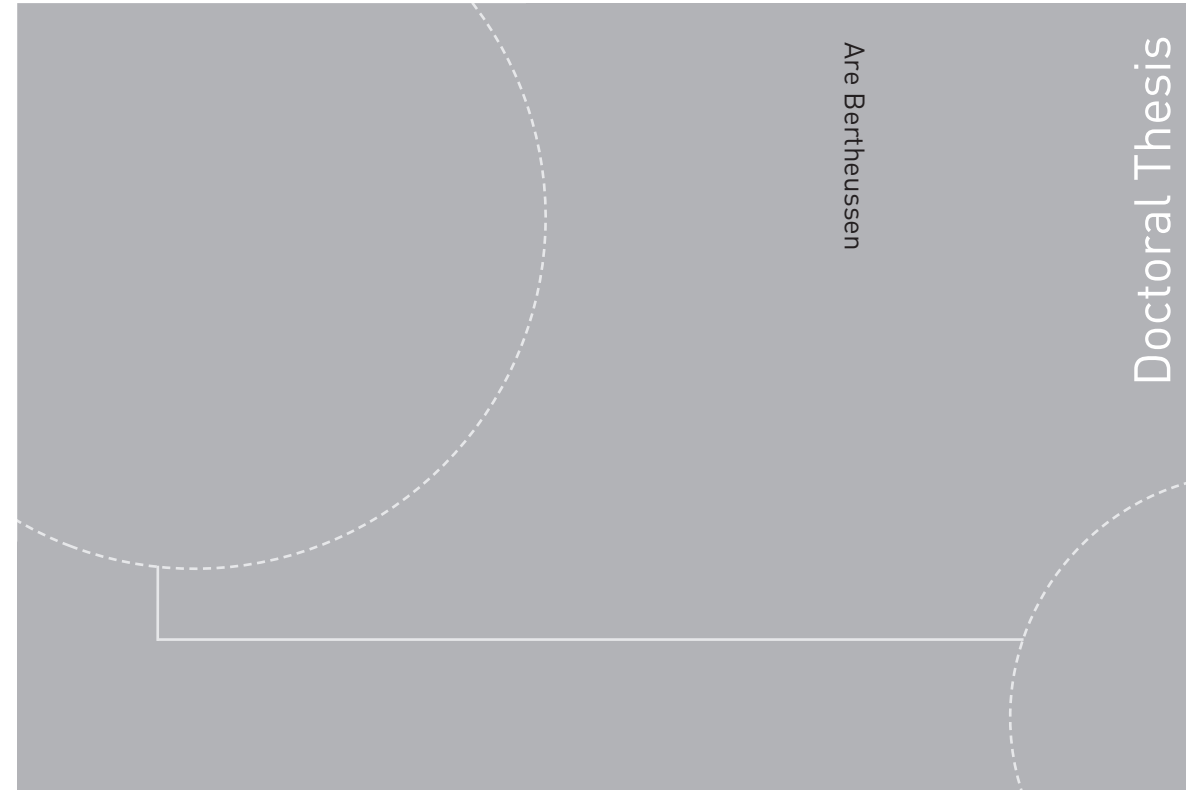


ISBN 978-82-326-3308-1 (printed version)  
ISBN 978-82-326-3309-8 (electronic version)  
ISSN 1503-8181



Doctoral theses at NTNU, 2018:259

Are Bertheussen

# Naphthenic acid solubility in produced water and their interactions with divalent cations

Doctoral theses at NTNU, 2018:259

**NTNU**  
Norwegian University of  
Science and Technology  
Faculty of Natural Sciences  
Department of Chemical Engineering

 **NTNU**  
Norwegian University of  
Science and Technology

 **NTNU**

 **NTNU**  
Norwegian University of  
Science and Technology

Are Bertheussen

# **Naphthenic acid solubility in produced water and their interactions with divalent cations**

Thesis for the degree of Philosophiae Doctor

Trondheim, September 2018

Norwegian University of Science and Technology  
Faculty of Natural Sciences  
Department of Chemical Engineering



Norwegian University of  
Science and Technology

**NTNU**

Norwegian University of Science and Technology

Thesis for the degree of Philosophiae Doctor

Faculty of Natural Sciences

Department of Chemical Engineering

© Are Bertheussen

ISBN 978-82-326-3308-1 (printed version)

ISBN 978-82-326-3309-8 (electronic version)

ISSN 1503-8181

Doctoral theses at NTNU, 2018:259



Printed by Skipnes Kommunikasjon as

As I stood today filling my car up with gasoline, I reminisced about the liquid flowing through the pump and how this is but the final storage this mixture of light hydrocarbons will experience before it is irreversibly changed to water and carbon oxide gases. I think that chemical engineers are one of the few who can truly appreciate the journey these hydrocarbons have travelled, just to now at last, they will soon be released once again to the atmosphere they left so many millions of years ago. They say science increases your understanding of the physical world around us, but alas even in a lifetime there is never enough time, and there is always more to study.





## Preface

This thesis is submitted in partial fulfilment of the requirements for the degree of Philosophiae Doctor (Ph.D.) at the Norwegian University of Science and Technology (NTNU). It consists of 5 papers that are based on work performed at the Ugelstad Laboratory, Department of Chemical Engineering, NTNU, under the supervision of Professor Johan Sjöblom and the co-supervision of Dr. Sébastien Simon. In addition, some of the modelling works were performed at the Institute for Energy Technology (IFE) in 2016.

I finished my degree in chemical engineering at the Department of Chemical Engineering, NTNU, in June 2015. In September 2015, I joined the Ugelstad laboratory to be involved in the Centre for Innovation-based Research (SFI) in subsea production and processing (SUBPRO). This project was funded by the Research Council of Norway, NTNU and major industry partners: ABB, Aker Solutions, Aker BP, DNV GL, Neptune energy (former Engie E&P, former GDF Suez E&P Norway), Lundin, Shell, Equinor (former Statoil) and VNG Norge.

## Acknowledgements

I would like to thank my supervisor Professor Johan Sjöblom, for hiring me into the laboratory he has built up and into the research centre on subsea technology and processing (SUBPRO), and for his guidance throughout the years. As work can be stressful I especially appreciated the good humor and social events he has arranged for the lab, which has made work more fun.

I would like to thank my co-supervisor Dr. Sébastien Simon for his patience, unwavering positivism without which this work would have been impossible.

I would like to thank my wonderful colleagues Sandra Rodríguez, Marcin Dudek, Jost Ruwoldt and Tomas Hjartnes for the enjoyable company on and off work.

Thanks to Jens, May and Bicheng for the daily lunch breaks.

I would like to thank my colleagues at the SUBPRO centre for enjoyable social events and introduction to new disciplines and problems.

I would like to thank my girlfriend, Anette Østbø Sørensen, simply for being perfect.

## Abstract

To keep up with the growing energy demands, the production of high acid crudes is increasing worldwide. This acidity is mainly caused by a subgroup of resins called naphthenic acids. With the increased production and normalization of new technology like seabed liquid-liquid separation, more knowledge about these acids is necessary to maintain a predictable production. One of the most important factors in understanding the physical and chemical behavior of crude oils has been found to be their content of polar components.

Multiple flow assurance problems can occur during crude oil production, as the temperature and pressure changes from the reservoir to the platform and over the lifetime of the field. The role of naphthenic acids in flow assurance relates mainly to issues like emulsion stability and naphthenate formation. Acids are prone to partition from the oil phase to the water phase, as the release of CO<sub>2</sub> during depressurization increases the water phase pH.

The goal of this thesis is to study the solubility and partitioning of naphthenic acids in oil-water systems as a function of the composition of the aqueous phase. The strategy adopted was the following. First, model acid and base compounds were studied experimentally and through modelling by dissipative particle dynamics (DPD). The partitioning of these acids and bases were determined. The thermodynamic characteristics determining this partitioning, the partition ratio, the dissociation constant and the solubility constant were determined. In order to be close to a real crude oil system, two mixtures of naphthenic acids were then studied, one commercial naphthenic acid mixture from Fluka and one extracted crude oil acid mixture. In order to analyze these mixtures, a GC/MS method was improved to provide a reliable structure distribution by considering fragmentation. The developed GC/MS techniques then allowed the study of the oil-water partitioning of these mixtures with pH in 3.5 wt. % NaCl water. The cologarithm of the partition ratio between the oil and water was found to increase linearly with the molecular weight of the acids. The relationship found for the commercial naphthenic acid mixture and crude oil extracted acids are similar, which seems to point to universal properties for naphthenic acids. Finally, the effect of the presence of calcium in the water phase on the partitioning of naphthenic acids was determined. Contrary to the precipitation observed for the single model acid 4-heptylbenzoic acid, the results obtained with naphthenic acid mixtures points to the formation of oil soluble calcium naphthenate at high pH.

The last part of the thesis is dedicated to determining the influence of solubilized naphthenic acids on oil-in-water emulsions. A microfluidic method was applied, and it was found that naphthenic acids in the water phase influences the coalescence of oil droplets in water. Moreover, the coalescence results with the commercial naphthenic acid mixture was found to be similar to the results obtained with dissolved crude oil components for three different crude oils.

## List of publications:

### **Paper I**

Bertheussen, Are.; Simon, Sébastien.; Sjöblom, Johan.,

“Equilibrium partitioning of naphthenic acids and bases and their consequences on interfacial properties.”

Colloids and Surfaces A: Physicochemical and Engineering Aspects **2017**, 529, 45-56

### **Paper II**

Skartlien, Roar.; Bertheussen, Are.; Simon, Sébastien.; Sjöblom, Johan.,

“Development of electrochemical DPD molecular simulations for oil/water partitioning of organic acids at varying pH.”

Journal of Dispersion Science and Technology **2017**, 39 (9), 1347-1375

### **Paper III**

Bertheussen, Are.; Simon, Sébastien.; Sjöblom, Johan.,

“Equilibrium partitioning of naphthenic acid mixture part 1: Commercial naphthenic acid mixture.”

Energy & Fuels **2018**, 32 (7), 7519-7538

### **Paper IV**

Bertheussen, Are.; Simon, Sébastien.; Sjöblom, Johan.,

“Equilibrium partitioning of naphthenic acid mixture part 2: Crude oil extracted naphthenic acids”

Accepted for publication in Energy & Fuels

### **Paper V**

Dudek, Marcin.; Bertheussen, Are.; Dumaire, Thomas.; Øye, Gisle.,

“Microfluidic tools for studying coalescence of crude oil droplets in produced water”

Chemical Engineering Science **2018**, 191, 448-458

All the experimental work and preparation of manuscripts for papers I, III, and IV was carried out by me at Ugelstad laboratory. In paper II, the simulations were performed by Roar Skartlien at the Institute for Energy Technology (IFE). My task was to define the system along with other co-authors and contribute to the writing of the manuscript. My role in paper V consisted to

perform experiments along with Marcin Dudek for the section involving dissolved components and to contribute to the preparation of the manuscript.

### **Additional publications and conferences**

Bertheussen, Are.; Simon, Sébastien.; Sjöblom, Johan.,

“Sequential separation, Research impact of fluid properties on oil-water separation and water quality”

Oral presentation at Subsea Valley **2017**, Bærum, Norway, April **2017**.

Bertheussen, Are.; Simon, Sébastien.; Sjöblom, Johan.,

“Equilibrium partitioning of naphthenic acids and bases and their interactions.”

Poster presentation at Petrophase **2017**, the 18th International Conference on Petroleum Phase Behavior and Fouling (PetroPhase) in Le Havre, France, June **2017**

Bertheussen, Are.; Simon, Sébastien.; Sjöblom, Johan.,

“How crude oil acids partition between oil and water phases.”

Oral presentation at the International workshop on “Advanced Hybrid Separation Techniques in Industrial Wastewater Management”, Kolkata, India, December **2017**.

Bertheussen, Are.; Simon, Sébastien.; Sjöblom, Johan.,

“Oil/Water Partitioning of Two Naphthenic Acid Mixtures.”

Oral presentation at Petrophase **2018**, the 19th International Conference on Petroleum Phase Behavior and Fouling, Park City, Utah, USA, July **2018**.







## Table of Contents

1	Introduction.....	1
1.1	Crude oil.....	2
1.2	Produced water.....	5
1.3	Upstream production.....	7
1.4	Subsea production and processing.....	8
2	Theoretical background.....	11
2.1	Naphthenic acids.....	11
2.1.1	Definition and structure.....	11
2.1.2	Analysis of naphthenic acids.....	13
2.2	Bases.....	16
2.3	Oil-water partitioning.....	16
2.4	Oil-water interfaces.....	23
2.4.1	Interfacial properties.....	23
2.4.1.1	Influence of structure and pH.....	23
2.4.1.2	Influence of cations.....	26
2.4.2	Emulsions.....	29
2.4.2.1	Definition and general concepts.....	29
2.4.2.2	Case of crude oil emulsions.....	32
2.5	Theory summary.....	41
3	Experimental techniques.....	42
3.1	Ultraviolet and visible (UV-Vis) spectroscopy.....	42
3.2	Surface tension (ST) and interfacial tension (IFT) measurements with the Du Noüy ring.....	43
3.3	Gas chromatography and mass spectrometry (GC/MS).....	44
3.4	Microfluidics.....	46
4	Main results.....	47
4.1	Paper I.....	47
4.2	Paper II.....	52
4.3	Paper III.....	54
4.4	Paper IV.....	59
4.5	Paper V.....	65
5	Concluding remarks.....	68
6	Scope for future work.....	71
7	References.....	73



# 1 Introduction

To keep up with the growing energy demands, the production of high acid crudes is increasing worldwide, now representing more than 15% of the global production <sup>1</sup>. This acidity is mainly caused by the content of a subgroup of resins called naphthenic acids. Acidic crude oils are more challenging to produce and refine due to the issues these, usually dense and viscous, fluids cause in flow assurance and later with corrosion and catalyst damage in refinery operations, not to mention the price penalty for acidic content <sup>2</sup>. In the field of subsea technology, seabed oil-water separation with reinjection or discharge of water circumvents the pressure drop of lifting the produced water, leading to increased production and smaller weight footprint of topside water treatment facilities. Three seabed liquid-liquid separators have already been installed and new technology is currently under evaluation for deeper seafloors <sup>3, 4</sup>, subsea discharge <sup>5</sup> and online water quality measurements <sup>6</sup>. A drawback of subsea processing is the reduced access to handle unforeseen flow assurance problems. Subsea solutions are often used in exploitation of marginal reserves in mature and infrastructure-rich fields, a development which hinges on accurate prediction of production <sup>7</sup>. To ensure the viability of the separation for the changing inlet conditions over the lifetime of the field, proper fluid characterization is required to anticipate challenges before they occur. In that respect, this work has been focused on the behavior of crude oil acids and bases in oil-water systems. Some of the equilibria involved are depicted in Figure 1.

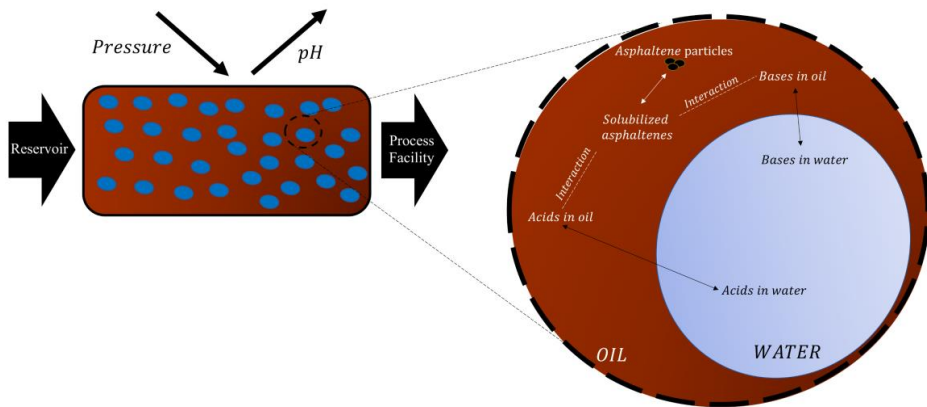
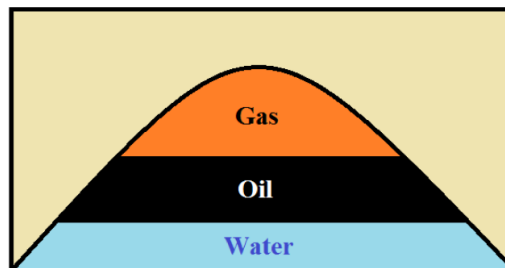


Figure 1: Schematic of the transfer of acids and bases between the oil phase and the water phase. The pressure drop in the well stream during production releases dissolved acidic gas ( $CO_2$ ) from the water phase. The consequent rise in water phase pH induces a transfer of crude oil acids. Asphaltenes are solubilized by resins including acids and bases in the oil phase <sup>8</sup>.

## 1.1 Crude oil

Crude oil is a naturally occurring hydrocarbon mixture with gaseous, liquid and solid components, on which our society is wholly dependent as a source of raw material for fuel, heating and plastics <sup>9</sup>. Large, but finite amounts of this resource are found in geological formations beneath the surface of the earth. As with the origin of life, there are two similarly named theories for the origin of crude oil: the biogenic and the abiogenic <sup>10</sup>. Traditionally, Western scientists have been proponents of the biogenic argument, while Eastern scientists from Russia and the Ukraine are proponents of the abiogenic side. The abiogenic theory states that petroleum is formed from carbon and hydrogen source material in the mantle of the earth and migrate up to the sedimentary rocks <sup>11</sup>, while the biogenic theory states that crude oil is organic material, sedimented and decomposed for millions of years under high temperatures and pressures <sup>9</sup>. The final petroleum will be influenced by the original organic material it was made from, which is why two adjacent reservoirs with different age can have various petroleum characteristics <sup>12</sup>. The formation of hydrocarbons leads to an increase in the specific volume <sup>13</sup>, which causes migration through cracks and capillaries. This migration from source rock to reservoir rock is referred to as the primary migration. In the reservoir rock, buoyancy forces squeeze the hydrocarbons through water filled pores until it hits a cap rock of low permeability. This is referred to as the secondary migration. Note that this implies that there will always be some associated water within the oil layer of the reservoir. A simplistic reservoir schematic is shown in Figure 2.



*Figure 2: Schematic of a petroleum reservoir.*

To extract the hydrocarbon resources, an oil well is drilled down into the reservoir and production is initiated as fluids are pushed to the surface by the high pressure of the reservoir. This production through pressure depletion is referred to as the primary recovery stage. For gas fields this pressure decline is counteracted by pumping down lean gas to recover more of the condensate from the rich gas in the reservoir, after which the reservoir is produced until the

pressure is depleted <sup>14</sup>. For oil fields, the natural pressure depletion alone would only extract around 10% of the available oil reserves. To counteract this decline in pressure, a secondary recovery stage is initiated where injection wells are drilled to pump down water and gas, which maintains the reservoir pressure and push the oil towards the production zone. This strategy offers a high return on investment, as around 35% of the oil reserves are expected to be produced <sup>9</sup>. Additional percentages of oil can be extracted through tertiary oil recovery, where enhanced oil recovery methods like thermal recovery, chemical injections or foam injections are employed.

From a compositional perspective, crude oil is a notoriously complex mixture, predominantly made up of different hydrocarbons. Other compounds contain various amounts of other elements like oxygen, nitrogen, sulfur vanadium and nickel. A typical elemental composition of crude oil can be described as 84-87% carbon, 11-14% hydrogen, <5% sulfur, <1% nitrogen and <2% oxygen. It was recently confirmed that the hydrocarbon composition increases in aromaticity, molecular weight, and heteroatom content as a function of boiling point <sup>15</sup>. As no two crude oils are alike, it would be useful to obtain the exact ingredients of each crude oil to systematize the causes behind observed behavior. Sadly, the enormous amount of unique molecules present in each crude oil make it impossible to quantify individual components <sup>16</sup>, although advances in mass spectrometry might allow for this option in the future. There are simpler and cruder fractionations in use however, where compounds are separated based on properties like boiling point, solvent solubility, chemical reactions or interfacial activity. Although the continuous molecular composition of crude oil will result in some degree of overlap for any boundaries established by these fractionation methods, useful comparative crude oil analysis can take place to infer how these fractions influence the crude oil behavior. One of the common fractionation methods is called SARA, where the crude oil is characterized into the following fractions: saturates, aromatics, resins and asphaltenes <sup>17</sup>. Figure 3 shows an illustration of such a SARA analysis of crude oil <sup>18</sup>.

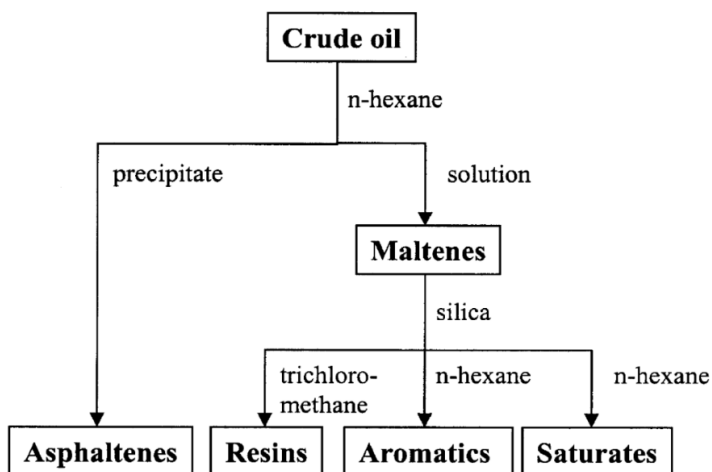


Figure 3: Illustration of the SARA fractionation of crude oil. Image reproduced from Sjöblom et al. <sup>18</sup>.

Asphaltenes are the largest and most polar molecules in crude oil, with molecular weights in the range of 500-1500 g/mol. This crude oil fraction contains both heteroatoms, such as nitrogen, oxygen and sulfur, and metals like nickel and vanadium. Asphaltenes are defined by their solubility: they precipitate in the presence of an excess of alkanes like pentane, hexane or heptane. These large polyaromatic molecules form aggregates that can deposit in flow lines <sup>19</sup> or stabilize emulsions <sup>20</sup>. The asphaltene content in crude oil is usually small, although in extreme cases it can encompass up to 17 wt. % <sup>21</sup>. After asphaltene precipitation the solute is referred to as maltenes, still containing the three fractions: resins, aromatics and saturates. Resins represent the remaining polar fraction after asphaltene extraction, which translates to functional groups containing oxygen, nitrogen and sulfur. This fraction is removed by adsorption onto polar surfaces or by precipitation in liquid propane <sup>9</sup>. The resin content ranges from 1-25 wt. % <sup>17,21</sup>. Naphthenic acids are a subclass of the resin fraction <sup>18</sup> and in general resins account for approximately 90% of the acidic functional groups in crude oil <sup>22-24</sup>. Other reports indicate resins to account for >85% of the basic groups in crude oil <sup>25,26</sup>. As both resins and asphaltenes are defined as a solubility class there exists an overlap in the arbitrary boundary between them. For example, pentane precipitated asphaltene has a larger weight fraction compared to heptane precipitated asphaltenes. Both these fractions, asphaltenes and resins, can cause more problems than they are worth, due to their involvement in flow assurance problems and catalyst poisoning in the refinery. Fortunately, the weight percentage of these fractions is usually small compared to the two last and most valuable fractions of the crude oil, saturates

(24-85 wt. %) and aromatics (10-45 wt. %). These fractions contain non-polar hydrocarbons of various size and proportion although they can still contain heteroatom groups like sulfur, nitrogen and oxygen <sup>27, 28</sup>. Production issues can also arise from the saturates fraction as temperature gradients along the transport pipe cause long chain paraffins or waxes to deposit, a problem which must be frequently remedied.

## 1.2 Produced water

As the reservoir formation is usually saturated with water prior to the hydrocarbon migration, and water is used to increase the production of oil, some water will inevitably be co-produced with the oil even at the start of production. This water phase is referred to as the produced water. Produced water can be a mix of water originating from the hydrocarbon zone (associated water), the water zone (free water) and from the injected water <sup>29</sup>, depending on the stage of production. The water cut in the well stream can vary from a couple of percent in the beginning to 98 % at the end of the field's lifetime <sup>30, 31</sup>. Worldwide, three barrels of water are on average produced per barrel of crude oil <sup>32</sup> which makes the produced water, by far, the biggest waste stream in the world.

Due to the prolonged exposure to hydrocarbons and rock in the reservoir, and mixing forces during production, produced water consists of a complex mixture of particulate, and dissolved organic and inorganic material <sup>31</sup>. Figure 4 gives an overview of produced water constituents<sup>33</sup>. Although the majority of the added production chemicals are primarily oil soluble, some water-soluble additives like biocide, oxygen scavengers and scale inhibitors also end up in the water phase <sup>34</sup>.



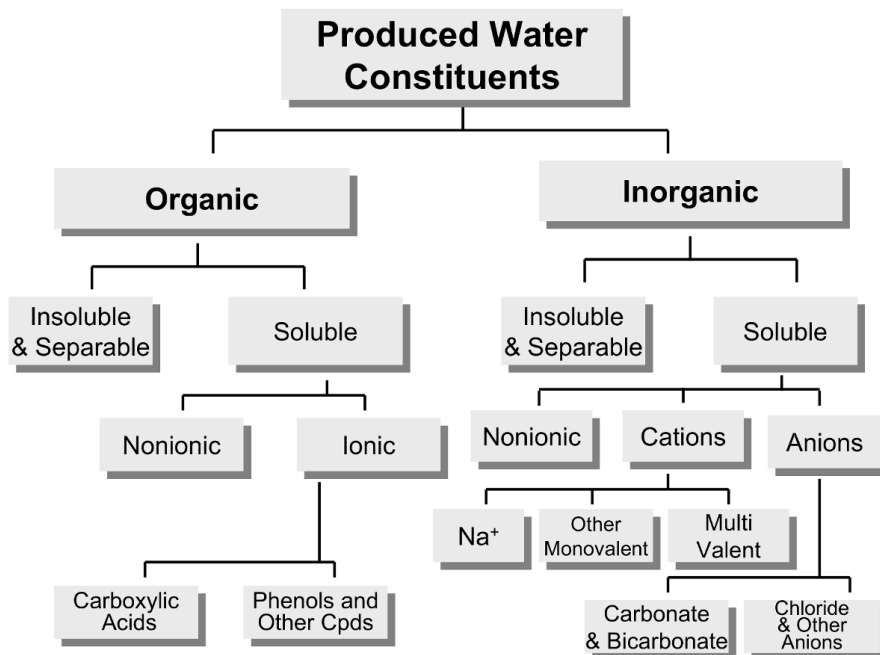


Figure 4: Representation of produced water constituents. Image reproduced from Hayes and Arthur <sup>33</sup>.

Produced water is subjected to treatment in order to meet local regulations for discharge <sup>35</sup> or injection criteria for injection into a reservoir. Examples of treatment units are hydrocyclones, c-tours, gas flotation units, membranes and filters. Produced water injection is especially common for onshore operations due to the lack of surrounding injection water sources or strict discharge rules <sup>29</sup>. In offshore operations, seawater is readily available for injection, which is why produced water has traditionally been discharged to the sea. These gigantic volumes of released wastewater with toxic and chronically harmful components have raised some environmental concerns <sup>31</sup>. A ten years study found that the effects on environmental harm on the Norwegian continental shelf are generally moderate although some long term effects remains to be mapped <sup>36</sup>. However, since the Norwegian government called on the oil industry to develop a zero discharge strategy <sup>37</sup>, reinjection of produced water is increasingly being employed on the Norwegian continental shelf <sup>38,39</sup>. Zero discharge requirements are already in effect in areas considered especially vulnerable like the Barents sea <sup>40</sup>. As of 2017, 24% of the produced water on the Norwegian continental shelf was injected back into the ground <sup>39</sup>. There have been some setbacks however, as the produced water reinjection (PWRI) plans for Ekofisk were halted due to reservoir souring <sup>41</sup>. In addition to reservoir souring by bacteria, other

challenges like oil and grease content, and especially suspended solids are also affecting the water injection <sup>42</sup>.

### 1.3 Upstream production

The production chain in the oil and gas industry is divided into three parts: upstream, midstream and downstream. The upstream part of the industry handles the exploration and the production of oil and gas, stabilized for transport. The midstream industry revolves around transportation, while the downstream industry transforms and purifies the raw material into marketable products for consumers or precursors for other industries.

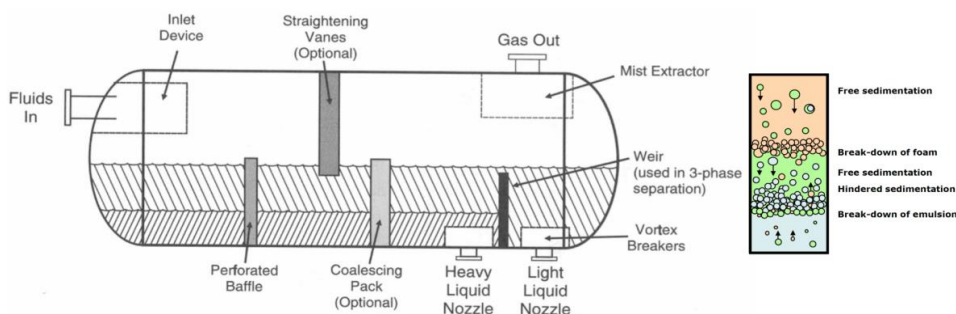


Figure 5: Schematic of the separator and the vertical flow in the phases. Images reproduced from Campbell, 1955 and Gramme, 2009 <sup>43, 44</sup>.

In the upstream part of the processing the first stage is a gravity separator, a large horizontal vessel in which the fluids are allowed to separate over a retention time of around five minutes. A schematic of a gravity separator is shown in Figure 5. From the three outlets the bulk phases of oil, water and gas go onto their respective processing trains. The crude oil goes on through a second and third separator with decreasing pressure to have a controlled vaporization of the volatile components. The water content is also progressively decreased through these stages before finally a coalescer brings the water content down to below the required 0.5 % v/v water content. The low water content is beneficial to avoid transporting water, and limit corrosion and scaling issues caused by salts dissolved in the water. From the water outlet of the first separator comes both water and coproduced sand or solids. First the solids are removed by a sand cyclone or desander. Then the water is treated with a hydrocyclone and a degasser unit to remove the dispersed oil droplets. Discharge regulations for oil-in-water content are usually set

around 15-40 ppm, while the injection criteria can be 10 ppm<sup>45</sup>, 100 ppm<sup>46</sup> or 1000 ppm<sup>47, 48</sup>. Oil droplets can have an adverse effect on the reservoir permeability<sup>49</sup>, and the injection criteria are based upon the type of the reservoir rock, the type of reservoir (production or disposal), injection strategy and injection tests<sup>50-53</sup>. The gas phase from the first stage separator is cooled and scrubbed for entrained and condensed liquids before it is compressed for transportation or injection. A schematic of the oil, gas and water processing trains is shown in Figure 6.

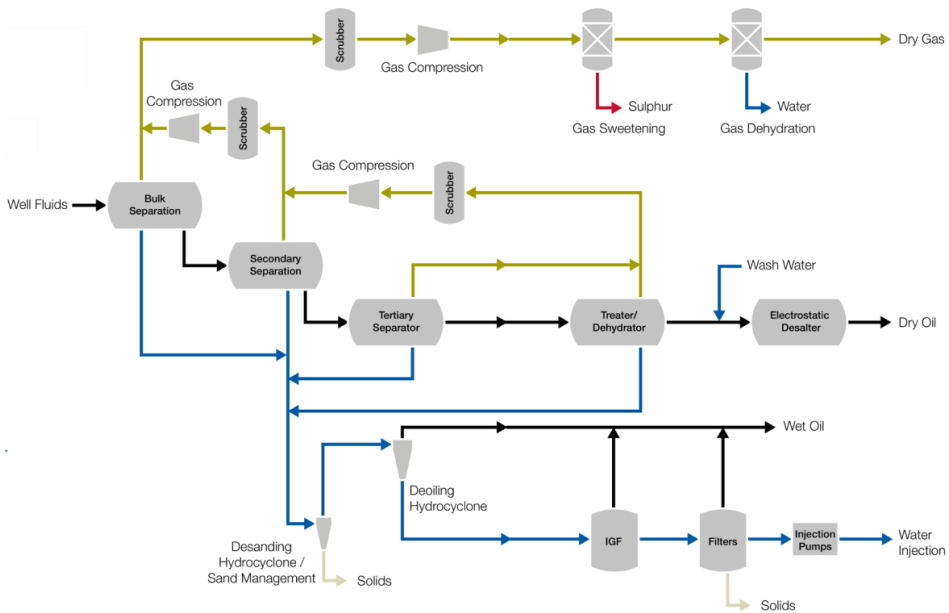


Figure 6: Schematic of a typical upstream processing system. Image reproduced from SULZER<sup>54</sup>.

#### 1.4 Subsea production and processing

As the most accessible crude oil resources are the first to be developed and depleted, the remaining resources are increasingly found in more remote areas and in deeper water<sup>55</sup>. Implementation of subsea solutions to these developments can offer an alternative where harsh weather conditions or weight limitations make traditional field developments economically unviable<sup>56, 57</sup>. In the recent decades, an increasing number of subsea production and processing solutions have gone from the drawing board to operated projects<sup>58</sup>. So far pumps, compressors, desanders, hydrocyclones and separators have been successfully implemented subsea, and new technologies are continuously being developed. Worldwide,

roughly 20% of the offshore oil and gas resources is recovered with subsea installations. In Brazil and Norway this percentage is much higher and most of the subsea milestones have been achieved in these countries.

One aspect of subsea processing entails liquid-liquid separation <sup>55, 56, 59</sup>. Declining reservoir pressure and increasing water cut over the lifetime of the field cause lowered production rate and cumulative oil recovery prospects, due to less pressure being available to lift a heavier production column from the reservoir to the surface. By removing most of the water at a lower point, the reservoir pressure does not have to lift all the water to the surface. As the water cut increases during production, the capacity of the water treatment topside can bottleneck the production, which is another reason to implement subsea water separation. Installment of additional equipment topside can be limited due to the weight or space restrictions on the platform. Subsea oil-water separation was successfully introduced in the early 2000s with the Troll C pilot and two more installments, Tordis and Marlim, have since followed <sup>47, 48, 60-62</sup>. The three installments were designed to remove most of the water from the production stream and inject it either into a disposal reservoir or a production reservoir.

Subsea separation also boasts more advantages than those listed above. For example, regarding the separation three points can be brought up. The separation can be performed at a higher pressure on the seabed leading to fewer problems related to depressurization of acidic oil <sup>63</sup>. The temperature of the fluids will be higher as they have less time to lose heat to the water around the pipes, which gives the separated fluids a larger density difference <sup>58</sup>. The shorter distance travelled from the reservoir to the seabed instead of from the reservoir to the surface, decreases the need for demulsifiers as stable emulsions have less time to form and age <sup>56</sup>. Regarding the flows coming out from the separator, they have different composition and reduced volume compared to the unseparated flow, decreasing the need for flow assurance chemicals <sup>64</sup> and decreasing the pipe dimension requirements. The separated phases are also less viscous than their water-in-oil emulsion counterpart, which reduces friction and increases the flow line capacity <sup>58</sup>. A testament to these advantages is mentioned in a report on the Troll C Pilot performance <sup>47</sup>.

Despite all the advantages, some operators have valid concerns regarding the reduced accessibility. Installations located at the seabed are more vulnerable to problems related to maintenance, inspection and start-up challenges, where the reduced access can blow otherwise routine problems out of proportion. The subsea installations need to allow for alternative

production methods and easy component replacement. The outside pressure on the equipment together with warmer, more pressurized wellstream fluids introduces massive strains on the separator system design. The separator is also expected to perform for the entire lifecycle of the field over a range of operational parameters<sup>6</sup>, which is why fluid characterization is one of the keys to ensure the long term viability of a subsea separation system<sup>58</sup>. Conventional gravity separators would require a thick shell to handle the hydrostatic pressure at great depths and thus it might simply be too heavy to lower down<sup>46</sup>. New separation technology, like the pipe separator, is designed to combat this issue<sup>64</sup>. Another important challenge lies in how to develop separation solutions that provide increased system efficiency and maintainability, while becoming more compact<sup>59</sup>. New aspects of subsea processing include implementation of compact electrocoalescers<sup>65</sup> and subsea water discharge<sup>5, 66</sup>. Standardization of available technologies may lead to future offshore oil and gas developments being invisible on the surface, as all the units, traditionally located on the oil platform, have been moved down to the seafloor<sup>67-69</sup>.

## 2 Theoretical background

### 2.1 Naphthenic acids

#### 2.1.1 Definition and structure

The term “naphthenic acids” has been used to describe all organic acids found in crude oil although the traditional definition describes a carboxylic acid with a naphthene ring <sup>12, 70</sup>. Like other crude oil components, they span over a large spectrum of sizes and structures. Size wise, they have been reported to have a molecular weight ranging between 200-700 g/mol <sup>71</sup> or C<sub>15</sub>-C<sub>55</sub> <sup>72</sup>, although their weight can exceed this number by far <sup>23</sup> like the tetrameric acid, ARN, with a molecular weight of 1230 g/mol <sup>73</sup>. Structure-wise, naphthenic acids are often described by the isomer formulas C<sub>n</sub>H<sub>2n+Z</sub>O<sub>2</sub> <sup>74</sup> for monoacids or C<sub>n</sub>H<sub>2n+Z</sub>O<sub>x</sub> <sup>75</sup> allowing for additional oxygen functional groups like acids with hydroxyl groups or diacids. In either case, the *n* refers to the number of carbon atoms, the *Z* is a negative integer referring to the hydrogen deficiency of the naphthenic acid molecule and the *x* refers to the number of oxygen atoms. This isomer formula is however limited, as it does not account for other heteroatoms like sulfur and nitrogen. As mentioned in section 1.1, crude oils have unique compositions. This is also true for their naphthenic acid sub-fraction. Acids from North Sea crude oils were found to be predominantly monoacidic carboxylic acids <sup>22, 76</sup>, in contrast to studies on crude oils from North, Central and South America <sup>72, 77, 78</sup>, which report that less than half of the identified acids can be described as “true naphthenic acids”, where the remaining acids contain nitrogen or sulfur functional groups or one or more aromatic rings. Headley, et al. <sup>79</sup> defined the term naphthenic acid fraction components (NAFC) aimed at giving scientists a more descriptive term for crude oil acids, accommodating for more functional group combinations with oxygen, sulfur, nitrogen and aromatic rings. Examples of these acids are shown in Figure 7.

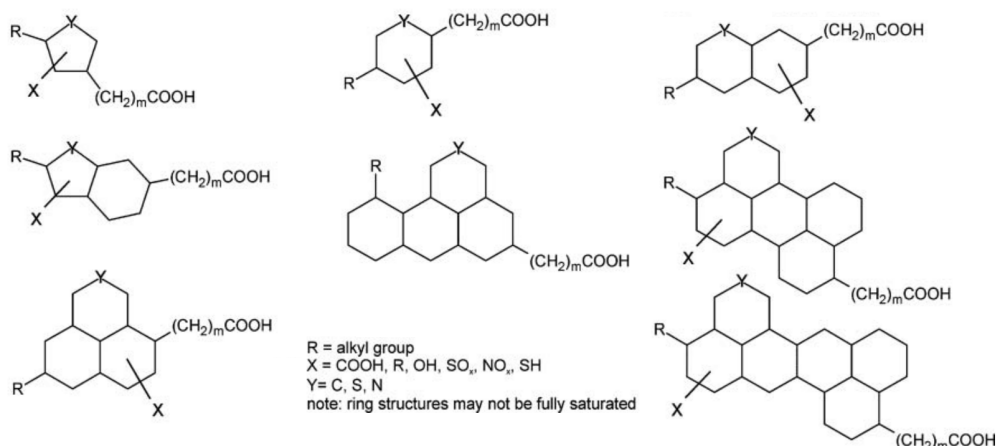


Figure 7: Examples of possible naphthenic acid fraction components (NAFC) as described by Headley, et al.<sup>80</sup>. Image reproduced from Headley et al.<sup>80</sup>

The amphiphilic properties of the naphthenic acids lead to an affinity for the interface between oil and water, which affects the stability of water-in-oil emulsions, and oil-in-water emulsions<sup>70, 81</sup>. Corrosion is another aspect of naphthenic acids<sup>82, 83</sup>, where they increase corrosion in combination with hydrogen sulfide<sup>84, 85</sup>, however the correlation between corrosion and acid content is not always clear cut<sup>24, 77, 86-88</sup>. In recent years, naphthenic acids have become immensely more popular as a research topic<sup>75</sup>, likely caused by the advent of concerns linked to open air tailing ponds of oil sands process-affected water (OSPW)<sup>89</sup> in Alberta, Canada, where some of the cyclic and aromatic naphthenic acids have been shown to be toxic and carcinogenic<sup>90</sup>. Another source of interest comes from the race to characterize the naphthenate deposition<sup>91</sup> found to clog upstream processing units with tons of sticky deposits. Naphthenic acids have also been shown to accelerate the degradation of polyamide used in flexible risers<sup>92</sup>, causing life time extension concerns for the current infrastructure especially if new tiebacks with acidic crude oils are installed. Despite their inherently problematic properties regarding flow assurance or environmental concerns, naphthenic acids have some redeeming properties through their dispersive properties of compounds prone to adhesion or sedimentation<sup>58</sup>. They have also been linked to anti-agglomerant behavior, inhibiting the formation of hydrates<sup>93, 94</sup>.

Regarding their origin, naphthenic acids can stem from three sources: they can come from the original sedimentation of plants and animals, following the biogenic theory. They can be

generated under both aerobic and anaerobic conditions during the biodegradation of crude oils <sup>24, 95-97</sup>. They can also come from the organic material in the bacteria themselves once they die and decompose. Biodegradation is the consumption of organic matter either aerobically or anaerobically by bacteria. As bacteria have a preference for the linear, followed by branched aliphatics, alicyclics and finally aromatic hydrocarbons <sup>98, 99</sup>, and they are often thought to degrade the crude oil economical value by turning hydrocarbons into resins and asphaltenes <sup>100</sup>. This structural preference is also evident by the general low content of aromatic rings in crude oil naphthenic acids <sup>77, 101, 102</sup>, although they are present in some degree <sup>103-105</sup>. The biodegradation of the lighter components causes an increase in the concentration of the more polar and heavy compounds known to lower the oil quality by, for example, decreasing the API gravity, and increasing acid and base content of the crude oil <sup>26, 106</sup>.

### 2.1.2 Analysis of naphthenic acids

The naphthenic acid content in crude oils is quantified by the total acid number (TAN), in which a crude oil is titrated to obtain a number indicating the mass of KOH necessary to neutralize one gram of oil,  $\text{mg}_{\text{KOH}}/\text{g}_{\text{oil}}$  <sup>102</sup>. Although other acidic functional groups are present in asphaltenes and other resins, the vast majority of the TAN value is usually attributed to the naphthenic acids <sup>22-24</sup>. TAN values for crude oils can reach values up to  $16 \text{ mg}_{\text{KOH}}/\text{g}_{\text{oil}}$  <sup>107</sup>, although the value is usually significantly lower. A TAN over 0.5 indicates a high acid crude <sup>12</sup> and the average TAN values for crude oils produced in the North Sea for example, is around  $0.35 \text{ mg}_{\text{KOH}}/\text{g}_{\text{oil}}$  <sup>1</sup>. Bitumen is known to have higher TAN values, where Athabasca bitumens from Alberta, Canada have TAN values from 3.2 to 5.5 <sup>108</sup>. Different extraction methods, liquid-liquid and liquid-solid based, are used to separate acids from crude oil or bitumen. A detailed discussion of these methods can be found in Saab, et al. <sup>101</sup>.

Fourier transformed infrared spectroscopy (FT-IR) can be used to analyze naphthenic acids due to the specific absorbance of the carboxylic group. Naphthenic acids forms dimers in solutions which affect the infrared absorption. For example the monomeric C=O bond absorbs photons at  $1743 \text{ cm}^{-1}$  while the dimer absorbs at  $1704 \text{ cm}^{-1}$  <sup>109</sup>. Naphthenic acid salts have an asymmetric absorbance at  $1600\text{-}1500 \text{ cm}^{-1}$  <sup>110-112</sup>. When it comes to quantification purposes, the use of commercial naphthenic acids as calibration standards has a negative effect on the



measurement accuracy as the acid composition rarely matches the composition in the sample <sup>63</sup>.

Otero, et al. <sup>113</sup> have claimed that the metal in metal carboxylates can be identified by their characteristic IR absorbance. Carboxylates bound to calcium for example was found to have a asymmetric stretch of the COO- bond at 1575-1580  $\text{cm}^{-1}$ , while the absorbance was 1585-1590  $\text{cm}^{-1}$  if copper was the cation <sup>113</sup>.

As naphthenic acids are a polydisperse mixture in crude oil, one useful method to study them is through mass spectrometry (MS). This method has been extensively used in multiple studies <sup>72, 75, 78, 114-117</sup>. With the general isomer formulas ( $\text{C}_n\text{H}_{2n+z}\text{O}_2$ ,  $\text{C}_n\text{H}_{2n+z}\text{O}_x$  or molecules including sulfur/nitrogen ) and high resolution MS, the abundance of each isomer can be extracted from the mass spectra to obtain the composition of the naphthenic acids in the sample <sup>98, 118</sup>. By using soft ionization techniques one major ion can be produced (and/or radical) from each compound with otherwise limited fragmentation, which simplifies subsequent interpretations <sup>75</sup>. Barrow, et al. <sup>119</sup> conducted parallel analysis on OSPW to compare the results obtained with atmospheric pressure photoionization (APPI) and electrospray ionization (ESI). They found that APPI was able to show a larger number of high molecular peaks due to its ability to ionize less polar molecules like naphthenoaromatic acids. APPI is able to show more species both in positive and negative mode since it can create radicals in addition to ions, an effect which is not obtained with ESI, although this can also make the data analysis more complicated <sup>118</sup>.

Compared to the direct injection mass spectrometry, there are advantages with prior separation of the sample to get a clearer picture, either through chromatographic separation columns, or prior fractionation. For example in their study of the OSPW naphthenic acid extracts, Martin, et al. <sup>120</sup> showed how different distributions are obtained in analysis with and without chromatographic separation prior to the MS detection. Clingenpeel, et al. <sup>121</sup> and Rowland, et al. <sup>122</sup> demonstrated how low molecular weight compounds, more prone to ionization, hid the presence of larger and less ionizable compounds in Fourier-transform ion cyclotron resonance (FT-ICR) MS studies of surface active components in bitumen and deasphalted bitumen. Prior fractionation through successive elutions in aminopropyl silica columns allowed larger, poorly ionizable compounds to be detected and analyzed. A similar approach has recently been used to suggest that the island structure of asphaltenes is not necessarily the dominant structure. It is argued that low molecular weight asphaltenes with

island structures mask the detection of higher molecular weight asphaltenes, where archipelago structures are shown to be more prominent<sup>123, 124</sup>. Due to their ability to form hydrogen bonds, naphthenic acids exist as dimers or trimers in organic solvents. This was found to be concentration-dependent and the aggregation tendency was found to decrease with boiling point<sup>125</sup>. This phenomenon can lead to them showing up in other forms than the monomer in mass spectra. This can be remedied by exposing the sample to infrared multiphoton dissociation (IRMPD)<sup>126</sup>. In chromatographic columns the hydroxyl group of the naphthenic acids causes other problems by forming a long elution tail as it exits the column. By derivatizing the carboxyl groups in naphthenic acids to esters<sup>127</sup>, chromatography can be used as a quantification method both by using high performance liquid chromatography (HPLC)<sup>128</sup> and gas chromatography (GC)<sup>102</sup>. Over the years multiple combinations of extraction methods, chromatography and mass spectrometry with different ionization sources and mass separators have been applied<sup>129-132</sup>.

GC/MS is a simpler form of analysis, which is often more affordable and therefore available in many research facilities. GC/MS often uses hard ionization sources causing excessive, but characteristic fragmentation, from which the original molecule can be identified with fragmentation libraries. This method is however, only valid for proper compound elution, and a recurring chromatographic problem with naphthenic acid mixtures is that the elution is not discontinuous, but rather appears as a continuous unresolved hump. A way around this problem, applied in several cases<sup>133, 134</sup>, entails derivatizing crude oil acids into esters with a BeF<sub>3</sub>/MeOH mixture followed by GC/MS selective ion monitoring for  $m/z = 74$ , typical to methyl esters. Methods for quantification of naphthenic acids with GC/MS have been developed by several authors<sup>102, 109</sup>. Scott, et al.<sup>109</sup> compared their quantitative method, which exploits the absence of C<sub>13</sub> in nature, to FTIR results and found that the naphthenic acids concentrations indicated by FTIR were often 2-4 times higher than that of the GC/MS. This was attributed to the GC/MS method not accounting for all acid structures.

Different methods have been developed to limit the excessive fragmentation of the hard ionization sources. By derivatizing naphthenic acids to their t-butyldimethylsilyl esters with N-methyl-N-(t-butyldimethylsilyl) trifluoroacetamide (MTBSTFA), stable fragments can be obtained with GC/MS. Using this method St. John, et al.<sup>135</sup> showed how naphthenic acid mixtures could be classified into distributions of carbon number and hydrogen deficiency using the standard isomeric formulas C<sub>n</sub>H<sub>2n+z</sub>O<sub>2</sub>. Although the low resolution of the masses prevented further classification into heteroatoms and additional functional groups, this method offered a

simple analytical solution in the study of polydisperse acid mixtures, and has since been applied by several authors <sup>98, 109, 132, 136-138</sup>. This derivatization agent has mostly been used on commercial acid samples and OSPW extracts, but it was also reported to work for heavy crude oil (Marlim) acids <sup>139</sup>. Later the derivatization agent chosen by St. John, et al. <sup>135</sup> would also be shown to have one of the best overall derivatization efficiency for different acid structures <sup>138</sup>, although some shortcomings regarding steric hindrance have been pointed out <sup>136</sup>.

## 2.2 Bases

The basic fraction in crude oil has been far less studied compared to their acidic counterparts, much owing to the naphthenic acid issues regarding tailing ponds and naphthenate depositions. The basic groups present in crude oil have been found to be nitrogen compounds, more specifically pyridine derivatives and not amine groups <sup>140-142</sup>. As mentioned in section 1.1 the nitrogen content in crude oils is normally under 1% and only a third to half of those nitrogen groups have basic functionality <sup>9, 25</sup>. As with the acidic fraction, the basic fraction is usually quantified through titration to obtain a total base number (TBN). Simon, et al. <sup>25</sup> and Barth, et al. <sup>26</sup> found two dozen crude oils to have TBN values ranging from ca. 0.15 to 6 mg<sub>KOH</sub>/g<sub>oil</sub>, which despite the seemingly low content of basic nitrogen groups in crude oils, often exceeded the total acid numbers in the same crude oils! A correlation factor between TAN and TBN of 0.75 have previously been reported in literature <sup>23</sup>. The total base number (TBN) increase with the biodegradation and the density of the crude oil <sup>25, 26</sup>. The basic groups fall predominantly into the resin fraction, although some basic groups are also found in the asphaltene fraction <sup>25, 26</sup>. Like acids, bases can also partition into the water phase <sup>143, 144</sup>.

## 2.3 Oil-water partitioning

Organic compounds have various degrees of water solubility, depending on their hydrophilic-lipophilic balance (HLB) value, their acid-base constant and parameters like pH, pressure, temperature. The larger the hydrophobic surface area of the molecule the less water-soluble it will be <sup>145</sup>. Linear aliphatic molecules will have a large hydrophobic area, compared to molecules of the same size with branching, ring structures or aromatic groups <sup>105</sup>. The salinity of the water phase also affects the solubility of organic compounds by making the water

molecules more ordered in hydration spheres and less available for the organic molecule to be dissolved<sup>145</sup>. This is called the salting out effect. Polar molecules like acids and bases, have the ability to be deprotonated or protonated in the water phase, which increases their polarity and therefore water solubility.

Equation sets to model behavior of acidic or basic crude oil components in oil-water systems have been formulated by several authors<sup>63, 146, 147</sup>. More simple models can predict the final pH of a crude oil-water system based on the TAN, TBN and initial pH<sup>144</sup>. One of the most comprehensive approaches was covered in Touhami, et al.<sup>146</sup>, which includes most of the equilibria encountered in oil-water systems, i.e. partitioning of indigenous polar compounds and added surfactants, dissociation, micellization and even metal naphthenate partitioning back into the oil phase.

In a liquid-liquid system, the concentration of a solute in each liquid can be described by the partitioning coefficient. Partition coefficients for organic compounds are important in biological systems with, for instance, applications in drug delivery<sup>148</sup>. This property is often presented with an octanol-water system as the standard and over the years, extensive libraries of partition coefficients have been gathered<sup>149</sup>. For acids and bases in oil-water systems the partitioning of the non-ionized forms of the monomer in each phase can be described by,

$$K_{wo,HA} = \frac{[HA]_w}{[HA]_o} \quad (1) \quad K_{wo,B} = \frac{[B]_w}{[B]_o} \quad (2)$$

where  $K_{wo,HA}$  and  $K_{wo,B}$  represents the partition coefficients for an acid or a base.  $[HA]_w$  and  $[B]_w$  represents the acid and base concentration in the water phase, and  $[HA]_o$  and  $[B]_o$  represents the nonionized monomers of acid and base concentration in the oil phase. This partition coefficient is independent of the concentration, but consideration should be given as to what species of the compound are being measured, since unaccounted equilibria like dimerization, micellization and hydration can make the measured partition coefficient concentration-dependent<sup>150</sup>. As acids have a tendency to form stable dimers in the oil phase, predominant over a wide range of concentrations<sup>151</sup>, another term for the partitioning was suggested by Scherrer and Howard<sup>152</sup>:

$$P_{wo} = \frac{[HA]_w}{[HA]_{o,tot}} = \frac{[HA]_w}{[HA]_o + 2[(HA)_2]_o} \quad (3)$$

where  $P_{wo}$  represents the partition ratio for an acid and  $[(HA)_2]$  represents the dimer concentration. Although this definition is not concentration independent, it is a practical term and negligible concentration dependency has been shown for 4-heptyl benzoic acid in oil-water systems at acidic pH<sup>150</sup>. Association in the oil phase can interfere with partitioning measurements, for example the association abilities of dibutyl phosphate in oil have been shown to give an unreasonably low partitioning in hexane-water systems<sup>149</sup>. Ionizable compounds like acids and bases require, in addition to the partition coefficient, the dissociation constants in aqueous phases,

$$K_{a,HA} = \frac{[A^-]_w [H^+]}{[HA]_w} \quad (4) \quad K_{a,HB^+} = \frac{[H^+] [B]_w}{[HB^+]_w} \quad (5)$$

where  $K_{a,HA}$  and  $K_{a,HB^+}$  represents the dissociation constants for an acid or a base, and  $[A^-]_w$  and  $[HB^+]_w$  are the conjugate base and acid of their respective acid and base in the water phase. By accounting for mass balances and excluding other phenomena like micellization, these expressions can be used to obtain expressions for the oil and water concentrations of acids and bases as a function of pH,

$$[HA]_{w,tot} = \frac{[HA]_{o,init}}{\frac{[H^+]}{P_{wo,acid}(K_{a,HA} + [H^+])} + \frac{V_w}{V_o}} \quad (6) \quad [B]_{w,tot} = \frac{[B]_{o,init}}{\frac{[K_{a,HB^+}]}{K_{wo,base}(K_{a,HB^+} + [H^+])} + \frac{V_w}{V_o}} \quad (7)$$

where  $[HA]_{o,init}$  and  $[B]_{o,init}$  represent the initial concentration of acid and base in the oil phase, and  $[HA]_{w,tot}$  and  $[B]_{w,tot}$  represent the sum of dissociated and undissociated acids and base in the water phase. The terms  $V_o$  and  $V_w$  denote the volume of the oil and water phase, respectively.

In the literature, authors sometimes use the same term to describe different measurements<sup>146, 150, 153, 154</sup>. Scherrer and Howard<sup>152</sup> have presented a comprehensive review explaining the use of different partitioning terms like the distribution ratio  $D_{wo}$ , defined as the ratio of all ionized and non-ionized forms of a compound between two phases.

$$D_{wo} = \frac{[HA]_{w,tot}}{[HA]_{o,tot}} = \frac{[HA]_w + [A^-]_w}{[HA]_o + 2[(HA)_2]_o} \quad (8)$$

When this term is equal to 1, the compound has equal partitioning in each phase. Through equations from Scherrer and Howard <sup>152</sup>, the pH at which this phenomenon occurs can be found. This pH has been referred to as the “apparent pK<sub>a</sub>” <sup>155</sup>, as it instead of describing the pH at which half the acids are in the dissociated form, it described the pH at which half the acids in the system are in the water phase. For monoprotic acids and bases this apparent pK<sub>a</sub>’ becomes pK<sub>a</sub> + pP<sub>wo</sub> for acids or pK<sub>a</sub> - pP<sub>wo</sub> for bases.

The choice of solvent also affects the partitioning. Indeed, more polar solvents like alcohols give a better solubility for polar organic compounds like acids and bases, compared to less polar solvents, e.g. aromatics or alkanes. A list of partition coefficient correlations between different solvents is available in the literature <sup>149</sup>.

Other parameters like pressure, temperature, salinity and pH, can influence the partitioning of polar species in crude oil. Simulations on how temperature affects the partitioning of naphthenic acids show that the partitioning coefficient goes towards unity at increased temperature <sup>156</sup>. This qualitatively correlates with the experimental findings of Bostick, et al. <sup>157</sup> who did an experimental matrix on a Gulf of Mexico crude oil with synthetic brine. With a pH of 7 and temperature from 25-75°C, the total amount of polar organics (most of which were found to be organic acids) in the water remained unchanged although the concentration of C<sub>10</sub>-C<sub>20</sub> components (more oil soluble) increased, while the concentration of C<sub>6</sub>-C<sub>10</sub> (more water-soluble) components decreased. Jacobs, et al. <sup>158</sup> report a temperature range from 3 to 80°C for produced water in the North Sea sector.

The same study by Bostick, et al. <sup>157</sup> found that pressure has a minor effect on the water-soluble organic content. However, these results were obtained with “dead”, depressurized oil and other results might have been obtained with a “live” wellstream sample, still containing the volatile gases originally present in the production system, or with a recombined sample with a similar gas makeup <sup>18, 159</sup>.

Several works have studied the effects of pH on acid base equilibria although most of them have only considered acids. As bases are protonated at low pH and acids are ionized at high pH, their water solubility increases. In order to predict the concentration in water however, the partition ratio needs to be taken into account <sup>63</sup>. The partition ratio is the reason why 90% of acids in the system with a pK<sub>a</sub> of 5 are not in the water phase at pH 6 <sup>155</sup>. This was demonstrated

by several authors. Havre, et al. <sup>147</sup> showed that acids start to transfer to the water phase at a pH much higher than their  $pK_a$  and Lord, et al. <sup>153</sup> demonstrate the same tendency for the base, dodecylamine, although in this case the partitioning occurs at a lower pH than the  $pK_a$  (since this is a base). Exceptions to this exist as Standal, et al. <sup>154</sup> reported equal total phase concentrations occurring at the  $pK_a$  in single compound partitioning of an acid, a phenol and a base. Eftekhardakhah, et al. <sup>143</sup> showed that after shaking crude oil with water, the nitrogen content in water increased at low pH indicating transfer of bases into water at low pH. Another group has observed a color change of the aqueous phase over the pH range when shaking crude oil with water, also indicating a transfer of bases and acids into water <sup>144, 160</sup>. Hutin, et al. <sup>160</sup> brings forth an interesting observation regarding the partitioning of crude oil bases, where the addition of sodium dodecyl benzenesulfonate (SDBS) makes previously unavailable bases suddenly become reactive and change the final pH dramatically upwards when the initial pH is low. The same effect is observed for acids at high pH as well, although to a lesser extent. A related effect can be observed between a heavy acidic oil and its deasphalted counterpart <sup>133</sup>, where while the basic influence on the final pH seemingly disappears, the acids become far more reactive. The opposite effect regarding the acidic species was recorded by Flesiski <sup>161</sup>. It can be argued that using pH change as a measure of phase transfer is too simplistic as interfacial exchange of protons and metal ions can take place without phase transfer of the acid species <sup>162</sup>, especially when asphaltene partitioning into water is justified only by a change in pH <sup>163</sup>.

Bostick, et al. <sup>157</sup> remarked that, in analyzing the effect of pH on water-soluble crude oil organics, significant quantities of C<sub>10</sub>-C<sub>20</sub> range compounds become markedly soluble above pH 7. Typical North Sea produced water pH values are reported to range between 5.8-8.5 <sup>71, 158, 164</sup>, while the pH in the North Sea formation water range from 5-6.5 <sup>165</sup>. These numbers serve to illustrate the increase in pH caused by the release of CO<sub>2</sub> to the gas phase as the pressure drops from the reservoir to the surface facilities <sup>63</sup>. This pH increase leads to the increased partitioning of naphthenic acids, from the oil phase to the water phase by ionization of the naphthenic acids. The pH increase also favors the precipitation of calcium carbonate, which can lead to inorganic scale formation <sup>166, 167</sup>. These parallel equilibria are shown in Figure 8.

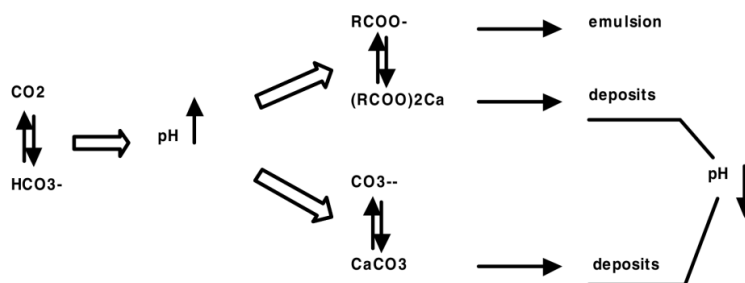


Figure 8: Scheme showing the effects of pH increase in the wellstream. Image reproduced from Rousseau et al. <sup>167</sup>.

Rousseau, et al. <sup>167</sup> also noted that bicarbonate acts as a buffer, maintaining the pH fairly constant and allowing more naphthenic acids to dissociate and/or partition.

The partitioning studies of Havre, et al. <sup>147</sup> on crude oil and commercial acids showed the naphthenic acids in crude oil to have a  $\text{pK}_a$  of 4.9, correlating to both earlier reports (5-6 reported by Brient, et al. <sup>168</sup>) and expected values for carboxylic acids <sup>169</sup>. There are however, contradictory views on this topic. For instance, a study showed high  $\text{pK}_a$  values for long chain acids, which only reach values close to 5 at infinite dilution <sup>170</sup>. This was attributed to pre-micellar aggregates. This determination was however, performed by titration of a high pH system in the absence of oil. At these pH values, the long chain acids could plausibly be partitioning into an oil-like medium as micelles at their apparent  $\text{pK}_a$ , as remarked by Passade-Boupat, et al. <sup>155</sup>.

Some studies have found a linear relationship between the logarithm of the partition coefficient and the carbon number in acids for low molecular weight acids by Reinsel, et al. <sup>171</sup> and higher molecular weight acids by Havre, et al. <sup>147</sup> (although it is unclear which water phase concentration Reinsel, et al. <sup>171</sup> actually measured). Similar relationships are also described earlier in the literature <sup>172</sup>.

Studies on more complex acids, like the tetraprotic synthetic acid (BP-10) <sup>173</sup>, synthesized to mimic the ARN acid <sup>174</sup> have been published. Here it was found that by including two dissociation steps in the partitioning equations (4) and (6) shown earlier, the oil-water behavior of these high molecular weight naphthenic acids could be modelled as well, even though the high values of  $\text{pK}_a$  showed an influence of micellization.

Insights into the dissociation of acids with molecular weight, or more specifically boiling point, are demonstrated by Rousseau, et al. <sup>167</sup>, who determined the pH at which the different boiling



point fractions of acids would dissociate. Here it can be seen that at pH 6.2, only acids with low boiling points 150 -230°C dissociate, compared to pH 7.2 where even some of the largest acids (400-550°C) will start to dissociate. Hurtevent, et al.<sup>63</sup> showed through experiments on 10 different crude oils that naphthenic acids can start to partition at pH values as low as 6.

The influence of molecular weight on the variation of partitioning with pH is also found in the experimental findings of Hemmingsen, et al.<sup>76</sup>, although here the water phase was a mixture of ethanol and water. North Sea crude oil successively mixed with pH 7, 10 and 14 in ethanol-water mixtures revealed narrow distributions for the pH 7 and 14 extractions, each on their side of the mass spectrum, while the pH 10 extraction had a much broader distribution. Although the solubility of naphthenic acids increases in ethanol water mixtures, 10% of the acids still remained in the oil phase after the pH 14 wash. A similar study<sup>130</sup> was conducted on another crude oil, this time without successive washes. Here the broadest distribution is obtained with the pH 14 wash.

With the high resolution of FT-ICR MS, Stanford, et al.<sup>105</sup> detected the presence of water-soluble acids as large as C<sub>41</sub>(~600 g/mol), even though the partitioning occurred at pH 7. While it has been shown that the interfacial material has similar double bond equivalent and carbon number distributions as the bulk phase polar components in the crude oil they come from<sup>175</sup>, the study by Stanford, et al.<sup>105</sup> showed this is not the case for the water-soluble components, which exhibit lower carbon numbers range and more aromatics for both acids and bases compared to their actual crude oil. It was widely shown that the high TAN crude oils contain the largest acid distributions<sup>24, 102</sup>. Contrary to expectations, Ligiero<sup>176</sup> showed that after contacting three crude oils with water, it was the crude oil with the lowest TAN (0.1 mg<sub>KOH</sub>/g<sub>oil</sub>) that gave the broadest distribution of acids in the water phase, some of them were even asphaltene-like (double bond equivalent (DBE) > 0.46 C<sub>n</sub>).

The salinity of the water phase affects the solubility of organic compounds through the salting out effect. This effect is demonstrated both for acids, bases and phenols in oil-water systems<sup>105, 154</sup>. In performing kinetic partitioning experiments with crude oils and model oils, Alvarado, et al.<sup>177</sup> found that higher salinity decreased the pH change over time, which went from 7 to 6 for high salinity and 6.5 to 4.5 for low salinity. Computer models showed a low impact of salinity on acid partitioning<sup>156</sup> and polar water-soluble organic partitioning were found not to be affected to a great extent. In his study Tichelkamp, et al.<sup>178</sup> found calcium to

greatly reduce the amount of water-soluble acids at high pH, while the same effect was not observed at pH 6.

A better understanding of the partitioning of polar crude oil compounds in oil-water systems could help minimize or overcome the production issues linked to these compounds <sup>63</sup>.

## 2.4 Oil-water interfaces

### 2.4.1 Interfacial properties

#### 2.4.1.1 *Influence of structure and pH*

Amphiphilic molecules have an affinity for the interface between oil and water due to their dualistic molecular structure, where one end is composed of a polar and hydrophilic functional group, and the rest of the molecule is otherwise apolar and hydrophobic. The relative size of the hydrophilic and hydrophobic parts of the molecule decides at which curvature of the interface the amphiphilic molecule adsorbs <sup>179</sup>. The polar crude oil components, asphaltenes and resins, thereunder organic acids and bases, usually have an amphiphilic nature, allowing them to adsorb/desorb to and from the oil-water interface and lower the interfacial tension (IFT) between oil and water like a surfactant.

It can be demonstrated through interfacial tension measurements that the resin fraction has the highest affinity for the interface <sup>180</sup>. This is a dynamic process, where compounds are either continuously adsorbed/desorbed or irreversibly adsorbed at the interface. If the adsorption rate is larger than the desorption, then the interfacial tension decreases over time until the desorption rate matches the adsorption rate and the interfacial tension is at equilibrium <sup>181</sup>. As with partitioning, the ionized form of the crude oil acids or bases tend to have a higher surface affinity compared to their less polar unionized forms. This can be demonstrated by showing crude oil interfaces to be positively charged at low pH where ionized bases are dominating the interface and negatively charged at neutral and high pH where acids become ionized <sup>182, 183</sup>. Although undissociated acids are less surface active than dissociated acids, they also decrease the interfacial tension as demonstrated by Havre, et al. <sup>147</sup>. Both Eftekhardakhah, et al. <sup>143</sup> and Nenningsland, et al. <sup>184</sup> found the surface activity of crude oil bases to be lower than the surface activity of crude oil acids, although the former study is limited to water-soluble species only.

Results by Luthy, et al.<sup>183</sup> showed similar surface active behavior for crude oils at high and low pH (Figure 9).

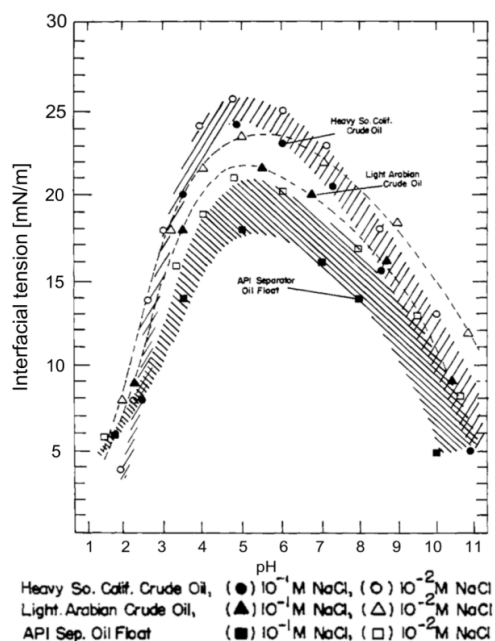


Figure 9: Graph displaying interfacial tension over the pH scale for three different crude oils and two different salt concentrations. Black dots belong to higher salt concentrations<sup>183</sup>. Reprinted (adapted) with permission from Luthy et al.<sup>183</sup>. Copyright 1977, American Chemical Society.

In order to exhibit surface active properties, a certain length of the hydrophobic part of the molecule is required. According to Seifert and Howells<sup>185</sup> the average molecular weights of interfacially active acids in crude oil range from 300 to 400 g/mol. It could be argued that this is the reason behind the uncommon interfacial tension responses recorded by Standal, et al.<sup>154</sup>. Of the single low molecular weight model compounds tested (an acid, a base (quinoline) and a phenol) only the phenol and the base seemed to change their interfacial activity with pH, and the base actually showed a lower IFT in its nonionic form. However, it can be noticed that molecules tested in this study are relatively low-molecular weight. Havre, et al.<sup>147</sup> showed that the interfacial tension of extracted crude oil acids remained constant from pH 2 to 8 before decreasing down to low values (<5 mN/m). Interestingly, Hemmingsen, et al.<sup>76</sup> showed that after successively washing a crude oil at three increasing pH values, 7, 10 and 14, and reacidifying (reprotonating) the obtained acid fractions, the acidic fraction obtained at pH 14 gave the lowest interfacial tension (~5 mN/m), followed by the pH 7 fraction (~10 mN/m),

while the pH 10 fraction only gave an interfacial tension of 16 mN/m. All these values were lower than the measured crude oil interfacial tension (~19 mN/m) and the water phase was non-pH-adjusted salt water. This shows that assuming surface active crude oil acids to be dissociated and exhibit surface active behavior at pH 6<sup>186</sup> could be wrong and this should be verified for each crude oil.

The effect of salinity on the interfacial tension is also demonstrated in Figure 9, where higher salinity leads to higher surface activity. This is likely caused by the suppression of the electrostatic repulsion between polar head groups, allowing surfactants to pack closer together at the interface. An extreme case of this phenomena was recorded by Spildo and Høiland<sup>150</sup>, where the interfacial tension was shown to remain constant even at high pH in an oil/distilled water system, with an acid otherwise shown to exhibit high surface activity at high pH. This effect has been linked to the interfacial pH through the following equation<sup>147, 187</sup>,

$$pH_{int} = pH_{bulk} + \frac{e\psi}{2.3kT} \quad (9)$$

where  $pH_{int}$  is the pH at the interface,  $pH_{bulk}$  is the pH in the bulk phase,  $e$  is the electric charge,  $\psi$  is the interfacial potential,  $k$  is the Boltzmann constant and  $T$  is the temperature. Danielli<sup>188</sup> showed that for acids in oil-water systems the difference between the interfacial pH and the bulk phase pH increased with bulk phase pH and decreased with salinity. The opposite effect was recorded for bases, where the difference was found to decrease with the bulk phase pH<sup>189</sup>. It would be interesting to see if the apparent  $pK_a'$  (i.e. the pH at which 50% of the total compound, protonated or deprotonated, is in each phase) and the interfacial pH for these systems with varying salinity overlap completely.

Rudin and Wasan<sup>190</sup> and Lord, et al.<sup>191</sup> reported that the interfacial tension of oleic and octanoic acids reach a minimum at the pH, where the acids showed equal distribution in both phases. A synergetic effect between the dissociated and undissociated groups was theorized to be the cause. Saeten, et al.<sup>192</sup> demonstrated with fatty acids and amines that acids and bases can react through proton transfer in solution to form ammonium carboxylate complexes, resulting in a 1:1 complex, or 3:1 complexes, with acid excess. The surface properties of these complexes showed increased surface activity<sup>193-195</sup>, compared to their individual components, an effect which is linked to the interfacial interactions between charged head groups. In a study with octanoic acid and octylamine, this effect was found to be greatest in systems with equimolar mixtures<sup>196</sup>.

### 2.4.1.2 Influence of cations

In addition to the ionic strength of the water phase, the ionic composition of the water phase can also affect the interfacial tension, if divalent cations are present in the water phase.

Calcium naphthenates have been a popular topic in the last 20 years<sup>197</sup>, since the first problems of calcium naphthenate deposits were reported in the late 1990's<sup>91, 167</sup>, causing costly production shut downs<sup>198</sup>. Although low molecular weight naphthenic acids were suspected to be the cause of the problem, the perpetrator was found to be a large 4-protic acid named ARN<sup>199</sup>. ARN molecules are aliphatic and have molecular weights around 1230 g/mol<sup>200-202</sup>. An example of this acid is shown in Figure 10. Although the ARN acid is present in ppm concentrations in crude oil<sup>203</sup>, the calcium naphthenate deposits were found to contain 28-41% ARN<sup>204</sup>. The rest likely consists of lower molecular weight acids<sup>205</sup> and solids.

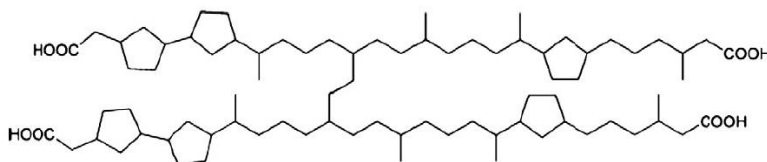


Figure 10: Structure of the most abundant isomer of the tetraacid with six rings, as determined by NMR spectroscopy<sup>201</sup>. Adapted from Ref. 200 with permission from The Royal Society of Chemistry.

The presence of ARN acids is not the only requirement for the formation of calcium naphthenate deposits, as some crude oil with ARN acids do not form deposits<sup>133</sup>. The reason ARN acids are more troublesome than other calcium naphthenates is the phenomena of a crosslinked, glue-like network at the interface between oil and water. While low molecular weight calcium carboxylates go into the bulk oil phase after formation<sup>63, 167</sup>, ARN accumulates at the interface and forms a sticky deposit insoluble in either phase. Our group published a review of the properties and experimental results regarding tetrameric acids in petroleum<sup>73</sup>.

With a term like “naphthenates” it can sometimes be hard to navigate what specifically the author is referring to, much like other generic terms like naphthenic acids or even asphaltenes before a standard terminology was developed. Turner and Smith<sup>206</sup> and Runham and Smith<sup>207</sup> suggested the use of terminology such as calcium naphthenate for phenomena relating to the depositions or the ARN acid, carboxylate soaps (i.e. calcium carboxylate and sodium carboxylate) for problems regarding soap or sludge emulsions and high calcium salt crudes i.e.

crudes with high calcium carboxylate content. This thesis has often used the term oil-soluble calcium naphthenate to describe calcium carboxylates and sodium naphthenates to describe sodium carboxylates.

When sodium or calcium carboxylates are formed, they either stay at the interface or they desorb into the bulk phases. Sodium carboxylates go to the water phase and calcium carboxylates go to the oil phase<sup>63</sup>. Due to their interfacial properties, sodium and calcium carboxylates can impact the emulsion stability.

The impact of sodium carboxylates/naphthenates/soaps on emulsion stability is more common in the industry as these problems can occur with low TAN, light oils<sup>133, 206</sup>. They are often referred to as sludge emulsions due to their high viscosity and can hold a high content of water. For example, one sludge emulsion formed with asphaltene and sodium carboxylate was found to have 85% water cut<sup>208</sup>. Most authors describe the sodium naphthenate emulsions to be formed by lower molecular weight fatty acids (~200–500 g/mol)<sup>179, 209, 210</sup>. The role of bicarbonate in the water phase is also brought up in several papers<sup>167, 179, 198</sup>, and is thought to be strongly correlated to the soap emulsion formation. Sodium naphthenates are also a water quality concern<sup>179, 180</sup> depending on the measurement method<sup>35</sup>. In the OSPAR method, which is used in the North Sea, the polar components like organic acids and phenols in the water are removed by florasil adsorbent before the measurement is taken, thus these species are not included in the result<sup>35</sup>. However, in the US the dissolved oil is included in the oil and grease measurement<sup>211</sup>.

Calcium carboxylates or oil-soluble calcium naphthenates are prone to create stable residual water content in heavier and more acidic crude oils<sup>133</sup>. However, the bigger concern with these compounds is their detrimental catalyst properties for the refineries, where they, as organic salts, can be hard to remove in the desalter<sup>212, 213</sup>. In the less problematic cases, the calcium content in the dry oil can range from 10 - 50 mg/L<sup>207</sup>, whereas in more severe cases the content can be several hundred ppm (85% of which is attributed to organic salts, rest inorganic)<sup>212</sup>. The exact pH required to increase the calcium content is not known. As an example the Dalia 2 crude oil, which ends up with 150 ppm calcium at the surface<sup>63</sup>, is reportedly produced with a pH increase from 6.5 to 7.5<sup>167</sup>, but this value is probably unique for every crude oil-water system based on the phase compositions and production parameters. Allen<sup>214</sup> and Sarac and Civan<sup>215</sup> reported a critical pH ~6 for metal soaps precipitation.

Deposits of calcium naphthenate are present in 10% or more of North Sea crudes, while soap emulsion or sludge occur in 30% of Southeast Asian crudes and 20% of West African crudes <sup>216</sup>. A detailed list of the characteristics for oils which form calcium naphthenate deposits or soap emulsions is listed in Gallup, et al. <sup>179</sup> and several industry case studies are available <sup>91, 112, 133, 179, 206, 209, 217</sup>.

After extensive studies by Havre <sup>218</sup> on the topic of calcium naphthenate formation, it was concluded that due to the low water solubility, calcium most likely does not react with dissociated acids in the water phase, but rather at the interface between oil and water <sup>219</sup>. Here Brandal <sup>219</sup> theorized that calcium formed 1:1 complexes and 1:2 complexes with dissociated acid head groups, where 1:2 complexes were thought to partition into the bulk phase and 1:1 complexes remain at the interface. This 1:1 complex formation is used to explain a permanent reduction in IFT for commercial acid mixture in systems with divalent cations at high pH, compared to a dip and then increase in the dynamic IFT for model acids <sup>162</sup>. Testing different distillation cuts of a crude oil acid mixture, the light cut acids were also seen to have a slow, but permanent reduction in IFT pointing to 1:1 complexes as seen for the commercial acid mixture. The higher cuts presented a dip before it increased again as shown for the model acids, although the increase was smaller for the polydisperse mixtures. This slow decrease and increase in IFT was attributed to surface restructuring and diffusion of 1:2 complexes from the interface. The pH does not necessarily need to be high to observe the effects of calcium, as network formation with large 4-protic acids and calcium are shown at pH 6.2 <sup>200, 220</sup>.

Precipitation of calcium soaps have been studied by several authors <sup>218, 221-223</sup>. Hanneseth, et al. <sup>221</sup> studied the precipitation of calcium naphthenates by optical density measurements in toluene-water systems. They found that the optical density increased more rapidly with acids containing aromatic ring compared to those with saturated rings, as unsaturated structures will penetrate deeper into the interface. If this is caused by the increased hydrophobicity, it could be suggested that acids with saturated rings would also react faster with calcium compared to aliphatic acids. It should be noted that in all these reports of oil-water systems, only single compounds have been studied. Polydisperse system like crude oil acid mixtures might present less or no precipitation.

In systems without oil, Havre <sup>224</sup> showed how a polydisperse crude oil acid mixture, dissolved in alkaline water, quickly formed precipitated calcium naphthenate upon addition of calcium.

Tichelkamp, et al. <sup>178</sup> showed that the ultra-low interfacial tension, achieved in crude oil brine systems with added surfactant, is affected by the calcium/sodium ratio of the brine, where it first dips and increase again with increasing calcium content. High temperature experiments in systems without added surfactants were also performed which showed that the increased calcium ratio increased the IFT. The increased calcium ratio in the brine also changed the dynamic IFT, where for systems with low calcium content, very low initial IFT values were observed in addition to a IFT rise due to partitioning. The low initial IFT and partitioning effects disappear with added calcium.

The water-soluble crude oil components are also a factor in produced water treatments like gas flotation, where they can change the surface tension of gas bubbles <sup>225</sup>, and affect the interactions between oil droplets and gas bubbles <sup>226</sup>. The presence of dissolved naphthenic acids in the water phase were found to decrease the oil removal efficiency for three crude oils, both at pH 6 and pH 10 <sup>227</sup>.

## 2.4.2 Emulsions

### 2.4.2.1 *Definition and general concepts*

An emulsion is a liquid-liquid mixture, where one liquid is dispersed in, and immiscible with, the other liquid. An example of this immiscibility is oil and water, where the polar water is immiscible in the apolar oil phase. Emulsions are present in our everyday life in the form of butter, milk and dressings, although they are also present in pharmaceutical, cosmetic and agricultural sectors <sup>228</sup>. Put simply, there are two classes of emulsions, macroemulsions and microemulsions. Macroemulsions are thermodynamically unstable <sup>229</sup>, whereas microemulsions is the exception from this rule as the entropic contributions takes over <sup>230</sup>. Although microemulsions have some relevance for oil production, for instance in EOR <sup>231</sup>, the following theory will describe regular emulsions, i.e. thermodynamically unstable emulsions. Notwithstanding the thermodynamic instability, emulsions can still have various degrees of kinetic stability, some of which can be beneficial. For example, food emulsions like milk and mayonnaise are less appetizing in their separated form. In other cases, this kinetic stability can be challenging if quick separation of the phases is required in a continuous process. This describes the challenges encountered in crude oil production where problems with mostly



water-in-oil emulsions (W/O) and some oil-in-water emulsions (O/W) can impede the required separation of the two phases (0.5% water-in-oil<sup>180</sup> and 10-1000 ppm of oil-in-water, depending on the water disposal strategy).

To form an emulsion an energy input is required to expand the interfacial area. A visualization of this available surface area energy can be described by the change in behavior for aluminum in bulk and dispersed state, where the stainless metal we use in cars and airplanes becomes highly explosive in its dispersed state<sup>232</sup>. The emulsion formation can be described in terms of the free energy by the following expression<sup>233</sup>,

$$\Delta G_f = \gamma A - T\Delta S_f \quad (10)$$

where  $\Delta G_f$  describes the total free energy of forming an emulsion with interfacial area  $A$ . The term  $T\Delta S_f$  is the entropic contribution which is always positive. A small interfacial tension  $\gamma$  would mean that smaller droplets can be achieved with the same energy input. Lowered interfacial tension is achieved through the presence of a surfactant. The surfactant also has a deciding role in which type of emulsion will be formed based on the Bancroft's rule: the phase in which the surfactant is most soluble, becomes the continuous phase. If the hydrophilic-lipophilic deviation (HLD) value of the surfactant is  $>7$  then a o/w emulsion is formed, while w/o emulsions occurs for values under 7<sup>234</sup>. The interfacial tension also affects the deformability of the droplets as droplets are prone to spherical geometry to minimize their surface area. This can be expressed through the Laplace pressure  $\Delta P$ ,

$$\Delta P = \gamma \left( \frac{1}{r_1} + \frac{1}{r_2} \right) \quad (11)$$

where the radii of curvature for the droplet,  $r_1$  and  $r_2$  are equal for spherical droplets.

In a dispersed system there are five destabilizing phenomena, where the first two, sedimentation and creaming are gravity based. They describe the vertical flow of droplets, before they collect together at the top or bottom. This effect increases as a function the density difference between the droplet and the continuous phase and decreases with the viscosity of the continuous phase according to Stokes's law. Another aspect is the droplet size, to which the final vertical velocity is very much dependent. Bigger droplets will rise or sink faster than smaller droplets. Another destabilizing phenomenon is Ostwald ripening, which describes the diffusion of dispersed phase from smaller droplets to bigger droplets. The driving force is the chemical potential difference between the two droplets, where lower surface to volume ratios

are preferred. Flocculation is the formation of droplet clusters, which is a reversible gathering of droplets in which they still retain their individual spherical geometries. These droplet flocs do however, cause an increase in sedimentation or creaming. The last step in destabilization is coalescence where two droplets collide and merge together, forming a new and bigger droplet or a droplet merge with a bulk fluid interface. The driving forces behind coalescence is the reduction in free energy by a reduction in the total surface area.

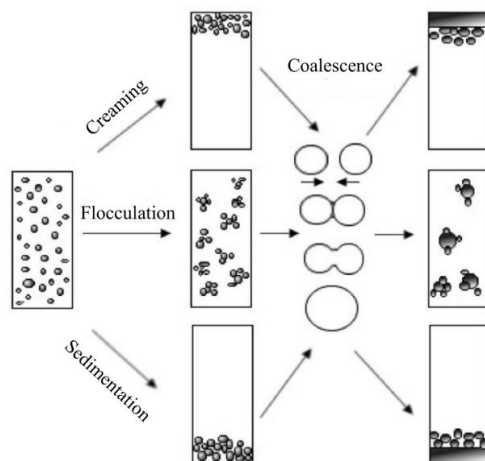


Figure 11: Processes taking place in an emulsion leading to emulsion breakdown and separation. Image reproduced from Aulfem et al. <sup>235</sup>.

As two droplets collide, their interface will stretch, and a flux of solvent will drag surfactants away from the point of impact (film drainage), causing an interfacial tension gradient. This effect is countered with the Gibbs-Marangoni effect, where the surfactants will have an inwards interfacial flow to reduce the thermodynamically unfavorable gradient <sup>236</sup>. In other words adsorbed surface active species at the interface would oppose any deformation of the droplet and provides a self-healing mechanism <sup>237</sup>. This is also described as elastic <sup>237</sup> or non-Newtonian behavior <sup>238</sup> and in general this will increase the emulsion stability <sup>180</sup>. A more rigid adsorbed layer on the interface would also slow down the film drainage and contribute to increased emulsion stability <sup>237</sup>.

Emulsions are stabilized by phenomena which hinder droplet coalescence. These stabilization mechanisms are:

Electrostatic repulsion, where electrically charged double layers of similar charge introduces a repulsive force between the droplets.

Steric stabilization, where large molecules can form a brush like layer on the interface blocking droplets from coming into close proximity of each other. This is explained by an osmotic pressure component counteracting the solvent concentration gradient that is created when sterically stabilized droplets collide.

Particle induced stability, also known as pickering emulsions, is were partially hydrophobic and hydrophilic solid particles, much smaller than the droplet <sup>239</sup>, at the interface form a physical layer keeping droplets apart.

Liquid crystal stability, where a lamellar gel network strengthens the droplet interface.

#### 2.4.2.2 *Case of crude oil emulsions*

The water in crude oil emulsions encountered in the oil industry has been the subject of hundreds of papers <sup>240</sup>. The formation occurs through mixing during production from the reservoir, especially when pressure drops are introduced over chokes and valves <sup>180, 241</sup>, and their stability can force operators to reduce the flow and hence the production <sup>242</sup>. The emulsion stability is controlled by the properties of the interface between oil and water. The presence of multiple components at this interface, asphaltenes, resins, biwettable particles like clay or sand, waxes, corrosion products and production chemicals <sup>243, 244</sup>, serves to illustrate the complexity of this topic. These components can all contribute in complex combinations and through different mechanisms, to change the interfacial tension and viscoelastic properties of the interface, altering the final stability of the system <sup>180</sup>. Hence it is difficult to predict emulsion stability solely based on fluid properties and interfacial components <sup>245</sup>.

The stability of an emulsion can be classified by separation kinetics. A loose crude oil emulsion separates into distinctive phases in minutes, a medium emulsion would require tens of minutes while a tight emulsion takes hours or days to separate out <sup>246</sup>. Water-in-oil emulsions are also known to be more viscous than pure oil and this viscosity can be problematic for pipeline transportation. The crucial factor controlling the viscosity of w/o emulsions is the phase volume ratio, where the viscosity increases with droplet volume fraction until phase inversion or a saturation point occurs <sup>228</sup>. The effect of the water cut and shear rate on the viscosities of w/o

emulsions was shown by Kokal <sup>246</sup>. The viscosities of oil-in-water based emulsions are much lower, both due to the properties of the water phase and the fact that most of the surfactants are oil soluble. This is exploited in the transport of heavy petroleum in pipelines, where an oil-in-water emulsion is formed in order to transport an otherwise very viscous mixture <sup>247</sup>.

The fact that the polar components are the source of emulsions stability is clearly shown in experiments by Sjöblom, et al. <sup>248</sup>, where first the polar components were removed from the crude oil and added to a model oil-water system. Then the emulsion stability of three oil-water systems are compared; original crude oil, crude oil stripped of polar components and model oil with added polar components from the crude oil. The emulsion formed with of the crude oil stripped of polar components is completely unstable and separates immediately, while emulsion stability behavior of the model oil with added polar components from the crude oil mirrors the behavior of the system with the original crude oil.

In these systems asphaltenes are considered to be the dominant factor of emulsion stability <sup>249</sup>, in their ability to form a film or skin on the droplet giving it a protective layer against coalescence <sup>229</sup>. A visualization could be trying to press two balloons together under water. This film was thought to be the more plausible explanation for observed emulsion stability compared to other emulsion stability mechanisms like electrostatic or steric stabilization <sup>250</sup> due to the low dielectric constant of oil and the low thickness of the asphaltene film <sup>251</sup>. The properties of this film are related to the aggregation state of asphaltenes in the bulk phase <sup>249</sup>. Even though asphaltenes are said to be soluble in aromatics, Mullins and Sheu <sup>252</sup> suggest nanoaggregates form at concentrations higher than 100 mg/L in toluene. Resins are also instrumental by how they interact with asphaltenes and the interface. Resins are found to form complexes with asphaltenes or compete with them for a position at the interface <sup>253</sup>.

It is often pointed out that asphaltenes are most surface active in the intermediate region between fully solvated or precipitated <sup>180, 254, 255</sup>. This is clearly shown for emulsion stability (resolved water) <sup>254</sup> and interfacial tension <sup>256</sup> as a function of solvent aromaticity, where a clear dip can be seen. An example of this effect regarding emulsion stability is shown in Figure 12. Although resins are known to solvate asphaltenes <sup>257</sup> the same up and down dip in emulsion stability is not always present when the resin to asphaltene ratio is altered <sup>8</sup>, probably due to resins contributing their own stability to the emulsion. In a review on water-in-oil emulsions, Kilpatrick <sup>240</sup> claims that the multiprotic acids and aromatic acids greatly enhance

the stability of asphaltene emulsions, while monoprotic acids at alkaline conditions greatly destabilize asphaltene emulsions.

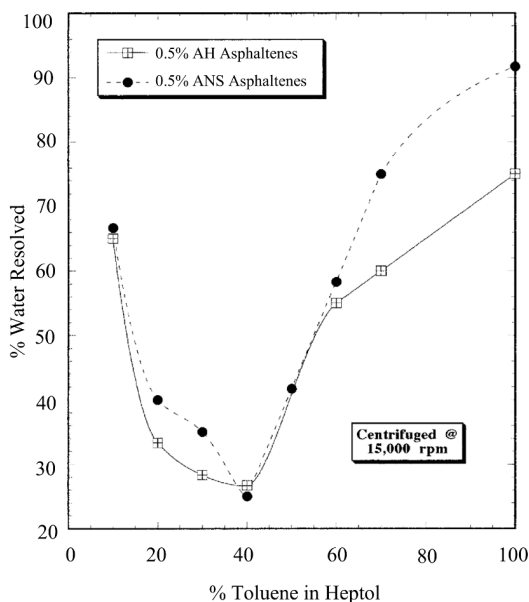


Figure 12: Effect of solvent aromaticity on emulsion stability. Reprinted from *Journal of Colloid and Interface Science*, Vol. 196, Joseph D. McLean, Peter K. Kilpatrick, *Effects of Asphaltene Aggregation in Model Heptane-Toluene Mixtures on Stability of Water-in-Oil Emulsions*, 12., Copyright 1997, with permission from Elsevier<sup>254</sup>

Hemmingsen, et al.<sup>258</sup> demonstrated the solvation effect of asphaltenes by resins, especially naphthenic acids, by showing the difference in precipitation onset upon saturate addition to a crude oil, before and after pH 14 wash (removing much of the resins), showing a clear difference in asphaltene precipitation. A comparison in emulsion stability was also shown for crude oil, deasphalted crude oil, pH 14 washed crude oil and deasphalted and pH 14 washed crude oil<sup>258</sup>. Comparing emulsions between crude oil and deasphalted crude oil, 3 out of 4 crudes were found to form completely unstable emulsions, while the last one remained unchanged in emulsion stability, pointing to another stabilizing mechanism. The pH 14 washed crude oils all showed increased emulsion stability showing the destabilizing effect of naphthenic acids on emulsion stability. However, the most interesting part was the pH 14 washed and deasphalted crude oil, which showed increased or similar emulsion stability with the crude oil. This is most likely caused by the resins left in the crude oil i.e. resins which are not 100% extracted in pH 14 ethanol-water. Without competition from the lower molecular

weight resins or asphaltenes for the interface, these resins, which are probably asphaltene-like, are also able to stabilize emulsions on their own.

In terms of crude oil production, the solubilization state of the asphaltenes will be affected by the depressurization during the production<sup>180</sup>. When the pressure decreases, the relative volume of light saturates will increase, thereby decreasing the asphaltene solubility, inducing their precipitation. After the pressure drops below a certain level (bubble point) these light components will go into the gas phase and the asphaltene solubility is increased in the now less saturated liquid oil phase. Further depressurization might cause a partitioning of the acidic resins to the water phase as an effect of the increase in pH. This would again reduce the asphaltene solubility as fewer asphaltene solvating resins are available.

The asphaltene film properties have been explored by several authors<sup>164, 259-264</sup>. The elastic skin behavior is linked to the crosslinking between asphaltenes which irreversibly adsorb to the interface forming 2D<sup>262</sup> or 3D<sup>265, 266</sup> gel like network structures<sup>249, 267</sup>. The aggregation and interactions between asphaltenes and resins can also be modelled in dissipative particle dynamics to reveal new insights into functional groups or structure<sup>268, 269, 270</sup>.

A visualization of this film can be observed in oil-in-water and water-in-oil droplet experiments, where a sudden reduction in volume makes the irreversibly adsorbed film crumble<sup>271, 272</sup>. The irreversibly adsorbed skins are also visible after droplet coalescence in a picture from Strassner<sup>271</sup>. These effects are shown in Figure 13 and Figure 14. By progressively adding bitumen to heptane, the properties of the film were seen to change from rigid to flexible<sup>273</sup>. This change from mobile to rigid film is also noted by Strassner<sup>271</sup> in an experiment changing the resin asphaltene ratio.

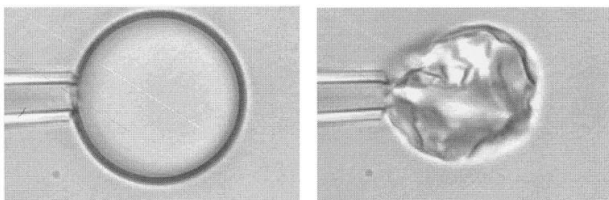


Figure 13: Pictures of skin formation upon retracting a water droplet in diluted bitumen. Reprinted from *Colloids and Surfaces A: Physicochemical and Engineering Aspects*, Vol. 174, A. Yeung, T. Dabros, J. Masliyah, J. Czarnecki, *Micropipette: a new technique in emulsion research*, Copyright 2000, with permission from Elsevier <sup>274</sup>

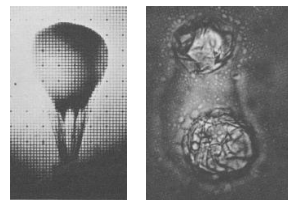


Figure 14: Pictures of skin formation upon retracting a crude oil droplet in water and the presence of these skins after coalescence of two water droplets in a crude oil emulsion. Copyright 1968, Society of Petroleum Engineers Inc. SPE. Reproduced with permission of SPE. Further reproduction prohibited without permission <sup>271</sup>.

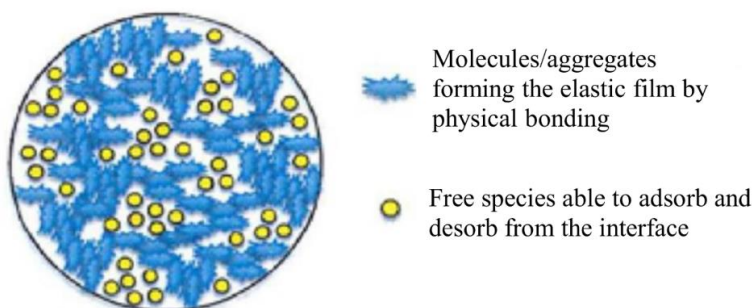
Numerous methods are available for isolation of the interfacial material, stabilizing crude oil emulsions, like extracting interfacial material through D<sub>2</sub>O <sup>275</sup>, washing <sup>134</sup>, wet silica <sup>276</sup> or various liquid-liquid extraction <sup>116, 138</sup>.

By isolating the interfacial material from the two types of films, flexible and rigid mentioned by Czarnecki and Moran <sup>273</sup>, Wu <sup>275</sup> showed that the rigid films had low H/C ratios compared to the flexible films, which contained carboxylic salts in addition to asphaltenes. Resins have been found to dominate the interfacial behavior when their interfacial content reach 40 wt. % <sup>260</sup>. Czarnecki <sup>277</sup> compared the composition of flexible and rigid films with FT-ICR MS and found their functional groups to be quite different from each other and also different from the functional group distributions in the bitumen and its “whole” asphaltene and “whole” resin fraction, compared to the analysis of the bitumen and its asphaltene and resins fraction. Similarities to the interfacial composition study on nine crude oils by Stanford, et al. <sup>175</sup> are also noted, especially regarding high interfacial concentration of molecules with both sulfur and oxygen groups. To make things more complicated, as asphaltenes are a solubility class, they have subfractions, only some of which are irreversible adsorbed <sup>278, 279</sup>.

Czarnecki <sup>277</sup> often stressed that only a small subfraction of asphaltenes are irreversibly adsorbed, and that the current use of SARA fractionation to describe the emulsion stability properties shown by “whole asphaltenes” is too simplistic. The most interfacially active asphaltenes were found to be below 2 wt. % of the whole asphaltenes by Yang, et al. <sup>280</sup>. According to Czarnecki and Moran <sup>273</sup> there are two fractions of crude oil components which

stabilize emulsions. A small subfraction of asphaltenes, which exhibit slow and irreversible adsorption, and low molecular weight surfactant-like material with fast adsorption.

Surface pressure measuring the change in film properties during compression is often linked to the emulsion stability<sup>251, 281, 282</sup>. In crude oil systems, resins alter this interface by being more surface active and making the interface more compressible<sup>260</sup>. A visualization of this interface disruption by resins is shown in Figure 15. Ortiz, et al.<sup>283</sup> showed how the pressure isotherms changed upon compression, where a flat curve was seen with surfactant indicating that the interface was dominated by them, while surface pressure increase is seen for the crude oil system without added surfactant. This was also correlated with the emulsion stability. Interestingly, after deasphalting a West African oil with heptane, thereby leaving the most resin like asphaltenes (pentane insoluble) in the oil, the oil got a mechanical rigid film upon droplet retraction which was not present before<sup>161</sup>.



*Figure 15: Schematic of a water/crude oil interface with interconnected elastic islands and holes filled with unconnected species that are more able to adsorb/desorb from the interface. Reprinted (adapted) with permission from Energy & Fuels, Copyright 2018, American Chemical Society<sup>253</sup>.*

Regarding the kinetics of interfacial adsorption, Ligiero<sup>176</sup> performed successive interfacial material isolations with the wet silica method<sup>276</sup>. They found that the molecular weight and surface elasticity increased for each successive extraction of the isolated material<sup>284, 285</sup>. Gel permeation chromatography inductively coupled plasma high-resolution mass spectrometry (GPC ICP HR MS) also showed a more significant sulfur content in the interfacial material which showed elastic properties, as was also found by Czarnecki<sup>277</sup>.

Partitioning of the surface-active components to the water phase can lead to a change in the film formation properties. This was shown by Moran and Czarnecki<sup>286</sup>, who changed the



composition of the water phase by adding sodium naphthenate. This addition of surfactant to the water phase changed the interfacial properties and the rigid film disappeared. These smaller and highly surface-active compounds likely diffuse fast from the less viscous water phase to the interface, compared to their larger counterparts in the oil. Washing crude oil or bitumen repeatedly with a fresh water phase, has been shown to either reduce<sup>177, 287</sup> or increase<sup>176, 288</sup> the emulsion stability. A remarkable finding was noted by Flesisnki<sup>161</sup>. A water phase which had been in contact with a West African oil crude oil, was put in contact with cyclohexane and showed viscoelastic interfacial properties, similar to the ones exhibited by the original crude oil and water<sup>161, 253</sup>. Interestingly, the water from the West African oil made more gel-like interface with the new oil phase than the already water-contacted West African oil with a new water phase<sup>161</sup>. A similar effect has been noted with a low TAN crude oil by Alvarado, et al.<sup>177</sup>, who found that emulsions with partitioned water and new crude oil were much more stable than emulsions with the three other combinations. Ligiero<sup>176</sup> noted a destabilizing influence on the interfacial rheology from the water phases with water-soluble crude oil species and concentrating these species increased this effect<sup>265</sup>. Hemmingsen, et al.<sup>76</sup> did successive water/ethanol pH washes on a crude oil and noted an emulsion stability increase after the pH 7 wash, no stability gain after the pH 10 wash and another stability increase after the pH 14 wash. In a study with a West African acidic oil and its heavy distillate fraction, both diluted in cyclohexane, a 2D gel-like interface was formed at pH 6.5<sup>289</sup>. At pH 8, naphthenates were found not to impede, but rather delay the 2D gel formation, in addition to reducing its strength. The slow interfacial restructuring and crosslinking behavior dynamics between large species at the interface, highlights the importance of aging on the measurement of interfacial film properties which is brought up by several authors<sup>176, 253, 265, 289</sup>.

Although increases in pH is often found to destabilize emulsions through increased resin activity<sup>8, 290, 291</sup>, in some cases the resins are found to be the main components stabilizing the emulsions. Strassner<sup>271</sup> showed increased emulsion stability at acidic or alkaline pH and Goldszal, et al.<sup>292</sup> recorded a massive increase in emulsion stability even at pH values as low as 6.6 for an acidic crude oil. Jones, et al.<sup>164</sup> showed the viscoelastic film stability to have an inverse bell function when it comes to pH, where the film has the highest viscoelasticity at intermediate pH and decreasing viscoelasticity at high or low pH. This was also found to match the stability of the formed emulsions. Complexes of fatty acids and fatty amines have been

observed to decrease the stability of emulsions<sup>192</sup>, although the author is not aware of research on this effect between the acids and pyridine derivatives in crude oil.

The emulsion stability of acidic oils is covered by the work of Hurtevent, et al.<sup>63</sup>. This stability is often linked to the formation of calcium or sodium naphthenates<sup>133, 155, 206, 207</sup>. However, crude oils with low TAN values have also been shown to form strong sodium naphthenate emulsions, shown to be mainly made up of fatty acids<sup>208, 210</sup>. Crude oil acids can also create a liquid crystal phase<sup>293</sup> or lamellar lyotropic liquid crystalline D-phase that can be important for W/O stabilization in acidic crude oils<sup>18, 294</sup> by forming a multilayer at the oil-water interface<sup>180</sup>. Havre and Sjöblom<sup>294</sup> prepared this liquid crystal phase with C<sub>16</sub> acids and showed how the addition of either commercial naphthenic acid mixture from Fluka or asphaltenes could increase and then decrease the w/o emulsion stability of the system. The degree of dissociation of naphthenic acids was also successfully correlated to the emulsion stability for an acidic oil in the work done by Hurtevent, et al.<sup>63</sup>, showing that the naphthenic acids were the main stabilizing compound in this crude oil. The emulsion type has also been recorded to change with the pH where o/w emulsions are commonly formed at high pH<sup>70, 81, 271, 290, 291</sup>.

The salinity of the water phase has been recorded to decrease the stability of crude oil emulsions<sup>255, 295, 296</sup>. Other cases show that salinity increases the emulsion stability<sup>297, 298</sup>. Maaref and Ayatollahi<sup>299</sup> reported that increased salinity increased the size of droplets formed, leading to lower emulsion stability. Opposite effect i.e. droplet size reductions have been reported for bitumen-in-water emulsions<sup>300</sup>. Divalent cations have also been found to decrease the emulsion stability<sup>63, 292</sup>. As salinity affects the dissociation ratio at the interface, this factor was found to be crucial in the naphthenate stabilized oils<sup>63</sup>. Hurtevent, et al.<sup>63</sup> showed that divalent calcium decreased the emulsions stability for two acidic oil while increasing the stability of another oil by forming a structured mesophase with viscoelastic properties. Calcium has been shown to change the interfacial film properties and prevent dissolution of the film to the bulk phase for a commercial acid mixture at pH values as low as 5.6<sup>301</sup>.

Demulsifiers are often used to destabilize the crude oil-water emulsions. Different demulsifiers are used for different crude oils depending on the main stabilizing components. These molecules are often large polymers with added functional groups, which alter their hydrophobic lipophilic balance. The optimal structure of these molecules also depends on the system parameters (salinity, pH, temperature) at the point where they are added. The drastic change in

effectiveness of one demulsifier with temperature is shown by Peña, et al.<sup>302</sup>. The concentration of a demulsifier is also paramount as overdosing can also stabilize the emulsion. This is shown in Goldszal, et al.<sup>292</sup>, where an increase in demulsifier concentration from 100 ppm to 200 ppm reduced the resolved water from 90% to 20%. Crude oil samples obtained by research laboratories often include production chemicals like demulsifiers<sup>176</sup>, which can cause uncertainties as to how much they affect the observed results. However, if their size and structure differs from the continuous size and structure spectrum of the crude oil<sup>15</sup>, their presence or absence can be identified. This was demonstrated in the study of interfacial material of a heavy crude oil by Lalli, et al.<sup>303</sup>.

Emulsions with water as the continuous phase have different properties compared to water-in-oil emulsions. As mentioned, they are often much less viscous. In addition, the high dielectric constant of water causes uneven interfacial charge distributions, which is the mechanism behind electrostatically stabilized emulsions. The electrostatic repulsion decreases with ionic strength, where a reduction in the zeta potential can be observed<sup>182,304</sup>. By using brine instead of pure water, Ese and Kilpatrick<sup>70</sup> showed that previously electrostatically stabilized emulsions immediately separated. The same effect is shown for an asphaltene stabilized model oil-in-water emulsions<sup>305</sup>, where the low salinity sample is opaque and the higher salinity sample is clear. Divalent cations also cause a higher reduction in the zeta potential as shown by other authors<sup>186,304</sup>. In addition to implications regarding the electrostatic repulsion of oil droplets in water, the ionic strength also screens the polar head group charge, allowing more surfactants to pack closer together at the surface, increasing the interfacial viscosity<sup>300</sup>. Acevedo, et al.<sup>300</sup> found that low salinity bitumen-in-water emulsions are electrostatically stabilized, while high salinity emulsions are stabilized by short range interaction forces. Other sources mention the presence of rigid chains on bitumen surfaces<sup>306</sup>. Laroche, et al.<sup>306</sup> showed these chains to increase in outwards direction from the bitumen droplet with asphaltene concentration and decrease with pH. This was attributed to a higher presence of smaller carboxylic acids at higher pH. Salou, et al.<sup>307</sup> found the resin to asphaltene ratio to be important in predicting bitumen-in-water stability. The emulsion stability was found to increase with R/A ratio and a shift in behavior was suggested around a R/A ratio of 2 to 3 in acidic water systems. Schorling, et al.<sup>308</sup> however found the emulsion stability to decrease with increased R/A ratio when using neutral water.

The reader is again reminded that most of the aforementioned findings were performed at ambient temperature and pressure settings. As crude oil production occurs at higher temperature and pressure levels, properties like solubility, viscosity, saturate/aromatic nature of oil phase will give different system characteristics. While thermal treatment is often used to destabilize emulsions, increased temperature was found to give extremely stable emulsions in the systems with a lamellar lyotropic liquid crystalline D-phase<sup>309</sup>. Temperature also increased the severity of naphthenate emulsions as the water phase solubility increases<sup>206</sup>. Decreased emulsion stabilities have also been recorded in high pressure systems, where gas bubble formation were theorized to rupture interfacial films or facilitate film drainage between droplets<sup>18</sup>. Studies also show that the emulsion stability is lower in “live” crude oils compared to “dead” or degassed crude oils which is recombined with a similar gas phase<sup>235</sup>.

## 2.5 Theory summary

By now it should be evident that naphthenic acids play an important role in crude oil production, both by influencing the oil-continuous and the water-continuous emulsions. It has been shown that even at normal operational pH levels their ability to influence the production can be remarkable, especially in systems with divalent cations. Their ability to partition into the water phase has also been recorded to influence the interfacial properties and the following emulsion stability. In order to gain better predictive models of system behavior, for example regarding the comingling of well-streams, the extent of partitioning and the impact of divalent cations on this partitioning behavior warrants further quantitative and qualitative insights, which is the aim of this thesis.

## 3 Experimental techniques

### 3.1 Ultraviolet and visible (UV-Vis) spectroscopy

Spectroscopy describes the interaction between matter and electromagnetic radiation. Light have different interactions with molecules depending on its location on the electromagnetic spectrum. Ultraviolet and visible, infrared, microwave and radiofrequency light cause respectively electron transitions, molecular vibrations, molecular rotations or align nuclei spin. Ultraviolet-visible spectroscopy ranges from 190 to 800 nm and can be used to transfer electrons to a higher energy orbital. This absorption energy is characteristic for a given molecular structure and by irradiating a sample with different energies from different wavelengths, an absorption spectrum for that sample can be measured. This absorption spectrum can then be used for quantitative and qualitative analysis. The electron transition or excitation involves moving an electron from a non-bonding (n) or bonding orbital ( $\sigma$  or  $\pi$ ) to an anti-bonding orbital ( $\sigma^*$  or  $\pi^*$ ). A non-bonding orbital is a lone pair of electrons found in elements to the right in the periodic table. Transitions from n to anti-bonding orbital,  $\sigma^*$ , and  $\sigma$  orbitals to anti-bonding orbitals,  $\sigma^*$  or  $\pi^*$  require higher energy (or shorter wavelengths) than what the UV-Vis spectrum can offer. Excitations from non-bonding n orbital or bonding  $\pi$  orbital to anti-bonding  $\pi^*$  orbital are the excitations that can be measured with UV-Vis spectroscopy. Saturated hydrocarbons are known to have negligible absorption in the UV-Vis portion of the spectrum<sup>310</sup>. Molecular structures like conjugated dienes can form a conjugated structure with their  $\pi$  orbitals giving the electrons a higher degree of delocalization. With a higher degree of delocalization comes lower energy required for the electron transition. In aromatics the  $\pi$ - electrons are delocalized and the higher the number of conjugated aromatic rings the bigger the delocalization. With a high enough degree of delocalization, the energy becomes low enough to absorb wavelengths in the visible light spectrum. This would then give the solution a color and is the reason these compounds are referred to as chromophores, which translates to color givers. For example, benzene needs a shorter (higher energy) wavelength and is colorless while polyaromatic core molecules like asphaltenes gives the solution a brown color.

By using a tungsten/halogen and deuterium lamp and controlling the wavelength output with a monochromator, the radiation required for the UV-Vis spectrum is achieved. The solute is then dissolved in a solvent and placed in a cuvette. Another cuvette filled with pure solvent is then

placed next to the cuvette with solute in the UV-Vis spectrophotometer to serve as a reference by showing how much absorption is caused by the solvent. Some solvents like aromatics can be unsuitable below a certain wavelength. The measured absorbance can be linked to the concentration through Beer–Lambert law:

$$A = \epsilon lc \quad (12)$$

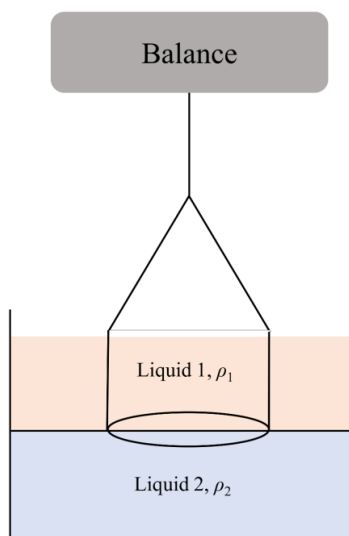
where  $A$  is the absorbance,  $\epsilon$  is the extinction coefficient,  $l$  is the optical path length and  $c$  is the concentration. Beer–Lambert law is a quantitative method for determining the concentrations of absorbing species. By measuring the absorbance of known solutions with known concentration of absorbing species, a calibration curve can be developed by linear regression of the absorbance at a specific wavelength. This linear equation gives a basis for determining the concentration of absorbing species in an unknown sample. This technique can for example be used to identify molecular compositions of reservoirs and predict the asphaltene correlated problems even before a physical sample is brought back to the laboratory. The correlation, however, is only valid for dilute solutions, as a non-linear response will occur at higher absorption.

### 3.2 Surface tension (ST) and interfacial tension (IFT) measurements with the Du Noüy ring

The Du Noüy ring is a technique which allows the measurement of surface tension between a liquid and air, and interfacial tension between two liquids. The working principle, also shared with another technique called the Wilhelmy plate method, is based on the capillary force on a platinum ring, where the maximum force, as the ring is pulled upwards, is related to the surface or interfacial tension. A schematic of the configuration is drawn in Figure 16. A flat beaker with one or two liquids is placed on a platform capable of vertical movement. The ring is suspended from a microbalance which measures the force maximum ( $Mg$ ) as the ring passes through the surface or interface as a function of time. The interfacial tension can be found through the radius of the ring ( $R$ ) and a correction factor  $f$ <sup>311, 312</sup>.

$$\gamma = \frac{Mg}{4\pi R} \cdot f \quad (13)$$

The advantages of this technique are its simplicity, where no prior calibration with other fluids is required, and the advantage of calculating surface tension from direct force measurements rather than indirect calculation. Due to the measurement time it is unsuited for dynamic interfacial tension measurements. Another critique is that measuring the interfacial tension on an expanding surface in non-equilibrium as the ring pulls upwards does not give a good representation of the equilibrium interfacial tension of the system, especially for systems with notoriously slow equilibrating surfactants like asphaltenes.



*Figure 16: Interfacial tension measurement technique Du Noüy Ring.*

### 3.3 Gas chromatography and mass spectrometry (GC/MS)

Gas chromatography coupled with a mass spectrometry detector is a commonly used analytical instrument. Gas chromatography refers to a separation process, where gas phase molecules of a sample are separated through a column based on their size, structure or properties. The separated compounds allow for individual detection and analysis as different molecules consecutively exit the column. Mass spectrometry is a powerful detection technique, which allows for quantitative and qualitative analysis of the molecules in a sample. A general description of the process is that molecules are ionized by an ionization source, their trajectory is altered with electrical fields and when they impact the detector, qualitative and quantitative data about registered mass to charge ( $m/z$ ) ratios at that time can be acquired.

Figure 17 depicts the process of a GC/MS. Sample is injected to a heated inlet for vaporization. Then the sample is carried by an inert gas into the column of the gas chromatograph. The column typically holds a low temperature initially before the temperature is gradually increased while a constant flow of inert gas passes through the column. As different molecules exit the column over time, they are ionized by an ionization source. Depending on the choice of ionization source (hard or soft), the degree of molecular fragmentation can be extensive or mild. One type of ionization source known for making extensive fragmentation is the electron ionization or EI, which bombards the molecules with electrons in order to ionize them. As the resulting ions are charged, their trajectory can be manipulated in the mass analyzer. A common mass analyzer is the quadrupole analyzer, in which the electrical field between two and two diagonally placed rods is varied over time<sup>313</sup>. This alters the trajectory of ions with different mass to charge ratio, allowing mass scanning as only certain ions are given a stable path through the analyzer to reach the detector at a given time. The detector correlates the signal received with the scan settings at the time of impact. As different compounds elute from the column, this scan allows their mass spectra to be captured, displaying the different intensities of the mass to charge ions registered. Soft ionization usually produces molecular ions in which case identification is rudimentary. Molecules excessively fragmented through hard ionization can also be identified through comparison of their characteristic fragmentation with fragmentation libraries.

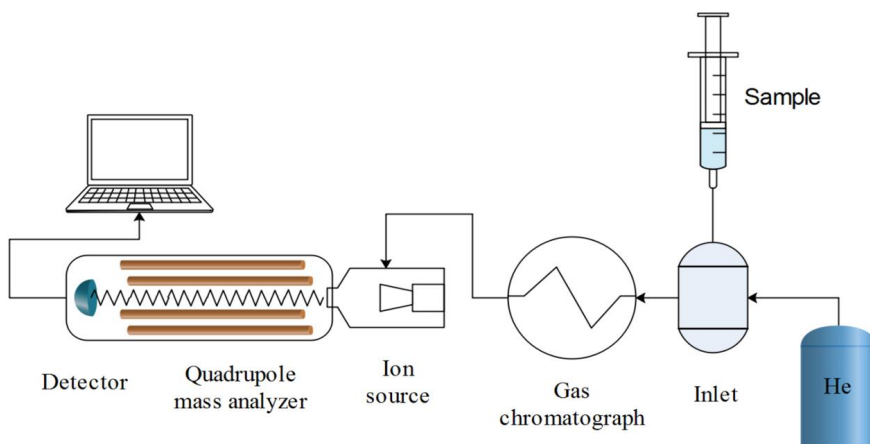


Figure 17: Illustration of a gas chromatograph coupled to a mass spectrometer detector



### 3.4 Microfluidics

Microfluidics refers to a technique where the flow behavior and properties of fluids are analyzed in small, micrometer scale channels. In these channels different fluids can be processed, mixed or separated, by using pumps and channel junctions. Fluid phenomena occurring over very short time scales, which is often the case in industrial applications, can be captured and analyzed with high speed imaging or other optical methods. There are many advantages to microfluidics, like quick measurement times and high repeatability. The small channels also limit the amount of sample and chemicals needed for experiments, in addition to reducing the waste. One subcategory is called droplet-based microfluidics. Droplets of one fluid are dispersed in another continuous fluid phase, where the two fluids are immiscible. Different channel geometries are used to generate droplets, like cross-flow, flow focusing and co-flow<sup>314</sup>. All these geometries produce monodisperse droplets through various regimes (e.g. dripping, squeezing or jetting), where the flow rate is the main parameter to control the droplet size and generation rate. Another advantage of microfluidics is the quickly reached equilibrium states during heat and mass transfer<sup>315</sup>, especially regarding the interfacial properties. One disadvantage is the limited channel height, which can lead to squeezed droplets between the top and bottom part of the channel. This limitation can cause deviations between studied systems compared to real unconstrained systems, however the trends observed in microfluidics should remain similar.

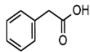
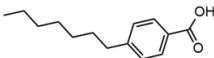
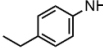
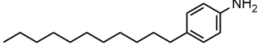
## 4 Main results

### 4.1 Paper I

*Equilibrium partitioning of naphthenic acids and bases and their consequences on interfacial properties*

The first paper starts with a literature review covering phenomena related to acid and base partitioning, interfacial tension, oil phase acid-base interactions and the influence of divalent cations. Secondly, the study of oil-water partitioning of crude oil components was initiated by considering model acids and bases. Two acids with different molecular weight were used: phenylacetic acid (PAA) and 4-heptylbenzoic acid (4HBA) with lower and higher molecular weight, respectively. Likewise, two derivatives of anilines differing by their molecular weight were analyzed: 4-ethylaniline (4EA) and 4-decylaniline (4DA), where 4DA had a higher molecular weight. Table 1 presents the structure of these model acids and bases. Instead of pyridines, anilines were chosen as the bases due to the lack of commercial availability for long alkyl pyridines. As mentioned in the introduction, the bases present in crude oils are predominantly pyridine derivatives. Previous literature involving crude oil bases have often used amines, which are much more basic compared to pyridines as evidenced by the  $pK_a$  values of their respective conjugate acids,  $\sim 10$  for amines and  $\sim 5.2$  for pyridines. Anilines with their conjugate acid  $pK_a$  of 4.6 were believed to be more suitable to represent pyridines in this regard.

*Table 1: Model acids and bases used to investigate oil-water partitioning and interfacial properties. Obtained  $pK_a$  and  $P_{wo}$  values are also shown.*

Name	Molecular mass (g/mol)	Chemical structure	$pK_a$	$P_{wo}$
Phenylacetic acid (PAA)	136		3.2	7.8
4-heptyl benzoic acid (4HBA)	220		4.6	$3.7 \times 10^{-4}$
4-ethylaniline (4EA)	121		5.1	$9.85 \times 10^{-2}$
4-decylaniline (4DA)	233		-	$7.8 \times 10^{-4}$

The equilibrium partitioning of these acids and bases were studied separately as a function of pH using heptane as the oil phase and 3.5 wt % NaCl as the aqueous phase. Through mass balances, partition ratios and dissociation constants, expressions for the oil and water concentrations of acids and bases were derived to model the partitioning with pH. These expressions are the following:

$$[HA]_{w,tot} = \frac{[HA]_{o,init}}{\frac{[H^+]}{P_{wo,acid}(K_{a,HA} + [H^+])} + \frac{V_w}{V_o}} \quad (S1) \quad [B]_{w,tot} = \frac{[B]_{o,init}}{\frac{[K_{a,HB^+}]}{P_{wo,base}(K_{a,HB^+} + [H^+])} + \frac{V_w}{V_o}} \quad (S2)$$

where  $[HA]_{o,init}$  and  $[B]_{o,init}$  represent the initial concentration of acid and base in the oil phase, and  $[HA]_{w,tot}$  and  $[B]_{w,tot}$  represent the sum of dissociated and undissociated acid and base in the water phase. The terms  $V_o$  and  $V_w$  denote the volume of the oil and water phases. The partition ratios  $P_{wo}$  represent the amount of nonionized compound in each phase:

$$P_{wo} = \frac{[HA]_w}{[HA]_{o,tot}} \quad (S3) \quad P_{wo} = \frac{[B]_w}{[B]_o} \quad (S4)$$

where  $[HA]_w$  and  $[B]_w$  represent the acid and base concentration in the water phase,  $[HA]_{o,tot}$  and  $[B]_o$  represent the acid and base concentration in the oil phase.  $[HA]_{o,tot}$  is used to include dimers in the oil phase. The dissociation constants,  $K_a$ , control the degree of dissociation in the water phase:

$$K_{a,HA} = \frac{[A^-]_w[H^+]}{[HA]_w} \quad (S5) \quad K_{a,HB^+} = \frac{[H^+][B]_w}{[HB^+]_w} \quad (S6)$$

where  $[A^-]_w$  and  $[HB^+]_w$  are the conjugate base and acid for of their respective acid and base in the water phase. A schematic of the occurring processes is depicted in Figure 18.

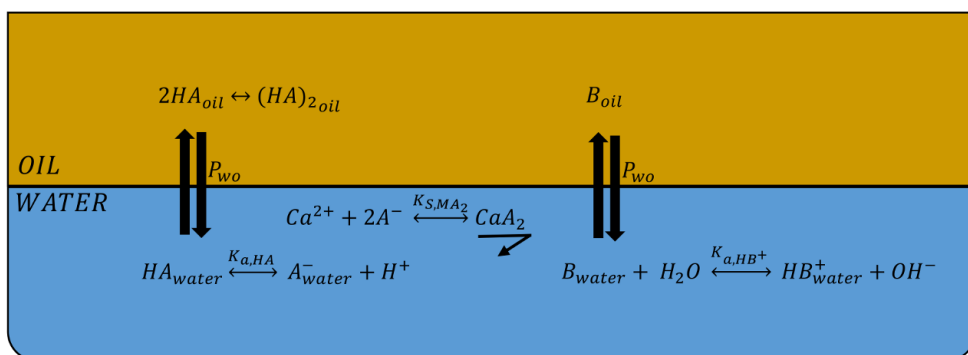


Figure 18: Schematic illustration of the acid and base equilibria that occurs in oil-water systems. Depicted are dimerization of acids in oil phase, partitioning of acid between oil and water phase, dissociation of acid in water phase, calcium naphthenate precipitation in the water phase, partitioning of the base between the oil and water phase and protonation of the base in the water phase.

The equilibrium partitioning between heptane and 3.5 wt. % NaCl water was mapped over the pH range and fitted to the partitioning equations. The small model acid, phenyl acetic acid, had a high affinity for the water phase, even at low pH values, giving a  $P_{wo}$  of 7.8. A small change in partitioning from around 90% to 100% acids in water gave, through fitting with the partitioning equations, a  $pK_a$  of 3.2, deemed to be inaccurate. The larger acid, 4-heptyl benzoic acid, had an initial affinity for the oil phase before a complete phase shift occurred around pH 8. The partitioning of the high molecular weight acid and the low molecular weight base is depicted in Figure 19. High volume, low pH experiments suggest a  $P_{wo}$  of  $3.7 \times 10^{-4}$ . Equations could be fitted to the partitioning with a  $pK_a$  of 4.6. A phase shift at pH 8.03 calculated from the distribution ratio equations corresponded well with the observed data. The consistent mass balance suggests that no sodium naphthenate partitions into the oil phase or precipitate.

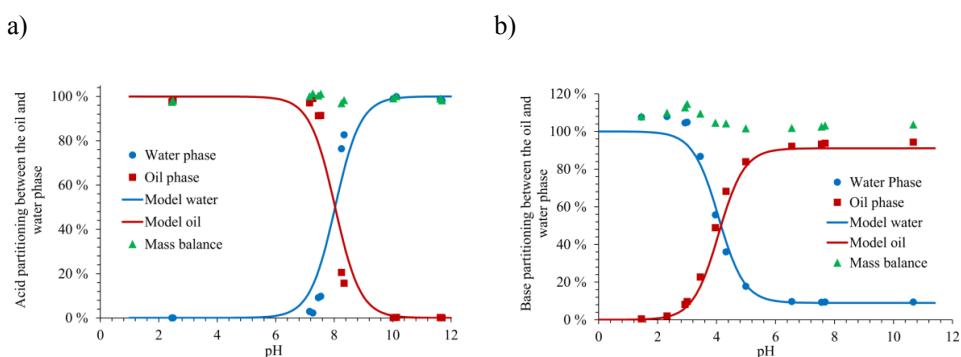


Figure 19: Equilibrium partitioning of a) high molecular weight acid, 4-heptylbenzoic acid (4HBA), b) low molecular weight base 4-ethylaniline(4EA), in a heptane and aqueous phase (3.5 wt. % NaCl) over a range of equilibrium pH values.

The small base, 4-ethylaniline, was solely water-soluble at low pH values. Around pH 4, there is a phase shift where 90% of the base goes into the oil phase while 10% of it stays in the water phase through pH 11. High pH measurements gave a  $P_{wo}$  of  $9.9 \times 10^{-2}$  and the equations fitted to the partitioning with a  $pK_a$  of 5.1. The distribution ratio equations suggested a phase shift at pH 4.15, corresponding well to the observed data. The large base, 4DA, showed little or no affinity for the water phase. High volume experiments with high and low pH had comparable base concentrations in the water phase, slightly higher for the low pH experiment, as would be expected. The  $P_{wo}$  was calculated to  $7.8 \times 10^{-4}$  while the  $pK_a$  could not be attained through the partitioning equations due to the low water solubility. It can be noted that acids are far more

water-soluble compared to bases of similar molecular weight. All the values of  $pK_a$  and  $P_{wo}$  are summarized in Table 1.

As the water phase in the crude oil production often contains various concentrations of divalent cations, the effect of calcium on the partitioning was analyzed. The partitioning of the larger acid, 4HBA, in the presence of the divalent cation calcium is shown in Figure 20. As can be observed, the mass balance for 4-heptyl benzoic acid did not add up to 100% for pH values higher than 6.8. This was caused by the visible precipitation of calcium naphthenate. Equations with precipitation were derived to fit the observed data by introducing a solubility constant of calcium 4-heptyl benzoate,  $K_s$ . The  $K_s$  was calculated by two different equations to be between  $1.5 \cdot 10^{-10}$  and  $2 \cdot 10^{-10}$ . For the small acid, the partitioning was unaffected by the presence of calcium.

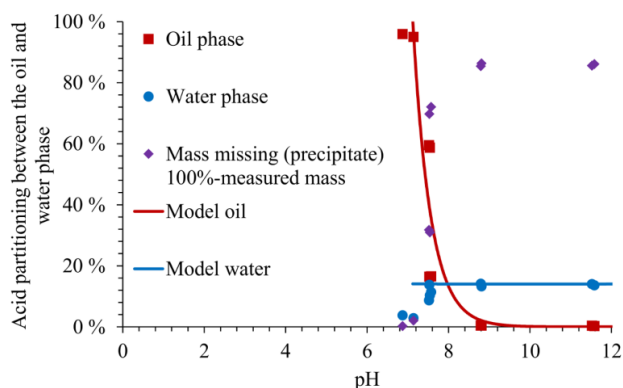


Figure 20: Partitioning of high molecular weight acid 4-heptylbenzoic acid, in heptane and aqueous phase over equilibrium pH (3.5 wt. % NaCl and 10mM CaCl<sub>2</sub>).

This paper also studied the influence of the acids and bases on the interfacial tension. Previous studies had suggested interfacial effects of acid and base complexes, where the surface activity of the mixtures was greater than that of the acids and bases alone, due to oppositely charged head group interactions<sup>193-196</sup>. To study this phenomena with our model acids and bases, interfacial tension measurements of systems with single components and mixtures were performed for the pH range 2-10. Equilibrium was arbitrarily set to the value after 6 hours of equilibration. Figure 21 shows the equilibrium interfacial tension of single acids and bases in heptane and water for different pH values. The first observation to notice is the effect of the hydrophobic tail on surface activity: neither the short chain base and the short chain acid

present any surface activity at any pH value. At low pH, i.e. when protonated, the large base, 4-decylaniline, showed surface active tendencies. In a separate experiment the interfacial tension was measured as low as 6 mN/m at pH 0.5. As the pH increases, the larger acid, 4-heptyl benzoic acid, starts to show interfacial activity, with a gradual decline from pH 2 to 6, before a marked decrease before and after the phase transfer at pH 8. There is also an interesting partitioning effect where the dynamic nature of the interfacial tension with continuous adsorption/desorption on the interface is observed over time for the larger acid. At higher pH values, the interfacial tension is initially very low (4-5 mN/m) before it gradually increases to 10 mN/m as the acid completes its partitioning over the interface. Figure 22 depicts the interfacial tension measurements for the systems with mixtures of acids and bases. Here it can be seen that the bases control the interfacial tension at low pH, while the acids are the main contributor at higher pH values. The almost identical values of interfacial tension between the mixture of acids and bases on one hand and only acids or only bases on the other hand, indicate an absence of surface active acid-base complexes. Most of the previous studies concerning interactions between acids and bases at the oil-water interface have used amines as model base. As the conjugate acids of amines have a much higher  $pK_a$  value compared to the conjugate acids of anilines, there is a pH window where both species could be dissociated at the interface at the same time. However, as most crude oil bases are pyridine homologues, the use of aniline as a model base is thought to be more representative for crude oil base behavior.

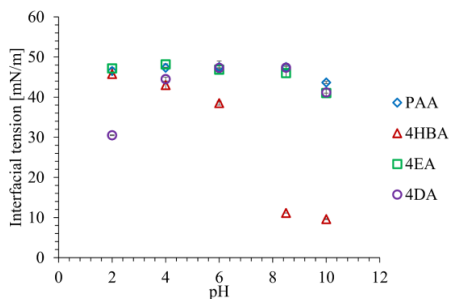


Figure 21: Interfacial tension of single components between heptane and aqueous buffers (3.5 wt. % NaCl).

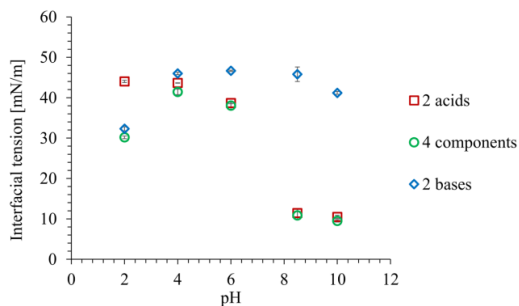
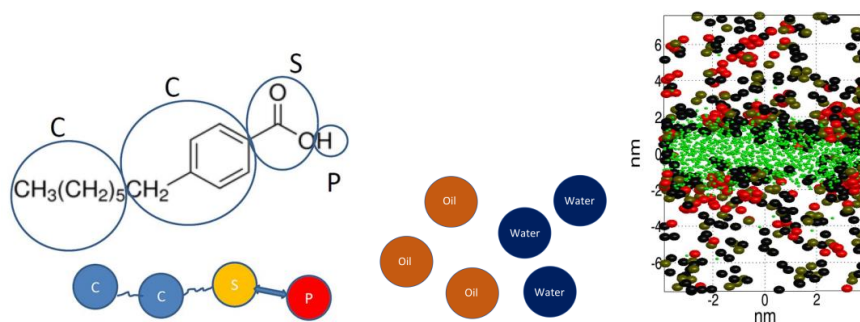


Figure 22: Interfacial tension between heptane and aqueous buffers (3.5 wt. % NaCl) where the oil phase initially contained 2 acids, 2 bases or all 4 components.

## 4.2 Paper II

### *Development of electrochemical DPD molecular simulations for oil/water partitioning of organic acids at varying pH*

The aim of this paper was to introduce acid partitioning in oil-water systems to dissipative particle dynamics (DPD) simulations. Dissipative particle dynamics have previously been used to study asphaltene aggregate formation and their interfacial behavior in oil/water systems<sup>268-270</sup>. Incorporating recently developed DPD methods for acid dissociation into an oil/water system, allows the study of acid partitioning mechanisms, involving dissociation at the oil/water interface followed by hydration of the dissociated acid. The results obtained for the model acid, 4-heptylbenzoic acid, in the heptane/3.5 wt. % NaCl water system from paper I, were used to calibrate the parameters used in the DPD simulation. The DPD system uses beads or particles to represent solvents and solutes as shown in Figure 23, and their behavior is controlled by the interaction parameters attributed to each bead type. Note that the solute molecule beads have two different types of bonds to allow dissociation of the proton bead.



*Figure 23: Visualization of the beads or particles used to model the 4-heptylbenzoic acid from paper I, the two solvents used in DPD simulations, and the simulation system.*

The proton dissociation is governed by the Morse potential energies between the proton bead and the three beads; oxygen group bead (S), water bead (W) and hydroxyl bead (W<sup>-</sup>). When dissociation occurs, the interaction between the oxygen bead and water beads is increased which facilitates the hydration of the dissociated molecule. In total there are three forces acting on the system: DPD forces replicating van der Waals forces for neutral beads, additional DPD forces for ionized beads and Morse forces to control the dissociation.

Computational restrictions on the number of beads in the system, visualized in Figure 23, limited the simulation pH window to high and low pH ranges, as just one hydroxyl bead  $W^-$  in the system corresponds to a pH of 11.47. To accommodate for this, the obtained results from the simulation system are recalibrated through a volume dilution of  $45^3$  times the original volume, with fixed concentration ratios between ions and organic acid, namely  $[H^+]/[HA_{tot}]$  for low pH and  $[OH^-]/[HA_{tot}]$  for high pH.

Appropriate force parameters allow comparable values to experimental values to be obtained through simulation, shown in Figure 24. As seen, the acid bead structures are predominantly in the oil phase at low pH, before they progressively dissociate and get hydrated as the pH increases.

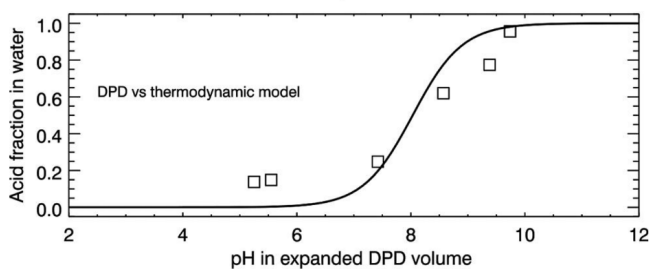


Figure 24: Results obtained from DPD simulation compared to the thermodynamic partitioning curve.

Preliminary analysis of the interface at high and low pH values also show some structural implications for the interface, although more work is needed to draw conclusive results from the interface as the current system is designed for partitioning. The main result from this work is the door opening DPD simulation method, incorporating partition equilibria and dissociation, which can allow for further research into transport mechanisms between lipophilic and hydrophilic media. This is not just limited to petroleum chemistry, but can also have numerous applications in biomedical research<sup>152</sup>.



### 4.3 Paper III

#### *Equilibrium partitioning of naphthenic acid mixture part I: Commercial naphthenic acid mixture*

Naphthenic acids in crude oil are a polydisperse mixture with thousands of different sizes and structures. Consequently, it was decided to extend the studies performed in papers I & II, involving model acids to a commercial mixture of naphthenic acids from Fluka. First, a new GC/MS method was developed to analyze the composition of the acid mixture, which afterwards was used to study the partitioning of these acids between oil and water as a function of pH. In the summaries of paper III and IV, all the masses correspond to the molecular weight of the acids before derivatization, except otherwise stated as “m/z”.

Naphthenic acids were analyzed by GC/MS after derivatization with MTBSTFA, a derivatization agent reputed to limit fragmentation during electron impact ionization in the MS analysis. To validate the efficiency of this derivatization agent, the fragmentation patterns of 17 organic acids with different sizes and structures were analyzed. The results validated the assumption of a dominant stable quasi-molecular mass fragment peak. Aliphatic acids produced the least fragmentation, followed by aromatic acids and alicyclic acids. The importance of molecular weight could be observed, where the other fragments produced by low molecular weight acids were too low in mass to register as a naphthenic acid (lower than 159 m/z). Larger acids however, could produce other fragments which could falsely register as a lower molecular weight naphthenic acid. Especially encouraging were the results obtained with dicarboxylic acids, where the intensity of double-charged mass fragments was small compared to the single-charged mass fragment.

The commercial naphthenic acid mixture from Fluka was analyzed after derivatization by GC/MS. The obtained chromatogram presented an unresolved hump with two different modes and several well-defined peaks consistent with saturated fatty acids. A close look analysis of the mass spectra revealed the presence of low molecular weight acids at high retention times. These low molecular weight species most likely represent fragments of higher molecular weight naphthenic acids, which is consistent with MS spectra obtained for the model naphthenic acids. Consequently, the chromatogram was split into different fractions differing by their molecular weight. Through minimum mass cutoff and recombination of mass spectra

normalized by the total elution time, an unbiased mass distribution could be achieved from the results given by the GC/MS. This distribution is shown in Figure 25.

Mass distributions from GC/MS show that the commercial acid mixture contain mostly aliphatic and alicyclic acids structures with a relatively narrow distribution of carbon number and hydrogen deficiencies. Average molecular weight of the commercial naphthenic acid mixture from Fluka was calculated from the distribution present in Figure 25 and compared with values determined from the elemental analysis and acid-base titration, shown in Table 2. The results show a good agreement between the different characterization methods, where the average molecular weight calculated from elemental analysis and titration results are similar, followed by a lower estimate based on the GC/MS distributions. This difference was attributed to the lower response factor of higher molecular weight compounds in the GC/MS.

Table 2: Summary of average molecular weight determinations of the commercial naphthenic acid mixture using 3 different methods.

Method	Average molecular weight
Elemental analysis	226 g/mol
Titration	231 g/mol
GC/MS	210 g/mol

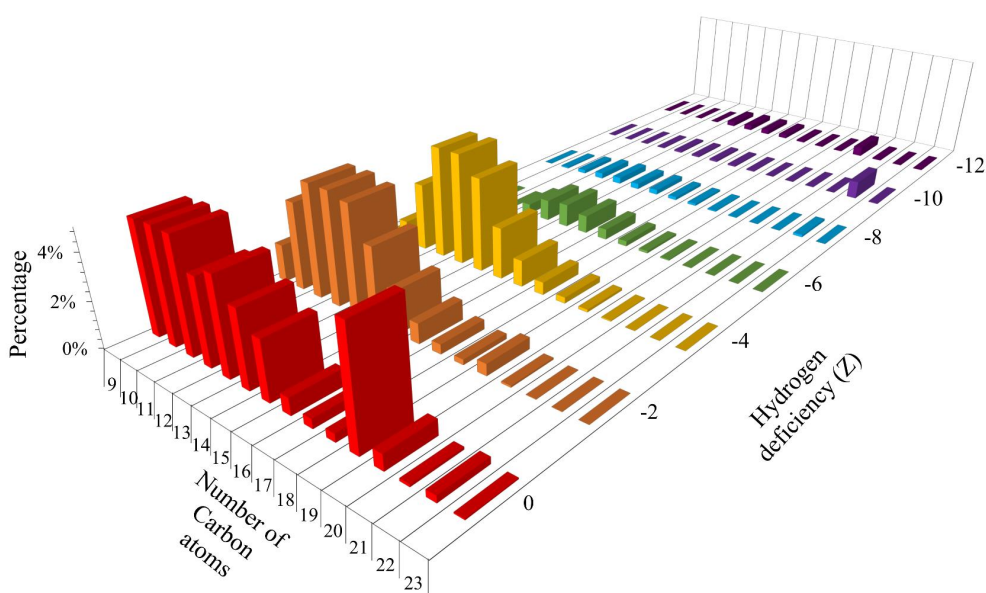


Figure 25: Mass distribution of the commercial NA mixture. The number of carbon atoms is visualized on one horizontal axis while the hydrogen deficiency,  $Z$ , is on the other horizontal axis. The number of ring structures in the acid structures decreases the  $Z$  number,  $Z=0$  signifies linear or branched acids and  $Z=-2$  signifies an acid structure with one ring.

The equilibrium partitioning of the commercial acid mixture between toluene and 3.5 wt. % NaCl aqueous buffers was mapped over the pH range. The initial oil phase concentrations corresponded to TAN values between 0.25 and 0.7  $\text{mg}_{\text{KOH}}/\text{g}_{\text{oil}}$ . This partitioning can be followed in Figure 26. An attempt to fit equation S1, and the equivalent equation for the total acid concentration in oil, to the partitioning of the entire acid mixture, using a single partitioning

ratio, was not able to successfully model the partitioning of the acid mixture since they present an average of properties. To provide a better prediction of the partitioning, it was decided to divide the chromatogram into narrower molecular weight ranges to obtain a partitioning curve that could be analyzed as a single specie.

The same method applied in the GC/MS characterization was implemented here, with increasing mass ranges of 25 g/mol each. An example of this partitioning of the naphthenic acid mass range 202 g/mol – 226 g/mol is shown in Figure 27. It was found that these mass ranges were narrow enough to be modeled by a single partition ratio, which increased with the molecular weight. These partition ratios could then be used to build up a summation model for the partitioning of the entire acid mixture, which logically, as a sum of its parts, fits the partitioning perfectly.

The mass balance was consistent for most of the measurements with two exceptions. First, at high molecular weight and high pH mass was lost, and this loss was attributed to the formation of sodium naphthenate particles. This loss is consistent with the observation of an opaque water phase after centrifugation at high pH. Second, at low molecular weight around pH 8, the mass balance would consistently exceed 100%. Despite our best efforts we were unable to find an explanation for this result.

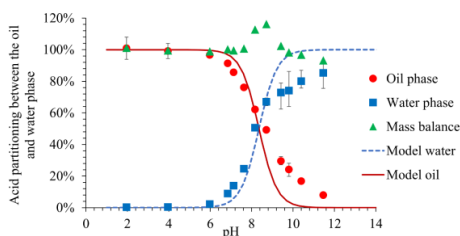


Figure 26: Equilibrium partitioning of the commercial acid mixture given as a function of equilibrium pH.

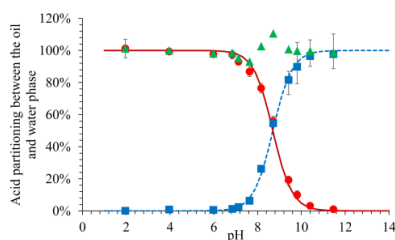


Figure 27: Equilibrium partitioning of the naphthenic acid mass fraction 202 g/mol – 226 g/mol, of the commercial acid mixture, given as a function of equilibrium pH.

Following up on the results obtained with divalent cations in the water phase in paper I, the partitioning of the commercial acid mixture in presence of calcium was also analyzed. The

behavior of the commercial acid mixture was different from the single model acids. Indeed, while 4HBA was found to form calcium naphthenate precipitate from pH 7, no precipitate was observed for the commercial naphthenic acid mixture and the mass balance was close to 100%. In addition, the partitioning of naphthenic acids to the water phase in the presence of calcium was reduced at high pH compared to the same system without calcium.

A closer look at how the partitioning of each mass range was affected revealed that the lower molecular weight acids ( $C_9$ - $C_{12}$ ) remained unchanged as was the case for the small model acid (PAA,  $C_8$ ) in paper I, while larger acids ( $C_{13}$ - $C_{19}$ ) had increasingly reduced the water phase partitioning, contrasting to the precipitate formation for the larger model acid ( $C_{14}$ ) in paper I. An example of this reduced partitioning for the mass range 202 g/mol – 226 g/mol can be seen in Figure 28. Elemental analysis of the equilibrated oil phase at low and high pH show an increasing presence of calcium in the oil phase with pH. This result points to the formation of oil-soluble calcium naphthenates. The elemental composition points to half the carboxyl groups in the oil phase being associated to calcium at pH 10 while this number increases to approximately 100% at pH 11.5.

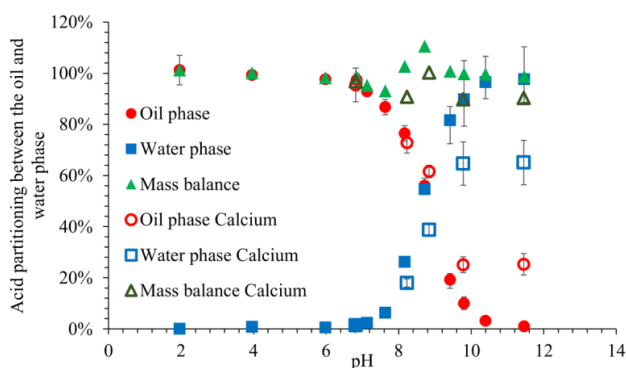


Figure 28: Equilibrium partitioning of the naphthenic acid mass fraction 202 g/mol – 226 g/mol, of the commercial acid mixture, with and without calcium in the water phase, given as a function of equilibrium pH.

#### 4.4 Paper IV

##### *Equilibrium partitioning of naphthenic acid mixture part 2: Crude oil extracted naphthenic acids.*

As a continuation of paper III, two naphthenic acid mixtures extracted from acidic crude oils were analyzed with the same methodology used as for the commercial acid mixture.

<sup>1</sup>H NMR of the extracted acids revealed a lack of aromatic rings in their structure, a recurring trend in the analysis of crude oil acids. The mass distributions of the extracted acids were determined by GC/MS. In paper III, the GC/MS method for the acid mixture analysis included a correction to avoid a distribution bias towards low molecular weight acids, by ensuring other fragments of high molecular weight acids were not considered in the distribution. The effect of this correction was not directly obvious for the commercial acid mixture, likely due to the low amount of large acids. For the extracted crude oil acids however, the effect is more prominent as can be observed in Figure 29 and Figure 30.

Here the non-corrected distribution in Figure 29, reveal a considerable presence of low molecular weight acids, however in the corrected distribution seen in Figure 30, it is revealed that many of these low molecular weight acids were not acids, but rather fragment artefacts from higher molecular weight acids. This is consistent with the mass spectra obtained for model acids presented in paper III. The corrected mass distribution obtained with GC/MS revealed that the two crude oil extracted acid mixtures had broad distributions regarding carbon number (C<sub>11</sub>-C<sub>40</sub>) with mostly alicyclic acid structures (hydrogen deficiencies (0 < Z < -12)), considering the absence of aromatic structures shown by NMR. Differences between the two extracted acid distributions were shown to be statistically insignificant, which is interesting as the crude oils they were extracted from, come from the same oil field, but have different TAN values (1.7 mg<sub>KOH</sub>/g<sub>oil</sub> vs. 3.1 mg<sub>KOH</sub>/g<sub>oil</sub>).

Characterization of the acids through elemental analysis, titration and GC/MS revealed a stark difference in the estimated average molecular weight as seen in Table 3. The lower estimate given by the GC/MS could be expected due to the bias of low response factor for higher molecular weight compounds in the GC/MS, and the GC/MS inability to analyze the largest molecular weight acids from crude oil. As it can be observed in the mass distribution in Figure 30, the extracted crude oil acids contain a large fraction of high molecular weight

compounds. The difference between the average molecular weight from the elemental analysis and the titration is harder to rationalize, although the elemental analysis method is very sensitive to the measured oxygen content and the titration result could be influenced by the presence of a non-acidic pollutant.

*Table 3: Summary of average molecular weights obtained by characterization of the extracted naphthenic acid mixtures with three different methods.*

Method	Average molecular weight Acid mixture A	Average molecular weight Acid mixture B
Elemental analysis	373 g/mol	395 g/mol
Titration	438* g/mol	454* g/mol
GC/MS	340 g/mol	360 g/mol

*\*Average molecular weight determination from TAN titration performed by Equinor at their facilities.*

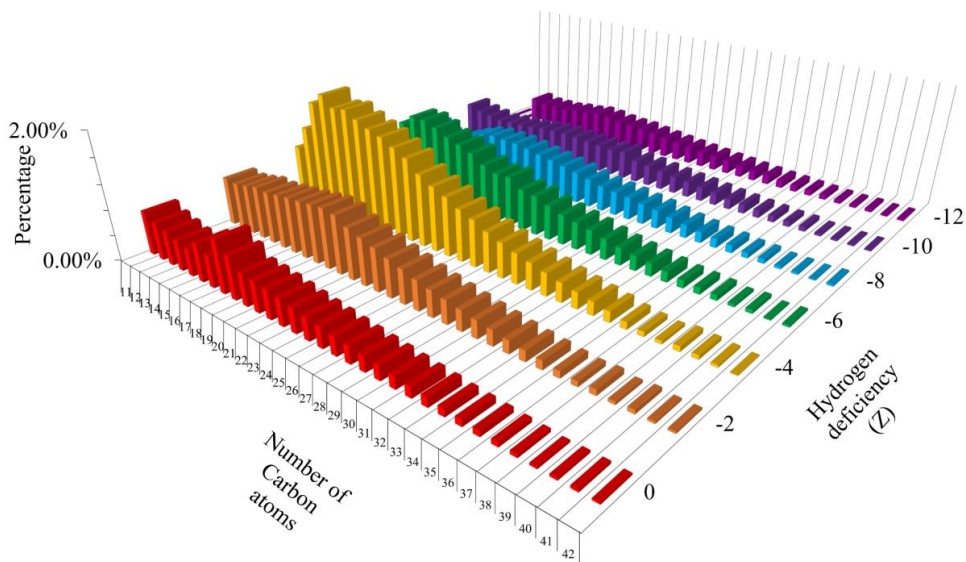


Figure 29: Uncorrected mass distribution of extracted crude oil acid mixture A.

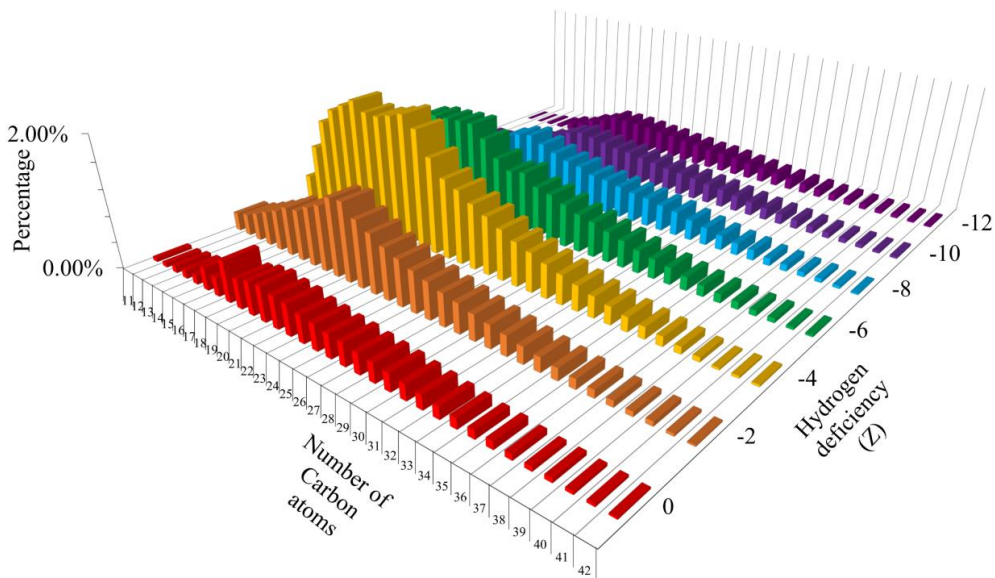


Figure 30: Corrected mass distribution of extracted crude oil acid mixture A.

Equilibrium partitioning experiments with the extracted crude oil acid mixture between toluene and 3.5 wt. % NaCl aqueous buffers were performed over a pH range from 4 to 12. The partitioning of the extracted acid mixture as shown in Figure 31, indicates that partitioning is limited when the entire naphthenic acid mixture is analyzed. However, a closer look at the data



shows that only a small fraction of the total acids (acids with molecular weight lower than 327 g/mol), could partition into the water phase, even at the highest pH. Consequently, the approach of evaluating the partitioning of molecular mass ranges from paper III was applied on the extracted acid mixture. This approach allows the partitioning of a narrower molecular weight range to be analyzed and fitted with partitioning equations as can be observed for the mass range 202 g/mol – 226 g/mol in Figure 32. In lower molecular weight ranges it can be observed that the partitioning into the water phase is complete at high pH. Summing up the partition ratio of lower molecular weight individual fractions in proportion to their area in the chromatogram allows to fit the partitioning of the water-soluble fraction of the extracted crude oil acid mixture (acids with molecular weight lower than 327 g/mol). The mass balance at high pH was lower than 100%. A light brown layer was present at the centrifuge tube wall for these pH values, which was attributed to sodium naphthenate precipitation, similar to the case for the commercial naphthenic acid mixture.

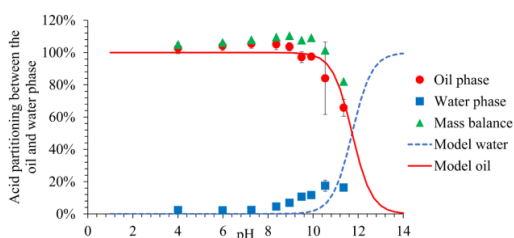


Figure 31: Equilibrium partitioning of the extracted crude oil acid mixture A given as a function of equilibrium pH.

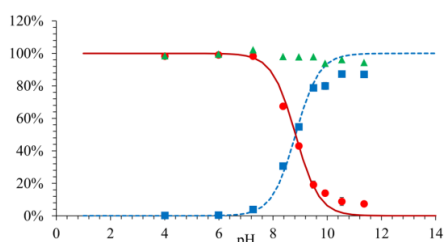


Figure 32: Equilibrium partitioning of the mass range 202 g/mol – 226 g/mol, of the extracted crude oil acid mixture A, given as a function of equilibrium pH.

The results from paper III and paper IV reveal that the partition ratios for equal molecular weight ranges are practically identical between the commercial acid mixture and the extracted acid sample, as illustrated in Figure 33. This result is interesting as although they both originate from petroleum, their origin is presumably different, suggesting universal applications for the obtained results.

This correlation was expanded into more fundamental derivations by considering the free energy contribution from each lipophilic group ( $-\text{CH}_x-$ ) and hydrophilic group ( $-\text{COOH}$ ) for

the partitioning of naphthenic acids. The obtained results ( $\Delta\mu_{L(-CH_x-)} = -2.63$  kJ/mol,  $\Delta\mu_{H(-COOH)} = 6.3$  kJ/mol) for the transfer from oil to water are similar to previously reported results regarding group free energy contributions, both for fatty acid partitioning Mukerjee<sup>316</sup> and micellization studies<sup>317, 318</sup>.

As crude oils inescapably are a mixture of saturates and aromatics, the influence of the solvent medium can be better understood by evaluating the difference in partitioning of the larger model acid from paper I, 4HBA, in the two solvents, heptane and toluene. The phase change occurred at a lower pH value in the saturated solvent, compared to the aromatic solvent, presumably due to the increased polarity of the aromatic solvent. The slope of the phase change was also sharper for the more non- aqueous solvent as described in earlier literature<sup>149</sup>.

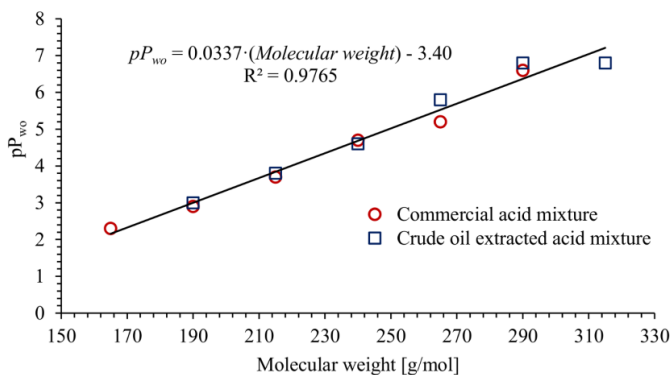


Figure 33: Graph indicating the linearity of the cologarithm of the partition ratio,  $pP_{w/o}$ , of acid mass ranges from two different naphthenic acid mixtures based on molecular weight. Linear regression is based on both data sets.

Comparing results obtained in paper III and IV with previously reported partitioning results requires some considerations to be taken as to what is being compared. For instance, the universally applied logP value for chemicals, usually referring to octanol-water equilibria, would need to be translated to a toluene-water system before comparisons can be made. Comparing the experimental results obtained in this work to the experimental results reported from Havre, et al.<sup>147</sup> on acid partitioning between crude oil and water, reveal great similarities, the small differences existing might be explained by the more saturated nature of crude oil as the organic phase, compared to toluene. The results obtained by Zhang, et al.<sup>319</sup> on the

partitioning of acids in OSPW however, reveal a large difference in partition ratios with results presented in Figure 33. Samples from the two studies could contain different acid structure isomers of similar molecular weight. Comparing the experimental data to values from solubility models like QSAR<sup>90</sup> and COSMO-RS<sup>156</sup> show that models have some limitations in predicting experimental partitioning values.

To finalize the work performed on the influence of calcium on partitioning covered in paper I and III, the influence of calcium on the partitioning of extracted crude oil acids were investigated. Calcium reduced the partitioning at high pH and gave a better mass balance (no precipitation observed). As seen in paper III, more details are revealed when considering the partitioning of narrower mass ranges. Once more, it was found that the calcium had little to no effect on the partitioning of the lowest molecular weight acids in the extracted acid mixture (C<sub>11</sub> – C<sub>12</sub>) while it increasingly reduced the partitioning of higher molecular weight acids (C<sub>13</sub>-C<sub>21</sub>) into the aqueous phase. This effect is shown in Figure 34. Elemental analysis of the oil phase from a high pH equilibrium experiment revealed calcium in the oil phase. Assuming the presence of oil soluble calcium naphthenates, it was calculated that all the acid groups left in the oil were bound to calcium at pH 11.5. In conclusion, the partitioning ratio values and the effects of calcium on the partitioning of the commercial acid mixture from paper III and the extracted crude oil acid mixture in this paper are almost identical, suggesting some universal trends for crude oil acid solubility in water at high pH.

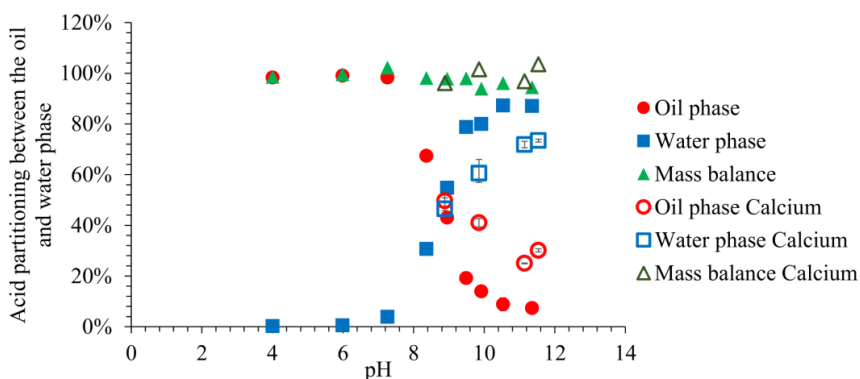


Figure 34: Equilibrium partitioning of the mass range 202 g/mol – 226 g/mol, of the extracted crude oil acid mixture A, with calcium in the water phase, given as a function of equilibrium pH.






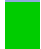
## 4.5 Paper V

### *Microfluidic tools for studying coalescence of crude oil droplets in produced water*

Having observed the equilibrium partitioning of model acids, a commercial acid mixture and extracted crude oil acids, the effect of these acids on the behavior of oil droplets in water was investigated with microfluidics. Water is inevitably co-produced with crude oil and the amount of water keeps increasing during the lifetime of the field. This produced water needs to be treated prior to discharge or injection/reinjection, where the treatment mainly revolves around the removal of dispersed crude oil. Whereas much attention has been given to the stability of oil continuous emulsions, fewer studies have been reported on the factors which influence the stability of water continuous petroleum emulsions.

This paper attempts to map the influence of various parameters on the coalescence of crude oil droplets in water. The microfluidic setup included a T-junction for droplet generation before a wider channel, which allowed droplets to interact with each other. Through high-speed imaging and image analysis the coalescence frequency for each system was obtained. Table 1 show the properties of the crude oil studied.

*Table 4: Properties of the crude oils studied.*

Crude oil	API [°]	Viscosity [mPa s] at 20°C	TAN [mgKOH/g <sub>oil</sub> ]	TBN [mgKOH/g <sub>oil</sub> ]	SARA [% wt.]				
					Saturates	Aromatics	Resins	Asphaltenes	
	A	19.2	354.4	2.2	2.8	50.6	31.2	15.7	2.5
	B	35.8	14.2	ND	1.0	84.0	13.4	2.3	0.3
	C	23.0	74.4	2.7	1.1	64.9	26.3	8.4	0.4
	D	36.3	10.2	0.2	1.1	71.5	23.1	5.1	0.3
	E	37.9	8.3	0.5	0.4	74.8	23.2	1.9	0.1
	F	39.7	7.5	0.1	0.6	78.5	18.9	2.5	0.1

In testing these crude oils in a diluted state (25% wt. with xylene) in systems with three different pH values (4, 6, 10) and two different salt compositions (NaCl and NaCl/CaCl<sub>2</sub>), the coalescence was always seen to decrease with increasing pH values, probably due to the

ionization of naphthenic acids and their adsorption at oil-water interface. The coalescence of the heavier crude oils was also notably lower for all systems studied compared to the lighter crude oils, even though their viscosity in the diluted state should be comparable. However, the content of surface active species (asphaltenes and resins) is higher in heavier crude oils. With a salt composition containing calcium, the coalescence generally increased at the highest pH, which was attributed to oil-soluble calcium naphthenate formation, removing these species from the interface. These results show the basic components in crude oil to be a destabilizing factor at low pH where coalescence frequency was found inversely proportional to TBN, although compared to the stabilizing influence of the acid fraction at high pH, the bases in crude oil provided much less stabilization against coalescence at pH 4.

To draw behavioral conclusions from the properties of the crude oils, a trend of lower coalescence frequency with the sum of the polar fractions, resins and asphaltenes, was found for all the crude oils irrespective of the pH and aqueous salt composition.

Three light crude oils (B, E and F) could, with the addition of an oil-soluble surfactant (200 ppm), be used undiluted, and these three crude oils were used to investigate the impact of the dissolved components in the water phase. First, the coalescence results were compared to results obtained with diluted oil and no added oil soluble surfactant, and the effect of the water composition were found to be similar for both systems, though undiluted crude oils were far more resistant towards coalescence. Dissolved components were introduced in the water phase. The dissolved components were: the model acid from paper I, 4-heptylbenzoic acid (4HBA) at pH 10, the commercial acid mixture from Fluka used in paper III, extracted at pH 6 and 10 (all at concentrations around 100 ppm), and dissolved components from each crude oil (Table 4) obtained through prolonged contact with water at pH 4, 6 and 10. In systems with 4HBA, the coalescence frequency was similar for all three crude oils at pH 10 as shown in Figure 35 indicating that 4HBA dominates the interfacial properties in these systems. In systems with the commercial acid mixture, however, the results were more crude oil specific, where the coalescence would either increase, decrease or stay the same. The viscosity, the resin/asphaltene ratio and the amount of water-soluble organic content in the crude oils were put forward as possible justifications for the observed trends.

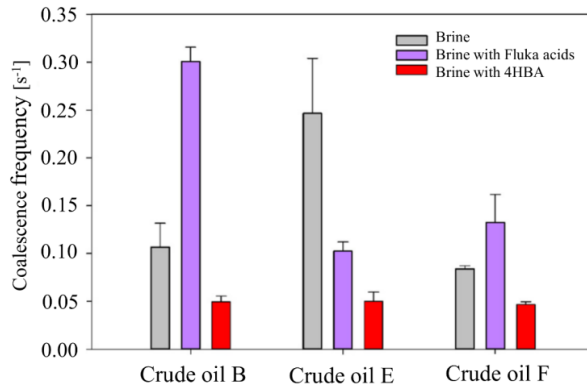


Figure 35: Coalescence frequencies at pH 10 for three crude oil with different water phase compositions regarding dissolved component. The water phase concentration for Fluka acids and 4HBA was 100 ppm.

Figure 36 presents the influence of the dissolved crude oil components on the coalescence on their respective crude oil. It can be observed that the trend is still crude oil dependent. Moreover, the trend observed for adding dissolved crude oil components is similar to the results obtained with the commercial acid mixture. This could show that the surface active dissolved crude oil components act similarly and most likely have a similar structure as the commercial acid mixture from Fluka, affecting the coalescence even at pH 6.

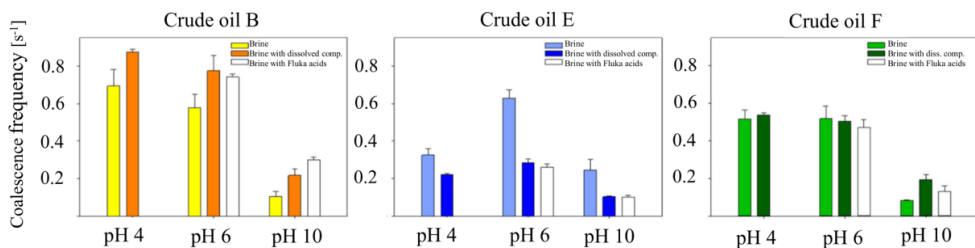


Figure 36: Coalescence frequencies for three crude oils with different water phase compositions regarding dissolved components.

Experiments in pressurized system revealed limited influence of pressure on coalescence frequency for pH 6 and 10, even at pressures of 40 bars. This was attributed to the lack of volatile crude oil components which would be directly influenced by pressure, namely the lighter alkanes, lost during the production.

## 5 Concluding remarks

In the pursuit of more predictable production conditions for less accessible processing systems like subsea oil-water separation systems, insights into dissolved surface-active species like naphthenic acids in the water phase might provide answers about the produced water composition at given parameters. This knowledge could prove useful when evaluating efficiency of the water treatment system over time.

The partitioning of acids and bases in crude oil were investigated using model acids and bases in a model system composed of heptane and 3.5 wt. % NaCl water. The low molecular weight acid, PAA, exhibited a large water solubility for all pH values, indicating that it and similar acids would partition to the water phase, maybe even in the reservoir. This was also proved by the lack of such low molecular weight acids in both the commercial acid mixture and the crude oil extracted acids. As these acids exhibit limited surface-active tendencies over the pH range, their presence could be inconsequential on the emulsion stability. The larger model acid, 4HBA, went from completely oil soluble to completely water-soluble as the pH increased. This acid also exhibited a strong surface affinity as dissociation of the acid took place. In fact, the initial concentration of 10 mM had to be drastically reduced as inseparable viscous mixtures would form at higher pH. Of the two model bases, the low molecular weight base, 4EA, exhibited partitioning with no surface activity, while the larger base 4DA, did not partition into the water phase at all, but showed surface activity. The influence of acid-base interaction on the interfacial tension were not observed with the model acids and bases used in this study. The presence of calcium on the partitioning of the two model acids, where found to only affect the larger model acid, 4HBA, which would form calcium naphthenate precipitate at higher pH. It is noted that the model bases, which are thought to be good representatives for crude oil bases, do not exhibit neither water solubility or interfacial activity in the pH range (6-7.7<sup>158</sup>) observed in oil production. However, if they are present in gas-condensate producing field which has a much lower pH (3.5-5.5<sup>158</sup>), their role might be amplified.

The effect of the oil phase solvent on partitioning was examined for the model acid 4HBA where the phase change occurred at pH 8 with heptane as the oil phase solvent and in a later experiment around pH 8.8 with toluene as the oil phase solvent. The behavior these acids would exhibit in a crude oil might be postulated to a pH in-between these two solvents as crude oil has both saturates and aromatic hydrocarbons, which is exactly the case reported earlier for

acids of similar size in a crude oil-water system where a phase change around pH 8.5 was predicted. However, the complexity of crude oil with other phase equilibria like for example resin-asphaltene interactions renders these speculations less certain.

A new dissipative particle dynamics (DPD) system was created by combining partitioning and dissociation of molecular bead structures. Interaction force parameters were tuned to match the partitioning behavior of the larger model acid 4HBA, a match which was made possible through a dilution of the system post simulation since limited computational capacity only allows a very small volume to be simulated. It is encouraging to see that partitioning properties can now be modelled and recreated in DPD simulations.

A method to study the partitioning and mass distribution of acid mixtures using standard GC/MS was developed and applied to two types of acid mixtures, one commercial naphthenic acid mixture from Fluka and two crude oil extracted acid mixtures. The characterization method to reduce mass distribution bias towards low molecular weight acids, due to fragmentation during the ionization step, was mostly evident for the two crude oil extracted acid mixtures. Both the partitioning of the commercial acid mixture and the partitioning of the water-soluble fraction of one extracted crude oil acid mixture could be successfully modelled by splitting up the chromatogram signal into narrow molecular weight ranges and recombining their partitioning behavior through normalization with the total area of the chromatogram. Similar molecular mass ranges for both types of acid mixtures exhibited the same partitioning behavior, indicating some universal properties.

The presence of calcium did affect the partitioning behavior of the acid mixtures, although in a different manner than what was observed for the large model acid (4HBA). Here no precipitate would form, instead the partitioning was increasingly reduced at high pH for acids larger than C<sub>13</sub>. Elemental analysis of the oil phase, after partitioning of acids to the water phase, showed an increasing calcium content in the oil phase with pH, indicating the formation of oil-soluble calcium naphthenates. This has implications to previous suggestions of pore blocking mechanisms for calcium naphthenate precipitation acidic crude oil reservoirs<sup>320</sup> or calcium naphthenate precipitation in the oil phase<sup>221, 222</sup>. Foregone conclusions might have reached by observing systems with single acids in toluene. In this work, calcium naphthenate precipitate did indeed form in the system with a single acid in heptane, while no precipitation was observed in the systems with acid mixtures in toluene as crystallization is inhibited by



polydispersity. Experiments with acid mixtures in heptane would need to be conducted prior to conclusive assertions, to rule out the influence of solvent.

The effect of dissolved components on the coalescence of oil droplets in water was tested by the means of microfluidics. First, it was established that for crude oils in their diluted form, an increase in the pH caused a decrease in coalescence and that even in their diluted state, heavier crude oils had a notably lower degree of coalescence. Both observations were attributed to polar fraction in the crude oils, specifically naphthenic acids and asphaltenes. Calcium in the water phase would cause an increase in coalescence at high pH. This last effect was attributed to the formation of oil soluble calcium naphthenates, removing surfactant from the interface and therefore rendering it more vulnerable to coalescence with other oil droplets. The effect of the dissolved components on the coalescence of three light crude oils, undiluted, were then tested. Dissolved model acid 4HBA were observed to dominate the coalescence behavior at high pH, evidenced by similar values obtained for all three crude oils. Dissolved commercial naphthenic acid mixture in the water phase would both decrease and increase the coalescence depending on the crude oil and the pH. Water phases with dissolved crude oil components from prolonged contact at three different pH values were obtained and tested with their respective crude oil. Here it was found that the dissolved crude oil components in the water phase which influence the coalescence had similar effect as the dissolved commercial naphthenic acid mixture even at pH 6. This points to crude oil acids as the main contributor from dissolved components on the coalescence stabilities of oil droplets in water, and it is interesting to see how their presence can both increase and decrease the coalescence.

Although this work investigates some of the effects these dissolved components have on the coalescence, this influence still requires more study to determine predictable behavior based on the system parameters: oil and water phase composition, emulsion type, pressure and temperature. After the water phase composition is decided based on the oil phase composition and the pressure (and therefore pH) and temperature, the influence of these components on the stability oil-in-water emulsions, water-in-oil emulsions, gas flotation and reinjection behavior can be evaluated.

## 6 Scope for future work

The results presented in this PhD thesis could be extended into different directions. First, it could be interesting to obtain information about the kinetics involved in naphthenic acid partitioning by assessing the partitioning over time in an emulsified system containing asphaltenes or other emulsion stabilizers. As the emulsion gradually destabilizes, the bulk phases could be analyzed to ascertain the quantity and character of the acids over time. This knowledge would allow assessment of the quality of produced water in a separator for instance.

Regarding the thermodynamics of partitioning, two points have been identified as topics for further study. First, although we have investigated the partitioning behavior of narrow naphthenic acid mass ranges from mixtures of naphthenic acids, these mass ranges still contain a large diversity of acids, both in functional groups and structure especially regarding the hydrogen deficiency,  $Z$ . A first step to determine the effect of naphthenic acid structures on the partitioning could entail considering the partitioning of specific naphthenic acid isomers to provide even more fundamental insight into the free energy contribution from different hydrocarbon structures. Second, this thesis has shown the influence of calcium on naphthenic acid partitioning. It would therefore be interesting to see if further investigation could reveal naphthenic acid structural information to the effect of calcium on partitioning as well. Quantification could be performed on the data gathered in this thesis to calculate the complexation constants for oil-soluble calcium naphthenate formation. The effect of temperature on calcium naphthenate partitioning into the oil phase could also be interesting to observe as partitioning constants are suggested to move towards unity as the temperature increases. The influence of molecular weight could be further investigated to discover the criteria for calcium naphthenate precipitation. Other variables, like kinetics and the influence of water cut, would also be interesting to include in this part.

The development of the GC/MS method of studying acid mixtures will allow a complex system to be split into narrower distribution fractions and every fraction could be studied separately in a reproducible manner. This technique should be incorporated into future studies on the influence of water-soluble crude oil acids at the Ugelstad laboratory and elsewhere.

Simulation of naphthenic acid partitioning between oil and water was studied by DPD. This methodology could be further developed to study the influence of naphthenic acid structure on partitioning. Data obtained by simulation would be supplementary to the data obtained in this

thesis and could allow the consideration of parameters which are difficult to study experimentally.

Another interesting topic for further work would be the interplay on the interface in systems containing a surface-active acid with partitioning abilities, and asphaltenes. Asphaltenes and naphthenic acids are among the most important emulsion stabilizers in crude oil. Knowledge of their interaction would allow to better predict the stability of crude oil emulsions. Droplet desorption studies of systems with naphthenic acids and asphaltenes with co-axial capillary could also shed some light on the complex interactions occurring at the ever-important oil-water interface.

## 7 References

1. Warner, R., Western European refineries and acidity in crude oil. In S&P-Global-Platts-Oil, Ed. S&P Global Inc: New York, USA, 2017; pp 1-6.
2. Bacon, R.; Tordo, S., Crude Oil Prices : Predicting Price Differentials Based on Quality. In *Public Policy Journal*, Viewpoint. World Bank: Washington, DC. USA, 2004; pp 1-4.
3. Shaiek, S.; Laurent, G., SpoolSep for Subsea Produced Water Separation, OTC-25934. In *Offshore Technology Conference*, 4-7 May, Houston, Texas, USA 2015.
4. Berntsen, J. S., Qualified technology (TRL 5) to remove produced water, at seafloor or topside, before it becomes difficult to treat. In *Tekna Produced Water Management Conference*, 24th-25th January, Stavanger, Norway, 2018.
5. Daigle, T. P., Ultra Deep Water Discharge of Produced Water and/or Solids at the Seabed In Research Partnership to Secure Energy for America, R., Ed. Fluor Offshore Solutions: Sugar Land, TX, USA, 2012.
6. Yang, M., Challenges for Water Quality Measurement for Produced Water Handling Subsea, OTC 23099. In *Offshore Technology Conference*, Offshore Technology Conference: 30 April–3 May, Houston, Texas, USA, 2012.
7. Mullins, O. C., Petroleomics and Structure–Function Relations of Crude Oils and Asphaltenes. In *Asphaltenes, Heavy Oils, and Petroleomics*, 1 ed.; Mullins, O. C.; Sheu, E. Y.; Hammami, A.; Marshall, A. G., Eds. Springer-Verlag New York: 2007.
8. McLean, J. D.; Kilpatrick, P. K., Effects of Asphaltene Solvency on Stability of Water-in-Crude-Oil Emulsions. *Journal of Colloid and Interface Science* **1997**, 189, (2), 242-253.
9. Speight, J. G., Heinemann, H., *The Chemistry and Technology of Petroleum*. Fourth Edition ed.; CRC Press Taylor & Francis group: Boca Raton, USA, 2006.
10. Sephton, M. A.; Hazen, R. M., On the Origins of Deep Hydrocarbons. *Reviews in Mineralogy and Geochemistry* **2013**, 75, (1), 449-465.
11. Kutcherov Vladimir, G.; Krayushkin Vladilen, A., Deep-seated abiogenic origin of petroleum: From geological assessment to physical theory. *Reviews of Geophysics* **2010**, 48, (1), 1-30.
12. Speight, J. G., *High Acid Crudes*. Gulf Professional Publishing: Oxford, United Kingdom, 2014.
13. Tissot, B. P.; Welte, D. H., Physicochemical Aspects of Primary Migration. In *Petroleum Formation and Occurrence*, Tissot, B. P.; Welte, D. H., Eds. Springer-Verlag Berlin Heidelberg, 1978.
14. El-Banbi, A. H.; Aly, A. M.; Lee, W. J.; McCain, W. D., Jr., Investigation of Waterflooding and Gas Cycling for Developing a Gas-Condensate Reservoir. In *SPE/CERI Gas Technology Symposium*, Society of Petroleum Engineers: Calgary, Alberta, Canada, 2000.
15. Chacón-Patiño, M., L.; Rowland, S. M.; Rodgers, R. P., The Compositional and Structural Continuum of Petroleum from Light Distillates to Asphaltenes: The Boduszynski Continuum Theory As Revealed by FT-ICR Mass Spectrometry. In *The Boduszynski Continuum: Contributions to the Understanding of the Molecular Composition of Petroleum*, Ovalles, C.; Moir, M. E., Eds. American Chemical Society: Washington, DC, USA, 2018; Vol. 1282, pp 113-171.
16. Sjöblom, J., Simon, S. , Oil films: Some basic concepts. In *Oil Spill Remediation: Colloid Chemistry-Based Principles and Solutions*, Somasundaran, P.; Patra, P.; Farinato, R. S.; Papadopoulos, K., Eds. John Wiley & Sons, Inc: Hoboken, New Jersey, 2014.
17. Aske, N.; Kallevik, H.; Sjöblom, J., Determination of Saturate, Aromatic, Resin, and Asphaltenic (SARA) Components in Crude Oils by Means of Infrared and Near-Infrared Spectroscopy. *Energy & Fuels* **2001**, 15, (5), 1304-1312.
18. Sjöblom, J.; Aske, N.; Harald Aulfem, I.; Brandal, Ø.; Erik Havre, T.; Sæther, Ø.; Westvik, A.; Eng Johnsen, E.; Kallevik, H., Our current understanding of water-in-crude oil emulsions.: Recent characterization techniques and high pressure performance. *Advances in Colloid and Interface Science* **2003**, 100–102, 399-473.

19. Hoepfner, M. P.; Limsakoune, V.; Chuenmeechao, V.; Maqbool, T.; Fogler, H. S., A Fundamental Study of Asphaltene Deposition. *Energy & Fuels* **2013**, *27*, (2), 725-735.
20. Zhang, L. Y.; Xu, Z.; Masliyah, J. H., Langmuir and Langmuir–Blodgett Films of Mixed Asphaltene and a Demulsifier. *Langmuir* **2003**, *19*, (23), 9730-9741.
21. Demirbas, A.; Taylan, O., Removing of resins from crude oils. *Petroleum Science and Technology* **2016**, *34*, (8), 771-777.
22. Binti Shafiee @ Ismail, N. S. Carboxylic acid composition and acidity in crude oils and bitumens. University of Newcastle upon Tyne, Newcastle, UK, 2014.
23. Barth, T.; Høiland, S.; Fotland, P.; Askvik, K. M.; Pedersen, B. S.; Borgund, A. E., Acidic compounds in biodegraded petroleum. *Organic Geochemistry* **2004**, *35*, (11–12), 1513-1525.
24. Meredith, W.; Kelland, S. J.; Jones, D. M., Influence of biodegradation on crude oil acidity and carboxylic acid composition. *Organic Geochemistry* **2000**, *31*, (11), 1059-1073.
25. Simon, S.; Nenningsland, A. L.; Herschbach, E.; Sjöblom, J., Extraction of basic components from petroleum crude oil. *Energy and Fuels* **2010**, *24*, (2), 1043-1050.
26. Barth, T.; Høiland, S.; Fotland, P.; Askvik, K. M.; Myklebust, R.; Erstad, K., Relationship between the Content of Asphaltenes and Bases in Some Crude Oils. *Energy & Fuels* **2005**, *19*, (4), 1624-1630.
27. Klein, G. C.; Angström, A.; Rodgers, R. P.; Marshall, A. G., Use of Saturates/Aromatics/Resins/Asphaltenes (SARA) Fractionation To Determine Matrix Effects in Crude Oil Analysis by Electrospray Ionization Fourier Transform Ion Cyclotron Resonance Mass Spectrometry. *Energy & Fuels* **2006**, *20*, (2), 668-672.
28. Gaspar, A.; Zellermann, E.; Lababidi, S.; Reece, J.; Schrader, W., Characterization of Saturates, Aromatics, Resins, and Asphaltenes Heavy Crude Oil Fractions by Atmospheric Pressure Laser Ionization Fourier Transform Ion Cyclotron Resonance Mass Spectrometry. *Energy & Fuels* **2012**, *26*, (6), 3481-3487.
29. Veil, J. A.; Puder, M. G.; Elcock, D.; Redweik, R. J., A White Paper Describing Produced Water from Production of Crude Oil, Natural Gas and Coal Bed Methane. In D.O.E., Ed. Argonne National Lab: Argonne, IL, USA, 2004.
30. Boysen, B.; Henthorne, L.; Johnson, H.; Turner, B., New Water-Treatment Technologies. Tackle offshore produced water challenges in EOR. *Oil and Gas Facilities, Society of Petroleum Engineers* **2013**, *2*, (3).
31. Neff, J.; Lee, K.; DeBlois, E. M., Produced Water: Overview of Composition, Fates, and Effects. In *Produced Water: Environmental Risks and Advances in Mitigation Technologies*, Lee, K.; Neff, J., Eds. Springer New York: New York, NY, 2011; pp 3-54.
32. Khatib, Z.; Verbeek, P., Water to Value - Produced Water Management for Sustainable Field Development of Mature and Green Fields. In *SPE International Conference on Health, Safety and Environment in Oil and Gas Exploration and Production*, Society of Petroleum Engineers: 20–22 March, Kuala Lumpur, Malaysia, 2002.
33. Hayes, T.; Arthur, D., Overview of emerging produced water treatment technologies In *The 11th Annual International Petroleum Environmental Conference*, October 12-15, Albuquerque, New Mexico, USA, 2004.
34. Johnsen, S.; Røe Utvik, T. I.; Garland, E.; de Vals, B.; Campbell, J., Environmental Fate And Effect Of Contaminants In Produced Water. In *SPE International Conference on Health, Safety, and Environment in Oil and Gas Exploration and Production*, Society of Petroleum Engineers: 29–31 March, Calgary, Alberta, Canada, 2004.
35. Yang, M., Measurement of Oil in Produced Water. In *Produced Water*, K. Lee, J. N., Ed. Springer Science Business Media, LLC: East Kilbride, Glasgow G75 0QF, UK, 2011.
36. RCN, Long-term effects of discharges to sea from petroleum-related activities. In *The Research Council of Norway*: Oslo, Norway, 2012.
37. KLD, White paper no. 58: Environmental policy for a Sustainable development - Joint Effort for the Future. In *Environment*, N. M. o. t., Ed. Government Administration Services: Oslo, Norway, 1996-1997.
38. Vik, E. A.; Janbu, A. O.; Garshol, F. K.; Henninge, L. B.; Engebretsen, S.; Kuijvenhoven, C.; Oilphant, D.; Hendriks, W. P., Nitrate Based Souring Mitigation of Produced Water - Side Effects and

- Challenges from the Draugen Produced Water re-Injection Pilot, SPE 106178. In *SPE International Symposium on Oilfield Chemistry*, Society of Petroleum Engineers: 28 February–2 March, Houston, Texas, U.S.A., 2007.
39. Association, T. N. O. a. G. *Environmental report 2017*; The Norwegian Oil and Gas Association: <https://www.norskoljeoggass.no/en>, 2017.
40. KLD, White paper: Integrated Management of the Marine Environment of the Barents Sea and the Sea Areas off the Lofoten Islands. In Environment, M. o., Ed. Norwegian government: Oslo, Norway, 2006; Vol. Report No. 8 to the Storting, p 9.
41. Voldum, K.; Garpestad, E.; Anderssen, N. O.; Henriksen, I. B., The CTour Process, An Option to Comply with Zero Harmful Discharge Legislation in Norwegian Waters - Experience of CTour Installation on Ekofisk After Start up 4th Quarter 2007, SPE 118012. In *Abu Dhabi International Petroleum Exhibition and Conference*, Society of Petroleum Engineers: 3-6 November, Abu Dhabi, UAE, 2008.
42. Bennion, D. B.; Thomas, F. B.; Imer, D.; Ma, T.; Schulmeister, B., Water Quality Considerations Resulting in the Impaired Injectivity of Water Injection and Disposal Wells. *Journal of Canadian Petroleum Technology* **2001**, 40, (6).
43. Gramme, P. E. In *Chemistry and Physics of Heavy Oil and other Dispersions*, Tekna Heavy Oil Technology for Offshore Applications, 14.-15. May 2009, Stavanger, Norway, 2009; 14.-15. May 2009, Stavanger, Norway, 2009.
44. Campbell, J. M., Know Your Separators. *Oil & Gas Journal* **1955**, 53, (45), 107-111.
45. Jacob, M.; Demangel, A.; Goldszal, A.; Rambeau, O.; Jouenne, S.; Cordelier, P. In *Impact of back produced polymer on tertiary water treatment performances*, Tekna Produced water management conference, Jan. 20–21, Stavanger, Norway, 2016; Jan. 20–21, Stavanger, Norway, 2016.
46. Euphemio, M. L.; Lima, I. F.; Orlowski, R.; Ribeiro, L. S.; Lourenco, I.; Pereira, R. d. S.; Inacio, F.; Gontijo, F.; Fletcher, n.; Trevisani, d., Marlim 3-Phase Subsea Separation System: Project Overview and Execution Strategy. In *Offshore Technology Conference*: 2012.
47. Horn, T.; Eriksen, G.; Bakke, W., Troll Pilot- Definition, Implementation and Experience. In *Offshore Technology Conference*, Offshore Technology Conference: 6-9 May 2002, Houston, Texas U.S.A., , 2002.
48. Gjerdsseth, A. C.; Faanes, A.; Ramberg, R., The Tordis IOR Project. In *Offshore Technology Conference*, Offshore Technology Conference: 30 April-3 May, Houston, Texas, U.S.A., , 2007.
49. Soo, H.; Radke, C. J., Flow mechanism of dilute, stable emulsions in porous media. *Industrial & Engineering Chemistry Fundamentals* **1984**, 23, (3), 342-347.
50. D. B. Bennion, F. B. T., D. Imer, T. Ma, B. Schulmeister, Water Quality Considerations Resulting in the Impaired Injectivity of Water Injection and Disposal Wells. **2000**.
51. Siqueira, A.; Mendes, R. A.; Furtado, C. J. A.; Vieira, L.; Serra De Souza, A. L.; Pereira, R. d. S.; Alves, A.; Ramalho, J.; De Melo, A. V.; Figueiredo, L.; Andrade, C.; Travalloni, A. M.; Penna, M.; Bezerra, M. C. M., Marlim 3-Phase Subsea Separation System (Petrobras): Introduction to the Involved Reservoir Background. In *Offshore Technology Conference*, Offshore Technology Conference: Houston, Texas, USA, 2012.
52. Anres, S. J.; Butin, N.; Evans, W.; Bignonneau, D., New Solutions for Subsea Produced Water Separation and Treatment in Deepwater. In *Offshore Technology Conference*: 2011.
53. McCurdy, R. In *Underground injection wells for produced water disposal*, USEPA Technical Workshops for the Hydraulic Fracturing Study: Water Resource Management., Arlington, VA, 2011; United States Environmental Protection Agency Office of Research and Development: Arlington, VA, 2011.
54. SULZER, Upstream Systems for Gas, Oil, Produced Water and Sand Processing. In brochure, P., Ed. Sulzer Ltd: 2017.
55. Lim, D.; Gruenhagen, H., Subsea Separation and Boosting—An Overview of Ongoing Projects SPE-123159-MS. In *Asia Pacific Oil and Gas Conference & Exhibition*, Society of Petroleum Engineers: 4–6 August, Jakarta, Indonesia, 2009.
56. Appleford, D. E.; Smith, R. G., Seabed Processing - Enabling Technology OTC-13194. In *Offshore Technology Conference*, Offshore Technology Conference: Houston, Texas, 2001.

57. de Lacotte, L. H.; Lopez, A.; Rivière, L.; Anfray, J., Deep Offshore - Needs for a Subsea / Topsides Integrated Approach OTC-25782-MS. In *Offshore Technology Conference*, Offshore Technology Conference: 4–7 May 2015, Houston, Texas, USA, 2015.
58. Friedemann, J. D., Design Criteria and Methodology for Modern Oil and Water Separation Systems. In *Emulsions and Emulsion Stability*, Sjöblom, J., Ed. CRC Press: Boca Raton, USA, 2005; pp 607-629.
59. Khoi Vu, V.; Fantoft, R.; Shaw, C. K.; Gruehagen, H., Comparison Of Subsea Separation Systems. In *Offshore Technology Conference*, Houston, Texas, USA, 4-7 May, OTC 20080, 2009.
60. Davies, S. R. H.; Bakke, W.; Ramberg, R. M.; Jensen, R. O., Experience to date and future opportunities for subsea processing in StatoilHydro, OTC 20619. In *Offshore Technology Conference*, Offshore Technology Conference: 3–6 May, Houston, Texas, USA, 2010.
61. Skjefstad, H. S.; Stanko, M., Subsea water separation: a state of the art review, future technologies and the development of a compact separator test facility. In *18th International Conference on Multiphase Production Technology*, BHR Group: Cannes, France, 2017.
62. de Oliveira, D. A.; Pereira, R. d. S.; Capela Moraes, C. A.; Baracho, V. P.; de Souza, R. d. S. A.; Euphemio, M. L. L.; da Silva, F. S.; Monteiro, A. S.; Casanova, C. C.; Duarte, D. G.; Raposo, G. M., Commissioning and Startup of Subsea Marlim Oil and Water Separation System. In *Offshore Technology Conference*: 2013.
63. Hurtevent, C.; Bourrel, M.; Rousseau, G.; Brocart, B., Production Issues of Acidic Petroleum Crude Oils. In *Emulsions and Emulsion Stability*, Sjöblom, J., Ed. CRC Press: Boca Raton, FL, USA, 2005; pp 477-516.
64. Jahnsen, O. F.; Storvik, M., Subsea Processing & Boosting In A Global Perspective. In *10th Offshore Mediterranean Conference and Exhibition*, Offshore Mediterranean Conference: March 23 - 25, Ravenna, Italy 2011.
65. Olson, M. D.; Grave, E. J.; Juarez, J. C.; Gul, K., Performance Testing of an Integrated, Subsea Compact Separation System with Electrocoalescence for Deepwater Applications, OTC-25695. In *Offshore Technology Conference*, *Offshore Technology Conference*: 4-7 May, Houston, Texas, USA, , 2015.
66. Yang, M.; Latif, Z., A Review of Recent Progress in Developing Water Quality Measurement Instruments for Subsea Separation and Produced Water Re-Injection or Discharge Applications. In *Offshore Technology Conference Asia*, Offshore Technology Conference: Kuala Lumpur, Malaysia, 2018.
67. Ruud, T.; Idrac, A.; McKenzie, L. J.; Høy, S. H., All Subsea: A Vision for the Future of Subsea Processing OTC-25735-MS. In *Offshore Technology Conference*, Offshore Technology Conference: 4–7 May, Houston, Texas, USA, 2015.
68. Kuhnle, T. I.; Grande, Ø.; Pedersen, F. B.; Yang, Y.; Jafar, M.; Sewraz, D.; Irvine, M. *All subsea – creating value from subsea processing*; Høvik, Norway, 2015.
69. Ramberg, R. M.; Davies, S. R. h.; Rognoe, H.; Oekland, O., Steps to the Subsea Factory OTC-24307-MS. In *OTC Brasil*, Offshore Technology Conference: 29–31 October, Rio de Janeiro, Brazil, 2013.
70. Ese, M.-H.; Kilpatrick, P. K., Stabilization of Water-in-Oil Emulsions by Naphthenic Acids and Their Salts: Model Compounds, Role of pH, and Soap : Acid Ratio. *Journal Of Dispersion Science And Technology* **2004**, 25, (3), 253-261.
71. Shepherd, A. G. A Mechanistic Analysis of Naphthenate and Carboxylate Soap-Forming Systems in Oilfield Exploration and Production. Heriot-Watt University, Edinburg, UK, 2008.
72. Qian, K.; Robbins, W. K.; Hughey, C. A.; Cooper, H. J.; Rodgers, R. P.; Marshall, A. G., Resolution and Identification of Elemental Compositions for More than 3000 Crude Acids in Heavy Petroleum by Negative-Ion Microelectrospray High-Field Fourier Transform Ion Cyclotron Resonance Mass Spectrometry. *Energy & Fuels* **2001**, 15, (6), 1505-1511.
73. Sjöblom, J.; Simon, S.; Xu, Z., The chemistry of tetrameric acids in petroleum. *Advances in Colloid and Interface Science* **2014**, 205, (0), 319-338.
74. Headley, J. V., McMartin, Dena W., A Review of the Occurrence and Fate of Naphthenic Acids in Aquatic Environments. *Journal of Environmental Science and Health Part A* **2004**, A39, (8), 1989–2010.

75. Grewer, D. M.; Young, R. F.; Whittall, R. M.; Fedorak, P. M., Naphthenic acids and other acid-extractables in water samples from Alberta: what is being measured? *Science of the Total Environment* **2010**, 408, (23), 5997–6010.
76. Hemmingsen, P. V.; Kim, S.; Pettersen, H. E.; Rodgers, R. P.; Sjöblom, J.; Marshall, A. G., Structural Characterization and Interfacial Behavior of Acidic Compounds Extracted from a North Sea Oil. *Energy & Fuels* **2006**, 20, (5), 1980-1987.
77. Tomczyk, N. A.; Winans, R. E.; Shinn, J. H.; Robinson, R. C., On the Nature and Origin of Acidic Species in Petroleum. 1. Detailed Acid Type Distribution in a California Crude Oil. *Energy & Fuels* **2001**, 15, (6), 1498-1504.
78. Rudzinski, W. E.; Oehlers, L.; Zhang, Y.; Najera, B., Tandem Mass Spectrometric Characterization of Commercial Naphthenic Acids and a Maya Crude Oil. *Energy & Fuels* **2002**, 16, (5), 1178-1185.
79. Headley, J. V.; Peru, K. M.; Mohamed, M. H.; Frank, R. A.; Martin, J. W.; Hazewinkel, R. R. O.; Humphries, D.; Gurprasad, N. P.; Hewitt, L. M.; Muir, D. C. G.; Lindeman, D.; Strub, R.; Young, R. F.; Grewer, D. M.; Whittall, R. M.; Fedorak, P. M.; Birkholz, D. A.; Hindle, R.; Reisdorph, R.; Wang, X.; Kasperski, K. L.; Hamilton, C.; Woudneh, M.; Wang, G.; Loescher, B.; Farwell, A.; Dixon, D. G.; Ross, M.; Pereira, A. D. S.; King, E.; Barrow, M. P.; Fahlman, B.; Bailey, J.; McMartin, D. W.; Borchers, C. H.; Ryan, C. H.; Toor, N. S.; Gillis, H. M.; Zuin, L.; Bickerton, G.; McMaster, M.; Sverko, E.; Shang, D.; Wilson, L. D.; Wrona, F. J., Chemical fingerprinting of naphthenic acids and oil sands process waters-A review of analytical methods for environmental samples. *Journal of Environmental Science and Health. Part A, Toxic/hazardous Substances & Environmental Engineering* **2013**, 48, 1145-1163.
80. Headley, J. V.; Barrow Mp Fau - Peru, K. M.; Peru Km Fau - Derrick, P. J.; Derrick, P. J., Salting-out effects on the characterization of naphthenic acids from Athabasca oil sands using electrospray ionization. *Journal of Environmental Science and Health, Part A, Toxic/Hazardous Substances and Environmental Engineering* **2011**, 46, (8), 844-854.
81. Häger, M.; Ese, M. H.; Sjöblom, J., Emulsion Inversion in an Oil-Surfactant-Water System Based on Model Naphthenic Acids under Alkaline Conditions. *Journal of Dispersion Science and Technology* **2005**, 26, (6), 673-682.
82. Barrow, M. P.; McDonnell, L. A.; Feng, X.; Walker, J.; Derrick, P. J., Determination of the Nature of Naphthenic Acids Present in Crude Oils Using Nanospray Fourier Transform Ion Cyclotron Resonance Mass Spectrometry: The Continued Battle Against Corrosion. *Analytical Chemistry* **2003**, 75, (4), 860-866.
83. Derungs, W. A., Naphthenic Acid Corrosion —An Old Enemy Of the Petroleum Industry. *Corrosion* **1956**, 12, (12), 41-46.
84. Laredo, G. C.; López, C. R.; Álvarez, R. E.; Castillo, J. J.; Cano, J. L., Identification of Naphthenic Acids and Other Corrosivity-Related Characteristics in Crude Oil and Vacuum Gas Oils from a Mexican Refinery. *Energy & Fuels* **2004**, 18, (6), 1687-1694.
85. Wu, X.; Jing, H.; Zheng, Y.; Yao, Z.; Ke, W., Erosion–corrosion of various oil-refining materials in naphthenic acid. *Wear* **2004**, 256, (1), 133-144.
86. Turnbull, A.; Slavcheva, E.; Shone, B., Factors Controlling Naphthenic Acid Corrosion. *The Journal of Science and Engineering, Corrosion* **1998**, 54, (11), 922-930.
87. Yépez, O., Influence of different sulfur compounds on corrosion due to naphthenic acid. *Fuel* **2005**, 84, (1), 97-104.
88. Yépez, O., On the chemical reaction between carboxylic acids and iron, including the special case of naphthenic acid. *Fuel* **2007**, 86, (7–8), 1162-1168.
89. Li, C.; Fu, L.; Stafford, J.; Belosevic, M.; Gamal El-Din, M., The toxicity of oil sands process-affected water (OSPW): A critical review. *Sci Total Environ* **2017**, 601-602, 1785-1802.
90. Scarlett, A. G.; West, C. E.; Jones, D.; Galloway, T. S.; Rowland, S. J., Predicted toxicity of naphthenic acids present in oil sands process-affected waters to a range of environmental and human endpoints. *Sci Total Environ* **2012**, 425, 119-27.
91. Vindstad, J. E.; Bye, A. S.; Grande, K. V.; Hustad, B.; Hustvedt, E.; Nergård, B., Fighting Naphthenate Deposition at the Heidrun Field. In *International Symposium on Oilfield Scale*, Society of Petroleum Engineers: January 29-30th, Aberdeen, UK, SPE 80375, 2003.



92. Hocker, S.; Rhudy, A. K.; Ginsburg, G.; Kranbuehl, D. E., Polyamide hydrolysis accelerated by small weak organic acids. *Polymer* **2014**, *55*, (20), 5057-5064.
93. Sinquin, A.; Arla, D.; Prioux, C.; Peytavy, J. L.; Glenat, P.; Dicharry, C., Gas Hydrate Formation and Transport in an Acidic Crude Oil: Influence of Salt and pH. *Energy & Fuels* **2007**, *22*, 721-728.
94. Erstad, K. The influence of crude oil acids on natural inhibition of hydrate plugs. UIB, Bergen, Norway, 2009.
95. Jaffé, R.; Gallardo, M. T., Application of carboxylic-acid biomarkers as indicators of biodegradation and migration of crude oils from the Maracaibo Basin, Western Venezuela. *Organic Geochemistry* **1993**, *20*, (7), 973-984.
96. Behar, F. H.; Albrecht, P., Correlations between carboxylic acids and hydrocarbons in several crude oils. Alteration by biodegradation. *Organic Geochemistry* **1984**, *6*, 597-604.
97. Aitken, C. M.; Jones, D. M.; Larter, S. R., Anaerobic hydrocarbon biodegradation in deep subsurface oil reservoirs. *Nature* **2004**, 431, 291.
98. Holowenko, F. M.; MacKinnon, M. D.; Fedorak, P. M., Characterization of naphthenic acids in oil sands wastewaters by gas chromatography-mass spectrometry. *Water Research* **2002**, *36*, (11), 2843-2855.
99. Cassani, F.; Eglinton, G., Organic geochemistry of Venezuelan extra-heavy crude oils 2. Molecular assessment of biodegradation. *Chemical Geology* **1991**, *91*, (4), 315-333.
100. Hollerbach, A., Influence of Biodegradation on the Chemical Composition of Heavy Oil and Bitumen. In *Exploration for heavy crude oils and natural bitumen*, Meyer, R. F., Ed. The American Association of Petroleum Geologists: Tulsa, Oklahoma, USA, 1987; Vol. 25, pp 243-247.
101. Saab, J.; Mokbel, I.; Razzouk, A. C.; Ainous, N.; Zydowicz, N.; Jose, J., Quantitative Extraction Procedure of Naphthenic Acids Contained in Crude Oils. Characterization with Different Spectroscopic Methods. *Energy & Fuels* **2005**, *19*, (2), 525-531.
102. Jones, D. M.; Watson, J. S.; Meredith, W.; Chen, M.; Bennett, B., Determination of Naphthenic Acids in Crude Oils Using Nonaqueous Ion Exchange Solid-Phase Extraction. *Analytical Chemistry* **2001**, *73*, (3), 703-707.
103. Seifert, W. K.; Teeter, R. M., Identification of polycyclic aromatic and heterocyclic crude oil carboxylic acids. *Analytical Chemistry* **1970**, *42*, (7), 750-758.
104. Jones, D.; West, C. E.; Scarlett, A. G.; Frank, R. A.; Rowland, S. J., Isolation and estimation of the 'aromatic' naphthenic acid content of an oil sands process-affected water extract. *Journal of Chromatography A* **2012**, 1247, (1873-3778 (Electronic)), 171– 175.
105. Stanford, L. A.; Kim, S.; Klein, G. C.; Smith, D. F.; Rodgers, R. P.; Marshall, A. G., Identification of Water-Soluble Heavy Crude Oil Organic-Acids, Bases, and Neutrals by Electrospray Ionization and Field Desorption Ionization Fourier Transform Ion Cyclotron Resonance Mass Spectrometry. *Environmental Science & Technology* **2007**, *41*, (8), 2696-2702.
106. Wenger, L. M.; Davis, C. L.; Isaksen, G. H., Multiple Controls on Petroleum Biodegradation and Impact on Oil Quality SPE-80168-PA. *SPE Reservoir Evaluation & Engineering* **2002**, *5*, (5), 375-383.
107. Li, M.; Cheng, D.; Pan, X.; Dou, L.; Hou, D.; Shi, Q.; Wen, Z.; Tang, Y.; Achal, S.; Milovic, M.; Tremblay, L., Characterization of petroleum acids using combined FT-IR, FT-ICR-MS and GC-MS: Implications for the origin of high acidity oils in the Muglad Basin, Sudan. *Organic Geochemistry* **2010**, *41*, (9), 959-965.
108. Smith, D. F.; Schaub, T. M.; Kim, S.; Rodgers, R. P.; Rahimi, P.; Teclamarium, A.; Marshall, A. G., Characterization of Acidic Species in Athabasca Bitumen and Bitumen Heavy Vacuum Gas Oil by Negative-Ion ESI FT-ICR MS with and without Acid-Ion Exchange Resin Prefractionation. *Energy & Fuels* **2008**, *22*, (4), 2372-2378.
109. Scott, A. C.; Young, R. F.; Fedorak, P. M., Comparison of GC-MS and FTIR methods for quantifying naphthenic acids in water samples. *Chemosphere* **2008**, *73*, (8), 1258-1264.
110. Papageorgiou, S. K.; Kouvelos, E. P.; Favvas, E. P.; Sapalidis, A. A.; Romanos, G. E.; Katsaros, F. K., Metal-carboxylate interactions in metal-alginate complexes studied with FTIR spectroscopy. *Carbohydrate Research* **2010**, *345*, (4), 469-473.

111. Robinet, L.; Corbeil-a, M.-C., The Characterization of Metal Soaps. *Studies in Conservation* **2003**, 48, (1), 23-40.
112. Shepherd, A. G.; van Dijk, M.; Koot, W.; Dubey, S. T.; Poteau, S.; Zabarar, G. J.; Grutters, M., Flow Assurance In Oil Systems: On the Role And Impact Of Naphthenic Acids. In Society of Petroleum Engineers: 2012.
113. Otero, V.; Sanches, D.; Montagner, C.; Vilarigues, M.; Carlyle, L.; Lopes, J. A.; Melo, M. J., Characterisation of metal carboxylates by Raman and infrared spectroscopy in works of art. *Journal of Raman Spectroscopy* **2014**, 45, (11-12), 1197-1206.
114. Clemente, J. S.; Fedorak, P. M., A review of the occurrence, analyses, toxicity, and biodegradation of naphthenic acids. *Chemosphere* **2005**, 60, (5), 585-600.
115. Damasceno, F. C.; Gruber, L. D. A.; Geller, A. M.; Vaz de Campos, M. C.; Gomes, A. O.; Guimaraes, R. C. L.; Peres, V. F.; Jacques, R. A.; Caramao, E. B., Characterization of naphthenic acids using mass spectroscopy and chromatographic techniques: study of technical mixtures. *Analytical Methods* **2014**, 6, (3), 807-816.
116. Lewis, A. T.; Tekavec, T. N.; Jarvis, J. M.; Juyal, P.; McKenna, A. M.; Yen, A. T.; Rodgers, R. P., Evaluation of the Extraction Method and Characterization of Water-Soluble Organics from Produced Water by Fourier Transform Ion Cyclotron Resonance Mass Spectrometry. *Energy & Fuels* **2013**, 27, (4), 1846-1855.
117. Headley, J. V.; Peru, K. M.; McMartin, D. W.; Winkler, M., Determination of dissolved naphthenic acids in natural waters by using negative-ion electrospray mass spectrometry. *Journal of AOAC International* **2002**, 85, 182-187.
118. Panda, S. K.; Andersson Jt Fau - Schrader, W.; Schrader, W., Mass-spectrometric analysis of complex volatile and nonvolatile crude oil components: a challenge. *Analytical and Bioanalytical Chemistry* **2007**, 389, (5), 1329-1339.
119. Barrow, M. P.; Witt, M.; Headley, J. V.; Peru, K. M., Athabasca Oil Sands Process Water: Characterization by Atmospheric Pressure Photoionization and Electrospray Ionization Fourier Transform Ion Cyclotron Resonance Mass Spectrometry. *Analytical Chemistry* **2010**, 82, (9), 3727-3735.
120. Martin, J. W.; Han, X.; Peru, K. M.; Headley, J. V., Comparison of high- and low-resolution electrospray ionization mass spectrometry for the analysis of naphthenic acid mixtures in oil sands process water. *Rapid Communications in Mass Spectrometry* **2008**, 22, (0951-4198 (Print)), 1919-1924.
121. Clingenpeel, A. C.; Rowland, S. M.; Corilo, Y. E.; Zito, P.; Rodgers, R. P., Fractionation of Interfacial Material Reveals a Continuum of Acidic Species That Contribute to Stable Emulsion Formation. *Energy & Fuels* **2017**, 31, (6), 5933-5939.
122. Rowland, S. M.; Robbins, W. K.; Corilo, Y. E.; Marshall, A. G.; Rodgers, R. P., Solid-Phase Extraction Fractionation To Extend the Characterization of Naphthenic Acids in Crude Oil by Electrospray Ionization Fourier Transform Ion Cyclotron Resonance Mass Spectrometry. *Energy & Fuels* **2014**, 28, (8), 5043-5048.
123. Chacón-Patiño, M. L.; Rowland, S. M.; Rodgers, R. P., Advances in Asphaltene Petroleomics. Part 1: Asphaltenes Are Composed of Abundant Island and Archipelago Structural Motifs. *Energy & Fuels* **2017**, 31, (12), 13509-13518.
124. Chacón-Patiño, M. L.; Rowland, S. M.; Rodgers, R. P., Advances in Asphaltene Petroleomics. Part 2: Selective Separation Method That Reveals Fractions Enriched in Island and Archipelago Structural Motifs by Mass Spectrometry. *Energy & Fuels* **2018**, 32, (1), 314-328.
125. Smith, D. F.; Schaub, T. M.; Rahimi, P.; Teclerian, A.; Rodgers, R. P.; Marshall, A. G., Self-Association of Organic Acids in Petroleum and Canadian Bitumen Characterized by Low- and High-Resolution Mass Spectrometry. *Energy & Fuels* **2007**, 21, (3), 1309-1316.
126. Rodgers, R. P.; Hendrickson, C. L.; Emmett, M. R.; Marshall, A. G.; Greaney, M.; Qian, K., Molecular characterization of petroporphyrins in crude oil by electrospray ionization Fourier transform ion cyclotron resonance mass spectrometry. *Canadian Journal of Chemistry* **2001**, 79, (5-6), 546-551.
127. Blau, K.; Halket, J. M., *Handbook of Derivatives for Chromatography*. John Wiley & Sons, Ltd: Chichester, UK, 1993.

128. Clemente, J. S.; Yen, T.-W.; Fedorak, P. M., Development of a high performance liquid chromatography method to monitor the biodegradation of naphthenic acids. *Journal of Environmental Engineering and Science* **2003**, 2, (3), 177-186.
129. Pereira, A. S.; Bhattacharjee, S.; Martin, J. W., Characterization of Oil Sands Process-Affected Waters by Liquid Chromatography Orbitrap Mass Spectrometry. *Environmental Science & Technology* **2013**, 47, (10), 5504-5513.
130. Colati, K. A. P.; Dalmaschio, G. P.; de Castro, E. V. R.; Gomes, A. O.; Vaz, B. G.; Romão, W., Monitoring the liquid/liquid extraction of naphthenic acids in Brazilian crude oil using electrospray ionization FT-ICR mass spectrometry (ESI FT-ICR MS). *Fuel* **2013**, 108, 647-655.
131. Wang, X.; Kasperski, K. L., Analysis of naphthenic acids in aqueous solution using HPLC-MS/MS. *Analytical Methods* **2010**, 2, (11), 1715-1722.
132. Merlin, M.; Guigard, S. E.; Fedorak, P. M., Detecting naphthenic acids in waters by gas chromatography–mass spectrometry. *Journal of Chromatography A* **2007**, 1140, (1–2), 225-229.
133. Brocart, B.; Hurtevent, C., Flow Assurance Issues and Control with Naphthenic Oils. *Journal of Dispersion Science and Technology* **2008**, 29, (10), 1496-1504.
134. Andersen, S. I.; Chandra, M. S.; Chen, J.; Zeng, B. Y.; Zou, F.; Mapolelo, M.; Abdallah, W.; Buiting, J. J., Detection and Impact of Carboxylic Acids at the Crude Oil–Water Interface. *Energy & Fuels* **2016**, 30, (6), 4475-4485.
135. St. John, W. P.; Rughani, J.; Green, S. A.; McGinnis, G. D., Analysis and characterization of naphthenic acids by gas chromatography–electron impact mass spectrometry of tert.-butyldimethylsilyl derivatives. *Journal of Chromatography A* **1998**, 807, (2), 241-251.
136. Schummer, C.; Delhomme, O.; Appenzeller, B. M. R.; Wennig, R.; Millet, M., Comparison of MTBSTFA and BSTFA in derivatization reactions of polar compounds prior to GC/MS analysis. *Talanta* **2009**, 77, (4), 1473-1482.
137. Clemente, J. S.; Fedorak, P. M., Evaluation of the analyses of tert-butyldimethylsilyl derivatives of naphthenic acids by gas chromatography–electron impact mass spectrometry. *Journal of Chromatography A* **2004**, 1047, (1), 117-128.
138. Shepherd, A. G.; van Mispelaar, V.; Nowlin, J.; Genuit, W.; Grutters, M., Analysis of Naphthenic Acids and Derivatization Agents Using Two-Dimensional Gas Chromatography and Mass Spectrometry: Impact on Flow Assurance Predictions. *Energy & Fuels* **2010**, 24, (4), 2300-2311.
139. Vaz de Campos, M. C.; Oliveira, E. C.; Filho, P. J. S.; Piatnicki, C. M. S.; Caramão, E. B., Analysis of tert-butyldimethylsilyl derivatives in heavy gas oil from Brazilian naphthenic acids by gas chromatography coupled to mass spectrometry with electron impact ionization. *Journal of Chromatography A* **2006**, 1105, (1), 95-105.
140. Aksenov, V. S.; Titov, V. I.; Kam'yanov, V. F., Nitrogen compounds of petroleum oils (review). *Chemistry of Heterocyclic Compounds* **1979**, 15, (2), 119-135.
141. Yamamoto, M.; Taguchi, K.; Sasaki, K., Basic nitrogen compounds in bitumen and crude oils. *Chemical Geology* **1991**, 93, (1–2), 193-206.
142. von Mühlen, C.; de Oliveira, E. C.; Zini, C. A.; Caramão, E. B.; Marriott, P. J., Characterization of Nitrogen-Containing Compounds in Heavy Gas Oil Petroleum Fractions Using Comprehensive Two-Dimensional Gas Chromatography Coupled to Time-of-Flight Mass Spectrometry. *Energy & Fuels* **2010**, 24, (6), 3572-3580.
143. Eftekhardakhah, M.; Kløcker, K. N.; Trapnes, H. H.; Gawel, B.; Øye, G., Composition and Dynamic Adsorption of Crude Oil Components Dissolved in Synthetic Produced Water at Different pH Values. *Industrial & Engineering Chemistry Research* **2016**, 55 (11), 3084–3090.
144. Hutin, A.; Argillier, J.-F.; Langevin, D., Mass Transfer between Crude Oil and Water. Part 1: Effect of Oil Components. *Energy & Fuels* **2014**, 28, (12), 7331-7336.
145. Turner, A., Salting out of chemicals in estuaries: implications for contaminant partitioning and modelling. *Science of The Total Environment* **2003**, 314–316, 599-612.
146. Touhami, Y.; Hornof, V.; Neale, G. H., Mechanisms for the Interactions between Acidic Oils and Surfactant-Enhanced Alkaline Solutions. *Journal of Colloid and Interface Science* **1996**, 177, (2), 446-455.
147. Havre, T. E.; Sjöblom, J.; Vindstad, J. E., Oil/Water-Partitioning and Interfacial Behavior of Naphthenic Acids. *Journal of Dispersion Science and Technology* **2003**, 24, (6), 789-801.

148. Bennion, B. J.; Be, N. A.; McNerney, M. W.; Lao, V.; Carlson, E. M.; Valdez, C. A.; Malfatti, M. A.; Enright, H. A.; Nguyen, T. H.; Lightstone, F. C.; Carpenter, T. S., Predicting a Drug's Membrane Permeability: A Computational Model Validated With in Vitro Permeability Assay Data. *The Journal of Physical Chemistry B* **2017**, 121, (20), 5228-5237.
149. Leo, A.; Hansch, C.; Elkins, D., Partition coefficients and their uses. *Chemical Reviews* **1971**, 71, (6), 525-616.
150. Spildo, K.; Høiland, H., Interfacial Properties and Partitioning of 4-Heptylbenzoic Acid between Decane and Water. *Journal of Colloid and Interface Science* **1999**, 209, (1), 99-108.
151. Goodman, D. S., The Distribution of Fatty Acids between n-Heptane and Aqueous Phosphate Buffer. *Journal of the American Chemical Society* **1958**, 80, (15), 3887-3892.
152. Scherrer, R. A.; Howard, S. M., Use of distribution coefficients in quantitative structure-activity relationships. *J Med Chem* **1977**, 20, (1), 53-8.
153. Lord, D. L.; Demond, A. H.; Hayes, K. F., Effects of Organic Base Chemistry on Interfacial Tension, Wettability, and Capillary Pressure in Multiphase Subsurface Waste Systems. *Transport in Porous Media* **2000**, 38, (1), 79-92.
154. Standal, S. H.; Blokhus, A. M.; Haavik, J.; Skauge, A.; Barth, T., Partition Coefficients and Interfacial Activity for Polar Components in Oil/Water Model Systems. *Journal of Colloid and Interface Science* **1999**, 212, (1), 33-41.
155. Passade-Boupat, N.; Rondon Gonzalez, M.; Hurtevent, C.; Brocart, B.; Palermo, T., Risk Assessment of Calcium Naphtenates and Separation Mechanisms of Acidic Crude Oil. In *SPE International Conference and Exhibition on Oilfield Scale*, Society of Petroleum Engineers: Aberdeen, UK, 30-31 May, SPE 155229, 2012.
156. Celsie, A.; Parnis, J. M.; Mackay, D., Impact of temperature, pH, and salinity changes on the physico-chemical properties of model naphthenic acids. *Chemosphere* **2016**, 146, 40-50.
157. Bostick, D. T.; Luo, H.; Hindmarsh, B. *Characterization of soluble organics in produced water*; Oak Ridge, Tennessee, US, 2002; pp 25-26.
158. Jacobs, R. P. W. M.; Grant, R. O. H.; Kwant, J.; Marquenie, J. M.; Mentzer, E., The Composition of Produced Water from Shell Operated Oil and Gas Production in the North Sea. In *Produced Water: Technological/Environmental Issues and Solutions*, Ray, J. P.; Engelhardt, F. R., Eds. Springer US: Boston, MA, 1992; pp 13-21.
159. Auflem, I. H.; Westvik, A.; Sjöblom, J., Destabilization of Water-in-Crude Oil Emulsions Based on Recombined Oil Samples at Various Pressures. *Journal of Dispersion Science and Technology* **2003**, 24, (1), 103-112.
160. Hutin, A.; Argillier, J.-F.; Langevin, D., Mass Transfer between Crude Oil and Water. Part 2: Effect of Sodium Dodecyl Benzenesulfonate for Enhanced Oil Recovery. *Energy & Fuels* **2014**, 28, (12), 7337-7342.
161. Flesisnki, L. Étude de la stabilité des émulsions et de la rhéologie interfaciale des systèmes pétrole brut/eau: Influence des asphaltènes et des acides naphthéniques. University of Pau and Pays de l'Adour (UPPA), Pau, France, 2011.
162. Brandal, Ø.; Hanneseth, A.-M.; Sjöblom, J., Interactions between synthetic and indigenous naphthenic acids and divalent cations across oil-water interfaces: effects of addition of oil-soluble non-ionic surfactants. *Colloid and Polymer Science* **2005**, 284, (2), 124-133.
163. Hutin, A.; Argillier, J.-F.; Langevin, D., Influence of pH on Oil-Water Interfacial Tension and Mass Transfer for Asphaltenes Model Oils. Comparison with Crude Oil Behavior. *Oil Gas Sci. Technol. – Rev. IFP Energies nouvelles* **2016**, 71, (4), 58.
164. Jones, T. J.; Neustadter, E. L.; Whittingham, K. P., Water-In-Crude Oil Emulsion Stability And Emulsion Destabilization By Chemical Demulsifiers. *Journal of Canadian Petroleum Technology* **1978**, 17, (02), 100-108.
165. McCartney, R. A.; Rein, E. In *Formation waters of the Norwegian Continental Shelf*, 16th International Symposium on Oilfield Chemistry, Geilo, Norway, 13-16 March, 2005; Geilo, Norway, 2005.
166. Goodwin, N.; Walsh, J. M.; Wright, R. J.; Dyer, S.; Graham, G. M., Modeling the Effect of Triazine Based Sulphide Scavengers on the in situ pH and Scaling Tendency. In *SPE International*

*Symposium on Oilfield Chemistry*, Society of Petroleum Engineers: 11-13 April, The Woodlands, Texas, USA, 2011.

167. Rousseau, G.; Zhou, H.; Hurtevent, C., Calcium Carbonate and Naphthenate Mixed Scale in Deep-Offshore Fields, SPE 68307. In *SPE 3rd International Symposium on Oilfield Scale*, Society of Petroleum Engineers: 30–31 January, Aberdeen, UK., 2001.
168. Brient, J. A.; Wessner, P. J.; Doyle, M. N., Naphthenic Acids. In *Encyclopedia of Chemical Technology*, Kirk-Othmer, Ed. John Wiley & Sons, Inc.: New York, 1995; pp 1017-1029.
169. Dewick, P. M., Acids and bases. In *Essentials of Organic Chemistry: For Students of Pharmacy, Medicinal Chemistry and Biological Chemistry*, Dewick, P. M., Ed. WILEY: West Sussex, England, 2006; p 130.
170. Kanicky, J. R.; Shah, D. O., Effect of Premicellar Aggregation on the pKa of Fatty Acid Soap Solutions. *Langmuir* **2003**, 19, (6), 2034-2038.
171. Reinsel, M. A.; Borkowski, J. J.; Sears, J. T., Partition Coefficients for Acetic, Propionic, and Butyric Acids in a Crude Oil/Water System. *Journal of Chemical & Engineering Data* **1994**, 39, (3), 513-516.
172. Cratin, P. D., Partitioning at the liquid-liquid interface. *Industrial & Engineering Chemistry* **1968**, 60, (9), 14-19.
173. Nordgård, E. L.; Ahmad, J.; Simon, S.; Sjöblom, J., Oil-Water Partitioning of a Synthetic Tetracarboxylic Acid as a Function of pH. *Journal of Dispersion Science and Technology* **2012**, 33, (6), 871-880.
174. Nordgård, E. L. k.; Sjöblom, J., Model Compounds for Asphaltenes and C80 Isoprenoid Tetraacids. Part I: Synthesis and Interfacial Activities. *Journal of Dispersion Science and Technology* **2008**, 29, (8), 1114-1122.
175. Stanford, L. A.; Rodgers, R. P.; Marshall, A. G.; Czarnecki, J.; Wu, X. A.; Taylor, S., Detailed Elemental Compositions of Emulsion Interfacial Material versus Parent Oil for Nine Geographically Distinct Light, Medium, and Heavy Crude Oils, Detected by Negative- and Positive-Ion Electrospray Ionization Fourier Transform Ion Cyclotron Resonance Mass Spectrometry. *Energy & Fuels* **2007**, 21, (2), 973-981.
176. Ligiero, L. M. Crude oil/water interface characterization and its relation to water-in-oil emulsion stability. University of Pau and Pays de l'Adour (UPPA), Pau, France, 2017.
177. Alvarado, V.; Wang, X.; Moradi, M., Role of Acid Components and Asphaltenes in Wyoming Water-in-Crude Oil Emulsions. *Energy & Fuels* **2011**, 25, (10), 4606-4613.
178. Tichelkamp, T.; Teigen, E.; Nourani, M.; Øye, G., Systematic study of the effect of electrolyte composition on interfacial tensions between surfactant solutions and crude oils. *Chemical Engineering Science* **2015**, 132, 244-249.
179. Gallup, D. L.; Curiale, J. A.; Smith, P. C., Characterization of Sodium Emulsion Soaps Formed from Production Fluids of Kutei Basin, Indonesia. *Energy & Fuels* **2007**, 21, (3), 1741-1759.
180. Sjöblom, J.; Hemmingsen, P. V.; Kallevik, H., The Role of Asphaltenes in Stabilizing Water-in-Crude Oil Emulsions. In *Asphaltenes, Heavy Oils, and Petroleomics*, Mullins, O. C.; Sheu, E. Y.; Hammami, A.; Marshall, A. G., Eds. Springer New York: New York, NY, 2007; pp 549-587.
181. Keleşoğlu, S.; Meakin, P.; Sjöblom, J., Effect of Aqueous Phase pH on the Dynamic Interfacial Tension of Acidic Crude Oils and Myristic Acid in Dodecane. *Journal of Dispersion Science and Technology* **2011**, 32, (11), 1682-1691.
182. Buckley, J. S.; Takamura, K.; Morrow, N. R., Influence of Electrical Surface Charges on the Wetting Properties of Crude Oils. *SPE Reservoir Engineering* **1989**, 4, (3), 332-340.
183. Luthy, R. G.; Selleck, R. E.; Galloway, T. R., Surface properties of petroleum refinery waste oil emulsions. *Environmental Science & Technology* **1977**, 11, (13), 1211-1217.
184. Nenningsland, A. L.; Simon, S.; Sjöblom, J., Surface properties of basic components extracted from petroleum crude oil. *Energy and Fuels* **2010**, 24, (12), 6501-6505.
185. Seifert, W. K.; Howells, W. G., Interfacially active acids in a California crude oil. Isolation of carboxylic acids and phenols. *Analytical Chemistry* **1969**, 41, (4), 554-562.
186. Ayirala, S. C.; Yousef, A. A.; Li, Z.; Xu, Z., Coalescence of Crude Oil Droplets in Brine Systems: Effect of Individual Electrolytes. *Energy & Fuels* **2018**, 32, (5), 5763-5771.

187. Cratin, P. D., Mathematical Modeling of Some pH-Dependent Surface and Interfacial Properties of Stearic Acid. *Journal of Dispersion Science and Technology* **1993**, 14, (5), 559-602.
188. Danielli, J. F., The Relations between Surface pH, Ion Concentrations and Interfacial Tension. *Proceedings of the Royal Society of London. Series B, Biological Sciences* **1937**, 122, (827), 155-174.
189. Peters, R. A., Interfacial Tension and Hydrogen-Ion Concentration. *Proceedings of the Royal Society of London. Series A, Containing Papers of a Mathematical and Physical Character* **1931**, 133, (821), 140-154.
190. Rudin, J.; Wasan, D. T., Mechanisms for lowering of interfacial tension in alkali/acidic oil systems: effect of added surfactant. *Industrial & Engineering Chemistry Research* **1992**, 31, (8), 1899-1906.
191. Lord, D. L.; Hayes, K. F.; Demond, A. H.; Salehzadeh, A., Influence of Organic Acid Solution Chemistry on Subsurface Transport Properties. 1. Surface and Interfacial Tension. *Environmental Science & Technology* **1997**, 31, (7), 2045-2051.
192. Saeten, J. O.; Sjoblom, J.; Gestblom, B., A dielectric spectroscopic study of fatty acid/amine complexes in solution. *The Journal of Physical Chemistry* **1991**, 95, (3), 1449-1453.
193. Góralczyk, D., Influence of Inorganic Electrolyte Concentration on Properties of Anionic-Cationic Adsorption Films. *Journal of Colloid and Interface Science* **1996**, 179, (1), 211-217.
194. Matsuki, H.; Aratono, M.; Kaneshina, S.; Motomura, K., Extremely Strong Interaction of Sodium Decyl Sulfate and Decyltrimethylammonium Bromide in Molecular Aggregates. *Journal of Colloid and Interface Science* **1997**, 191, (1), 120-130.
195. Ebeltoft, H.; Sjoblom, J.; Saeten, J. O.; Olofsson, G., Fatty Acid/Base Interactions in Model Systems. A Langmuir Film, Surface Tension, and Calorimetric Study. *Langmuir* **1994**, 10, (7), 2262-2266.
196. Spildo, K.; Blokhuis, A. M.; Andersson, A., Surface and Interfacial Properties of Octanoic Acid-Octylamine Mixtures in Isooctane-Water Systems: Influence of Acid: Amine Molar Ratio and Aqueous Phase pH. *Journal of Colloid and Interface Science* **2001**, 243, (2), 483-490.
197. Kelland, M. A., *Production Chemicals for the Oil and Gas Industry*. Second Edition ed.; CRC Press Boca Raton, FL, USA, 2014.
198. Williams, H.; Dyer, S.; Graham, G. M., Understanding the Factors Influencing the Formation and Control of Calcium Naphthenate Solids and Stabilised Emulsions Using a Novel Laboratory Flow Rig, SPE 106499. In *SPE International Symposium on Oilfield Chemistry*, Society of Petroleum Engineers: 28 February–2 March, Houston, Texas, U.S.A., 2007.
199. Mediaas, H.; Wolf, N. O.; Baugh, T. D.; Grande, K. V.; Vinstad, J. E., The Discovery of High Molecular Weight Naphthenic Acids (ARN Acid) Responsible for Calcium Naphthenate Deposits. In *SPE International Symposium on Oilfield Scale, 11-12 May*, SPE 93011: Society of Petroleum Engineers: Aberdeen, United Kingdom, 2005.
200. Simon, S.; Subramanian, S.; Gao, B.; Sjöblom, J., Interfacial Shear Rheology of Gels Formed at the Oil/Water Interface by Tetrameric Acid and Calcium Ion: Influence of Tetrameric Acid Structure and Oil Composition. *Industrial & Engineering Chemistry Research* **2015**, 54, (35), 8713-8722.
201. Lutnaes, B. F.; Brandal, O.; Sjoblom, J.; Krane, J., Archaeal C80 isoprenoid tetraacids responsible for naphthenate deposition in crude oil processing. *Organic & Biomolecular Chemistry* **2006**, 4, (4), 616-620.
202. Lutnaes, B. F.; Krane, J.; Smith, B. E.; Rowland, S. J., Structure elucidation of C80, C81 and C82 isoprenoid tetraacids responsible for naphthenate deposition in crude oil production. *Organic & Biomolecular Chemistry* **2007**, 5, (12), 1873-1877.
203. Sutton, P. A.; Rowland, S. J., Determination of the Content of C80 Tetraacids in Petroleum. *Energy & Fuels* **2014**, 28, (9), 5657-5669.
204. Simon, S.; Nordgård, E.; Bruheim, P.; Sjöblom, J., Determination of C80 tetra-acid content in calcium naphthenate deposits. *Journal of Chromatography A* **2008**, 1200, (2), 136-143.
205. Ahmed, M. M. Characterization, modelling, prediction and inhibition of naphthenate deposits in oilfield production. PhD thesis, Heriot-Watt University, Edinburgh, UK, 2010.

206. Turner, M. S.; Smith, P. C., Controls On Soap Scale Formation, Including Naphthenate Soaps - Drivers And Mitigation, SPE 94339. In *SPE International Symposium on Oilfield Scale*, Society of Petroleum Engineers: 11–12 May, Aberdeen, United Kingdom, 2005.
207. Runham, G.; Smith, P. C., Successful Naphthenate Scale and Soap Emulsion Management, SPE 121522. In *SPE International Symposium on Oilfield Chemistry*, 20–22 April, Society of Petroleum Engineers: The Woodlands. Texas, USA, 2009.
208. Pauchard, V.; Sjöblom, J.; Kokal, S.; Bouriat, P.; Dicharry, C.; Müller, H.; al-Hajji, A., Role of Naphthenic Acids in Emulsion Tightness for a Low-Total-Acid-Number (TAN)/High-Asphaltenes Oil. *Energy & Fuels* **2009**, *23*, (3), 1269-1279.
209. Mohammed, M. A.; Sorbie, K. S., Naphthenic acid extraction and characterization from naphthenate field deposits and crude oils using ESMS and APCI-MS. *Colloids and Surfaces A: Physicochemical and Engineering Aspects* **2009**, *349*, (1–3), 1-18.
210. Mapolelo, M. M.; Stanford, L. A.; Rodgers, R. P.; Yen, A. T.; Debord, J. D.; Asomaning, S.; Marshall, A. G., Chemical Speciation of Calcium and Sodium Naphthenate Deposits by Electrospray Ionization FT-ICR Mass Spectrometry. *Energy & Fuels* **2009**, *23*, (1), 349-355.
211. Hart, P. R., Removal of Water-Soluble Organics From Produced Brine Without Scale Formation. **2004**.
212. Wu, B.; Zhu, J.; Li, X., Distribution of calcium, nickel, iron, and manganese in super-heavy oil from Liaohe Oilfield, China. *Petroleum Science* **2014**, *11*, (4), 590-595.
213. Xu, X.; Yang, J.; Jiang, Y.; Gao, J., Effects of Process Conditions on Desalting and Demetalization of Crude Oil. *Petroleum Science and Technology* **2006**, *24*, (11), 1307-1321.
214. Allen, L. H., The importance of pH in controlling metal-soap deposition. *Tappi Journal* **1988**, *71*, (1), 61-64.
215. Sarac, S.; Civan, F., Mechanisms, Parameters, and Modeling of Naphthenate Soap-Induced Formation Damage. In *SPE International Symposium and Exhibition on Formation Damage Control*, Society of Petroleum Engineers: Lafayette, Louisiana, U.S.A., 2008.
216. Staff, J. P. T. In *Techbits: Naphthenate Deposits, Emulsions Highlighted in Technology Workshop*, Journal of Petroleum Technology, 10–13 March, Pau, France, 2008/7/1/, 2008; Society of Petroleum Engineers: 10–13 March, Pau, France, 2008.
217. Hurtevent, C.; Ubbels, S., Preventing Naphthenate Stabilised Emulsions and Naphthenate Deposits on Fields Producing Acidic Crude Oils. In *SPE International Oilfield Scale Symposium*, SPE 100430, Society of Petroleum Engineers: 30 May-1 June 2006, Aberdeen, Scotland, U.K., , 2006.
218. Havre, T. E. Formation of Calcium Naphthenate in Water/Oil Systems, Naphthenic Acid Chemistry and Emulsion Stability. PhD thesis, NTNU, Trondheim, Norway, Trondheim, 2002.
219. Brandal, Ø. Interfacial (o/w) Properties of Naphthenic Acids and Metal Naphthenates, Naphthenic Acid Characterization and Metal Naphthenate Inhibition. PhD thesis, NTNU, Trondheim, Norway, 2005.
220. Nordgård, E. L.; Simon, S.; Sjöblom, J., Interfacial Shear Rheology of Calcium Naphthenate at the Oil/Water Interface and the Influence of pH, Calcium, and in Presence of a Model Monoacid. *Journal of Dispersion Science and Technology* **2012**, *33*, (7), 1083-1092.
221. Hanneseth, A. M. D.; Brandal, Ø.; Sjöblom, J., Formation, Growth, and Inhibition of Calcium Naphthenate Particles in Oil/Water Systems as Monitored by Means of Near Infrared Spectroscopy. *Journal of Dispersion Science and Technology* **2006**, *27*, (2), 185-192.
222. Dyer, S. J.; Graham, G. M.; Arnott, C., Naphthenate Scale Formation - Examination of Molecular Controls in Idealised Systems. In *International Symposium on Oilfield Scale*, 29-30 January, Society of Petroleum Engineers: Aberdeen, United Kingdom, 2003.
223. Sarac, S.; Civan, F., Experimental Investigation and Modeling of Naphthenate Soap Precipitation Kinetics in Petroleum Reservoirs. In *International Symposium on Oilfield Chemistry*, Society of Petroleum Engineers: 28 February-2 March, Houston, Texas, U.S.A. SPE-106074, 2007.
224. Havre, T. E., Near-IR spectroscopy as a method for studying the formation of calcium naphthenate. *Colloid and Polymer Science* **2004**, *282*, (3), 270-279.
225. Eftekhardakhah, M.; Øye, G., Dynamic Adsorption of Organic Compounds Dissolved in Synthetic Produced Water at Air Bubbles: The Influence of the Ionic Composition of Aqueous Solutions. *Energy & Fuels* **2013**, *27*, (9), 5128-5134.

226. Eftekhardakhah, M.; Øye, G., Induction and Coverage Times for Crude Oil Droplets Spreading on Air Bubbles. *Environmental Science & Technology* **2013**, *47*, (24), 14154-14160.
227. Dudek, M.; Øye, G., Removal of Crude Oil Droplets through Spreading on Gas Bubbles Studied with Microfluidics. *Submitted* **2018**.
228. Forster, T.; Rybinski, W. v., Chapter 12 Applications of Emulsions. In *Modern Aspects of Emulsion Science*, Binks, B. P., Ed. The Royal Society of Chemistry: Cambridge, UK, 1998; pp 395-426.
229. Sjöblom, J.; Stenius, P.; Simon, S.; Grimes, B. A., Emulsion Stabilization. In *Encyclopedia of Colloid and Interface Science*, Tadros, T., Ed. Springer: New York, NY, USA, 2013.
230. Dukhin, S. S.; Sjöblom, J.; Sæther, Ø., An Experimental and Theoretical Approach to the Dynamic Behavior of Emulsions. In *Emulsion and Emulsion Stability*, 2nd ed.; Sjöblom, J., Ed. CRC Press: Boca Raton, FL, 2006.
231. Sjöblom, J.; Lindberg, R.; Friberg, S. E., Microemulsions — phase equilibria characterization, structures, applications and chemical reactions. *Advances in Colloid and Interface Science* **1996**, *65*, 125-287.
232. Maoling, L., Research on Protection Measures and Explosion about Aluminum Dust. *Procedia Engineering* **2012**, *43*, 516-518.
233. Tadros, T., Emulsification. In *Encyclopedia of Colloid and Interface Science*, Tadros, T., Ed. Springer Berlin Heidelberg: Berlin, Heidelberg, 2013; pp 363-364.
234. Walstra, P.; Smulders, P. E. A., Chapter 2 Emulsion Formation. In *Modern Aspects of Emulsion Science*, Binks, B. P., Ed. The Royal Society of Chemistry: Cambridge, UK, 1998; pp 56-99.
235. Auflem, I. H. Influence of Asphaltene Aggregation and Pressure on Crude Oil Emulsion Stability. NTNU, Trondheim, Norway, 2002.
236. McClements, D., Colloidal Interactions. In *Food Emulsions. Principles, Practices, and Techniques*, McClements, D., Ed. CRC Press: Boca Raton, FL, USA, 2005.
237. Lucassen-Reynders, E. H., Interfacial viscoelasticity in emulsions and foams *Food Structure* **1993**, *12*, 1-12.
238. Czarnecki, J.; Tchoukov, P.; Dabros, T., Possible Role of Asphaltenes in the Stabilization of Water-in-Crude Oil Emulsions. *Energy & Fuels* **2012**, *26*, (9), 5782-5786.
239. Tambe, D. E.; Sharma, M. M., Factors Controlling the Stability of Colloid-Stabilized Emulsions: I. An Experimental Investigation. *Journal of Colloid and Interface Science* **1993**, *157*, (1), 244-253.
240. Kilpatrick, P. K., Water-in-crude oil emulsion stabilization: Review and unanswered questions. *Energy and Fuels* **2012**, *26*, (7), 4017-4026.
241. Sjöblom, J.; Skodvin, T.; Holt, Ø.; Nilsen, F. P., Colloid chemistry and modern instrumentation in offshore petroleum production and transport. *Colloids and Surfaces A: Physicochemical and Engineering Aspects* **1997**, *123-124*, 593-607.
242. Davies, G. A.; Nilsen, F. P.; Gramme, P. E., The formation of Stable Dispersions of Crude oil and Produced Water: The Influence of Oil Type, Wax & Asphaltene Content, SPE 36587. In *SPE Annual Technical Conference and Exhibition*, Society of Petroleum Engineers: 6-9 October, Denver, Colorado, USA, 1996.
243. Sztukowski, D. M.; Yarranton, H. W., Oilfield solids and water-in-oil emulsion stability. *Journal of Colloid and Interface Science* **2005**, *285*, (2), 821-833.
244. Kralova, I.; Sjöblom, J.; Øye, G.; Simon, S.; Grimes, B. A.; Paso, K., Heavy Crude Oils/Particle Stabilized Emulsions. *Advances in Colloid and Interface Science* **2011**, *169*, (2), 106-127.
245. Arntzen, R.; Andresen, P. A. K., Three-phase Wellstream Gravity Separation. In *Encyclopedic Handbook of Emulsion Technology*, Sjöblom, J., Ed. CRC Press: 2001.
246. Kokal, S. L., Crude Oil Emulsions: A State-Of-The-Art Review. *SPE Production & Facilities* **2005**, *20*, (01).
247. Salager, J.-L.; Forgiarini, A. M., Emulsion Stabilization, Breaking, and Inversion Depends upon Formulation: Advantage or Inconvenience in Flow Assurance. *Energy & Fuels* **2012**, *26*, (7), 4027-4033.



248. Sjöblom, J.; Urdahl, O.; Børve, K. C. N.; Mingyuan, L.; Saeten, J. O.; Christy, A. A.; Gu, T., Stabilization and destabilization of water-in-crude oil emulsions from the norwegian continental shelf. Correlation with model systems. *Advances in Colloid and Interface Science* **1992**, 41, 241-271.
249. Kilpatrick, P. K.; Spiecker, P. M., Asphaltene Emulsions. In *Encyclopedic Handbook of Emulsion Technology*, Sjöblom, J., Ed. Marcel Dekker: New York, NY, USA, 2001; pp 707–730.
250. Nordli, K. G.; Sjöblom, J.; Kizling, J.; Stenius, P., Water-in-crude oil emulsions from the Norwegian continental shelf 4. Monolayer properties of the interfacially active crude oil fraction. *Colloids and Surfaces* **1991**, 57, (1), 83-98.
251. Yarranton, H. W.; Sztukowski, D. M.; Urrutia, P., Effect of interfacial rheology on model emulsion coalescence: I. Interfacial rheology. *Journal of Colloid and Interface Science* **2007**, 310, (1), 246-252.
252. Mullins, O. C.; Sheu, E. Y., *Structures and Dynamics of Asphaltenes*. Springer Science & Business Media: New York, NY, USA, 1998; p 438.
253. Bourrel, M.; Passade-Boupat, N., Crude Oil Surface Active Species: Consequences for Enhanced Oil Recovery and Emulsion Stability. *Energy & Fuels* **2018**, 32, (3), 2642-2652.
254. McLean, J. D.; Kilpatrick, P. K., Effects of Asphaltene Aggregation in Model Heptane–Toluene Mixtures on Stability of Water-in-Oil Emulsions. *Journal of Colloid and Interface Science* **1997**, 196, (1), 23-34.
255. van der Waarden, M., Stability of emulsions of water in mineral oils containing asphaltenes. *Kolloid-Zeitschrift* **1958**, 156, (2), 116-122.
256. Fossen, M.; Sjöblom, J.; Kallevik, H.; Jakobsson, J., A New Procedure for Direct Precipitation and Fractionation of Asphaltenes from Crude Oil. *Journal of Dispersion Science and Technology* **2007**, 28, (1), 193-197.
257. Östlund, J.-A.; Nydén, M.; Auflem, I. H.; Sjöblom, J., Interactions between Asphaltenes and Naphthenic Acids. *Energy & Fuels* **2003**, 17, (1), 113-119.
258. Hemmingsen, P. V.; Li, X.; Peytavy, J. L.; Sjöblom, J., Hydrate Plugging Potential of Original and Modified Crude Oils. *Journal of Dispersion Science and Technology* **2007**, 28, (3), 371-382.
259. Spiecker, P. M.; Kilpatrick, P. K., Interfacial rheology of petroleum asphaltenes at the oil-water interface. *Langmuir* **2004**, 20, (10), 4022-32.
260. Ese, M. H.; Yang, X.; Sjöblom, J., Film forming properties of asphaltenes and resins. A comparative Langmuir–Blodgett study of crude oils from North Sea, European continent and Venezuela. *Colloid and Polymer Science* **1998**, 276, (9), 800-809.
261. Aske, N.; Orr, R.; Sjöblom, J., Dilatational Elasticity Moduli of Water–Crude Oil Interfaces Using the Oscillating Pendant Drop. *Journal of Dispersion Science and Technology* **2002**, 23, (6), 809-825.
262. Bouriat, P.; El Kerri, N.; Graciaa, A.; Lachaise, J., Properties of a Two-Dimensional Asphaltene Network at the Water–Cyclohexane Interface Deduced from Dynamic Tensiometry. *Langmuir* **2004**, 20, (18), 7459-7464.
263. Gafonova, O. V.; Yarranton, H. W., The Stabilization of Water-in-Hydrocarbon Emulsions by Asphaltenes and Resins. *Journal of Colloid and Interface Science* **2001**, 241, (2), 469-478.
264. Georgieva, D.; Schmitt, V.; Leal-Calderon, F.; Langevin, D., On the Possible Role of Surface Elasticity in Emulsion Stability. *Langmuir* **2009**, 25, (10), 5565-5573.
265. Tchoukov, P.; Yang, F.; Xu, Z.; Dabros, T.; Czarnecki, J.; Sjöblom, J., Role of Asphaltenes in Stabilizing Thin Liquid Emulsion Films. *Langmuir* **2014**, 30, (11), 3024-3033.
266. Siffert, B.; Bourgeois, C.; Papirer, E., Structure and water–oil emulsifying properties of asphaltenes. *Fuel* **1984**, 63, (6), 834-837.
267. Freer, E. M.; Radke, C. J., Relaxation of asphaltenes at the toluene/water interface: Diffusion exchange and surface rearrangement. *The Journal of Adhesion* **2004**, 80, (6), 481-496.
268. Skartlien, R.; Simon, S.; Sjöblom, J., DPD Molecular Simulations of Asphaltene Adsorption on Hydrophilic Substrates: Effects of Polar Groups and Solubility. *Journal of Dispersion Science and Technology* **2016**, 37, (6), 866-883.

269. Skartlien, R.; Simon, S.; Sjöblom, J., A DPD study of asphaltene aggregation: The role of inhibitor and asphaltene structure in diffusion-limited aggregation. *Journal of Dispersion Science and Technology* **2017**, 38, (3), 440-450.
270. Zhang, S.-F.; Sun, L. L.; Xu, J.-B.; Wu, H.; Wen, H., Aggregate Structure in Heavy Crude Oil: Using a Dissipative Particle Dynamics Based Mesoscale Platform. *Energy & Fuels* **2010**, 24, (8), 4312-4326.
271. Strassner, J. E., Effect of pH on Interfacial Films and Stability of Crude Oil-Water Emulsions. *Journal of Petroleum Technology* **1968**, 20, (3), 303-312.
272. Yeung, A.; Dabros, T.; Czarnecki, J., On the interfacial properties of micrometre-sized water droplets in crude oil. *Proceedings of the Royal Society A: Mathematical, Physical and Engineering Sciences* **1999**, 455, (1990), 3709-3723.
273. Czarnecki, J.; Moran, K., On the Stabilization Mechanism of Water-in-Oil Emulsions in Petroleum Systems. *Energy & Fuels* **2005**, 19, (5), 2074-2079.
274. Yeung, A.; Dabros, T.; Masliyah, J.; Czarnecki, J., Micropipette: a new technique in emulsion research. *Colloids and Surfaces A: Physicochemical and Engineering Aspects* **2000**, 174, (1), 169-181.
275. Wu, X., Investigating the Stability Mechanism of Water-in-Diluted Bitumen Emulsions through Isolation and Characterization of the Stabilizing Materials at the Interface. *Energy & Fuels* **2003**, 17, (1), 179-190.
276. Jarvis, J. M.; Robbins, W. K.; Corilo, Y. E.; Rodgers, R. P., Novel Method To Isolate Interfacial Material. *Energy & Fuels* **2015**, 29, (11), 7058-7064.
277. Czarnecki, J., Stabilization of Water in Crude Oil Emulsions. Part 2. *Energy & Fuels* **2009**, 23, (3), 1253-1257.
278. Andersen, S. I., Separation of asphaltenes by polarity using liquid-liquid extraction. *Petroleum Science and Technology* **1997**, 15, (1-2), 185-198.
279. Qiao, P.; Harbottle, D.; Tchoukov, P.; Wang, X.; Xu, Z., Asphaltene Subfractions Responsible for Stabilizing Water-in-Crude Oil Emulsions. Part 3. Effect of Solvent Aromaticity. *Energy & Fuels* **2017**.
280. Yang, F.; Tchoukov, P.; Pensini, E.; Dabros, T.; Czarnecki, J.; Masliyah, J.; Xu, Z., Asphaltene Subfractions Responsible for Stabilizing Water-in-Crude Oil Emulsions. Part 1: Interfacial Behaviors. *Energy & Fuels* **2014**, 28, (11), 6897-6904.
281. Sjöblom, J.; Mingyuan, L.; Christy, A. A.; Gu, T., Water-in-crude-oil emulsions from the Norwegian continental shelf 7. Interfacial pressure and emulsion stability. *Colloids and Surfaces* **1992**, 66, (1), 55-62.
282. Wang, X.; Pensini, E.; Liang, Y.; Xu, Z.; Chandra, M. S.; Andersen, S. I.; Abdallah, W.; Buiting, J. J., Fatty acid-asphaltene interactions at oil/water interface. *Colloids and Surfaces A: Physicochemical and Engineering Aspects* **2017**, 513, 168-177.
283. Ortiz, D. P.; Baydak, E. N.; Yarranton, H. W., Effect of surfactants on interfacial films and stability of water-in-oil emulsions stabilized by asphaltenes. *J Colloid Interface Sci* **2010**, 351, (2), 542-55.
284. Ligiero, L. M.; Bouriat, P.; Dicharry, C.; Passade-Boupat, N.; Lalli, P. M.; Rodgers, R. P.; Barrère-Mangote, C.; Giusti, P.; Bouyssièrè, B., Characterization of Crude Oil Interfacial Material Isolated by the Wet Silica Method. Part 1: Gel Permeation Chromatography Inductively Coupled Plasma High-Resolution Mass Spectrometry Analysis. *Energy & Fuels* **2017**, 31, (2), 1065-1071.
285. Ligiero, L. M.; Dicharry, C.; Passade-Boupat, N.; Bouyssièrè, B.; Lalli, P. M.; Rodgers, R. P.; Barrère-Mangote, C.; Giusti, P.; Bouriat, P., Characterization of Crude Oil Interfacial Material Isolated by the Wet Silica Method. Part 2: Dilatational and Shear Interfacial Properties. *Energy & Fuels* **2017**, 31, (2), 1072-1081.
286. Moran, K.; Czarnecki, J., Competitive adsorption of sodium naphthenates and naturally occurring species at water-in-crude oil emulsion droplet surfaces. *Colloids and Surfaces A: Physicochemical and Engineering Aspects* **2007**, 292, (2), 87-98.
287. Xu, Y.; Dabros, T.; Hamza, H.; Shefantook, W., Destabilization of water in bitumen emulsion by washing with water. *Petroleum Science and Technology* **1999**, 17, (9-10), 1051-1070.

288. Gu, G.; Xu, Z.; Nandakumar, K.; Masliyah, J. H., Influence of water-soluble and water-insoluble natural surface active components on the stability of water-in-toluene-diluted bitumen emulsion. *Fuel* **2002**, 81, (14), 1859-1869.
289. Arla, D.; Flesisnki, L.; Bouriat, P.; Dicharry, C., Influence of Alkaline pH on the Rheology of Water/Acidic Crude Oil Interface. *Energy & Fuels* **2011**, 25, (3), 1118-1126.
290. Poteau, S.; Argillier, J.-F.; Langevin, D.; Pincet, F.; Perez, E., Influence of pH on Stability and Dynamic Properties of Asphaltenes and Other Amphiphilic Molecules at the Oil–Water Interface. *Energy & Fuels* **2005**, 19, (4), 1337-1341.
291. Arla, D.; Sinquin, A.; Palermo, T.; Hurtevent, C.; Graciaa, A.; Dicharry, C., Influence of pH and Water Content on the Type and Stability of Acidic Crude Oil Emulsions†. *Energy & Fuels* **2007**, 21, (3), 1337-1342.
292. Goldszal, A.; Hurtevent, C.; Rousseau, G., Scale and Naphthenate Inhibition in Deep-Offshore Fields. In *SPE Oilfield Scale Symposium*, Society of Petroleum Engineers: 30-31 January, Aberdeen, United Kingdom, , 2002.
293. Horváth-Szabó, G.; Czarniecki, J.; Masliyah, J. H., Sandwich Structures at Oil–Water Interfaces under Alkaline Conditions. *Journal of Colloid and Interface Science* **2002**, 253, (2), 427-434.
294. Havre, T. E.; Sjöblom, J., Emulsion stabilization by means of combined surfactant multilayer (D-phase) and asphaltene particles. *Colloids and Surfaces A: Physicochemical and Engineering Aspects* **2003**, 228, (1–3), 131-142.
295. Moradi, M.; Alvarado, V.; Huzurbazar, S., Effect of Salinity on Water-in-Crude Oil Emulsion: Evaluation through Drop-Size Distribution Proxy. *Energy & Fuels* **2011**, 25, (1), 260-268.
296. Wang, X.; Alvarado, V., Effects of Aqueous-Phase Salinity on Water-in-Crude Oil Emulsion Stability. *Journal of Dispersion Science and Technology* **2012**, 33, (2), 165-170.
297. Alves, D. R.; Carneiro, J. S. A.; Oliveira, I. F.; Façanha, F.; Santos, A. F.; Dariva, C.; Franceschi, E.; Fortuny, M., Influence of the salinity on the interfacial properties of a Brazilian crude oil–brine systems. *Fuel* **2014**, 118, 21-26.
298. Rocha, J. A.; Baydak, E. N.; Yarranton, H. W.; Sztukowski, D. M.; Ali-Marcano, V.; Gong, L.; Shi, C.; Zeng, H., Role of Aqueous Phase Chemistry, Interfacial Film Properties, and Surface Coverage in Stabilizing Water-in-Bitumen Emulsions. *Energy & Fuels* **2016**, 30, (7), 5240-5252.
299. Maaref, S.; Ayatollahi, S., The effect of brine salinity on water-in-oil emulsion stability through droplet size distribution analysis: A case study. *Journal of Dispersion Science and Technology* **2018**, 39, (5), 721-733.
300. Acevedo, S.; Gutierrez, X.; Rivas, H., Bitumen-in-Water Emulsions Stabilized with Natural Surfactants. *Journal of Colloid and Interface Science* **2001**, 242, (1), 230-238.
301. Havre, T.; Ese, M.-H.; Sjöblom, J.; Blokhuis, A., Langmuir films of naphthenic acids at different pH and electrolyte concentrations. *Colloid and Polymer Science* **2002**, 280, (7), 647-652.
302. Peña, A. A.; Hirasaki, G. J.; Miller, C. A., Chemically Induced Destabilization of Water-in-Crude Oil Emulsions. *Industrial & Engineering Chemistry Research* **2005**, 44, (5), 1139-1149.
303. Lalli, P. M.; Corilo, Y. E.; Rowland, S. M.; Marshall, A. G.; Rodgers, R. P., Isomeric Separation and Structural Characterization of Acids in Petroleum by Ion Mobility Mass Spectrometry. *Energy & Fuels* **2015**, 29, (6), 3626-3633.
304. Liu, J.; Xu, Z.; Masliyah, J., Studies on Bitumen–Silica Interaction in Aqueous Solutions by Atomic Force Microscopy. *Langmuir* **2003**, 19, (9), 3911-3920.
305. Sanders, R. S.; Chow, R. S.; Masliyah, J. H., Deposition of Bitumen and Asphaltene-Stabilized Emulsions in an Impinging Jet Cell. *Journal of Colloid and Interface Science* **1995**, 174, (1), 230-245.
306. Laroche, I.; Wu, X.; Masliyah, J. H.; Czarniecki, J., Dynamic and static interactions between bitumen droplets in water. *J Colloid Interface Sci* **2002**, 250, (2), 316-26.
307. Salou, M.; Siffert, B.; Jada, A., Study of the stability of bitumen emulsions by application of DLVO theory. *Colloids and Surfaces A: Physicochemical and Engineering Aspects* **1998**, 142, (1), 9-16.

308. Schorling, P. C.; Kessel, D. G.; Rahimian, I., Influence of the crude oil resin/asphaltene ratio on the stability of oil/water emulsions. *Colloids and Surfaces A: Physicochemical and Engineering Aspects* **1999**, 152, (1), 95-102.
309. Skurtveit, R.; Sjöblom, J.; Høiland, H., Emulsions under elevated temperature and pressure conditions. *Journal of Colloid and Interface Science* **1989**, 133, (2), 395-403.
310. Celis, M. T.; Garcia Rubio, L. H., Characterization of Emulsions: A Systematic Spectroscopy Study. *Journal of Dispersion Science and Technology* **2008**, 29, (1), 20-26.
311. Harkins, W. D.; Jordan, H. F., A method for the determination of surface and interfacial tension from the maximum pull on a ring. *Journal of the American Chemical Society* **1930**, 52, (5), 1751-1772.
312. Macy, R., Surface tension by the ring method. Applicability of the du Nouy apparatus. *Journal of Chemical Education* **1935**, 12, (12), 573-576.
313. Hoffmann, E., Stroobant V., *Mass Spectrometry: Principles and Applications*. 3rd ed.; John Wiley & Sons, Inc.: West Sussex, England, 2007.
314. Baroud, C. N.; Gallaire, F.; Dangla, R., Dynamics of microfluidic droplets. *Lab Chip* **2010**, 10, (16), 2032-45.
315. Mashaghi, S.; Abbaspourrad, A.; Weitz, D. A.; van Oijen, A. M., Droplet microfluidics: A tool for biology, chemistry and nanotechnology. *TrAC Trends in Analytical Chemistry* **2016**, 82, 118-125.
316. Mukerjee, P., Dimerization of Anions of Long-Chain Fatty Acids in Aqueous Solutions and the Hydrophobic Properties of the Acids. *The Journal of Physical Chemistry* **1965**, 69, (9), 2821-2827.
317. Pestman, J. M.; Kevelam, J.; Blandamer, M. J.; van Doren, H. A.; Kellogg, R. M.; Engberts, J. B. F. N., Thermodynamics of Micellization of Nonionic Saccharide-Based N-Acyl-N-alkylaldosylamine and N-Acyl-N-alkylamino-1-deoxyalditol Surfactants. *Langmuir* **1999**, 15, (6), 2009-2014.
318. Heerklotz, H.; Epand, R. M., The Enthalpy of Acyl Chain Packing and the Apparent Water-Accessible Apolar Surface Area of Phospholipids. *Biophysical Journal* **2001**, 80, (1), 271-279.
319. Zhang, K.; Pereira, A. S.; Martin, J. W., Estimates of Octanol-Water Partitioning for Thousands of Dissolved Organic Species in Oil Sands Process-Affected Water. *Environmental Science & Technology* **2015**, 49, (14), 8907-8913.
320. Sarac, S.; Civan, F., Mechanisms, Parameters, and Modeling of Naphthenate-Soap-Induced Formation Damage. *Society of Petroleum Engineers Journal* **2009**, 14, (2), 259-266.



PAPER I

---

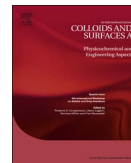
Equilibrium partitioning of naphthenic acids and bases and their consequences on interfacial properties





Contents lists available at ScienceDirect

## Colloids and Surfaces A

journal homepage: [www.elsevier.com/locate/colsurfa](http://www.elsevier.com/locate/colsurfa)

# Equilibrium partitioning of naphthenic acids and bases and their consequences on interfacial properties

Are Bertheussen\*, Sébastien Simon, Johan Sjöblom

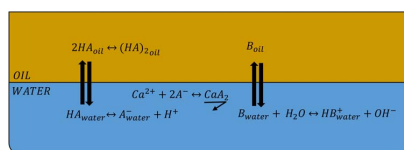
Ugelstad Laboratory, Department of Chemical Engineering, Norwegian University of Science and Technology (NTNU), N-7491 Trondheim, Norway



## HIGHLIGHTS

- Partitioning of acids and bases to determine water quality of produced water.
- Equilibrium partitioning of acids and bases vs pH, with or without calcium.
- No interfacial interactions were detected between acids and bases.

## GRAPHICAL ABSTRACT



## ARTICLE INFO

### Keywords:

Equilibrium partitioning  
Interfacial tension  
Interfacial interaction  
Partition ratio  
Distribution ratio

## ABSTRACT

This article aims to create a model to accurately predict the equilibrium partitioning of naphthenic acids and basic crude oil components between the oil and water phase. The model was tested on 2 acids and 2 bases. After a review of the properties of crude oil acids and bases, the equilibrium partitioning of acids and bases with different molecular weight was analyzed over a pH interval using heptane as the oil phase and 3.5 wt.% NaCl as the water phase. Phenylacetic acid would represent the low molecular weight acid while 4-heptylbenzoic acid was chosen to represent the high molecular weight one. Likewise, 4-ethylaniline and 4-decylaniline were chosen as corresponding bases. The partitioning of the two acids and the low molecular weight base was successfully modelled by considering the acid dissociation constant  $pK_a$  in aqueous phase and the partition ratio  $P_{wo}$  of the non-ionized species between oil and aqueous phase. The high molecular weight base did not significantly partition into the aqueous phase at the pH range studied. The results show that acid species are more water soluble than basic species of similar molecular weight. In presence of calcium the partitioning of acids is successfully modelled by accounting for the precipitation of naphthenate soap with a solubility constant  $K_s$ . The kinetic interfacial tension between heptane and 3.5% NaCl aqueous buffer was also analyzed with oils that contained single compounds, two bases, two acids and all four components over a pH interval to identify any interfacial acid-base interactions. No significant interfacial interaction could be identified, mostly due to similar  $pK_a$  values.

## 1. Introduction

Crude oils have been produced for over one hundred years. The conventional oil resources are slowly running out [1] while energy demands continue to increase [2]. Development of demanding fields can become economically viable by implementing new technological solutions in areas like subsea production and processing [3,4]. One aspect of subsea processing entails liquid–liquid separation [1,3,5]. Three subsea liquid–liquid separators have been installed to date: Troll

C, Tordis and Marlim; all of which were designed to inject (e.g. into a disposal reservoir) or reinject (e.g. into the production reservoir) the produced water [6]. Produced water is generated during the production of oil and gas [7] and it contains both dissolved and dispersed oil components [8]. Several oil companies have envisioned a futuristic scenario where an entire production and processing facility would operate on the seafloor, eliminating the need for topside processing all together [6,9,10]. To achieve export quality crude oil from such a facility, additional oil dehydration steps would be required. The water

\* Corresponding author.

E-mail address: [are.bertheussen@ntnu.no](mailto:are.bertheussen@ntnu.no) (A. Bertheussen).

<http://dx.doi.org/10.1016/j.colsurfa.2017.05.068>

Received 6 March 2017; Received in revised form 2 May 2017; Accepted 23 May 2017

Available online 26 May 2017

0927-7757/© 2017 Elsevier B.V. All rights reserved.



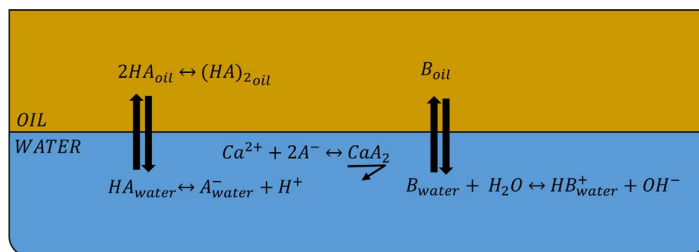


Fig. 1. Schematic illustration of the acid and base equilibria that occurs in oil water systems. Depicted are dimerization of acids in oil phase, partitioning of acid between oil and water phase, dissociation of acid in water phase, metal soap precipitation in the water phase or at the interface, partitioning of the base between the oil and water phase and protonation of the base in the water phase.

quality from these dehydration steps might require additional or different treatment to reach injection or discharge criteria. This paper will focus on the dissolved components in the produced water.

Production of biodegraded crude oil is increasing as reserves of conventional light oil are running low [11]. Biodegradation is known to lower the oil quality by, for example, decreasing the API gravity and increasing the total acid number (TAN) of the crude oil [12]. The total base number (TBN) has also been found to increase with biodegradation [13]. These acids and bases in crude oil will partition themselves between the oil and water phase or at the interface depending on parameters like molecular size, structure and pH [14,15]. This article will focus on the equilibrium partitioning of naphthenic acids and bases and the interfacial interactions between such compounds.

## 2. Structure and properties of acids and bases

### 2.1. Definition

The term “naphthenic acids” has become ambiguous as noted by Grever, Young, Whittall and Fedorak [11]. Although the traditional definition is that of a carboxylic acids with a naphthene ring, it can apparently be used to describe all organic acids found in crude oil [16,17]. Naphthenic acids have a high diversity in size and structure [18] with an average molecular weight of 300–500 g/mol [19]. On a structural basis, they are often described by the isomer  $C_nH_{2n+z}O_2$ . The  $n$  represents the number of carbon atoms while  $z$  is a negative, even integer specifying the hydrogen deficiency [20,21]. Oxy-naphthenic acids with the general formula  $C_nH_{2n+z}O_x$  have also been introduced to describe naphthenic acids with added hydroxyl groups or multiple carboxylic groups ( $x \geq 3$ ) [22] like the ARN acid responsible for calcium naphthenate deposition [23,24]. Naphthenic acids can stabilize water in oil (W/O) and oil in water (O/W) emulsions depending on several conditions, especially pH [17,25], cause corrosion [26] or naphthenate deposits [27]. They have a detrimental effect on the environment and are toxic to a variety of aquatic organisms [28]. Although acidic crude oils are problematic, the naphthenic acids can also, through their dispersive properties, limit problems related to adhesion or sedimentation [29].

The basic components in crude oil are nitrogen compounds, especially pyridines and its homologues [30–32]. Amines are generally not present or at low concentration in crude oils [30]. However, they have been used to model crude oil bases as mentioned below. The nitrogen content in crude oil is generally around 0.1%–0.9%wt [33] and studies suggest that only 30%–50% of the nitrogen compounds are basic nitrogen compounds [33,34]. There are basic components in both the resin and asphaltene fractions of crude oil although some studies found the basic fraction of asphaltenes to be small compared to the basic fraction of resins [13,34]. Both Eftekhardadkhal, Kløcker, Trapnes, Gawel and Øye [35] and Nenningsland, Simon and Sjöblom [36] found that basic crude oil species had lower surface affinity at low pH when they are protonated compared with acidic crude oil species at high pH when they are ionized.

### 2.2. Oil water partitioning

In oil water systems, acids and bases will partition between the oil and water phase, depending on parameters like pH, pressure, temperature and the hydrophilic-lipophilic balance (HLB) value of the compounds. Fig. 1 depicts some of the equilibria encountered when considering acids and bases in oil water systems.

Havre, Sjöblom and Vindstad [14] studied the partitioning of naphthenic acids using crude oil acids and commercial acids. The study found that naphthenic acids in crude oil water systems had a  $pK_a$  of 4.9, which is in the lower range of the 5–6 reported by Brient, Wessner and Doyle [20]. The study also found that the linear relationship between the logarithm of the partitioning constant and the number of carbons in the molecule, reported for low molecular weight fatty acids by Reinsel [37], is also valid for higher molecular weight naphthenic acids. Touhami, Hornof and Neale [38] presented a comprehensible partitioning diagram and set of equations, accounting most of the equilibria encountered for organic acid in oil water systems, even for the partitioning of naphthenate soap back into the oil phase.

Stanford, Kim, Klein, Smith, Rodgers and Marshall [39] analyzed the water solubility of nitrogen compounds in crude oils. They found that the basic water soluble fractions of the crude oil had a lower hydrogen to carbon ratio and more nitrogen compared to the molecular distribution of bases in the two crude oils, as would be expected due to lower hydrophobic part and higher polarity. Eftekhardadkhal, Kløcker, Trapnes, Gawel and Øye [35] studied the effect of pH on the solubility of nitrogen compounds in produced water. By mixing 7 crude oils with water at different pH they found that nitrogen concentration in water decreased with increasing pH from 2 to 8 for 6 of the 7 crude oils tested. This trend is likely caused by pyridinic nitrogen compounds which ionize at low pH. The exception could be caused by the presence of zwitterionic compounds. Hutin, Argillier and Langevin [15] studied the mass transfer of acidic and basic species from the oil phase to the water phase. A model based on the equations from Havre, Sjöblom and Vindstad [14] and Hurtevent, Bourrel, Rousseau and Brocart [19] was fitted with initial pH and final pH measurement to obtain average partitioning constants for the acids and bases. With the obtained average partitioning constants, their model could to some degree predict the final pH of a crude oil water system based on TAN, TBN and the initial pH. In a subsequent study they also reported significantly higher mass transfer of bases from crude oil when the surfactant sodium dodecyl benzenesulfonate (SDBS) was present [40]. Lord, Demond and Hayes [41] measured the distribution of dodecylamine in xylene salt-water systems over a pH range from 3 to 11. Their results show that the base had a greater affinity for the oil phase at pH values over 6 and that although the  $pK_a$  for the base was 10.6 the interfacial tension did not start to change before lowering the pH to < 8. Celsie, Parnis and Mackay [42] used COSMO-RS solvation theory to model how salinity, temperature and pH would affect the naphthenic acid concentration in water for 55 representative naphthenic acids. The predicted partition ratios had adequate fits to experimental data. Their model showed that the partitioning tendency over increasing temperature was towards unity i.e. mainly oil soluble components became more water soluble

and vice versa. They concluded that salinity has modest impact on partition and distribution ratios compared to the high impact of temperature and pH. Their model also includes some interesting predictions of how the inclusion of a sulphur/nitrogen atom or changing a ring from aromatic to non-aromatic would change the behavior of an otherwise similar naphthenic acid.

In this study, the equilibrium partitioning of acids and bases with lower and higher molecular weight will be considered over the pH range. The goal is to determine the partitioning ratio for model acids and bases and obtain insight into how molecular weight influences the behavior of these compounds in two phase systems.

### 2.3. Modelling partition ratio with pH

In an oil-water system, the acids and bases in the system would partition themselves between the phases through the following equilibria.



These equilibria can be described by the following partition constants

$$K_{wo,HA} = \frac{[HA]_w}{[HA]_o} \quad (3)$$

$$K_{wo,B} = \frac{[B]_w}{[B]_o} \quad (4)$$

where  $[HA]_w$  and  $[B]_w$  represents the acid and base concentration in the water phase,  $[HA]_o$  and  $[B]_o$  represents the acid and base concentration in the oil phase,  $K_{wo,HA}$  represents the partition constant of the acid and  $K_{wo,B}$  represents the partition constant of the base. This partition constant is independent of concentration, but varies with temperature and pressure. Concentrations were used instead of activities as activity coefficients were assumed to be equal to 1 due to low concentrations. The carboxylic group makes the acids prone to associate into dimers in the oil phase [43]. Goodman [43] reported dimer association constants for C<sub>8</sub>-C<sub>14</sub> fatty acids in heptane to be 10<sup>3</sup>–10<sup>4</sup>, showing the dimer to be a stable and predominant form in the organic over a wide range of concentrations. Dimers form in the oil phase through the following equilibria



where  $(HA)_2$  is the dimer. The article by Havre, Sjöblom and Vindstad [14] stays true to the IUPAC definition [44] of the partition constant where only the monomer in each of the two phases is considered, but the article does not account for dimers in the mass balance. Equilibria like dimers give rise to numerous definitions of partition coefficient and similar terms reported in the literature [38,41,45,46]. Mukerjee [47] studied dimerization of fatty acid anions in the water phase. They showed that the formation of trimers and higher aggregates are negligible compared to dimers and that the dimerization constant increase with increasing alkyl chain length, up until palmitate. Dimers of amines are also mentioned in the literature, this time in the water phase [41]. Unaccounted equilibria like dimerization, micellation and hydration can make the measured partition constant  $K_{wo}$  concentration dependent, which is why consideration should be given to what species of the compound are measured by the chosen method of analysis [45].

Scherrer and Howard [48] defined a partition ratio  $P_{wo}$  (then called partition coefficient) by the amount of nonionized compound in each phase which seems to be interpreted as the following equation.

$$P_{wo} = \frac{[HA]_w}{[HA]_{o,tot}} = \frac{[HA]_w}{[HA]_o + 2[(HA)_2]_o} \quad (6)$$

$$P_{wo} = \frac{[B]_w}{[B]_{o,tot}} \quad (7)$$

The partition ratio term is not independent of concentration, as the ratio of the two monomers in each phase would be, but it can be a more practical term due to ease of measurement. Spildo and Høiland [45] showed that the partition ratio of 4-heptylbenzoic acid did not vary much with concentration at acidic pH.

Scherrer and Howard [48] also defined a distribution ratio  $D_{wo}$  (then called distribution coefficient) which accounts for all forms of the compound in each phase.

$$D_{wo} = \frac{[HA]_{w,tot}}{[HA]_{o,tot}} = \frac{[HA]_w + [A^-]_w}{[HA]_o + 2[(HA)_2]_o} \quad (8)$$

This term can be useful when the compound can dissociate in water. For monoprotic acids and bases the term can be linked to the partition ratio by the following equations.

$$\log(D_{wo,acids}) = \log(P_{wo,acids}) - \log\left(\frac{1}{1 + 10^{pH-pK_a}}\right) \quad (9)$$

$$\log(D_{wo,bases}) = \log(P_{wo,bases}) - \log\left(\frac{1}{1 + 10^{pK_a-pH}}\right) \quad (10)$$

Eqs. (9) and (10) can be used to calculate the pH at which a phase shift would occur, if the  $pK_a$  and  $P_{wo}$  of the compound is known by setting the left side term to zero.

Standal, Blokhuis, Haavik, Skauge and Barth [46] compared the distribution ratios of an acid (1-Naphtoic acid), a phenol (5-Indanol) and a base (Quinoline), and showed how they varied with pH. They found that the phase transfer occurred at the  $pK_a$  for all three compounds, which differs with the results from other authors [14,48]. They also found that the unprotonated base had a higher affinity for the oil phase than both the phenol and the acid due to the lower polarity.

In the water phase, the acids and bases can also deprotonate/protonate to form their conjugate bases and acids through the following equilibria.



These can be described by the following dissociation constants.

$$K_{a,HA} = \frac{[A^-]_w [H^+]_w}{[HA]_w} \quad (13)$$

$$K_{a,HB^+} = \frac{[H^+]_w [B]_w}{[HB^+]_w} \quad (14)$$

By introducing some new terms, the following mass balances can be applied to the system,

$$[HA]_{o,init} V_o = [HA]_{w,tot} V_w + [HA]_{o,tot} V_o \quad (15)$$

$$[B]_{o,init} V_o = [B]_{w,tot} V_w + [B]_o V_o \quad (16)$$

where  $[HA]_{o,init}$  and  $[B]_{o,init}$  represents the initial concentration of acid and base in the oil phase, and  $[HA]_{w,tot}$  and  $[B]_{w,tot}$  represents the sum of dissociated and undissociated acids and base in the water phase. The terms  $V_o$  and  $V_w$  denote the volume of the oil and water phase.

The equation sets consisting of Eqs. ((6), (13), (15)) for acids and Eqs. ((7), (14), (16)) for bases can be combined to form an expression for the total acid or base content in the water phase as presented below.

$$[HA]_{w,tot} = \frac{[HA]_{o,init}}{\frac{[H^+]_w}{P_{wo,acid}(K_{a,HA} + [H^+]_w)} + \frac{V_w}{V_o}} \quad (17)$$

$$[B]_{w,tot} = \frac{[B]_{o,init}}{\frac{[K_{a,HB^+}]}{P_{wo,base}(K_{a,HB^+} + [H^+]_w)} + \frac{V_w}{V_o}} \quad (18)$$

It is assumed that the protonated base  $HB^+$  and deprotonated acid

$A^-$  are completely insoluble in oil phase.

If the water phase contains divalent cations like calcium, other phenomena can occur, like precipitation of metal naphthenates [49] or solvating metal naphthenates in the crude oil [50]. Spildo and Høiland [45] found that the distribution ratio was greatly affected by calcium in their studies on 4-heptylbenzoic acid. The problems related to naphthenate deposits [27] led to increased research effort for mapping the behavior of naphthenic acids in systems with divalent cations [51–54].

The solubility product constant for divalent cations with monoprotic naphthenic acids can be expressed by the following equation.

$$K_{S,MA_2} = [M^{2+}][A^-]^2 \quad (19)$$

This can be combined with Eqs. (6) and (13) to make the following expressions for the acid concentration in oil and water at the solubility limit.

$$[HA]_{w,tot} = \sqrt{\frac{K_{S,MA_2}}{[M^{2+}]}} \left( 1 + \frac{[H^+]}{K_{a,HA}} \right) \quad (20)$$

$$[HA]_{o,tot} = \sqrt{\frac{K_{S,MA_2}}{[M^{2+}]}} \left( \frac{[H^+]}{P_{wo}K_{a,HA}} \right) \quad (21)$$

The equations with solubility products are only valid for systems with precipitate.

#### 2.4. Interfacial tensions of naphthenic acids and bases

Organic acids and bases can have an amphiphilic nature which allows them to adsorb and desorb at the oil-water interface and lower the interfacial tension. If the adsorption rate is larger than the desorption, then the interfacial tension decreases over time until the desorption rate matches the adsorption rate and the interfacial tension is at equilibrium [55]. Crude oil can contain both surface active acids and bases as shown by Buckley, Takamura and Morrow [56]. They demonstrated that the interfacial charge changed from negative to positive at low pH, indicating both acidic and basic species at the interface. Interfacial tension in oil water systems with an organic acid has been reported to decrease with pH [14,57,58], go through a minimum [59,60] or remain constant [45,46].

Rudin and Wasan [59] and [60] found that the interfacial tension of oleic and octanoic acid went through a minimum upon increasing the pH. The minimum occurred at the point where the acid had equal distribution in both phases and it was theorized to be a synergetic effect between ionized and non-ionized acids at the interface. Interfacial tension of naphthenic acids has been studied by multiple authors [14,46]. As with organic acids, the interfacial tension of organic bases depend on pH [61]. Lord, Demond and Hayes [41] studied the interfacial tension of dodecylamine over various pH values and found that the interfacial tension first started to decrease well below the  $pK_a$  of the compound. Likewise, Cratin [57] showed that the interfacial tension for stearic acid continued to decrease at pH values much higher than the  $pK_a$  of the acid. The pH at the interface was shown to be related to the bulk phase pH through the following equation [14,57].

$$pH_{int} = pH_{bulk} + \frac{e\psi}{2.3kT} \quad (22)$$

where  $pH_{int}$  is the pH at the interface,  $pH_{bulk}$  is the pH in the bulk phase,  $e$  is the electronic charge,  $\psi$  is the interfacial potential,  $k$  is the Boltzmann constant and  $T$  is the temperature. The interfacial  $pK_a$  of the acids studied by Cratin [57] and Joos [62] were calculated to be 3–5 pH values above the bulk phase  $pK_a$ , which explains why the interfacial tension continues to decrease well above the bulk phase  $pK_a$  of the acid. Much of the previously mentioned work builds on Danielli [58] who used the Donnan equilibrium to relate the interfacial pH to the bulk phase pH in his work on oleic and palmitic acid. They found that the difference between bulk pH and interfacial pH increased with bulk

phase pH for acids and decreased with salinity. For organic bases it was shown by using experimental data on hexadecylamine from Peters [63] that the difference between interfacial pH and bulk pH decreased with increasing bulk pH as one would expect. Spildo and Høiland [45] demonstrated the salinity dependence of the interfacial pH vs the bulk pH when they showed that the interfacial tension in an oil-water system with 4-heptylbenzoic acid remained unchanged at increasing pH for distilled water.

Standal, Blokhuis, Haavik, Skauge and Barth [46] compared the interfacial tension over pH for acid (1-Naphtic acid), a phenol (5-Indanol) and a base (Quinoline) of similar structure. Their results show the interfacial tension of the system with the acid to be unaffected by pH, while the system with the phenol shows a decrease of interfacial tension as the pH reaches the  $pK_a$ . The system with the base exhibits a drop in interfacial tension around pH 6, which according to the authors, show that the unprotonated base is more interfacially active than the protonated base. It should however be mentioned that none of these molecules include a hydrophobic tail.

Acids and bases can react through proton transfer in solution to form ammonium carboxylate complexes, resulting in an 1:1 complex or in the case of acid excess, 3:1 complexes as demonstrated with fatty acids and amines by Saeten, Sjoblom and Gestblom [64]. Surface properties of these complexes have also been studied [65–67] and found that the surface activity of the mixtures are greater than that of the individual components due to the strong interaction between the oppositely charged head groups. It is also reported that the ratio is usually of an equimolar nature and that the complex interactions decrease with ionic strength. Ebeltoft, Sjoblom, Saeten and Olofsson [67] compared the compression stabilities of Langmuir films made up of one of two acids (Stearic acid and Arachidic acid) combined with one of three amines (butyl, hexyl and octyl). They found that stearic acid was only able to make a stable film with octylamine, whereas arachidic acid could make stable films with the two smaller amines. Complexes of fatty acids and fatty amines have been observed to drastically change the properties of emulsions [64]. Spildo, Blokhuis and Andersson [68] studied the interfacial interactions between octanoic acid and octylamine to find that the interfacial tension was significantly lower when both acid and base were present at the interface, compared to either compound alone. The effect was shown to be greatest for equimolar mixtures. The synergetic effect was only observed when the pH of the system was such that both species were ionized. Experimenting with amines and carboxylic acids in oil-water systems, Peters [63] mentions the appearance of a tension buffering effect, which keeps the interfacial tension around the same value over a large range of different bulk pH values.

This article aims to assess how relevant acids and bases partition between the oil phase and the water phase. The influence of chain length of acids and bases will be determined. The partition ratio  $P_{wo}$  will be evaluated at the pH where no ionized acid or base is present in the water phase. Eqs. (17) and (18) will be used to obtain the dissociation constant  $pK_a$  of the acid or base that gives the model the best fit. The effect of divalent cations on the partitioning behavior of the acids will be evaluated to observe if the partitioning changes in the presence of calcium.

The interfacial tension of single components and mixtures of organic acids and anilines will be analyzed to observe possible acid base interactions. Bases present in crude oil are pyridine-derivatives. However, long chain pyridines are not commercially available. Consequently, we have chosen to use aniline-derivatives as the base components due to its  $pK_a$  being like the  $pK_a$  of pyridine. The choice is not a perfect one. However, we think this is better than using amine-derivatives as frequently seen in the literature. Dimerization of bases will not be considered in this study. Dimerization of carboxylates in the aqueous phase will not be considered either, based on the dimerization constants from Mukerjee [47]. Partitioning of metal soaps into the oil phase can occur, but this has not been included into the model. Data obtained through

these studies will be used as a basis for subsequent studies into the kinetics of acid and base partitioning and modelling through dissipative particle dynamics (DPD).

### 3. Materials and methods

#### 3.1. Chemicals

The chemicals used as model acids and bases for crude oil acids and bases of different molecular weight are listed in Table 1, along with their abbreviations. The compounds were used without further purification. Compounds with an aromatic ring were chosen to be measured with Ultraviolet (UV) spectroscopy. Heptane was obtained from Sigma Aldrich, > 99% purity.

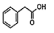
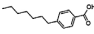
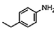
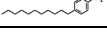
#### 3.2. Equilibrium partitioning

Heptane solutions with the following concentrations were prepared: 1 mM 4HBA, 10 mM PAA, 10 mM 4EA and 10 mM 4DA. 3.5 wt.% NaCl aqueous solutions were prepared with ultra-pure water (MilliQ resistivity of 18.2  $\Omega$  millipore), adjusted with 0.1 M NaOH or 0.1 M HCl solutions which also contained 3.5 wt.% NaCl. Equal volumes of oil and water phase (between 10 and 15 mL) were shaken at 200 rpm for 24 h. Complete phase separation was often obtained within minutes; centrifugation was used when necessary. The pH was measured before and after. The equilibrium concentrations of both phases were determined by UV spectroscopy. When some concentrations fell below the detection limit of the UV spectroscopy, a larger volume (100 mL or 400 mL of each phase) was shaken before the water phase was removed. The pH of the water phase was adjusted before a smaller volume of pure heptane was added to the water phase and shaken over night to extract acids or bases from the water phase. The heptane phase was then evaporated to increase the concentration before UV analysis. The water phase in the high-volume experiment with low pH for the high molecular weight base (4DA) was adjusted to high pH before extraction. The water phase in the experiments with calcium contained 3.5 wt.% NaCl and 10 mM CaCl<sub>2</sub>. The pH of the solutions was adjusted with 0.1 M HCl solution with 3.5 wt.% NaCl and 10 mM CaCl<sub>2</sub> or 0.1 M NaOH solution with 3.5 wt.% NaCl.

#### 3.3. UV spectroscopy

Calibration standards of the acids and bases in both phases were used to create calibration curves for quantification. A water phase adjusted to pH 12 was necessary to dissolve the high molecular weight acid 4HBA in the water phase. A calibration curve for the high molecular weight base 4DA in water could not be obtained due to limited solubility of this compound. The UV-vis recording spectrophotometer was of the type SHIMADZU UV-2401PC. It should be noted that the UV spectra are sensitive to pH of the aqueous phase. Adjusting the pH to lower than 2 in case of bases or higher than 12 in case of acid assures complete ionization in the aqueous solution to analyze ensured consistent absorption spectra.

**Table 1**  
Chemicals used as model acids and bases, their properties, structure, supplier and quality.

Name	Molecular mass (g/mol)	Chemical structure	Supplier	Purity
Phenylacetic acid (PAA)	136		Sigma	99%
4-heptyl benzoic acid (4HBA)	220		VWR	99%
4-ethylaniline (4EA)	121		Sigma	98%
4-decylaniline (4DA)	233		Sigma	97%

#### 3.4. Interfacial tension studies

Interfacial tension measurements were performed using a Du Nöuy ring connected to a KSV Sigma 70 tensiometer. Heptane was used as the oil phase and the water phase was made up of 3.5 wt.% NaCl and the aqueous buffers listed in Table 2.

Single compound experiments had heptane solutions with 1 mM of a single acid or single base.

Multi compound experiments had heptane solutions containing either 1 mM of each acid, 1 mM of each base or 1 mM of each acid and each base.

15 mL of buffer was added to the glass vessel and its surface tension was measured to check the absence of surface active impurities. 15 mL of oil phase was added carefully to the glass vessel with the ring submerged under the aqueous surface. The interfacial tension was then measured for 6 h. Over the course of the experiment the acids and bases in the oil phase would partition themselves between the phases depending on the pH. Evaporation of heptane was limited by covering the samples. pH was measured before and after the experiment and no variation of pH was observed.

### 4. Results and discussion

#### 4.1. Equilibrium partitioning of the low molecular weight model acid

The equilibrium partitioning of phenylacetic acid (PAA) between heptane and 3.5 wt.% NaCl water as a function of equilibrium pH is presented in Fig. 2. PAA shows a high affinity for the water phase even at low pH levels and fully partition into the water phase when the pH reaches around 4.5. The partition ratio  $P_{wo}$  was calculated from the lowest pH experiments where the acid was assumed to be fully protonated in the water phase and was found to be 7.8. The  $pK_a$  was fitted to Eq. (17) and was found to be 3.2, which is much lower than the reported value of 4.3 [70]. Benzoic acid is reported to have a  $pK_a$  of 4.2 and acids with the carboxyl group farther away from the aromatic ring like phenylacetic acid would be expected to have a higher  $pK_a$  [70]. However, the uncertainty associated to the  $pK_a$  value is high because the concentration of PAA in water changes by only 10% over the pH range. Consequently, the fitting of the data points with Eq. (17) is difficult.

#### 4.2. Equilibrium partitioning of the high molecular weight model acid

The equilibrium partitioning of 4-heptylbenzoic acid (4HBA) in heptane and 3.5 wt.% NaCl water as a function of equilibrium pH is shown in Fig. 3. The larger acid, 4-heptylbenzoic acid, has a low affinity for the water phase at lower pH values before a complete phase transfer to heptane around pH 8 as seen in Fig. 3. The acid was first studied at the same initial concentration as the rest of the model compounds (10 mM), but was diluted due to the formation of an inseparable viscous mixture at high pH levels. Spildo and Høiland [45] also encountered this problem at pH values around 8, using 1.5 mM initial concentration, 42% water cut. They noted that the problem only occurred for water containing NaCl and not with the distilled water. To measure the water concentration at low pH levels, high volume experiments with initial

**Table 2**  
List of different aqueous buffers prepared [69].

pH	Buffers
2	0.01 M HCl
4	0.1 M CH <sub>3</sub> COOH adjusted with NaOH
6	0.2 M KH <sub>2</sub> PO <sub>4</sub> adjusted with NaOH
8.5	0.05 M Borax adjusted with HCl
10	0.05 M Borax adjusted with NaOH

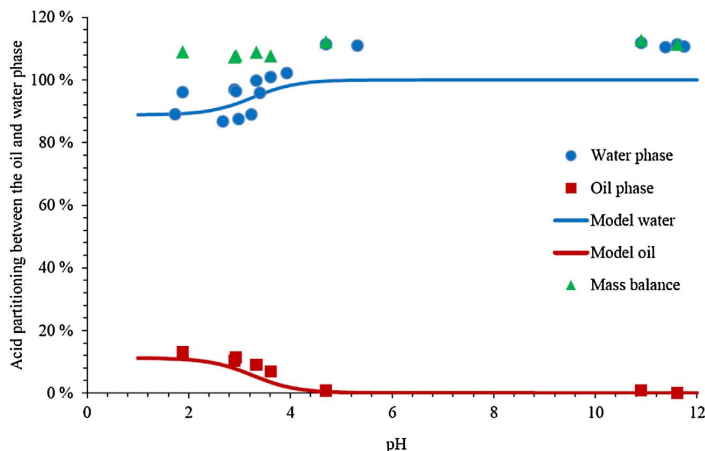


Fig. 2. Equilibrium partitioning of the low molecular weight acid, Phenylacetic acid (PAA) in a heptane and aqueous phase (3.5 wt.% NaCl) over a range of equilibrium pH values. Initial concentration in heptane was 10 mM, data fitted by Eq. (17).

acid concentration of 10 mM were conducted. From the low pH experiments the partition ratio  $P_{wo}$  was calculated to be  $3.7 \times 10^{-4}$ . By fitting the data to Eq. (17) the  $pK_a$  of 4.6 was calculated, which is somewhat lower than the  $pK_a$  of 5–6 for naphthenic acids reported by [20], although acids with an aromatic ring would be expected to have a lower  $pK_a$ . Havre, Sjöblom and Vindstad [14] obtained similar values for 4HBA with a  $pK_a$  to be 5 and the  $P_{wo}$  to be  $1.2 \times 10^{-4}$ , although they mention that the  $pK_a$  found was unexpectedly high and that other equilibria might have interfered. There is a discrepancy between the concentration profile predicted by Eq. (17) and the measured values. This might be caused by other equilibria not accounted for in the mass balance like dimerization, hydration, micelle formation. With the obtained values  $P_{wo}$  and  $pK_a$  the distribution ratio from Scherrer and Howard [48] (Eq. (9)) predicts a phase transfer around pH 8.03 which corresponds perfectly with the observed behavior. Since the maximum concentration of acid in the aqueous phase equals the initial concentration in the oil phase, the sodium naphthenate soap does not partition into the oil phase at any measurable level.

#### 4.3. Equilibrium partitioning of the low molecular weight model base

The equilibrium partitioning of 4-ethylaniline (4EA) in heptane and 3.5% NaCl water as a function of equilibrium pH is shown in Fig. 4. 4-Ethylaniline is solely water soluble at low pH values, before it partially partitions into the oil phase around pH 4. At higher pH levels, around 10% of the base remains in the water phase irrespective of pH. The  $P_{wo}$

was calculated at high pH to be 0.099 and the  $pK_a$  was calculated with Eq. (18) to be 5.1. This matches literature values for *n*-ethylaniline [71]. With the obtained  $P_{wo}$  and  $pK_a$ , the distribution ratio (Eq. (10)) indicate a phase transfer at pH 4.15, from mostly water soluble at low pH to mostly oil soluble at high pH, which fits well with the observed values. The incomplete phase transfer is likely due to the increased affinity of aromatic rings towards the aqueous phase.

#### 4.4. Equilibrium partitioning of the high molecular weight model base

The equilibrium partitioning of 4-decylaniline (4DA) in heptane and 3.5 wt.% NaCl water as a function of equilibrium pH is shown in Fig. 5. The high molecular weight base 4DA did not partition into the water phase, even at low pH levels which in turn meant no water phase calibration curve could be obtained. No UV signal was registered from the water phases after the equilibrium studies. High volume (100 mL of each phase) experiments at high pH (pH 12) and low pH (pH 2) followed by heptane extraction showed that the 4DA has comparable partitioning into the water phase at both high and low pH, albeit, slightly higher for the low pH experiments as would be expected. From the high volume, high pH equilibrium experiments, the  $P_{wo}$  was calculated to be  $7.8 \times 10^{-4}$ . The  $pK_a$  could not be found through Eq. (18) because of the low solubility of this compound in the aqueous phase.

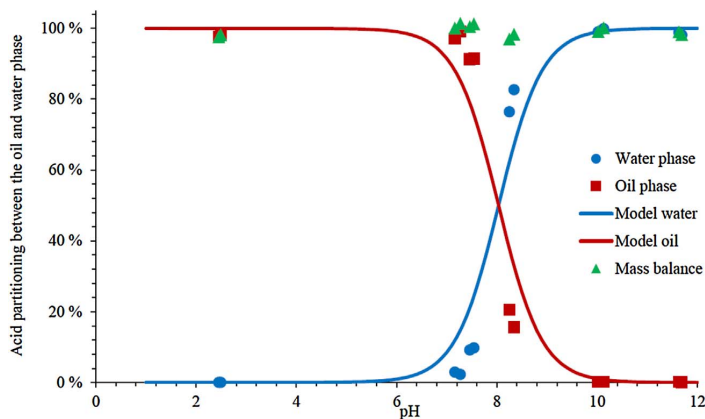


Fig. 3. Equilibrium partitioning of the high molecular weight acid, 4-heptylbenzoic acid (4HBA), in heptane and aqueous phase (3.5 wt.% NaCl) over a range of equilibrium pH values. The initial concentration in the oil phase was 1 mM. The data was fitted by Eq. (17).

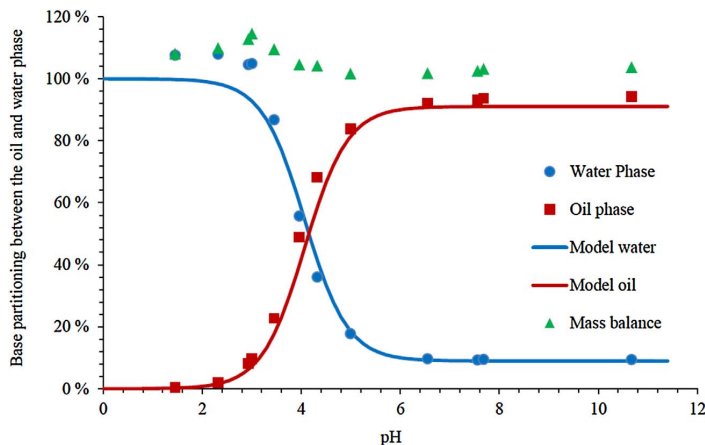


Fig. 4. Equilibrium partitioning of the low molecular weight base 4-ethylaniiline(4EA) in heptane and aqueous phase (3.5 wt.% NaCl) given as a function of equilibrium pH. Initial concentration in heptane was 10 mM and the data was fitted with Eq. (18).

4.5. Comparison of  $P_{wo}$  and  $pK_a$

Table 3 presents the  $P_{wo}$  and  $pK_a$  of the 2 model acids and 2 model bases studied in the equilibrium partitioning experiments. From the table, it can be noted that acids are more soluble than bases of equivalent molecular weight. The  $pK_a$  of the acids and bases are also similar. A good fit can be obtained with Eqs. (17) and (18), but it seems the influence of other equilibria can be seen in Fig. 3 with 4HBA. It should be pointed out again that the partition ratio, by the way it is defined, is concentration dependent to some degree if dimerization takes place in the oil phase. However, it is used as a constant when Eqs. (17) and (18) are used to find the  $pK_a$ .

4.6. Partitioning of the low molecular weight acid in presence of calcium

The influence of calcium on the partition of phenylacetic acid (PAA) can be observed in Fig. 6. The addition of 10 mM  $CaCl_2$  to the aqueous phase does not seem to affect the partitioning of the low molecular weight acid in the heptane water system at any pH, and the curve in Fig. 6 is indeed very similar to the curve without calcium from Fig. 2. From the low pH equilibrium concentrations, the  $P_{wo}$  was calculated to be 4.56 and by fitting the data to Eq. (17) the  $pK_a$  was calculated to be 2.19. The uncertainties related to the calculated  $pK_a$  is discussed in the previous section regarding this acid.

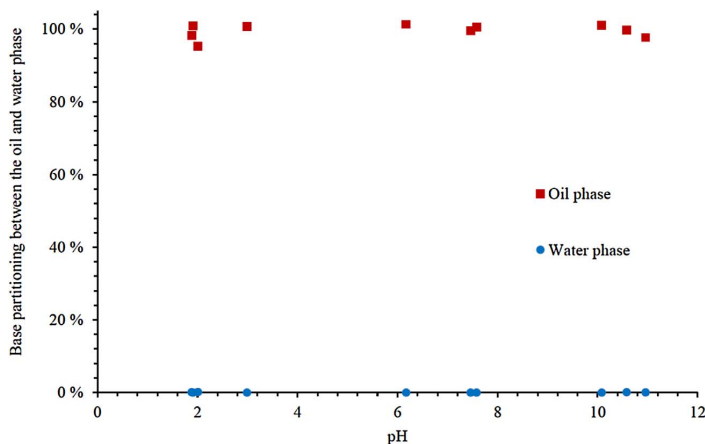


Fig. 5. Partitioning of high molecular weight base 4-decylaniline (4DA) in heptane and aqueous phase over equilibrium pH (3.5 wt.% NaCl). Initial concentration was 10 mM in heptane.

Table 3  
Partition ratio and dissociation constants for model acids and bases.

Model compound	Initial concentration	$P_{wo}$	$pK_a$
PAA	10 mM	7.8	3.2
4HBA	1 mM <sup>a</sup>	$3.7 \times 10^{-4}$	4.6
4EA	10 mM	$9.85 \times 10^{-2}$	5.1
4DA	10 mM	$7.8 \times 10^{-4}$	-

<sup>a</sup> The  $P_{wo}$  for 4HBA was found by using 10 mM as initial concentration due to the low absorbance in UV in oil phase obtained by using 1 mM.

4.7. Partitioning of the high molecular weight acid in the presence of calcium

Fig. 7 shows how 4-heptylbenzoic acid (4HBA) partition between heptane and water over equilibrium pH when divalent cations like calcium are present. When the pH was below pH 6.8, the mass balance from the measurement of the oil and water phase added up to 100%. However, when the pH was higher than 6.8, the mass balance did not add up and 4HBA started to form precipitate of calcium naphthenate. This precipitate would place itself at the interface and the amount was observed to increase with the equilibrium pH, mirroring the increasing amount of missing mass from the mass balance. Comparing the curves in Figs. 3 and 7 it can be seen that with 10 mM of calcium present in the system, 4HBA transfers phase from oil to water at a lower pH (0.5) than



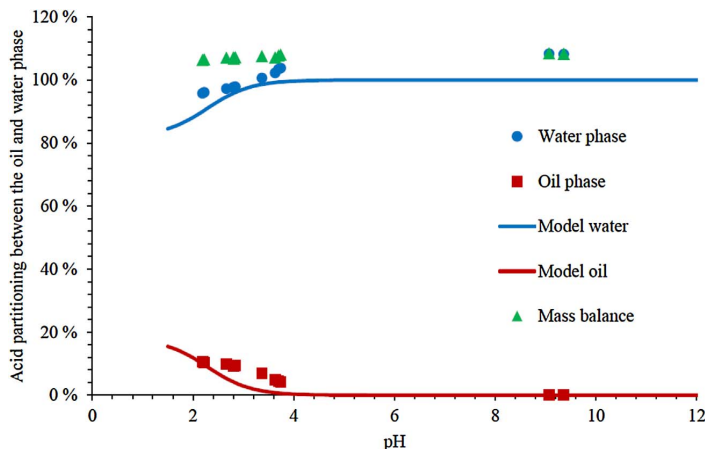


Fig. 6. Partitioning of the low molecular weight acid(PAA) in heptane and aqueous phase over equilibrium pH (3.5 wt.% NaCl and 10 mM CaCl<sub>2</sub>). The initial concentration in heptane was 10 mM and the data is fitted with Eq. (17).

when the system only contained sodium ions. Spildo and Høiland [45] reported stable emulsion formation at pH values over 7 upon adding calcium to their partitioning studies of 4HBA. No such stable emulsions were formed in these experiments, although it should be mentioned that the systems used are somewhat different, particularly regarding calcium concentration (10 x more).

As seen in Fig. 7, the concentrations of 4HBA in the water and oil phase are well-fitted by Eqs. (20) and (21) when pH > 6.8, where precipitates start to form. The  $K_s$  was calculated from Eqs. (19) and (21) to be between 1.5 and  $2 \times 10^{-10}$ .

4.8. Interfacial tension analysis

Before measuring the interfacial tension of solutions with acids and bases, the interfacial tension between heptane and MQ water was measured to be 51 mN/m, and it did not change significantly for the buffer solutions. The interfacial tension for the single acids and bases considered in this study are shown for various pH values in Fig. 8. It can be observed that only the long chain acid 4HBA and base 4DA presents interfacial activity at high and low pH. The low molecular weight acid PAA and low molecular weight base 4EA, show no interfacial activity at the pH values explored here. This might be expected due to the short hydrophobic part of these molecules. The system with the high molecular weight acid (4HBA) decreases slowly towards pH 6 before a noticeable drop between pH 6 and 8.5 followed by a small decrease towards pH 10. This interfacial tension change at higher pH than bulk

phase  $pK_a$  is in accordance with the interfacial  $pK_a$  theories previously mentioned [57,58]. The high molecular weight base 4DA only becomes interfacially active between pH 4 and 2. In a separate experiment it has been observed that the interfacial tension for 4DA at pH 0.5 goes towards 6 mN/m.

Fig. 9 shows the dynamic interfacial tension of the high molecular weight acid 4HBA and gives some interesting insight into the phase transfer over the oil-water interface. A logarithmic plot of the interfacial tension data reveal that equilibrium is not completely reached after 6 h. The values after 6 h were reported as equilibrium values for practical reasons and are considered close to the equilibrium due to the slow variation of interfacial tension we see after 6 h. For high pH experiments, the interfacial tension starts out at around 5 mN/m due to the fast adsorption of 4HBA at the interface, and then slowly increases towards equilibrium as the 4HBA partitions into the aqueous phase, depleting the oil phase of acids. This is in accordance with the kinetic partitioning experiments by Spildo and Høiland [45] which show partitioning of 4HBA at pH 8 takes about 5 h to reach equilibrium.

4.9. Interfacial interactions

The interfacial tension between heptane and aqueous buffers was measured with oil phases containing 2 acids, 2 bases or all 4 components as shown in Fig. 10. By comparing Figs. 8 and 10, the interfacial tensions of the mixtures are observed to be completely dominated by the high molecular weight acid and base at their respective active pH

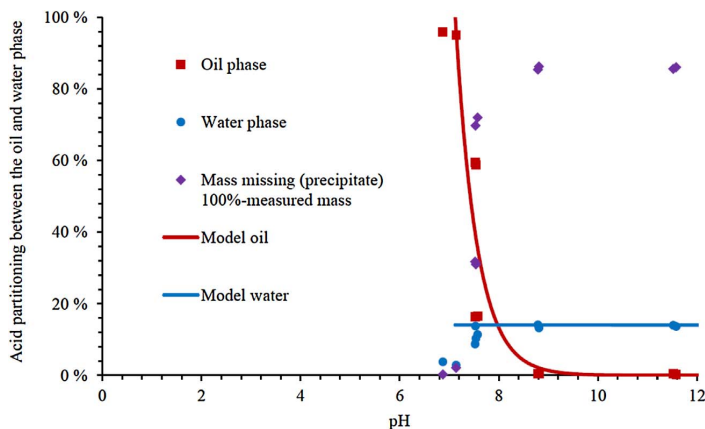


Fig. 7. Partitioning of the high molecular weight acid 4-heptylbenzoic acid in heptane and aqueous phase over equilibrium pH (3.5 wt.% NaCl and 10 mM CaCl<sub>2</sub>). Precipitation of calcium naphthenate particles occurs. Eqs. (20) and (21) were used to fit the water and oil phase concentration at pH > 6.8.

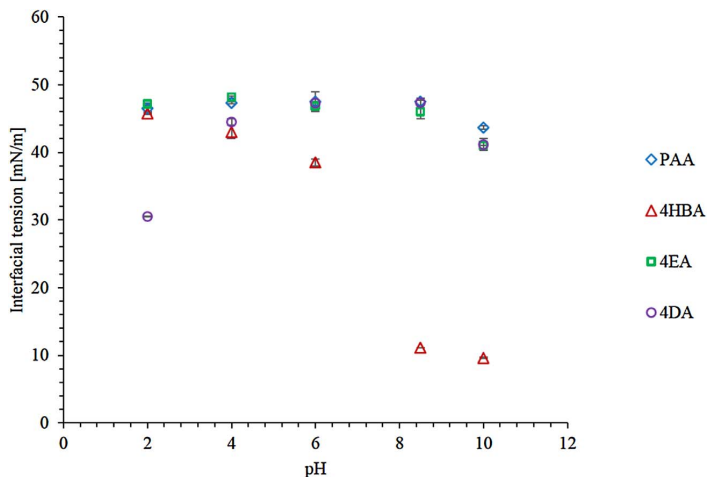


Fig. 8. Interfacial tension of single components between heptane and aqueous buffers (3.5 wt.% NaCl). The components were: Low molecular weight acid (PAA), high molecular weight acid (4HBA), low molecular weight base (4EA) and high molecular weight base (4DA). The initial concentration of each compound in heptane was 1 mM. Values were measured after 6 h of equilibration. The pH was measured before and after to assure no change occurred. The values are the average of two measurements where the error bars represent the range of values.

values. The interfacial tension of the mixture with 2 acids and 2 bases, is similar to the interfacial tension of the mixture with 2 acids at all other pH values considered. From these observations, it can be deduced that there are no interactions between acids and bases that would influence the interfacial tension. In their studies of crude oil bases, Nenningsland, Simon and Sjöblom [36] obtained a similar curve to the one seen in Fig. 10 for the three mixtures of crude oil, extracted bases and non-basic crude oil.

Table 4 presents a summary of the equilibrium interfacial tension study of the chosen acids and bases. The bases control interfacial tension at low pH. At pH 4 their contribution to interfacial tension is about equal, before the acids take control of the interfacial tension at pH 6 and above. The lack of interaction of acids and bases is most likely because the pH window, where both acid and base would both exist in the dissociated state, is much smaller for anilines and carboxylic acids than for the amines and carboxylic acids studied by previous authors. The synergistic effect of octylamine and octanoic acid occurred at pH 7 in the experiments by Spildo, Blokhus and Andersson [68]. Here, the  $pK_a$  of the amine and acid were respectively 4.8 and 10.6, indicating that the synergistic effect would occur at a pH where the distribution ratios for both species goes towards 1 (Eq. (8)), i.e. the acid and base had almost equal solubility in both phases. In this respect, there might

not exist a synergistic pH window where the aniline and organic acid can interact at the interface. These results also indicate that acid base complexes formed in the oil or water phase, if they exist, does not affect the interfacial tension. Moreover, since crude oil bases are mainly pyridine homologues, use of anilines with similar  $pK_a$  would give a more accurate representation to phenomena in crude oil systems compared to amines which are not present in crude oil to any large extent.

#### 4.10. Comparison of interfacial tension and partitioning

In Fig. 11 the interfacial tension can be seen versus the total amount of 4HBA and corresponding carboxylate in the system. The biggest drop in interfacial tension with pH occurs between ca. 6 and 8, which corresponds to approximately the pH range at which 4HBA transfer from the oil phase to the water phase. The decrease of the interfacial tension is therefore correlated to the partition of the high molecular weight acid.

The situation is different in the case of the base 4DA. Indeed, the interfacial tension increases when the pH varies from 2 to 4 while the base stays in the oil phase as seen in Figs. 5 and 8. Consequently, such correlation between interfacial tension and partitioning does not exist for this compound at the pH range studied.

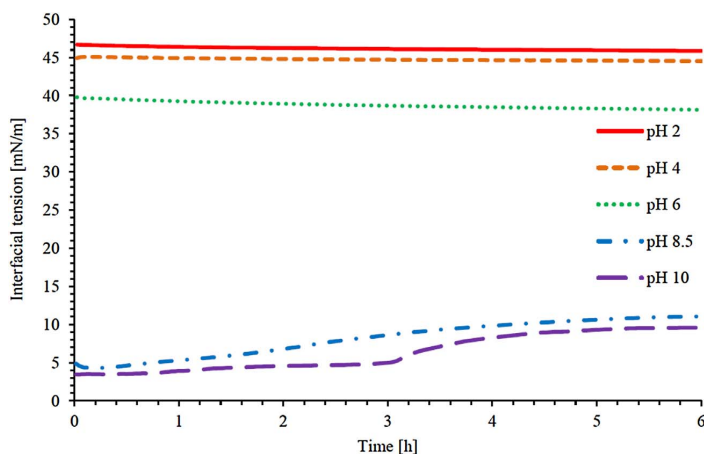


Fig. 9. Dynamic interfacial tension curves for the high molecular weight acid 4HBA in oil phase over aqueous buffers of different pH values. The initial concentration in the oil phase was 1 mM.



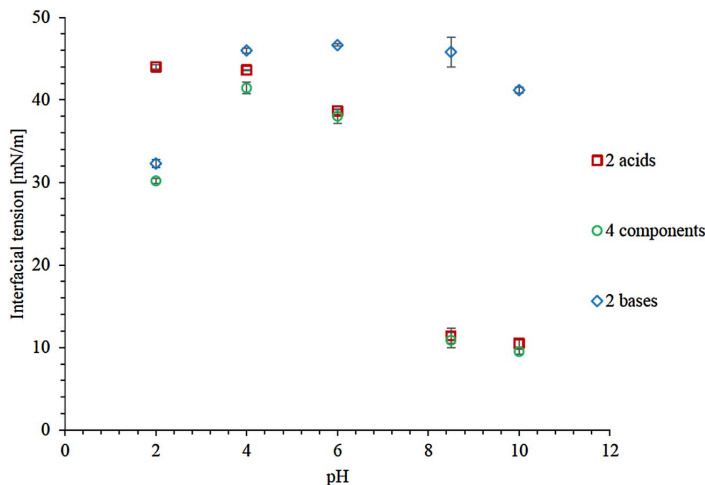


Fig. 10. Interfacial tension between heptane and aqueous buffers (3.5 wt.% NaCl) where the oil phase initially contained 2 acids, 2 bases or all 4 components. The heptane solution with 2 acids contained 1 mM PAA and 1 mM 4HBA, the solution with 2 bases contained 1 mM 4EA and 1 mM 4DA. The heptane solution with 4 components contained 1 mM of each acid and 1 mM of each base. The values are the average of two measurements where the error bars represent the range of values. Values measured after 6 h of equilibration.

Table 4  
Summary of equilibrium interfacial tensions measured for heptane aqueous buffer (3.5 wt.% NaCl) systems with 2 acids (1 mM of each acid), 2 bases (1 mM of each base) or 4 components (1 mM of each acid and 1 mM of each base) initially in the heptane phase.

pH	2 acids	4 components	2 bases
2	44 mN/m	30 mN/m	33 mN/m
4	43 mN/m	41 mN/m	46 mN/m
6	39 mN/m	37 mN/m	46 mN/m
8.3	12 mN/m	10 mN/m	44 mN/m
9.6	11 mN/m	10 mN/m	41 mN/m

5. Conclusion

A simple system with model acids and bases in heptane was used to represent crude oil containing acidic and basic species. Low molecular weight acids like phenylacetic acid (PAA) would to a high degree partition in the water phase regardless of pH or cations present in the water phase. Larger acids like 4-heptylbenzoic acid (4HBA) would exist in the oil phase with moderate interfacial activity at low pH. At higher pH, the acid would be activated to accumulate at the interface and diffuse into the water phase. The high molecular weight acid is highly affected by higher valence cations like calcium and readily form calcium precipitate at higher pH values. Low molecular weight bases like

4-ethylaniline would exist in the water phase at low pH and partition into the oil phase at pH 4 and higher.

The high molecular weight base did not partition to the water phase for any of the pH values explored in this article. Acids were observed to be much more soluble in water compared to bases of equal molecular weight. These results can be the basis for more studies into the kinetics of acid and base partitioning and dissipative particle dynamics (DPD) modelling.

No interfacial interactions between acids and bases could be indicated by interfacial tension studies. The reason for this is most likely the pH window in which both the acids and the base can exist in the dissociated state simultaneously. This pH window might not exist due to similar  $pK_a$  values. There is no indication of oil phase complexation between the studied acids and bases affecting the interface.

Acknowledgements

This work was carried out as a part of SUBPRO, a Research-based Innovation Centre within Subsea Production and Processing. The authors gratefully acknowledge the financial support from SUBPRO, which is financed by the Research Council of Norway, major industry partners and NTNU.

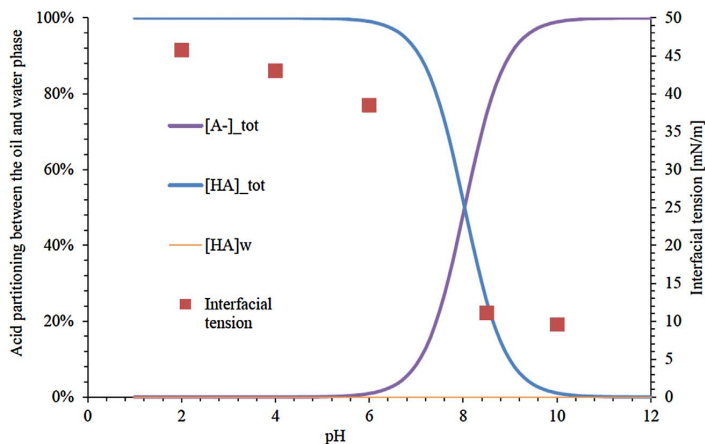


Fig. 11. Summary graph showing the partitioning of the high molecular weight acid 4HBA (1 mM) and the interfacial tension at different pH values. The lines were calculated from Eq. (17) and  $pK_a$  and  $P_{wo}$  reported in Table 3. Interfacial tension values measured after 6 h of equilibration.

## References

- [1] V. Khoi Vu, R. Fantoft, C.K. Shaw, H. Gruehagen, Comparison of subsea separation systems OTC-20080-MS, Offshore Technology Conference, Houston, Texas, 2009.
- [2] C.N. Prescott, Subsea separation and processing of oil, gas & produced water, in: F.O. Solutions (Ed.), Past, Present and Future. Why We Need It Now, Rice Global E & C Forum, Houston, Texas, 2012.
- [3] D.E. Appleford, R.G. Smith, Seabed processing – enabling technology OTC-13194, Offshore Technology Conference, Offshore Technology Conference, Houston, Texas, 2001.
- [4] L.H. de Lacotte, A. Lopez, L. Rivière, J. Anfray, Deep offshore – needs for a subsea/topsides integrated approach OTC-25782-MS, Offshore Technology Conference, Offshore Technology Conference, Houston, Texas, 2015.
- [5] D. Lim, H. Gruehagen, Subsea separation and boosting—an overview of ongoing projects SPE-123159-MS, Asia Pacific Oil and Gas Conference & Exhibition, Society of Petroleum Engineers, Jakarta, Indonesia, 2009.
- [6] T.I. Kuhnle, O. Grande, F.B. Pedersen, Y. Yang, M. Jafar, D. Sewraz, M. Irvine, All subsea – creating value from subsea processing, in: D. GL (Ed.), DNV GL Strategic Research & Innovation Position Paper, 2015.
- [7] J. Neff, K. Lee, E.M. DeBlolis, Produced Water: Overview of Composition, Fates, and Effects Produced Water. Environmental Risks and Advances in Mitigation Technologies, in: K. Lee, J. Neff (Eds.), Springer New York, New York, NY, 2011, pp. 3–54.
- [8] M. Yang, Measurement of oil in produced water, in: J.N.K. Lee (Ed.), Produced Water, Springer Science Business Media, LLC, East Kilbride, Glasgow G75 0QF, UK, 2011.
- [9] T. Ruud, A. Idrac, L.J. McKenzie, S.H. Hoy, All subsea: a vision for the future of subsea processing OTC-25735-MS, Offshore Technology Conference, Offshore Technology Conference, Houston, Texas, USA, 2015.
- [10] R.M. Ramberg, S.R.H. Davies, H. Rognoe, O. Oekland, Steps to the subsea factory OTC-24307-MS, OTC, Brasil, Offshore Technology Conference, Rio de Janeiro, Brazil, 2013.
- [11] D.M. Grewer, R.F. Young, R.M. Whittal, P.M. Fedorak, Naphthenic acids and other acid-extractables in water samples from Alberta: what is being measured? Sci. Total Environ. 408 (2010) 5997–6010.
- [12] L.M. Wenger, C.L. Davis, G.H. Isaksen, Multiple controls on petroleum biodegradation and impact on oil quality SPE-80168-PA, SPE Reservoir Eval. Eng. 5 (2002).
- [13] T. Barth, S. Høiland, P. Fotland, K.M. Askvik, R. Myklebust, K. Erstad, Relationship between the content of asphaltenes and bases in some crude oils, Energy Fuels 19 (2005) 1624–1630.
- [14] T.E. Havre, J. Sjöblom, J.E. Vindstad, Oil/water-partitioning and interfacial behavior of naphthenic acids, J. Dispers. Sci. Technol. 24 (2003) 789–801.
- [15] A. Hutin, J.-F. Argillier, D. Langevin, Mass transfer between crude oil and water. Part 1: effect of oil components, Energy Fuels 28 (2014) 7331–7336.
- [16] J.G. Speight, High Acid Crudes, Gulf Professional Publishing, Oxford, United Kingdom, 2014.
- [17] M.-H. Ese, P.K. Kilpatrick, Stabilization of water-in-oil emulsions by naphthenic acids and their salts: model compounds, role of pH, and soap: acid ratio, J. Dispers. Sci. Technol. 25 (2004) 253–261.
- [18] C.S. Hsu, G.J. Dechert, W.K. Robbins, E.K. Fukuda, Naphthenic acids in crude oils characterized by mass spectrometry, Energy Fuels 14 (2000) 217–223.
- [19] C. Hurtevent, M. Bourrel, G. Rousseau, B. Brocart, Production Issues of Acidic Petroleum Crude Oils, Emulsions and Emulsion Stability, CRC Press, 2005, pp. 477–516.
- [20] J.A. Brient, P.J. Wessner, M.N. Doyle, Naphthenic acids, in: Kirk-Othmer (Ed.), Encyclopedia of Chemical Technology, John Wiley & Sons, Inc., New York, 1995, pp. 1017–1029.
- [21] J.S. Clemente, P.M. Fedorak, A review of the occurrence, analyses, toxicity, and biodegradation of naphthenic acids, Chemosphere 60 (2005) 585–600.
- [22] M.P. Barrow, M. Witt, J.V. Headley, K.M. Peru, Athabasca oil sands process water: characterization by atmospheric pressure photoionization and electrospray ionization fourier transform ion cyclotron resonance mass spectrometry, Anal. Chem. 82 (2010) 3727–3735.
- [23] H. Mediaas, N.O. Wolf, T.D. Baugh, K.V. Grande, J.E. Vinstad, The discovery of high molecular weight naphthenic acids (ARN acid) responsible for calcium naphthenate deposits SPE-93011-MS, SPE International Symposium on Oilfield Scale, Society of Petroleum Engineers, Aberdeen, United Kingdom, 2005.
- [24] J. Sjöblom, S. Simon, Z. Xu, The chemistry of tetrameric acids in petroleum, Adv. Colloid Interface Sci. 205 (2014) 319–338.
- [25] M. Häger, M.H. Ese, J. Sjöblom, Emulsion inversion in an oil-surfactant-water system based on model naphthenic acids under alkaline conditions, J. Dispers. Sci. Technol. 26 (2005) 673–682.
- [26] M.P. Barrow, L.A. McDonnell, X. Feng, J. Walker, P.J. Derrick, Determination of the nature of naphthenic acids present in crude oils using nanospray fourier transform ion cyclotron resonance mass spectrometry: the continued battle against corrosion, Anal. Chem. 75 (2003) 860–866.
- [27] J.E. Vindstad, A.S. Bye, K.V. Grande, B.M. Hustad, E. Hustvedt, B. Nergård, Fighting naphthenate deposition at the heidrun field, SPE 80375, International Symposium on Oilfield Scale, Society of Petroleum Engineers (2003).
- [28] B. Zhao, R. Currie, H. Mian, Catalogue of Analytical Methods for Naphthenic Acids Related to Oil Sands Operations, Oil Sands Research and Information Network, University of Alberta, School of Energy and the Environment, Edmonton Alberta, 2012.
- [29] J.D. Friedemann, Design criteria and methodology for modern oil and water separation systems, in: J. Sjöblom (Ed.), Emulsions and Emulsion Stability, CRC Press, Boca Raton, USA, 2005, pp. 607–629.
- [30] V.S. Aksenov, V.I. Titov, V.F. Kam'yanov, Nitrogen compounds of petroleum oils (review), Chem. Heterocycl. Compd. 15 (1979) 119–135.
- [31] M. Yamamoto, K. Taguchi, K. Sasaki, Basic nitrogen compounds in bitumen and crude oils, Chem. Geol. 93 (1991) 193–206.
- [32] C. von Mühlen, E.C. de Oliveira, C.A. Zini, E.B. Caramão, P.J. Marriott, Characterization of nitrogen-containing compounds in heavy gas oil petroleum fractions using comprehensive two-dimensional gas chromatography coupled to time-of-flight mass spectrometry, Energy Fuels 24 (2010) 3572–3580.
- [33] J.G. Speight, H. Heinemann, The Chemistry and Technology of Petroleum, Fourth edition, CRC Press Taylor & Francis group, Boca Raton, USA, 2006.
- [34] S. Simon, A.L. Nenningsland, E. Herschbach, J. Sjöblom, Extraction of basic components from petroleum crude oil, Energy Fuels 24 (2010) 1043–1050.
- [35] M. Eftekhardakhah, K.N. Kløcker, H.H. Trappes, B. Gaweł, G. Øye, Composition and dynamic adsorption of crude oil components dissolved in synthetic produced water at different pH values, Ind. Eng. Chem. Res. 55 (2016) 3084–3090.
- [36] A.L. Nenningsland, S. Simon, J. Sjöblom, Surface properties of basic components extracted from petroleum crude oil, Energy Fuels 24 (2010) 6501–6505.
- [37] A.M. Reinsel, J.J. Borkowski, J.T. Sears, Partition Coefficients for Acetic, Propionic, and Butyric Acids in a Crude Oil/Water System, Journal of Chemical & Engineering Data 39 (1994) 513–516.
- [38] Y. Touhami, V. Hornof, G.H. Neale, Mechanisms for the interactions between acidic oils and surfactant-enhanced alkaline solutions, J. Colloid Interface Sci. 177 (1996) 446–455.
- [39] L.A. Stanford, S. Kim, G.C. Klein, D.F. Smith, R.P. Rodgers, A.G. Marshall, Identification of water-soluble heavy crude oil organic-acids, bases, and neutrals by electrospray ionization and field desorption ionization fourier transform ion cyclotron resonance mass spectrometry, Environ. Sci. Technol. 41 (2007) 2696–2702.
- [40] A. Hutin, J.-F. Argillier, D. Langevin, Mass transfer between crude oil and water. Part 2: effect of sodium dodecyl benzenesulfonate for enhanced oil recovery, Energy Fuels 28 (2014) 7337–7342.
- [41] D.L. Lord, A.H. Demond, K.F. Hayes, Effects of organic base chemistry on interfacial tension, wettability, and capillary pressure in multiphase subsurface waste systems, Transp. Porous Media 38 (2000) 79–92.
- [42] A. Celsie, J.M. Parnis, D. Mackay, Impact of temperature, pH, and salinity changes on the physico-chemical properties of model naphthenic acids, Chemosphere 146 (2016) 40–50.
- [43] D.S. Goodman, The distribution of fatty acids between n-heptane and aqueous phosphate buffer, J. Am. Chem. Soc. 80 (1958) 3887–3892.
- [44] IUPAC, Partition coefficient, in: A. Wilkinson, A.D. McNaught (Eds.), Compendium of Chemical Terminology, Blackwell Scientific Publications Oxford, 1997, pp. 1067–1069.
- [45] K. Spildo, H. Høiland, Interfacial properties and partitioning of 4-heptylbenzoic acid between decane and water, J. Colloid Interface Sci. 209 (1999) 99–108.
- [46] S.H. Standal, A.M. Blokhus, J. Haavik, A. Skauge, T. Barth, Partition coefficients and interfacial activity for polar components in oil/water model systems, J. Colloid Interface Sci. 212 (1999) 33–41.
- [47] P. Mukerjee, Dimerization of anions of long-chain fatty acids in aqueous solutions and the hydrophobic properties of the acids, J. Phys. Chem. 69 (1965) 2821–2827.
- [48] R.A. Scherrer, S.M. Howard, Use of distribution coefficients in quantitative structure-activity relationships, J. Med. Chem. 20 (1977) 53–58.
- [49] Ø. Brandal, J. Sjöblom, Interfacial behavior of naphthenic acids and multivalent cations in systems with oil and water. II: formation and stability of metal naphthenate films at oil-water interfaces, J. Dispers. Sci. Technol. 26 (2005) 53–58.
- [50] C.E. Cooke Jr., R.E. Williams, P.A. Kolodziej, Oil recovery by alkaline waterflooding, J. Petrol. Technol. 26 (1974).
- [51] T.E. Havre, Formation of calcium naphthenate in water/oil systems, Naphthenic Acid Chemistry and Emulsion Stability, Department of Chemical Engineering, Norwegian University of Science and Technology, Trondheim, 2002.
- [52] Ø. Brandal, Interfacial (o/w) properties of naphthenic acids and metal naphthenates, Naphthenic Acid Characterization and Metal Naphthenate Inhibition, Department of Chemical Engineering, NTNU, 2005.
- [53] A.M.D. Hanneseth, Ø. Brandal, J. Sjöblom, Formation, growth, and inhibition of calcium naphthenate particles in oil/water systems as monitored by means of near infrared spectroscopy, J. Dispers. Sci. Technol. 27 (2006) 185–192.
- [54] S. Simon, C. Reisen, A. Bersås, J. Sjöblom, Reaction between tetrameric acids and Ca<sup>2+</sup> in oil/water system, Ind. Eng. Chem. Res. 51 (2012) 5669–5676.
- [55] S. Keleşoğlu, P. Meakin, J. Sjöblom, Effect of aqueous phase pH on the dynamic interfacial tension of acidic crude oils and myristic acid in dodecane, J. Dispers. Sci. Technol. 32 (2011) 1682–1691.
- [56] J.S. Buckley, K. Takamura, N.R. Morrow, Influence of electrical surface charges on the wetting properties of crude oils, SPE Reservoir Eng. 4 (1989) 332–340.
- [57] P.D. Cratin, Mathematical modeling of some pH-dependent surface and interfacial properties of stearic acid, J. Dispers. Sci. Technol. 14 (1993) 559–602.
- [58] J.F. Danielli, The relations between surface pH, ion concentrations and interfacial tension, Proc. R. Soc. London Ser. B Biol. Sci. 122 (1937) 155–174.
- [59] J. Rudin, D.T. Wasan, Mechanisms for lowering of interfacial tension in alkali/acidic oil systems: effect of added surfactant, Ind. Eng. Chem. Res. 31 (1992) 1899–1906.
- [60] D.L. Lord, K.F. Hayes, A.H. Demond, A. Salehzadeh, Influence of organic acid solution chemistry on subsurface transport properties. 1. Surface and interfacial tension, Environ. Sci. Technol. 31 (1997) 2045–2051.
- [61] A.M. Gaudin, T.G. Decker, Contact angles and adsorption in the system quartz-water-dodecane modified by dodecyl ammonium chloride, J. Colloid Interface Sci. 24 (1967) 151–158.

- [62] P. Joos, Effect of the pH on the collapse pressure of fatty acid monolayers evaluation of the surface dissociation constant, *Bull. Soc. Chim. Belges* 80 (1971) 277–281.
- [63] R.A. Peters, Interfacial tension and hydrogen-ion concentration, *Proc. R. Soc. London Ser. A Contain. Pap. Math. Phys. Charact.* 133 (1931) 140–154.
- [64] J.O. Saeten, J. Sjoblom, B. Gestblom, A dielectric spectroscopic study of fatty acid/amine complexes in solution, *J. Phys. Chem.* 95 (1991) 1449–1453.
- [65] D. Góralczyk, Influence of inorganic electrolyte concentration on properties of anionic–cationic adsorption films, *J. Colloid Interface Sci.* 179 (1996) 211–217.
- [66] H. Matsuki, M. Aratono, S. Kaneshina, K. Motomura, Extremely strong interaction of sodium decyl sulfate and decyltrimethylammonium bromide in molecular aggregates, *J. Colloid Interface Sci.* 191 (1997) 120–130.
- [67] H. Ebeltoft, J. Sjoblom, J.O. Saeten, G. Olofsson, Fatty acid/base interactions in model systems. A Langmuir film, surface tension, and calorimetric study, *Langmuir* 10 (1994) 2262–2266.
- [68] K. Spildo, A.M. Blokhus, A. Andersson, Surface and interfacial properties of octanoic acid–octylamine mixtures in isoctane–water systems: influence of acid: amine molar ratio and aqueous phase pH, *J. Colloid Interface Sci.* 243 (2001) 483–490.
- [69] D.R. Lide, *CRC Handbook of Chemistry and Physics: a Ready-reference Book of Chemical and Physical Data*, in: D.R. Lide (Ed.), CRC Press Inc., Boca Raton, 1997, p. 842.
- [70] P.M. Dewick, *Acids and bases*, in: P.M. Dewick (Ed.), *Essentials of Organic Chemistry: For Students of Pharmacy, Medicinal Chemistry and Biological Chemistry*, Wiley, West Sussex, England, 2006, p. 130.
- [71] X. Zhang, *Monoliths and Small Particle-packed Columns for Liquid Chromatography*, Department of chemistry, University at Buffalo, 2007 (pp. 54).

## PAPER II

---

Development of electrochemical DPD molecular simulations for oil/water partitioning of organic acids at varying pH

Not included due to copyright



## PAPER III

---

Equilibrium partitioning of naphthenic acid mixture part 1: Commercial naphthenic acid mixture



# Equilibrium Partitioning of Naphthenic Acid Mixture, Part 1: Commercial Naphthenic Acid Mixture

Are Bertheussen,\*<sup>✉</sup> Sébastien Simon, and Johan Sjöblom

Ugelstad Laboratory, Department of Chemical Engineering, Norwegian University of Science and Technology (NTNU), N-7491 Trondheim, Norway

## Supporting Information

**ABSTRACT:** Crude oil contains naphthenic acids that can partition into water. This phenomenon is a function of several parameters, such as the naphthenic acid composition, pH, and water phase salinity. This article is a continuation of previous work regarding the partitioning between oil and water of model acids and bases in model systems, with regard to pH and salinity. The present work will focus on a commercial naphthenic acid mixture from Fluka, while the next work will deal with extracted naphthenic acids from a crude oil. The composition of the acid mixture was determined by GC/MS and it was found that the commercial naphthenic acid mixture is mostly composed of saturated acids with 0–3 ring structures. The partitioning of the commercial naphthenic acid mixture was determined. The equilibrium partitioning of acids with different molecular weight was determined over a large pH interval, using toluene as the oil phase and 3.5 wt % NaCl aqueous buffers as the water phase. The partitioning of the naphthenic acid mixture with pH was successfully modeled by dividing the naphthenic acid mixture into narrow molecular weight range fractions characterized by a single partitioning ratio ( $pP_{wo}$ ). The variation of the  $pP_{wo}$  of the fractions with molecular weight was found to be linear. In the presence of calcium and high pH, the partitioning of higher-molecular-weight acids was reduced, likely because of the formation of oil-soluble calcium naphthenates, since no precipitation was observed. The partitioning of low-molecular-weight acids was not affected by calcium.

## 1. INTRODUCTION

As the world energy demand continues to increase, energy companies prepare to utilize more complicated oil resources.<sup>1,2</sup> Biodegraded crude oil can be more difficult to produce, because of its lower API gravity, elevated total acid number (TAN), and total base number (TBN).<sup>3–5</sup> These acids and bases in crude oil can partition and solubilize into the coproduced water phase, which is a tendency that is affected by parameters such as pH, temperature, and molecular weight.

Subsea solutions for produced water discharge and achieving export-quality crude oils subsea are close to becoming a reality.<sup>6</sup> To predict how the oil and water quality will be affected by inlet conditions such as the composition and properties of the well stream over the lifetime of the fields, more knowledge is needed about the partitioning behavior of crude oil components such as naphthenic acids. This paper is the first in a series of companion papers to discuss and explore the composition and equilibrium partitioning of naphthenic acid mixtures.

## 2. THEORY

**2.1. Definition and Prevalence.** The term “naphthenic acids” has been used to describe all organic acids found in crude oil, although the traditional definition describes a carboxylic acid with a naphthene ring. The weight percent in crude oil varies from 0 wt % to 3 wt %.<sup>7</sup> As with other crude oil components, naphthenic acids have large variations in size and structural conformations; however, a good rule of thumb is that they have a molecular weight of 200–700 g/mol (from ref 8) and a structure described by the isomer  $C_nH_{2n+Z}O_2$ .<sup>9</sup> So-called oxy-naphthenic acids  $C_nH_{2n+Z}O_x$  isomer formulas have

also been used to include naphthenic acids with added hydroxyl or acidic functional groups.<sup>10</sup> In either case, the parameter  $n$  refers to the number of carbon atoms, while the  $Z$  is a negative integer referring to the hydrogen deficiency of the naphthenic acid molecule, the  $x$  refers to the number of oxygen atoms. However, this view of naphthenic acids might be too limiting, as noted by Grever et al.,<sup>10</sup> who reported that less than half of the peak abundancies in the acid oil extracts and commercial acid mixtures examined could be grouped into the  $C_nH_{2n+Z}O_x$  isomer. Headley et al.<sup>11</sup> defined the term naphthenic acid fraction components (NAFC), which allowed for more combinations with functional groups containing oxygen, sulfur, nitrogen, and aromatic rings. Qian et al.<sup>12</sup> in their identification of 3000 acids from a south American crude oil found that crude oil acids range from  $C_{15}$ – $C_{55}$ . Several authors,<sup>12–14</sup> have concluded that, after experimenting with crude oils from North, Central, and South America, less than half of the acids are “true naphthenic acids”, while the rest consists of acids with one or more aromatic, nitrogen, or sulfur groups such as alkyl sulfonic acid. Hemmingsen et al.,<sup>15</sup> on the other hand, found acids from a North Sea crude oil to consist predominantly of conventional naphthenic acids, i.e., molecules with one carboxyl group.

Naphthenic acids are corrosive,<sup>16</sup> although using TAN as an indicator for corrosiveness is unreliable and researchers suspect a smaller subgroup of acids might be culpable.<sup>13</sup> Naphthenic acids affect the stability of water in oil emulsions and oil-in-

Received: April 28, 2018

Revised: June 5, 2018

Published: June 12, 2018



water emulsions<sup>17,18</sup> and cause pipe or formation pore blockage through precipitation.<sup>19,20</sup> Some of the cyclic and aromatic naphthenic acids has been shown to be toxic and carcinogenic,<sup>21</sup> which is why dissolved naphthenic acids are considered major contaminants in oil sands process-affected water (OSPW).<sup>22</sup> Produced water discharge from offshore installations also contains naphthenic acids, which raises some environmental concerns.<sup>23</sup>

Mass spectrometry has been extensively used to characterize naphthenic acids in multiple studies.<sup>10,12–14,24–31</sup> With high-resolution mass spectroscopy (MS), such as Fourier transform–ion cyclotron resonance mass spectroscopy (FT-ICR MS), the abundance of each isomer can be extracted from the mass spectra to obtain the composition of the naphthenic acids in the sample.<sup>32</sup> However, this technique presents some pitfalls. For instance, Clingenpeel et al.<sup>33</sup> performed FT-ICR MS on fractions according to their hydrophobicity from acidic interfacial material isolated from a bitumen sample. They revealed that, when analyzed unfractionated, the most ionizable compounds, i.e., the least hydrophobic, low-molecular-weight monoacids, masked the presence of larger compounds. Fractionation showed that the acid fraction that gave the tightest emulsion was composed of asphaltene-like acids, with regard to size and aromaticity. Stanford et al.<sup>34</sup> used FT-ICR MS to compare the composition of the polar components of nine crude oils to the surface-active material from the corresponding crude oil. They found that, generally, the double bond equivalent (DBE) and carbon number distributions of the interfacial material overlaps with the polar components of the parent crude oil. For water-soluble species, however, the distributions of polar species do not match that of the parent oil. Less-hydrophobic species such as acids with aromatic ring structures would, for example, be relatively more abundant in the water phase.<sup>28</sup>

Jones et al.<sup>35</sup> developed a gas chromatography/mass spectroscopy (GC/MS) method for routine quantification of naphthenic acids in both light and heavy oils. Scott et al.<sup>25</sup> also describes a quantitative naphthenic acid detection method based on GC/MS,<sup>36,37</sup> which exploits the general absence of C<sub>13</sub> acids in nature. When used in comparison with results obtained from FTIR, they found that in all but one case, the FTIR results showed higher concentrations than the GC/MS, often 2–4 times higher. This difference was attributed to hydroxy-naphthenic acids not being included in the GC/MS quantification. In 1998, St. John et al. developed a GC/MS method that uses *N*-methyl-*N*-(*t*-butyldimethylsilyl) trifluoroacetamide (MTBSTFA) to derivatize naphthenic acids to their *t*-butyldimethylsilyl esters. This derivatization method produces a stable ion fragment [M+57], where M is the molecular weight of the naphthenic acid. Through these characteristic ions, individual components eluting within the usually large, unresolved hump of naphthenic acids can be classified, providing the composition of the naphthenic acids based on Z and carbon numbers.<sup>26</sup> This method has later been applied by several authors.<sup>25,26,36,38–40</sup> Upon testing multiple derivatization agents on different model acid structures, Shepherd et al.<sup>40</sup> found MTBSTFA to give one of the best yields overall, although recent research has claimed pentafluorobenzyl bromide (PFBBR) to be superior to MTBSTFA.<sup>41</sup>

Mass spectra of commercially available NA mixtures and OSPW or crude oil extracts have been studied by several authors,<sup>8,10,13,14,36,42–48</sup> and Saab et al.<sup>49</sup> discusses various naphthenic acid extraction methods. Generally speaking,

research has found commercial acid mixtures to contain more saturated and lighter acids, compared to acids extracted from crude oil or oil sand. Caution should be used when comparing the results obtained with previously published data, as West et al.<sup>50</sup> warns that different batches of commercially available NA mixtures from the same vendor might differ.

**2.2. Oil–Water Partitioning.** Some crude oil components have some solubility in water. Hydrophobic surface area is inversely related to the aqueous solubility.<sup>51</sup> Alkyl chains increase hydrophobic surface area while branching, polar, or aromatic groups decrease this area.<sup>28</sup> Production alterations in terms of pH, pressure, and temperature also affect solubility,<sup>52</sup> in effect changing the composition of the oil and water phase. The polarity of the crude oil acids makes them more water-soluble than their nonpolar counterparts. The partitioning of naphthenic acids between oil and water is strongly dependent on the pH of the aqueous phase. At low pH, naphthenic acids are neutral and their solubility in water is limited. As the pH increases, naphthenic acids are ionized and, therefore, their partitioning in the aqueous phase increases. The ionization of acids is classically characterized by an acid constant, pK<sub>a</sub>. The pK<sub>a</sub> of short-chain acids is close to 5. However, higher values have been reported for long-chain acids.<sup>53</sup> Kanicky and Shah<sup>53</sup> have shown that pK<sub>a</sub> decreases with the concentration of acid and reaches values close to 5 at infinite dilution. This behavior was attributed to the presence of long-chain acid premicellar aggregates, which, at higher concentrations, would influence acid–base equilibria. Upon extracting crude oil acids with neutral water, Stanford et al.<sup>28</sup> detected water-soluble acids up to C<sub>41</sub> (~600 g/mol). The extent of the partitioning is dependent on the structure (hydrophobicity) of the naphthenic acid. In their study of naphthenic acid partitioning, Havre et al.<sup>42</sup> found that naphthenic acids in crude oil–water systems had a pK<sub>a</sub> of 4.9, which corresponds to the pK<sub>a</sub> range reported by Brient et al.,<sup>54</sup> and varying pP<sub>wo</sub> values, depending on the molecular weight of the acids. Different partitioning models are reported in the literature. The most comprehensive one found was covered in Touhami et al.,<sup>55</sup> which includes most of the equilibria encountered in oil–water systems, i.e., partitioning of indigenous polar compounds and added surfactants, dissociation, micellization, and even metal naphthenate partitioning back into the oil phase. Based on previous models,<sup>42,56</sup> Hutin et al.<sup>57</sup> developed a model that could predict the final pH of a crude oil–water system based on the TAN, TBN, and initial pH.

In this study, the equilibrium partitioning of a commercial naphthenic acid (NA) mixture will be considered over the pH range. The goal is to determine the partition ratio for acids and obtain insight into how molecular weight influences the behavior of these compounds in two-phase systems.

**2.3. Modeling of Partition Ratio with pH.** In this section, a classical thermodynamic model for the partitioning of naphthenic acids is presented. For instance, this model has already been applied by Havre et al.,<sup>42</sup> Nordgård et al.,<sup>58</sup> Bertheussen et al.,<sup>59</sup> and others in their work.

In an oil–water system, the acids in their protonated form would partition themselves between the phases, according to the following partition constant:

$$K_{\text{wo,HA}} = \frac{[\text{HA}]_{\text{w}}}{[\text{HA}]_{\text{o}}} \quad (1)$$

**Table 1.** List of Chemicals Used As Model Acids, Their Molecular Weight, Supplier, Purity, Stable Mass Fragment after Derivatization with MTBSTFA, Actual Mass Difference between the Molecular Weight of the Acid and the Stable Ion Fragment, Abundances of the Stable Ion Fragments, and Mass and Abundance of the Isotope 2+<sup>a</sup>

acid (C number, Z number)	molecular weight [g/mol]	supplier	purity [%]	stable ion fragment after derivatization, [M+57] <sup>b</sup> [m/z]	mass difference [m/z]	[M+57] abundance [%]	[M+57] 2+ Isotope	
							mass [m/z]	abundance [%]
3-cyclopentylpropionic acid (8,-2)	142	Aldrich	98	199	+57	92	201	5
propyl benzoic acid (10,-8)	164	Aldrich	97	221	+57	95	223	0 <sup>c</sup>
cyclohexanebutyric acid (10,-2)	170	Acros Organics	99	227	+57	89	229	5
capric acid (10,0)	172	Fluka	99	229	+57	96	231	0 <sup>c</sup>
5-phenylvalerian acid (11,-8)	178	Aldrich	99	235	+57	97	237	0 <sup>c</sup>
1-naphthaleneacetic acid (12,-14) <sup>d</sup>	186	Sigma	>95	243	+57	92	245	0 <sup>c</sup>
trans-4-pentylcyclohexanecarboxylic acid (12,-2)	192	Acros Organics	98	255	+57	91	257	5
tridecanoic acid (13,0)	214	Fluka	99.7	271	+57	89	273	6
4-heptylbenzoic acid (14,-8)	220	Alfa Aesar	99	277	+57	76	279	5
myristic acid (14,0)	228	Acros Organics	99.5	285	+57	89	287	6
palmitic acid (16,0)	256	Sigma-Aldrich	99	313	+57	87	315	6
6-heptylnaphthalene-2-carboxylic acid (18,-14) <sup>d,e</sup>	270	Chiron AS	99.9	327	+57	61	329	5
stearic acid (18, 0)	284	Fluka	97	341	+57	85	343	6
hexadecanedioic acid (16, 0) <sup>d</sup>	286	Fluka	98	457	+114+57	61	459	8
behenic acid (22,0)	341	Fluka	99	398	+57	80	399	7
β-cholanic acid (24, -8)	360	Sigma	99	417	+57	44	419	4
docosanedioic acid (22, -0) <sup>d</sup>	370	Sigma-Aldrich	95	541	+114+57	52	543	9

<sup>a</sup>All abundances are calculated based on the sum of fragment intensities that match naphthenic acid masses (cutoff 159 m/z) listed in Table S1 in the Supporting Information. Acid abundances do not add up to 100% because of the presence of other ion fragments. The isotope +1 is not included in calculations for this table, since it does not fit into the naphthenic acid mass distribution table given in the Supporting Information (Table S1). <sup>b</sup>[M+57] refers to the stable mass fragment after derivatization with MTBSTFA, where M is the molecular weight of the acid. For the sake of simplicity, the term [M+57] is also used to describe the stable ion fragment for diacids, even though it technically should be [M+57+114]. <sup>c</sup>Indicates that this value would not be counted, since it does not fit into the naphthenic acid mass distribution table given in the Supporting Information (Table S1). <sup>d</sup>Indicates a structure that does not match how this ion would be attributed on the mass distribution (Table S1), which assumed only monoacids and Z ≤ 12. For instance, 1-naphthaleneacetic acid (12, -14) would be counted as a C = 11, Z = 0 acid, while docosanedioic acid would be counted as a C = 33, Z = -10 acid. <sup>e</sup>Internal standard.

where  $[HA]_w$  represents the protonated acid concentration in the water phase,  $[HA]_o$  represents the acid concentration in the oil phase, and  $K_{wo,HA}$  represents the partition constant of the acid. This partition constant is independent of concentration, but varies with temperature and pressure. Because of the dimer considerations discussed in a previous article,<sup>59</sup> the partition ratio defined by Scherrer and Howard<sup>60</sup> will be used in the following models. The ratio accounts for the nonionized compounds in each phase, as seen in eq 2.

$$P_{wo} = \frac{[HA]_w}{[HA]_{o,tot}} = \frac{[HA]_w}{[HA]_o + 2[(HA)_2]_o} \quad (2)$$

In the water phase, the acids can also deprotonate/protonate, as described by the following dissociation constant:

$$K_{a,HA} = \frac{[A^-]_w [H^+]_w}{[HA]_w} \quad (3)$$

where  $[A^-]_w$  represents the concentration of dissociated acid in the water phase and  $K_{a,HA}$  represents the dissociation constant of the acid. By introducing some new terms, the following mass balance can be applied to the system:

$$[HA]_{o,init} V_o = [HA]_{w,tot} V_w + [HA]_{o,tot} V_o \quad (4)$$

where  $[HA]_{o,init}$  represents the initial concentration of acid in the oil phase, and  $[HA]_{w,tot}$  represents the sum of dissociated and undissociated acids in the water phase. The terms  $V_o$  and  $V_w$  denote the volume of the oil and water phase, respectively.

The equation sets consisting of eqs 2, 3, and 4 can be combined to form an expression for the total acid content in the water phase and oil phase, as presented below.

$$[HA]_{w,tot} = \frac{[HA]_{o,init}}{\frac{[H^+]_w}{P_{wo,acid}(K_{a,HA}^w[H^+]_w)} + \frac{V_w}{V_o}} \quad (5)$$

$$[HA]_{o,tot} = \frac{[HA]_{o,init}}{1 + \frac{V_w P_{wo,acid}(K_{a,HA}^w[H^+]_w)}{V_o [H^+]_w}} \quad (6)$$

It is assumed that the deprotonated acid  $[A^-]$  is completely insoluble in the oil phase. With divalent cations in the oil phase, other phenomena, such as the formation of oil-soluble naphthenates<sup>61</sup> and precipitation of metal naphthenates<sup>62</sup> can occur. Since production problems with calcium naphthenates were first encountered in the 1990s,<sup>19</sup> there has been much research on the effect of divalent cations on naphthenic acids in oil-water systems<sup>7,8,63-66</sup> and, therefore, part of this article is dedicated to this effort.

This article aims to assess how a petroleum-cut commercial acid mixture partitions between the oil phase and the water phase. After characterization of the naphthenic acid and molecular weight mostly by GC/MS, the influence of molecular weight on oil–water partitioning will be determined. The partition ratio ( $P_{wo}$ ) will be obtained by fitting eqs 5 and 6 with a constant  $pK_a$  of 5. The effect of divalent cations on the partitioning behavior of the acids will be evaluated to determine if  $Ca^{2+}$  has specific interaction with the naphthenic acid mixture. This study will be extended for naphthenic acid mixtures extracted from crude oil in a companion article.<sup>67</sup> Data obtained through these studies will be used as a basis for ongoing studies into the kinetics of acid partitioning. An acid mixture from Fluka was chosen as the commercial acid mixture in this study, because it contains both aliphatic and alicyclic acids, as previously shown in the work of Lo et al.<sup>46</sup> and Hindle et al.<sup>47</sup>

### 3. MATERIALS AND METHODS

**3.1. Chemicals.** The following chemicals were used as received from the manufacturer without further purification: toluene (Sigma–Aldrich, anhydrous, 99.8%), deuterated chloroform (Sigma–Aldrich, 99.96 at % D), *n*-tert-butyltrimethylsilyl-*N*-methyltrifluoroacetamide with 1% tert-butyltrimethylchlorosilane (MTBSTFA + 1% TBDMSCL) (Sigma–Aldrich, ≥95%), acetic acid (Sigma–Aldrich, >99.99%), potassium dihydrogen phosphate (Merck, ≥99.5%), sodium tetraborate decahydrate (Sigma–Aldrich, ≥99.5%), sodium chloride (Merck, 99.5%), sodium bicarbonate (Sigma–Aldrich, 99.5%), and calcium chloride dihydrate (Sigma–Aldrich, 99%). A commercial naphthenic acid mixture from Fluka was used with specifications from the manufacturer (density,  $d_4^{20} = 0.95$ , acid number = 230 mg<sub>KOH</sub>/g) and it looks like a thick golden liquid. Different carboxylic acids were used to test the gas chromatography/mass spectroscopy (GC/MS) procedure; their features are listed in Table 1.

**3.2. Characterization.** Hydrogen 1 (<sup>1</sup>H) and carbon 13 (<sup>13</sup>C) nuclear magnetic resonance (NMR) analyses were performed with a Bruker Avance NMR spectrometer (400 MHz). Naphthenic acid samples were prepared to a concentration of 1 wt % for <sup>1</sup>H and 10 wt % for <sup>13</sup>C in CDCl<sub>3</sub>. The elemental composition (C, H, N, O, S, Ca, Cl, Na) was determined by the Laboratory SGS Multilab (Evry, France) using thermal conductivity measurements for C, H, and N, by infrared measurements for O and S, by mineralization and ICP/AES for Ca and Na and potentiometric titration for Cl. The TAN values were determined according to ASTM Method D664-95 on a Titrand unit (Metrohm) that was fitted with a 6.0229.100 LL solvotrode.

**3.3. Equilibrium Partitioning.** **3.3.1. With Monovalent Cations.** At least two parallels of oil–water experiments from pH 2–12 were performed. Solutions of the commercial acid mixture in toluene were prepared at two different concentrations: 10 mM (2.3 g/L) and 4 mM (0.9 g/L). These concentrations correspond to TAN values between 0.25 and 0.7 mg<sub>KOH</sub>/g. 3.5 wt % NaCl aqueous buffers listed in Table 2 were prepared with ultrapure water (Milli-Q, Millipore, resistivity of 18.2 MΩ cm) as the water phase. Equal volumes of oil and water phase (8 mL) were shaken at 250 rpm for 24 h on a horizontal shaker (IKA HS 501). Samples were then centrifuged at 11 000 rpm for 30

min. The pH was measured before contact with the oil phase and after centrifugation. The oil phase is directly analyzed as explained in section 3.4.1, while the naphthenic acids in the water phase are first extracted through the following procedure. Six milliliters (6 mL) of the water phase was recovered and adjusted to pH < 2 by adding 0.6–3 mL of 1 M HCl in 3.5 wt % NaCl solution, depending on the pH of the aqueous buffer. Naphthenic acids present in the low pH water phase were back-extracted into a toluene volume equal to the recovered water before pH adjustment (6 mL) by shaking for 24 h. The extraction yield was assumed to be 100%, considering the  $pP_{wo}$  values and mass balances obtained in this work. To obtain a signal for the water phase in pH 2 experiments, 200 mL of both phases were used and the oil from the back-extracted water phase concentrated through evaporation prior to analysis. After centrifugation, the water phase of the experiments with pH 11 and 12 buffers had a slightly opaque water phase.

**3.3.2. With Divalent Cations.** At least two parallels of oil–water experiments were performed at pH 7, 8.4, 9, 10, and 12. The conditions were similar to those mentioned in the paragraph above, except that, here, the aqueous buffers contained 3.5 wt % NaCl and 10 mM CaCl<sub>2</sub>. Another exception was that the results for pH 7 were obtained through using a high initial pH (10.6) unbuffered solution due to KH<sub>2</sub>PO<sub>4</sub>/CaCl<sub>2</sub> incompatibility. Washing the oil phase with low pH water was considered, since calcium naphthenates would presumably be unavailable for derivatization, but this treatment was found to only affect the pH 12 sample, with regard to the internal standard peak. The post-centrifugation opaqueness of the high pH buffers mentioned in the previous paragraph was not observed in these experiments.

To obtain enough dry sample for elemental analysis after equilibrium partitioning with calcium, higher volumes (450 mL of both phases) were used.

**3.4. GC/MS.** **3.4.1. Preparation and Analysis of the Samples.** A quantity of 0.7 g of 0.22 mM 6-heptylnaphthalene-2-carboxylic acid in toluene (used as an internal standard) was added to 1.6 g of sample prior to derivatization. The criterion for the internal standard was an acid with elution time close to the hump of the acid mixture. 6-Heptylnaphthalene-2-carboxylic acid was selected to elute after the commercial acid mixture. A mass of 0.36 g of toluene solutions with naphthenic acids and internal standard were added to a microinsert inside a 1.5-mL glass vial, along with 0.04 g of *N*-tert-butyltrimethylsilyl-*N*-methyltrifluoroacetamide with 1% tert-butyltrimethylchlorosilane (MTBSTFA + 1% TBDMSCL), giving a >30 times excess of derivatization agent. The glass vials were sealed with Teflon-lined caps, and the samples were heated in a water bath at 65 °C for 30 min and weighed before and after. The weight did not change. GC/MS analysis was performed on an Agilent GC(7890)/MS(S977) equipped with an Agilent J&W DB-1HT Nonpolar, 100% dimethylpolysiloxane, capillary column (30 m × 0.25 mm × 0.10 μm film thickness). The injection was run in splitless mode. The helium carrier gas flow rate was kept at 1 mL min<sup>-1</sup>. The inlet temperature and the GC/MS interface temperature were both kept at 330 °C. An initial temperature of 100 °C was held for 5 min before a ramp of 5 °C/min until a maximum temperature of 325 °C, which was held for 10 min. Solvent delay was set to 5 min. The GC/MS was operated in electron impact ionization mode with ion source temperature and quadrupole temperature at 230 and 150 °C respectively. This instrument was set to scan from *m/z* 42 to *m/z* 600 with a scan rate of 5 scans per second. An injection volume of 0.3 μL was chosen to ensure that saturation would not occur, i.e., no *m/z* peak could exceed 8.5 × 10<sup>6</sup> counts. Every five samples, pure solvent was run with the same method to serve as a blank. Chromatograms and spectra were acquired and analyzed using the Masshunter Acquisition Data qualitative analysis program.

**3.4.2. Mass Chromatogram Analysis.** Mass spectra were extracted from the chromatogram peaks with a height filter, only considering peaks with a relative height of >0.1% of the largest peak. Spectra from corresponding blank solvent runs were subtracted from the sample spectra. The *m/z* values obtained were used to determine the NA molecular weight, the carbon number, and the hydrogen deficiency

Table 2. List of Different Aqueous Buffers Prepared<sup>68</sup>

pH	buffer
2	0.01 M HCl
4	0.1 M CH <sub>3</sub> COOH adjusted with NaOH
6–7.9	0.1 M KH <sub>2</sub> PO <sub>4</sub> adjusted with NaOH
8.4–9	0.025 M borax adjusted with HCl
9.5–10	0.025 M borax adjusted with NaOH
11	0.05 M NaHCO <sub>3</sub> adjusted with NaOH
12	0.01 M NaOH

(Z). The procedure was described as follows. First, the  $m/z$  values were rounded by setting the values between  $(x - 1).7$  and  $(x).7$  to  $x$ , since most atoms weigh more than the nominal mass. For example, both 237.7  $m/z$  and 238.69  $m/z$  would be rounded to 238  $m/z$ . The  $n$  and  $Z$  then were determined using the matrix presented in Table S1 in the Supporting Information. Table S1 is an example of a matrix of the possible naphthenic acids within the carbon number range of 5–37, with 0–6 rings ( $Z = 0$  to  $-12$ ); the masses shown are those of  $[M + 57]$  ions. Some isomer combinations are excluded by the rules set up by Holowenko et al.<sup>26</sup> (for example, nonexistent molecules with five carbons and six rings). Contrary to Holowenko et al.,<sup>26</sup> aromatic structures were considered in this work. The shortcoming of MTBSTFA, with regard to steric hindrance,<sup>38</sup> was not investigated.

**3.4.3. Quantification.** The equilibrium concentrations of both phases were determined by GC/MS. Total ion chromatograms (TIC) are chromatograms that show the sum of all intensities for all masses registered by the detector over time. The extracted ion chromatogram (EIC) shows the sum of intensities for a specific mass or mass range registered by the detector over time. The total NA concentration and the concentration of NA of specific molecular weight ranges were determined using the following methodology. Extracted ion chromatograms (EIC) were obtained from total ion chromatograms (TIC). After subtraction of solvent blanks obtained during the same analysis session and integration of the peak, the naphthenic acid concentration was determined after normalization with internal standard peak area (6-heptylnaphthalene-2-carboxylic acid, retention time = 33.7 min) and comparison with the corresponding calibration curve.

## 4. RESULTS AND DISCUSSION

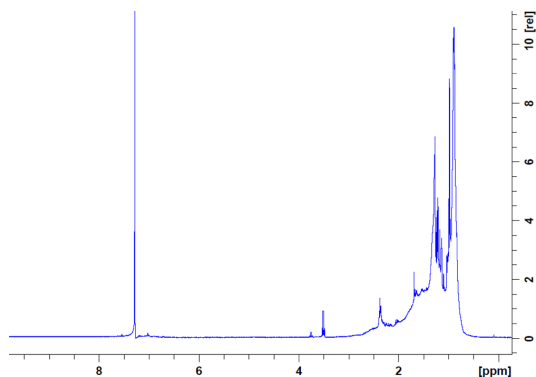
**4.1. Characterization.** **4.1.1. Characterization by Total Acid Number (TAN), Elemental Analysis, and Nuclear Magnetic Resonance (NMR).** The total acid number (TAN) of the commercial NA mixture was measured to 242  $\text{mg}_{\text{KOH}}/\text{g}_{\text{oil}}$  through titration, which indicates an average molecular weight of 231 g/mol, assuming monoprotic acids, which is in good agreement with the data provided by the manufacturer. The elemental composition of the commercial acid mixture is listed in Table 3. The acids in the commercial acid mixture

**Table 3. Elemental Composition of the Commercial Naphthenic Acid Mixture**

element	symbol	composition [wt %]
carbon	C	74.1
hydrogen	H	11.54
oxygen	O	14.26
sulfur	S	<0.1
nitrogen	N	<0.05

contains almost no sulfur or nitrogen. Assuming pure carboxylic acids with isomer  $\text{C}_n\text{H}_{2n+Z}\text{O}_2$ , the percentages of C, H, and O are consistent with an average combination with  $n = 14$  and  $Z = -2$ , indicating a molecular weight of 226 g/mol, which is similar to the molecular weight obtained by titration. The elemental analysis compares well to the one reported on the same commercial acid by Rudzinski et al.<sup>14</sup> 74.2% C, 11.23% H, and 14.5% O, with negligible N and S. Consequently, the average molecular weight was also equivalent, although they did not round  $n$  to the nearest integer.

$^1\text{H}$  NMR and  $^{13}\text{C}$  NMR spectra of the commercial NA mixture are depicted in Figures 1 and 2, respectively. Figure 1 show the  $^1\text{H}$  NMR spectrum conducted on a 1 wt % solution of the commercial acid mixture. The peaks with chemical shifts lower than 1 ppm are related to termination methyl groups,



**Figure 1.**  $^1\text{H}$  NMR spectrum for the commercial naphthenic acid mixture in  $\text{CDCl}_3$ .

while peaks between 1.15 and 2.33 ppm corresponds to  $\text{CH}_2$  methylene bridges with increasing proximity to the carboxyl group.<sup>69,70</sup> The absence of peaks at 7–8 ppm indicate that there are few or no aromatic groups in the commercial naphthenic acid mixture.<sup>49</sup> The  $^{13}\text{C}$  NMR spectrum performed on 10 wt % solution shown in Figure 2 concur with these findings by showing an almost-negligible intensity hump at 130 ppm for aromatic carbons. As with the hydrogen spectrum, most of the signal is in the aliphatic (primary to quaternary) region from 5 ppm to 60 ppm. The peak at 180–185 corresponds to COOH, and there are no noticeable peaks from C–O bonds. Rudzinski et al.<sup>14</sup> in performing a  $^{13}\text{C}$  NMR analysis on a commercial acid mixture from the same vendor, reported a composition of 7.1% aromatic carbons. However, as argued by West et al.,<sup>50</sup> commercial acid mixtures from petroleum cuts might differ, even when supplied by the same vendor. This might be attributed to shifts in crude oil stock or refinery strategies.

**4.1.2. Characterization by GC/MS.** **4.1.2.1. Assessment of Derivatization Efficiency.** More information about the composition of acid mixtures can be determined by GC/MS. Prior to the analysis of the commercial NA mixture, the performances of the chosen derivatization agent (MTBSTFA) was investigated using model acids of known structure (see Table 1). MTBSTFA derivatizes hydroxyl, carboxyl, thiol groups, and primary and secondary amines and creates stable ion fragments  $[M+57]$ , where M is the molecular weight of the acid.<sup>71</sup> To avoid confusion, mass fragments of MTBSTFA derivatized acids will always be denoted with  $m/z$  and the real molecular weights of acids will be given in units of g/mol. For simplicity,  $[M+57]$  is used to describe stable ion fragment for acids with multiple functional groups such as diacids as well, even though it technically should be denoted  $[M+57+114]$  for diacids (Table 1). A table of masses for the isomer  $\text{C}_n\text{H}_{2n+Z}\text{O}_2$  is listed as Table S1 in the Supporting Information. This table allows for  $n$  and  $Z$  to be ascertained from their molecular weight, as explained in section 3.4.2.

The double bond equivalent (DBE) described in eq 7<sup>72</sup> gives the average unsaturation for naphthenic acids structures.

$$\text{DBE} = \frac{2C + 2 - H}{2} \quad (7)$$

DBEs can be attributed to hydrogen deficiency ( $Z$ ), as denoted in eq 8.<sup>73</sup>

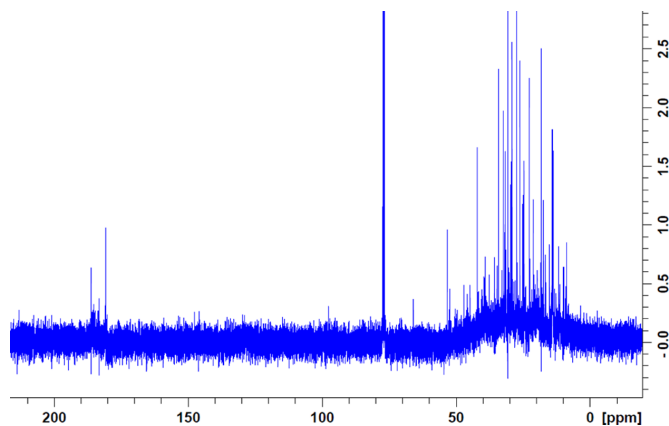


Figure 2.  $^{13}\text{C}$  NMR spectrum for the commercial naphthenic acid mixture in  $\text{CDCl}_3$ .

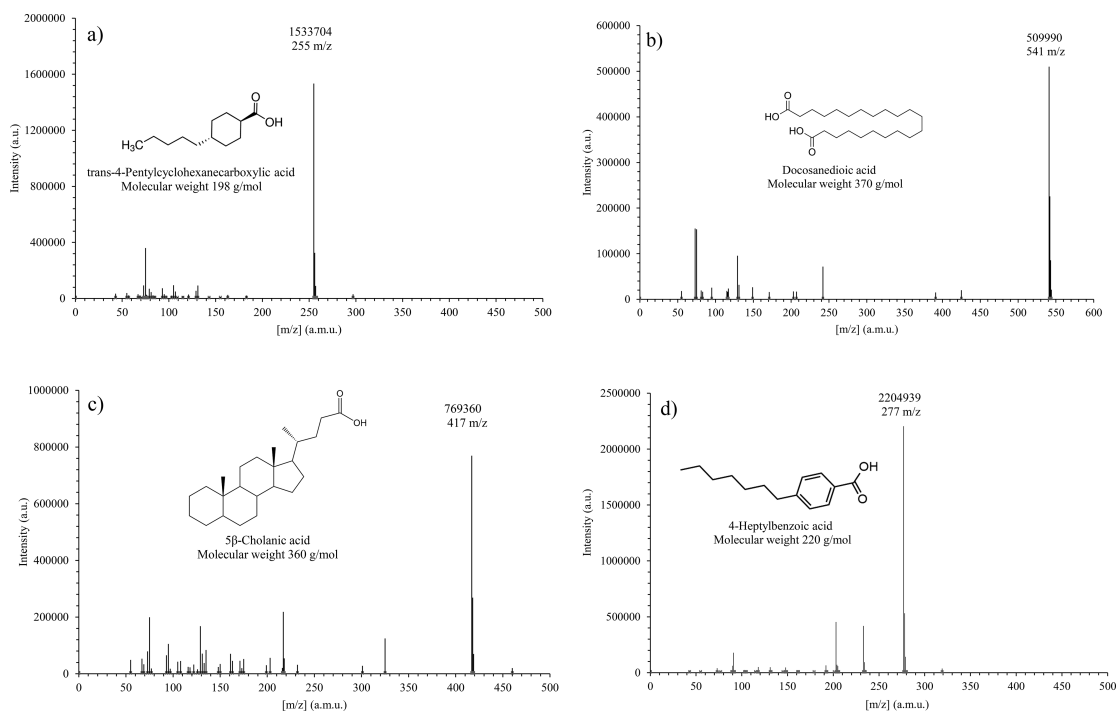


Figure 3. Mass spectra of chromatogram peaks and structures for (a) trans-4-pentylcyclohexanecarboxylic acid, (b) docosanedioic acid, (c) 5 $\beta$ -cholanic acid, and (d) 4-heptylbenzoic acid after derivatization with MTBSTFA.

$$Z = -2\text{DBE} + 2 \quad (8)$$

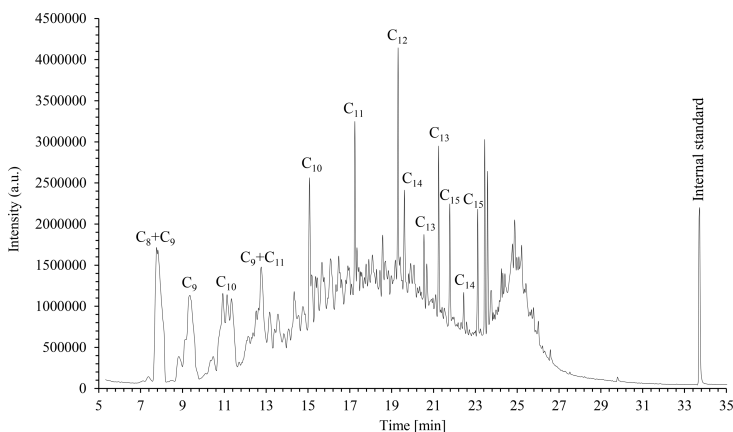
where  $C$  and  $H$  are the number of carbon and hydrogen atoms in the formula. Since alkenes are typically not present in crude oil,<sup>74</sup> the hydrogen deficiency ( $Z$ ) is used to assign cyclic or aromatic structures.

Acids with aromatic functional groups have traditionally been excluded from the  $\text{C}_n\text{H}_{2n+Z}\text{O}_2$  isomer mass tables, either because they fall outside the traditional definition<sup>26</sup> or because low-molecular-weight aromatic acids are present in very low concentrations in petroleum acid extracts.<sup>35</sup> However, larger

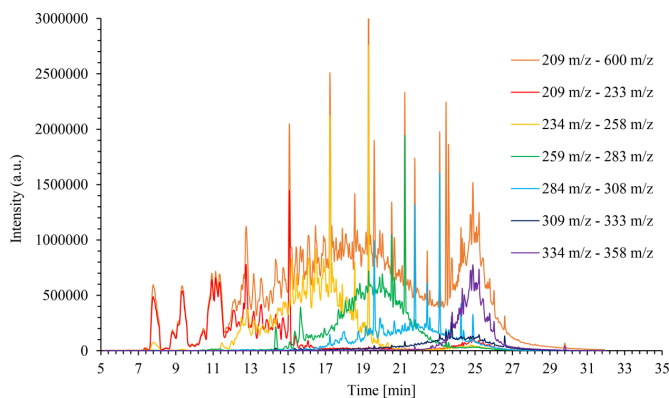
aromatic acids are present in both oil sands and petroleum,<sup>75,76</sup> and this article has included aromatic ring combinations, as seen in Table S1, to cover as diverse a range of carboxylic acids as possible. Indeed,  $Z$  can be less than or equal to  $-8$  in Table S1, which could match molecules containing one aromatic ring.

A mixture of model acids from Table 1 was derivatized with MTBSTFA and analyzed with GC/MS. As can be seen in Figure 3, the derivatization method produces a single dominant mass fragment for different acid structures, such as saturated, diacids, aromatic, and polycyclic. It appears that the





**Figure 4.** Chromatogram of the commercial NA mixture. The peak at a retention time of 33 min corresponds to the internal standard 6-heptylnaphthalene-2-carboxylic acid. Major peaks listed have stable ion fragments consistent with saturated fatty acids. Their carbon number is indicated on the figure.



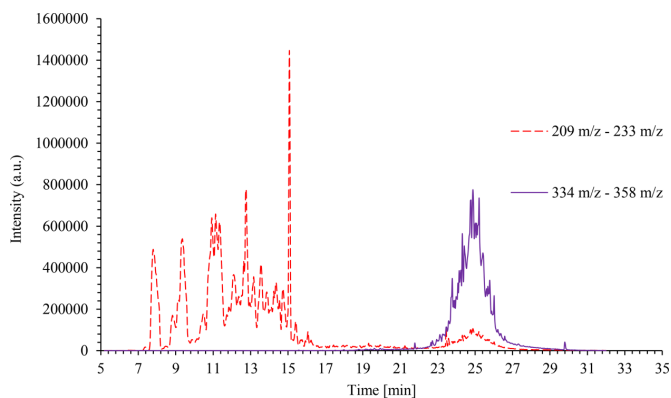
**Figure 5.** Chromatograms showing the EIC with a mass range of 209–600  $m/z$  and shorter mass ranges.

dominance of the single-ion fragment is more evident for saturated acids and single ring acids, compared to aromatic and polycyclic acids. This is also evident when evaluating the acid fragmentation findings by Clemente and Fedorak,<sup>39</sup> who wrote a comprehensive analysis about GC/MS analysis of naphthenic acids derivatized by MTBSTFA. Their method compares how the acid fragments would be interpreted by the mass distribution matrix given in Table S1 (note that the isotope  $[M+57]+1$  would not be counted in this matrix). Generally, the ion abundance of the stable mass fragment  $[M+57]$  declines with both molecular weight and hydrogen deficiency. Larger acids can also give a false presence of another acid. For example, as can be seen in Table 1, ~9% of the real Behenic acid ( $C_{22}$   $Z = 0$ ) peak would appear as a  $C_{23}$   $Z = -12$  acid, because of the isotopes of carbon and silicon. However, this isotope bias in the determination of the naphthenic acid distribution is statistically insignificant, as shown by Clemente and Fedorak.<sup>39</sup>

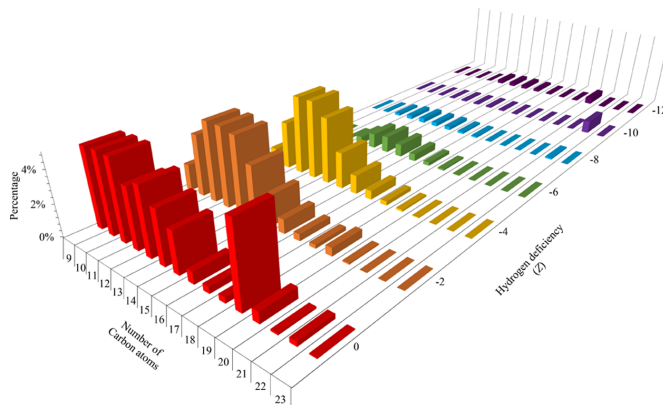
The mass spectra of 5-phenylvalerian acid, propyl benzoic acid, and 1-naphthaleneacetic acid present a higher fragmentation, which is consistent with their aromaticity. However, the intensity abundance of the stable  $[M+57]$  peak indicated in

Table 1 is very high (97%, 95%, and 92%, respectively). This discrepancy comes from the fact that the fragments from these compounds are too small to be counted as naphthenic acids in Table S1.

The excessive fragmentation of compound with higher molecular weight, aromatic rings, or polycyclic structures would create a distribution bias toward low-molecular-weight acids and should be considered when making mass distributions of naphthenic acid mixtures. The opposite effect, where smaller acids appear to be larger acids, can also occur in the situation when, for example, two methyl silyl groups are grafted onto a diacid. The results obtained in Table 1 show that the base peak for derivatized diacids (hexadecanedioic acid, docosanedioic acid) corresponds to  $[M+57+114]$  i.e., both acid groups have been derivatized but only one has been subsequently ionized. This was also noted by St. John et al.<sup>24</sup> on the diacid camphoric acid. As a result, docosanedioic acid ( $C_{22}H_{42}O_4$ ) would appear as a monoacid with  $C_{33}$  and  $Z = -10$  in our analysis. Similar conclusions were drawn by Bataineh et al.<sup>77</sup> for hydroxylated acids. Nevertheless, some diacids are doubly ionized,  $[M+57 + 57]/2$  (242  $m/z$  peak for docosanedioic acid in Figure 3 and 200  $m/z$  peak for



**Figure 6.** Chromatogram showing response for extracted ion chromatograms (EIC) with mass ranges of 209–233  $m/z$  and 333–358  $m/z$ . The response of the EIC with a mass range of 209–233  $m/z$  at minute 25 is considered as fragments.



**Figure 7.** Mass distribution of commercial NA mixture. An attempt to reduce the effects of fragmentation was performed by splitting up the mass spectra with different mass ranges (see Table 4) before recombination (see the text for details). The untreated distribution was not significantly different.

hexadecanedioic acid, not shown). As the doubly charged species for both diacids tested have even  $m/z$  numbers, doubly charged ion peaks do not influence the distribution, because they are not counted as naphthenic acids, according to Table S1. However, this is a mere coincidence, as it can easily be demonstrated that every other diacid produces an odd numbered doubly charged peak, which would influence the naphthenic acid distribution. For instance, the diacid  $C_9H_{16}O_4$  with a molecular weight of 188 g/mol, would give a doubly charged ion peak at 151  $m/z$ .

**4.1.2.2. GC/MS Analysis of the Commercial Naphthenic Acid Mixture.** The commercial NA mixture was analyzed by GC/MS to give the chromatogram presented in Figure 4. The chromatogram elutes as an unresolved hump with two different modes and several well-defined peaks. This means that the Fluka NA mixture is so complex that GC cannot separate all the molecules present. The well-defined peaks appear to have a hydrogen deficiency of 0 and, therefore, it can be speculated that they correspond to linear saturated fatty acids of different molecular weight. Their carbon numbers are indicated in Figure 4. It can be observed that saturated acid peaks elute roughly consecutively until  $C_{12}$  (retention time = 19 min); at

longer retention times, saturated  $C_{13}$ ,  $C_{14}$ , and  $C_{15}$  acids can be identified. As there are several peaks corresponding to  $C_{13}$  and  $C_{14}$ , it must correspond to different isomers, and, consequently, nonlinear saturated carboxylic acids are most likely present. The second mode at a retention time of 25 min corresponds to molecules in  $C_{19}$ . The mass spectrum averaged over the entire elution hump was analyzed with regard to the stable mass ion fragments for naphthenic acids listed in Table S1 to yield a distribution shown in Figure 7 (presented later in this work). A response factor of 1 was assumed for all acids.

The separation in GC fitted with a nonpolar column is based on boiling point, i.e., molecular weight for a given class of molecule. To check the consistency of results, a visualization of increasing EIC mass ranges is shown in Figure 5. These EIC mass ranges revealed that part of the mass range 209–233  $m/z$ , corresponding to small acids, elute later in the chromatogram, where acids of much larger molecular weight elute, as seen in Figure 6. These were thought to be either fragments of higher-molecular-weight compounds, as seen in Figure 3, or nonacid pollutants. The obtained distribution also indicated a high amount (9% of the intensities corresponding to naphthenic acids in Table S1) of low-molecular-weight acids with stable

mass fragments from 159  $m/z$  to 208  $m/z$ . Upon closer examination of the EIC for the mass range of 159–208  $m/z$ , it was observed that these compounds do not elute early with a mass specific elution hump in the start of the chromatogram, but rather elute upon low intensity over the entire hump. These were deemed to be fragments of high-molecular-weight species, hence, Figure 7 starts at the next mass range 209–233  $m/z$  or  $C_9$ . As can be seen in Table S1, the mass ranges below 209  $m/z$  contains few possible acid structures and small molecules also have fewer structural isomers.<sup>47</sup> St. John et al.<sup>24</sup> noted that it was difficult to find masses below 200  $m/z$  using the MTBSTFA technique on acid mixtures, because of the presence of other fragment ions. The same article also argues that 97% of naphthenic acids have nine carbon atoms or more. As was seen in previous work,<sup>59</sup> low-molecular-weight acids are preferably water-soluble, even at low pH values. Much of the reported results from the literature could be skewed in this regard, as smaller acids could have been lost from the oil to the produced water or desalter water before entering the refinery.

There are larger fragments ( $\geq 209$   $m/z$ ) as well, as shown in Figure 6. From the EIC mass ranges (Figure 5), it was determined that the elution of increasing acid masses starts and is completed at specific times. As an example, in Figure 6, the acids in the mass range of 209–233  $m/z$  were found to elute over a range of 7.5–17 min. Consequently, all signal responses from this mass range above 17 min were disregarded as small fragments from larger acids or as nonacid molecules. Based on the elution humps for different EIC mass ranges shown in Figure 5, the total chromatogram was split into time segments with increasing minimum  $m/z$  cutoffs shown in Table 4, before

**Table 4. How the Chromatogram Segments Are Considered To Ensure That Fragments Do Not Skew the Mass Distribution in Favor of Lower-Molecular-Weight Acids**

chromatogram segment	minimum $m/z$ cutoff
7.5–17 min	209
17–22 min	233
22–24 min	258
24–27 min	283
27–29 min	308
29–32 min	333

the intensity averages of each time segment was normalized and summed up to reconstruct the mass distribution for the entire chromatogram. However, the mass distributions did end up looking similar, which indicates that most fragments were found in the mass range of 159–208  $m/z$  and that the commercial NA mixture contains mainly low-molecular-weight acids that, when derivatized with MTBSTFA, do not produce high amounts of fragments with mass higher than 209  $m/z$ .

Figure 7 shows that the commercial naphthenic acid mixture consists mainly of aliphatic ( $Z = 0$ ) and alicyclic structures ( $Z > -8$ ). The distribution is narrow, with regard to carbon number and hydrogen deficiency, with  $C_9$ – $C_{19}$  and 0–3 ring structures. Indeed, there are nearly no acids with  $Z = -8$ , which is the hydrogen deficiency corresponding to a single aromatic ring or 4-ring structures. This result is consistent with the NMR spectra in Figures 1 and 2. The biggest proportion of peaks seems to fall in the  $C_9$ – $C_{15}$  and 0–2 ring ranges, although a second mode at  $C_{19}$  can be observed, in agreement with the chromatogram presented in Figure 4. The peaks seen at  $Z = -12$  are most likely a measurement artifact. Indeed, it

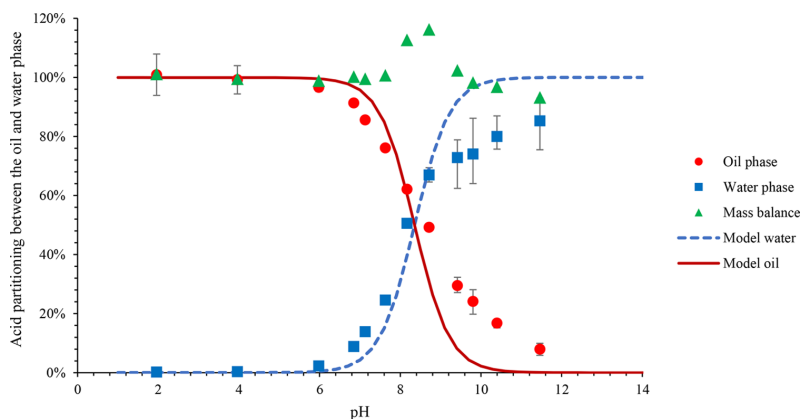
can be seen in Table 1 that, because of the isotopic composition of C and Si, peaks at  $[M+57]+2$  are present in the mass spectrum with an intensity of  $\sim 5\%$ – $9\%$  of the stable ion fragment peak  $[M+57]$ . Consequently, because of the periodic structure of Table S1, the peaks at  $Z = -12$  could just correspond to  $[M+57]+2$  isotopes of  $[M+57]$  species with  $Z = 0$ . The number-average molecular weight calculated from the GC/MS mass distribution was 210 g/mol. A comparison of average molecular weight determined by different methods show that this number is lower than the average molecular weight determined by elemental analysis or acid number, as seen in Table 5. This could be attributed to the lower response

**Table 5. Summary of Results Obtained by Characterization of the Commercial NA Mixture**

method	average molecular weight (g/mol)
elemental analysis	226
titration	231
GC/MS	210

factors of higher-molecular-weight compounds. It must be mentioned that different separation conditions were tested by varying the GC temperature program, which all provided similar NA distributions. A well-defined double peak at 387  $m/z$  ( $C_{22}$   $Z = -10$ ) was observed in the chromatogram. This compound would partition into water at any pH, including acidic ones. Consequently, it is thought that this compound is not a carboxylic acid, although it likely contains some functional group that reacts with MTBSTFA, since it disappeared when the commercial NA mixture was injected without a derivatization agent. By taking the total intensity as the sum of all intensities from 209  $m/z$  to 600  $m/z$ , the masses in Table S1 representing the isomer  $C_nH_{2n+Z}O_2$  accounted for 80% of the total intensities registered. Using another table with  $[M+57]+1$   $m/z$ , because of the isotopes of silicon and carbon accounts for 18% of the total intensities. The remaining 2% falls outside the masses in Table S1 and was considered either an uncertainty or a contribution from phenols<sup>50</sup> or molecules containing oxygen, nitrogen, or sulfur groups, which do not react with MTBSTFA. It should be mentioned that matching nominal masses could encompass a large amount of different structures, as seen in Table S1; every other mass is counted as an acid when above 259  $m/z$ . This would exclude some naphthenic acids, nitrogen combinations as these would get an even nominal mass. The larger proportion of naphthenic acids with added oxygen, sulfur, or other nitrogen functional groups would get odd stable mass fragments so close to those in Table S1 that they could not be distinguished with the available precision. However, with the low values for sulfur and nitrogen from the elemental analysis and the assumption that commercial acid mixtures contains few  $O_3$  and  $O_4$  species,<sup>10</sup> we still presume to compare our results with the findings of more-precise MS analysis on the same commercial NA mixture. Lo et al.<sup>46</sup> and Rudzinski et al.<sup>14</sup> examined a commercial NA mixture from Fluka via ESI-MS without prior fractionation to obtain a mass distribution with a large presence of unsaturated compounds filling out hydrogen deficiency columns up to  $Z = -12$ , much different from the distribution shown in Figure 7. On the other hand, Hindle et al.<sup>47</sup> using HPLC TOF HRMS obtained a completely different distribution from the two previous studies, which does seem to completely overlap with the distribution in Figure 7. This





**Figure 8.** Equilibrium partitioning of the 209–600  $m/z$  fraction, given as a function of equilibrium pH. The total concentration of the commercial NA mixture was 10 mM or 4 mM for  $\text{pH} > 9$ . Aqueous buffers (3.5 wt % NaCl) were used as the water phase. Data were fitted with eqs 5 and 6. The values are the average of two or three measurements, where the error bars represent the range of obtained values. Some of the error bars are smaller than the symbols. The mass balance error bars are not specified for the sake of clarity.

discrepancy in distributions is most likely due to the aforementioned differences between commercial acid mixtures of the same vendor, although part of it could be attributed to the differences seen in analysis with and without chromatographic separation prior to the MS detection.<sup>78</sup> Merlin et al.<sup>36</sup> analyzed a commercial NA mixture from the same vendor with GC/MS and MTBSTFA. The article reported the abundance of three mass fragments  $\text{C}_{13} Z = -4$   $m/z = 267$ ,  $\text{C}_{13} Z = -6$   $m/z = 265$ , and  $\text{C}_{14} Z = -6$   $m/z = 279$  with abundances of 9%, 1%, and 1% of total ions, respectively. As can be seen in Figure 7, our results show abundances of 6%, 1%, and 1% of the same mass fragments, which is consistent with Merlin et al.<sup>36</sup>

**4.2. Determination of the Partition Ratio.** Commercial NA mixture in toluene were shaken in the presence of aqueous buffers, and the separated phases were derivatized and analyzed with GC/MS. The partition ratio of naphthenic acids was studied using toluene as the oil-phase solvent. Choice of the model solvent is not trivial, since different equilibria such as dimerization<sup>79</sup> are influenced by the polarity of the solvent. Aromatic solvents have been used in numerous studies as model solvent for crude oil to study compounds such as asphaltenes and resins.<sup>80–82</sup> The extracted ion chromatograms (EICs) between 209  $m/z$  and 600  $m/z$  of derivatized naphthenic acids were extracted from the total ion chromatograms (originally, the mass range of 159–600  $m/z$  was chosen, because this range corresponds to the smallest acids listed in Table S1; however, as mentioned in the previous section, the masses that registered as acids below  $\text{C}_9$  were thought to be smaller fragments, because of their constant elution over the entire acid hump). The area under the chromatogram was used to build calibration curves after recombination with the area of the internal standard peak.

The equilibrium partitioning for the commercial acid mixture is shown in Figure 8. At low pH values, all the acids have a low affinity for the water phase. At pH 6, partitioning starts and at the highest pH value (11.5), ~8% of the acids remain in the oil phase. The pH at which 50% of the naphthenic acids are in water and 50% of the naphthenic acids are in the oil phase is close to 8.4. Since the  $\text{p}K_a$  value for carboxylic acids and naphthenic acids have been found to have

a  $\text{p}K_a$  of 4–6,<sup>42,54,83</sup> the  $\text{p}K_a$  in these calculations has been fixed to a value of 5. From the partitioning equations offered in several papers,<sup>59,60,84</sup> it can be deduced that the apparent  $\text{p}K'_a$  value (i.e.m the point where the acid(s) is/are equally distributed between the two phases) is equal to the sum of  $\text{p}P_{\text{wo}}$  and  $\text{p}K_a$ , as shown in eq 9.

$$\text{p}K'_a = \text{p}K_a + \text{p}P_{\text{wo}} \quad (9)$$

Headley et al.,<sup>31</sup> in researching how pH affected solid phase extraction (SPE) recoveries of naphthenic acids from water, agitated a commercial NA mixture from Fluka in various aqueous buffers. The extraction recovery by SPE was reported to be 100% at pH 3, 63% at pH 7, and 50% at pH 9, which matches the results obtained in Figure 8, assuming that close to 100% of the acids in the water phase are dissociated.

Equations 5 and 6 predicts a  $\text{p}P_{\text{wo}}$  of 3.4, which gives an apparent  $\text{p}K'_a$  of 8.4, which technically is the point where phase transfer becomes predominant. However, compared to sharp phase transfers of single compounds,<sup>59</sup> the phase transfer of a polydisperse acid mixture happens on a much wider pH range. Consequently, eqs 5 and 6 do not give an accurate fit for the partitioning as a function of pH with a single  $\text{p}P_{\text{wo}}$ .

To obtain an equation to model the partitioning of the polydisperse mixture, it was decided to divide the chromatogram into range fractions to obtain narrower molecular weight ranges. This strategy is similar to that adopted to obtain the commercial NA mixture carbon numbers and hydrogen deficiency distribution in Figure 7. Indeed, the distribution of the naphthenic acids present in the water phase after partitioning at pH 8 (Figure S1 in the Supporting Information) shows that the lowest-molecular-weight acids are preferentially partitioned into the aqueous phase. The retention times and the mass range of the different fractions are summarized in Table 6. Note that this table is consistent with Table 4. A calibration curve was built for every fraction considered in Table 6, normalized by the internal standard. The signal obtained from mass ranges above 358  $m/z$  were small and did not yield accurate enough data. Although individual response factors were not used, the data should still be regarded as quantitative, as separate calibration curves were built for every

**Table 6. Mass Ranges Considered for Quantitative Partition Analysis of Extracted Ion Chromatograms (EICs) of the Commercial NA Mixture and the Elution Time Segment Considered to Be Whole Acids and Not Fragments**

EIC mass fragment range <sup>a</sup> [ <i>m/z</i> ]	integrated time interval of EIC	R <sup>2</sup> , linear range of 0.4–15 mM, 0.092–3.4 g/L	chromatogram area [%]
209–600	7.5–32 min	0.998	100
209–233	7.5–17 min	0.997	16
234–258	10–22 min	0.999	26
259–283	14–24 min	0.999	21
284–308	12–27 min	0.999	12
309–333	15–29 min	0.997	5
334–358	18–30 min	0.995	9

<sup>a</sup>Masses included in the mass ranges are based on naphthenic acid masses [M+S7] from Table S1 including their isotope [M+S7]+1.

fraction, reducing the impact of lower response factors with molecular weight.

In total, the areas used for concentration determination of the different fractions encompassed 90% of the total chromatogram area spanning from 209 *m/z* to 600 *m/z*. The lacking 10% can be attributed to nonincluded fragment humps, as seen in Figure 6 and masses above 358 *m/z*.

The equilibrium partitioning of the mass range of 209–233 *m/z* is shown in Figure 9. As seen in Table S1, this mass range corresponds to C<sub>9</sub>/C<sub>10</sub> acids. The EIC intensity of this fraction comprises 16% of the total chromatogram area. The acids in this mass range are completely oil-soluble below pH 6 and transfer completely to the water phase from pH 6 to pH 9. Equations 5 and 6 give an adequate fit with the data when the  $pP_{wo}$  is 2.3, indicating that the molecular weight range is narrow enough to be modeled by a single  $pP_{wo}$ . However, the mass balance is quite noisy in this mass segment. The apparent  $pK'_a$  indicates a phase transfer from pH 7.3.

The equilibrium partitioning of the mass range of 234–258 *m/z*, corresponding to C<sub>11</sub>/C<sub>12</sub> acids, is shown in Figure 10. The EIC intensity of this fraction comprises 26% of the total chromatogram area. Equations 5 and 6 give a good fit with the data when  $pP_{wo} = 2.9$  (higher than the value found for the mass

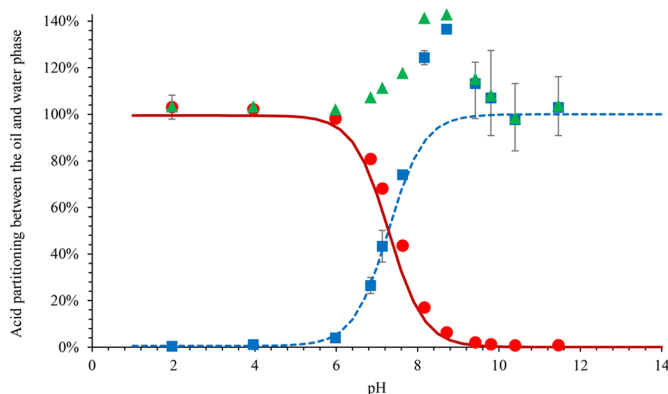
range of 209–233 *m/z*) which indicates a phase transfer at the apparent  $pK'_a$  of 7.9.

The equilibrium partitioning of the mass ranges of 259–283 *m/z* and 284–308 *m/z* are shown in Figures 11 and 12, respectively. These mass ranges correspond to C<sub>13</sub>/C<sub>14</sub> acids and C<sub>15</sub>/C<sub>16</sub> acids, respectively, and similarly comprise 21% and 12% of the total chromatogram area. A good fit with  $pP_{wo} = 3.7$  is obtained for mass range of 259–283 *m/z*, which gives an apparent  $pK'_a$  that indicates a phase transfer at pH 8.7, as seen in Figure 11. Equations 5 and 6 give a good fit with the data for mass range 284–308 *m/z* when  $pP_{wo} = 4.7$ , indicating a phase transfer at pH 9.7.

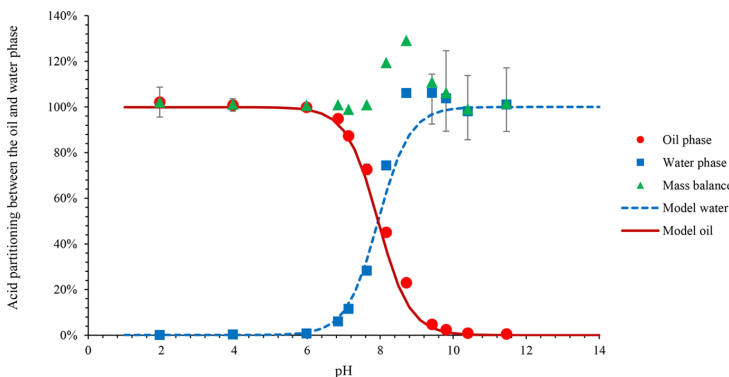
The equilibrium partitioning of the mass ranges of 309–333 *m/z* and 334–358 *m/z* are shown in Figures 13 and 14. These mass ranges correspond to C<sub>17</sub> acids and C<sub>18</sub>/C<sub>19</sub> acids, respectively, and similarly comprise 5% and 9% of the total chromatogram area. An adequate fit with a  $pP_{wo}$  of 5.2 is obtained for mass range of 309–333 *m/z*, which gives an apparent  $pK'_a$  indicating a phase transfer at pH 10.2, as seen in Figure 13. Equations 5 and 6 do not give a good fit with the data for a mass range of 334–358 *m/z*, because of incomplete partitioning. The obtained  $pP_{wo}$  value of 6.7 does not accurately predict the system behavior at high pH. The  $pP_{wo}$  values will be further discussed later in this work, in Figure 16.

The mass balances were systematically determined for all the systems tested and reported in Figures 8–14. This mass balance is generally close to 100%, except in two specific situations.

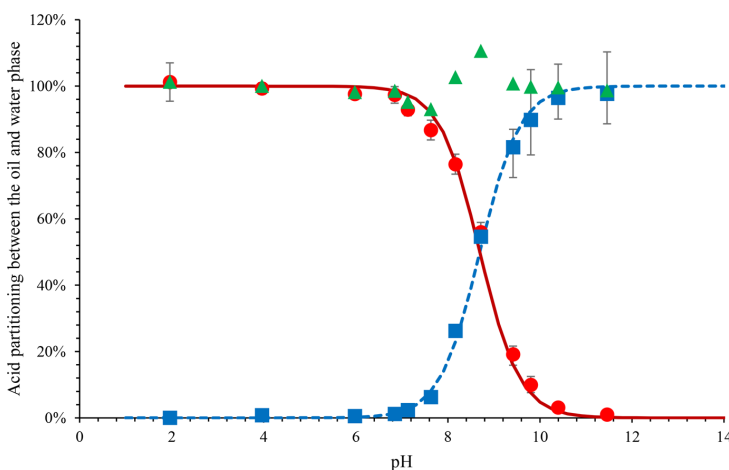
First, at high pH and for higher molecular weight (Figures 13 and 14), the mass balance is lower than 100%. Here, incomplete mass balances at high pH values can be observed, which contribute uncertainty to model predictions. Two explanations can be attributed to this loss. The surface activity of naphthenic acids increases with pH, as shown by Havre et al.,<sup>42</sup> with interfacial tension studies on the same commercial acid mixture used in this article. The increased surface activity means more naphthenic acids are present at the interface. However, the surface area between oil and water is low (a few cm<sup>2</sup>) and therefore the mass present at the interface should represent a negligible part of the total mass of naphthenic acids



**Figure 9.** Equilibrium partitioning of the 209–233 *m/z* fraction, given as a function of equilibrium pH. The total concentration of the commercial NA mixture was 10 mM, or 4 mM for pH >9. Aqueous buffers (3.5 wt % NaCl) were used as the water phase. Data were fitted with eqs 5 and 6. The values are the average of two or three measurements where the error bars represent the range of obtained values. Some of the error bars are smaller than the symbols. The mass balance error bars are not specified, for the sake of clarity.



**Figure 10.** Equilibrium partitioning of the 234–258  $m/z$  fraction, given as a function of equilibrium pH. The total concentration of the commercial NA mixture was 10 mM, or 4 mM for  $\text{pH} > 9$ . Aqueous buffers (3.5 wt % NaCl) were used as a water phase. Data were fitted with eqs 5 and 6. The values are the average of two or three measurements where the error bars represent the range of obtained values. Some of the error bars are smaller than the symbols. The mass balance error bars are not specified, for the sake of clarity.



**Figure 11.** Equilibrium partitioning of the 259–283  $m/z$  fraction, given as a function of equilibrium pH. The total concentration of the commercial NA mixture was 10 mM or 4 mM for  $\text{pH} > 9$ . Aqueous buffers (3.5 wt % NaCl) were used as a water phase. Data were fitted with eqs 5 and 6. The values are the average of two or three measurements, where the error bars represent the range of obtained values. Some of the error bars are smaller than the symbols. The mass balance error bars are not specified, for the sake of clarity.

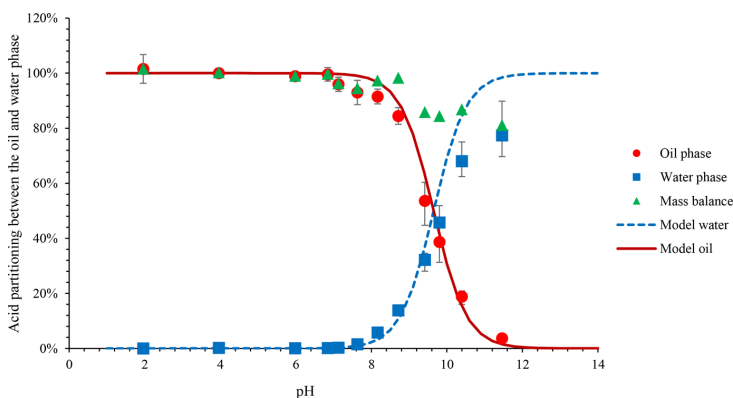
in the system. Another explanation can be attributed to the slightly opaque water obtained after centrifugation in experiments with initial pH 11 and 12 ( $\text{pH}_i = 10.4$  and  $11.4$ ), where this opaqueness is suspected to be the cause of the sample loss. It was impossible to improve the separation. It was attempted to dissolve 4 mM of pure commercial NA mixture in 3.5 wt % NaCl at pH 12 ( $\text{pH}_i = 11.4$ ) by shaking overnight. Part of the naphthenic acid mixture did not solubilize and, therefore, the turbidity seen at high pH in partitioning experiments are most likely attributed to sodium naphthenate particles, which is consistent with the low mass balance. This precipitation of sodium naphthenate is not predicted in the model tested in this article. This should be considered in the prediction for high-molecular-weight naphthenic acids at high pH for better prediction.

Second, the mass balance could be higher than 100% at intermediate pH (ca. 8), as seen in Figures 9 and 10. Multiple experiments including the testing of different solvents for the

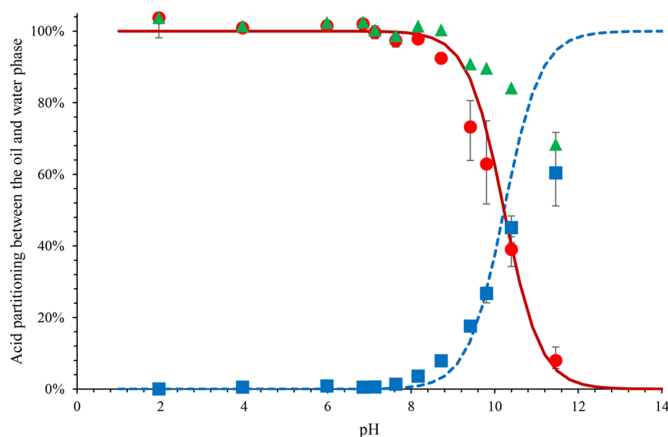
back-extraction procedure, building up the calibration curve several times, testing the repeatability, were performed to obtain a better mass balance, but these attempts were unsuccessful. We do not have an explanation concerning this discrepancy, but we can notice this only concerns a few points. This point should be investigated further to improve the accuracy of the method.

The mass ranges above 358  $m/z$  correspond to only 3% of the total chromatogram area and do not appear to partition into the water phase. The total naphthenic acid concentration in oil and water can be determined by doing the summation of every individual fraction in proportion to their ratios of the total chromatogram area, as seen in eqs 10 and 11.

$$[\text{HA}]_{w,\text{tot}} = \sum_{i=1}^n \omega_i \frac{[\text{HA}]_{o,\text{init}}}{\frac{[\text{H}^+]}{P_{w,o,\text{acid},i}(K_{a,\text{HA}} + [\text{H}^+])} + \frac{V_w}{V_o}} \quad (10)$$



**Figure 12.** Equilibrium partitioning of the 284–308  $m/z$  fraction, given as a function of equilibrium pH. The total concentration of the commercial NA mixture was 10 mM, or 4 mM for  $\text{pH} > 9$ . Aqueous buffers (3.5 wt % NaCl) were used as a water phase. Data were fitted with eqs 5 and 6. The values are the average of two or three measurements, where the error bars represent the range of obtained values. Some of the error bars are smaller than the symbols. The mass balance error bars are not specified, for the sake of clarity.



**Figure 13.** Equilibrium partitioning of the 309–333  $m/z$  fraction, given as a function of equilibrium pH. The total concentration of the commercial NA mixture was 10 mM or 4 mM for  $\text{pH}$  higher than  $> 9$ . Aqueous buffers (3.5 wt % NaCl) were used as the water phase. Data were fitted with eqs 5 and 6. The values are the average of two or three measurements where the error bars represent the range of obtained values. Some of the error bars are smaller than the symbols. The mass balance error bars are not specified, for the sake of clarity.

$$[\text{HA}]_{\text{o,tot}} = \sum_{i=1}^n \omega_i \frac{[\text{HA}]_{\text{o,init}}}{1 + \frac{V_w P_{\text{wo,acid},i} (K_{\text{a,HA}} [\text{H}^+])}{V_o [\text{H}^+]}} \quad (11)$$

Here, the  $\omega_i$  and  $P_{\text{wo,acid},i}$  are the chromatogram area fraction and partition ratio for each mass range, respectively.

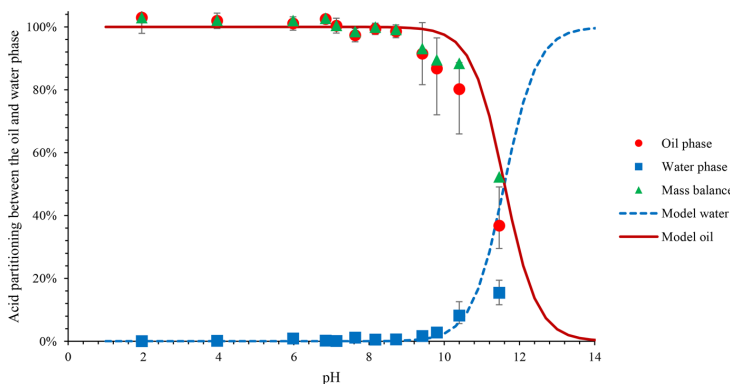
This summation model fits the partitioning data of the entire commercial NA mixture perfectly, as seen in Figure 15.

The findings for the partitioning of the commercial NA mixture are summarized in Table 7. Here, the  $pP_{\text{wo}}$  and apparent  $pK_{\text{a}}$  can be seen to progressively increase with the size of the acids. With few or no aromatic groups in the acid mixture, this size increase can only increase the hydrophobic surface area, lowering the water solubility.<sup>28,51</sup> The increasing molecular weight of acids in the water phase with pH is also found in the experimental findings of Hemmingsen et al.<sup>15</sup> This can also be observed in Figure 16, where the linear relationship between molecular weight and  $pP_{\text{wo}}$  previously

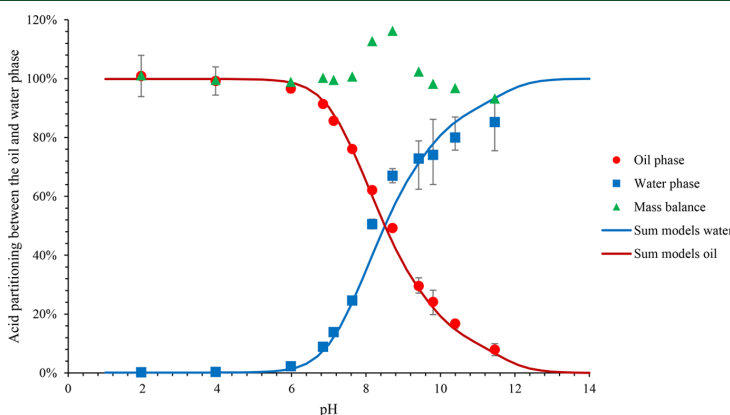
seen in the work of Reinsel et al.<sup>85</sup> and Havre et al.<sup>42</sup> is expanded. The meaning of the  $pP_{\text{wo}}$ , the variation with molecular weight, and their comparison with model components will be discussed in the companion article.<sup>67</sup>

Havre et al. have determined the CMC of a commercial NA mixture from Fluka at pH 11.3 and found a value of 0.8 mM. This means that micelles could be formed in some of our systems if the concentration of acids in the aqueous phase is higher than this value. The formation of micelles is not considered into the model presented in eqs 5 and 6. By considering the small chromatograms areas of the lowest concentrations considered in the calibration curves, partitioning experiments with similar concentrations under the CMC were deemed unreliable.

**4.3. Influence of Divalent Cation on Partitioning.** As seen in previous work,<sup>59</sup> the addition of 10 mM of a divalent cation such as calcium to the water phase affected the partitioning of the larger tested acid 4-heptylbenzoic acid with



**Figure 14.** Equilibrium partitioning of the 334–358  $m/z$  fraction, given as a function of equilibrium pH. The total concentration of the commercial NA mixture was 10 mM, or 4 mM for  $\text{pH} > 9$ . Aqueous buffers (3.5 wt % NaCl) were used as the water phase. Data were fitted with eqs 5 and 6. The values are the average of two or three measurements where the error bars represent the range of obtained values. Some of the error bars are smaller than the symbols. The mass balance error bars are not specified for the sake of clarity.



**Figure 15.** Equilibrium partitioning of the 209–600  $m/z$  fraction, given as a function of equilibrium pH. The total concentration of the commercial NA mixture was 10 mM, or 4 mM for  $\text{pH} > 9$ . Aqueous buffers (3.5 wt % NaCl) were used as the water phase. Data were fitted with eqs 10 and 11. The values are the average of two or three measurements where the error bars represent the range of obtained values. Some of the error bars are smaller than the symbols. The mass balance error bars are not specified, for the sake of clarity.

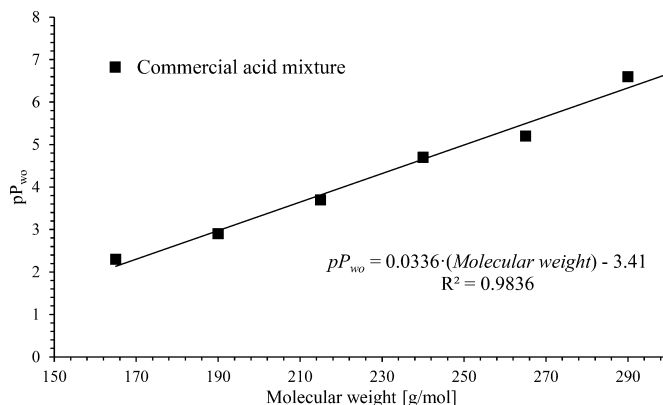
**Table 7. Mass Ranges and Equivalent Molecular Weight Shown with Their Respective  $\text{p}P_{\text{wo}}$  Calculated by Imposing  $\text{p}K_{\text{a}} = 5$  in eqs 5 and 6 (the Area Fraction of the Elution Hump of Each Mass Range Is Also Indicated)**

mass range	molecular weight	approximate carbon numbers	$\text{p}K_{\text{a}}^{\text{a}}$	$\text{p}P_{\text{wo}}$	chromatogram area [%]	$\text{p}K_{\text{a}}^{\text{c}}$
209–233 $m/z$	152–176 g/mol	$\text{C}_9/\text{C}_{10}$	5	2.3	16	7.3
234–258 $m/z$	177–201 g/mol	$\text{C}_{11}/\text{C}_{12}$	5	2.9	26	7.9
259–283 $m/z$	202–226 g/mol	$\text{C}_{13}/\text{C}_{14}$	5	3.7	21	8.7
284–308 $m/z$	227–251 g/mol	$\text{C}_{15}/\text{C}_{16}$	5	4.7	12	9.7
309–333 $m/z$	252–276 g/mol	$\text{C}_{17}$	5	5.2	5	10.2
334–358 $m/z$	277–301 g/mol	$\text{C}_{18}/\text{C}_{19}$	5	6.6 <sup>b</sup>	9	11.6
>359 $m/z$	>302 g/mol	> $\text{C}_{19}$	no partitioning at pH 12		3	
209–600 $m/z$	152–543 g/mol		5	3.4	100 <sup>c</sup>	8.4

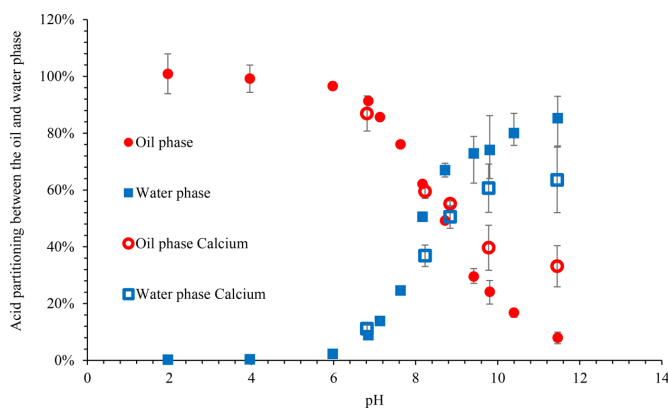
<sup>a</sup>A value of  $\text{p}K_{\text{a}} = 5$  imposed for naphthenic acids in all mass ranges. <sup>b</sup> $\text{p}P_{\text{wo}}$  calculated on incomplete partitioning in water at high pH. <sup>c</sup>Elution hump area does not add up to 100%, because of fragments registering as naphthenic acids, as can be seen in Figure 6.

the precipitation of calcium naphthenate  $\text{CaA}_2$  at pH 7 and higher, whereas no significant difference was seen for the partitioning of the small tested acid, phenylacetic acid. To map how calcium would affect the partitioning of a polydisperse mixture of acids, the same experimental setup used in section

4.2 was repeated, with the exception that 10 mM  $\text{CaCl}_2$  was added to the water phase. As mentioned, the separated water phases from the experiments with the two highest pH values in section 4.2, in the absence of  $\text{CaCl}_2$ , were slightly opaque, indicating the presence of colloids such as emulsions or



**Figure 16.** Graph indicating the linearity of the partition ratio  $pP_{wo}$  of acid mass ranges from the commercial NA mixture, based on molecular weight. The molecular weight indicated corresponds to the middle of the mass ranges.



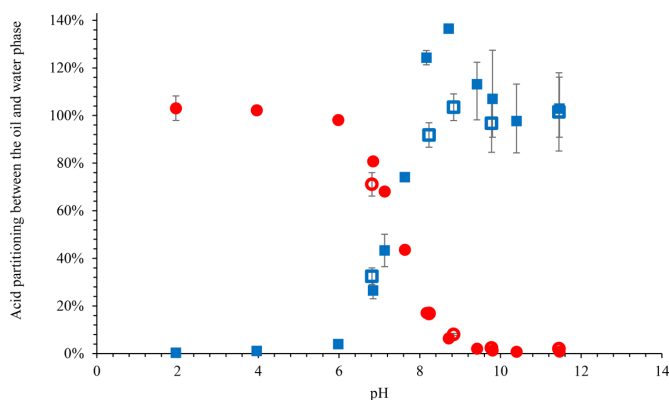
**Figure 17.** Equilibrium partitioning of the 209–600  $m/z$  fraction, given as a function of equilibrium pH. The total concentration of the commercial NA mixture was 10 mM, or 4 mM for  $\text{pH} > 9$ . Aqueous buffers with 3.5 wt % NaCl or 10 mM  $\text{CaCl}_2$  and 3.5 wt % NaCl were used as the water phase. The values are the average of two or three measurements, where the error bars represent the range of obtained values. Some of the error bars are smaller than the symbols. For the sake of clarity, figures without mass balances are presented here, and figures with mass balances are presented in the [Supporting Information](#).

particles. No opaqueness in the separated oil or water phases was observed in the partitioning experiments with calcium. In [Figure 17](#), we see the overall effect of calcium on the whole acid mass range of 209–600  $m/z$ . It can be observed that, at lower pH values, the acid partitioning seems unaffected, whereas a reduction in partitioning can be observed at higher pH values. Since the aqueous and oil phases at this pH were not turbid, the presence of precipitated calcium naphthenate can be ruled out. The influence of calcium on high-pH oil–water mixtures was also reported by Dudek et al.,<sup>86</sup> where it was found to exert a stabilizing effect on oil-in-water emulsions. This is believed to be caused by calcium complexes or oil-soluble calcium naphthenates. Oil-soluble calcium naphthenates have been discussed in the literature.<sup>56,61,87</sup>

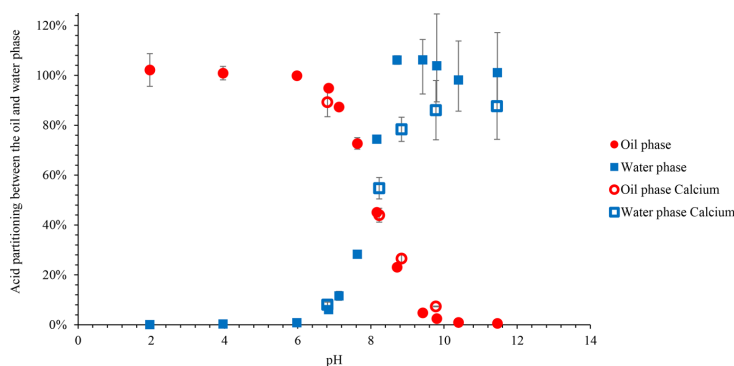
To study this in more detail, the mass ranges were considered individually, to determine how calcium affected different naphthenic acid sizes. As seen in [Figures 18 and 19](#), which present the partitioning of the mass ranges of 209–233  $m/z$  ( $C_9/C_{10}$ ) and 234–258  $m/z$  ( $C_{11}/C_{12}$ ), the smaller naphthenic acids are largely unaffected by the presence of

calcium, as was the case for the small model acid, phenylacetic acid (which would have a stable mass fragment of 193  $m/z$ ) in a previous article.<sup>59</sup>

[Figures 20a–d](#) compare the acid partitioning with and without calcium present for the remaining mass ranges of 259–283  $m/z$  ( $C_{13}/C_{14}$ ), 284–308  $m/z$  ( $C_{15}/C_{16}$ ), 309–333  $m/z$  ( $C_{17}$ ), and 334–358  $m/z$  ( $C_{18}/C_{19}$ ). At low pH values, calcium still does not affect the partitioning. At higher pH values, the partitioning is reduced as the molecular weight of the acids increases. A stable mass balance (as can be observed in [Figure S2](#) in the [Supporting Information](#)) also indicates little or no loss of sample due to precipitation of calcium naphthenate particles, as confirmed by visual inspection of the samples after centrifugation, where no visible turbidity or particles were observed. The difference in partitioning between systems with and without calcium could come from either a salting-out effect from  $\text{CaCl}_2$  or the presence of oil-soluble calcium naphthenates. Indeed, it has been previously recorded that calcium preferentially forms oil-soluble calcium naphthenate with higher-molecular-weight acids.<sup>87</sup>



**Figure 18.** Equilibrium partitioning of the 209–233  $m/z$  fraction, given as a function of equilibrium pH. The total concentration of the commercial NA mixture was 10 mM, or 4 mM for pH >9. Aqueous buffers with 3.5 wt % NaCl or 10 mM  $\text{CaCl}_2$  and 3.5 wt % NaCl were used as a water phase. The values are the average of two or three measurements, where the error bars represent the range of obtained values. Some of the error bars are smaller than the symbols. For the sake of clarity, figures without mass balances are presented here, and figures with mass balances are presented in the [Supporting Information](#).



**Figure 19.** Equilibrium partitioning of the 234–258  $m/z$  fraction, given as a function of equilibrium pH. The total concentration of the commercial NA mixture was 10 mM, or 4 mM for pH >9. Aqueous buffers with 3.5 wt % NaCl or 10 mM  $\text{CaCl}_2$  and 3.5 wt % NaCl were used as a water phase. The values are the average of two or three measurements, where the error bars represent the range of obtained values. Some of the error bars are smaller than the symbols. For the sake of clarity, figures without mass balances are presented here, and figures with mass balances are presented in the [Supporting Information](#).

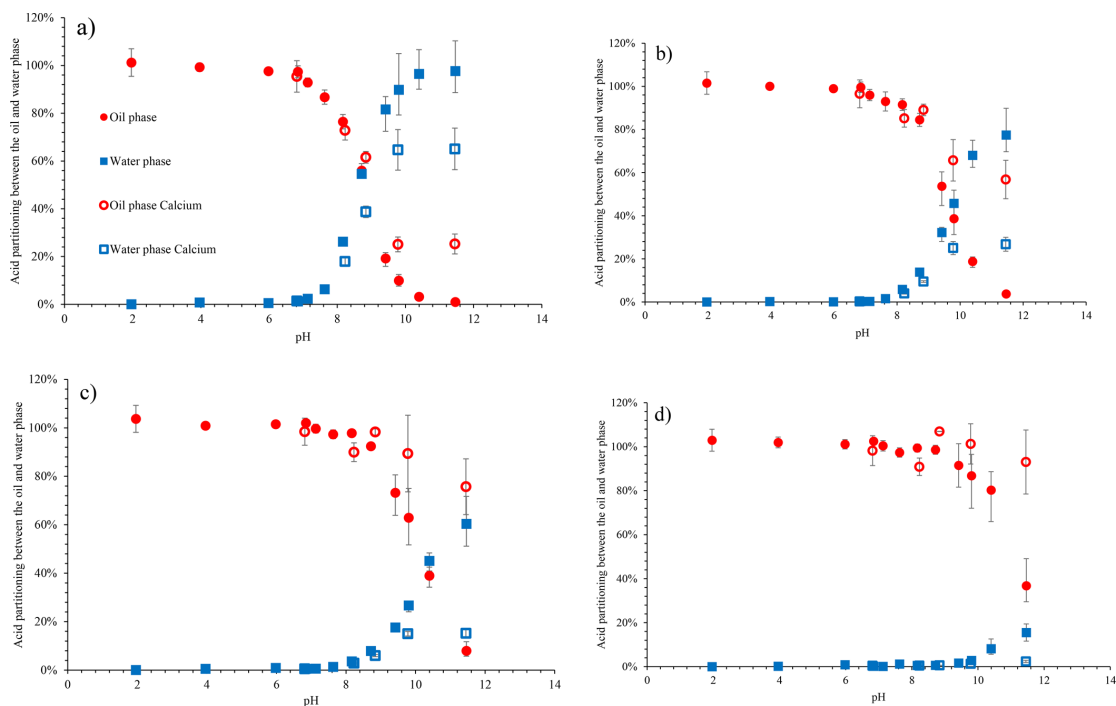
To determine which explanation is the most likely, the elemental composition, especially calcium content of the oil phase after evaporation of toluene was determined at three different pH values (2, 10, and 12), as seen in [Table 8](#). The samples were all prepared in duplicate and analyzed. The table shows that the compositions are slightly different between the two parallels, but the trends are reproducible. The composition at low pH is relatively similar to that of the commercial NA mixture, since negligible partitioning occurs at this pH. At higher pH, the percentage of oxygen decreases, which could be attributed to an increase of the molecular weight of the naphthenic acid in the oil phase. This increase is consistent with the variation of the  $pP_{wo}$  with molecular weight. At high pH, the carbon:oxygen ratio indicated a high average carbon number, varying from  $\text{C}_{33}$  to  $\text{C}_{66}$ , depending on the pH and the parallel, i.e., bigger than the largest molecule present in the Fluka naphthenic acid mixture (see [Figure 7](#)). These surprising values are difficult to explain and could result from the possible presence of neutral impurities present in the Fluka naphthenic

acid samples; these impurities would be more preponderant in the elemental analysis at high pH, because most of the naphthenic acids would have partitioned into the water phase.

The ratio between the moles of oxygen and calcium was calculated to determine the number of Ca atoms per carbonyl group. The results show that, at pH  $\sim$ 10, only half of the carbonyl groups in the oil are bound to calcium (note that 2  $\text{RCOO}^-$  are needed per  $\text{Ca}^{2+}$ ), whereas, at higher pH, all the carbonyl groups in the oil phase are bound to calcium. This effect is likely caused by a higher degree of acid dissociation at higher pH.

In summary, it seems that, from the mass range of 209–258  $m/z$  ( $\text{C}_9$ – $\text{C}_{12}$ ), calcium does not seem to affect the acid partitioning. In contrast, in the mass range of 259–358  $m/z$  ( $\text{C}_{13}$ – $\text{C}_{19}$ ), calcium reduces the partitioning at high pH, most likely by forming oil-soluble calcium naphthenates, which is consistent with the composition of calcium in the oil phase.





**Figure 20.** Equilibrium partitioning of the fractions (a) 259–283  $m/z$ , (b) 284–308  $m/z$ , (c) 309–333  $m/z$ , and (d) 334–358  $m/z$ , given as a function of equilibrium pH. The total concentration of the commercial NA mixture was 10 mM, or 4 mM for pH >9. Aqueous buffers with 3.5 wt % NaCl or 10 mM  $\text{CaCl}_2$  and 3.5 wt % NaCl were used as a water phase. The values are the average of two or three measurements, where the error bars represent the range of obtained values. Some of the error bars are smaller than the symbols. For the sake of clarity, figures without mass balances are presented here, and figures with mass balances are presented in the [Supporting Information](#).

**Table 8. Elemental Composition of Evaporated Oil Phase Acids after Shaken to Equilibrium with pH 2, 10, and 12 Buffers with 3.5% NaCl and 10 mM  $\text{CaCl}_2$ <sup>a</sup>**

final pH	carbon [%]	hydrogen [%]	oxygen [%]	calcium [%]	sodium [%]	chlorine [%]	mol calcium/mol $\text{COO}^-$
1.94	75.3/77.1	11.5/12.1	13.1/10.9	<0.01/<0.01	<0.01/<0.01	<0.4/<0.4	~0
9.8	78.6/82.0	12.4/13.2	6.25/3.31	1.6/0.87	0.03/0.01	<0.4/<0.4	0.21/0.21
11.5	76.4/78.2	11.9/12.5	6.2/4.2	3.7/2.5	0.02/0.02	<0.4/<0.4	0.48/0.46

<sup>a</sup>The slash (/) separates the results of the analysis of two independently prepared samples.

## 5. CONCLUSION

Model acids and a commercial naphthenic acid mixture from Fluka were analyzed using low-resolution GC/MS. The derivatization agent produced a dominant stable mass fragment ion for all model acid structures tested. Other ion fragments from predominantly aromatic acids, polycyclic acids, and high-molecular-weight acids in general, would influence the analysis of the commercial naphthenic acid mixture. A method to analyze mass spectra was developed to avoid this pitfall, primarily consisting of dividing the chromatogram into different mass range fractions. The GC/MS analysis shows that the commercial naphthenic acid mixture contains exclusively saturated acids with up to 19 carbon atoms and hydrogen deficiencies from 0 to -6 or 0–3 ring structures. The partitioning of the commercial naphthenic acid mixture versus pH was analyzed with GC/MS. The acids had an almost-complete partitioning over the pH range of 6–12. A model with one partition ratio for the polydisperse acid mixture did

not manage to represent the experimental results of the entire naphthenic acid mixture. Consequently, a new method was developed consisting of the analysis of narrow molecular weight ranges (width of 25 g/mol) to determine their partition ratio  $pP_{\text{wo}}$ . By summing up contributions from each mass range, a model was constructed that predicted the partitioning of the entire naphthenic acid mixture perfectly. Low mass balance for high-molecular-weight naphthenic acids indicated the possible precipitation of sodium naphthenate, not considered in the model. Adding calcium to the water phase did not affect partitioning at low pH and reduced the partitioning at high pH. Elemental analysis indicated that the likely cause was the formation of oil-soluble calcium naphthenates. Calcium seemed to increasingly reduce the partitioning of high-molecular-weight acids, while the partitioning of the smaller acids seemed unaffected. This work has given valuable insight into acid partitioning, which will be further explored in the examination of extracted crude oil acids. Future work could include the comparison of the data obtained



in this article with  $pK_a$  values of the naphthenic acids partitioned into water determined by potentiometric titration.

## ■ ASSOCIATED CONTENT

### 📄 Supporting Information

The Supporting Information is available free of charge on the ACS Publications website at DOI: 10.1021/acs.energyfuels.8b01494.

Table S1, which displays the naphthenic acid masses for increasing carbon numbers and hydrogen deficiencies; Figure S1, which shows a mass distribution of naphthenic acids in the water phase at pH 8; Figure S2, which are graphs showing equilibrium partitioning of naphthenic acids with and without calcium and the mass balances (DOCX)

## ■ AUTHOR INFORMATION

### Corresponding Author

\*Tel.: (+43) 73 55 09 24. E-mail: are.bertheussen@ntnu.no.

### ORCID

Are Bertheussen: 0000-0003-3235-659X

### Notes

The authors declare no competing financial interest.

## ■ ACKNOWLEDGMENTS

This work was carried out as a part of SUBPRO, a Research-based Innovation Centre within Subsea Production and Processing. The authors gratefully acknowledge the financial support from SUBPRO, which is financed by the Research Council of Norway, major industry partners, and NTNU. The authors would like to thank Bicheng Gao (NTNU) for determination of the NMR spectra.

## ■ REFERENCES

- (1) Khoi Vu, V.; Fantoft, R.; Shaw, C. K.; Gruehagen, H. Comparison of Subsea Separation Systems. In *Offshore Technology Conference*, May 4–7, 2009, Houston, TX; Paper No. OTC 20080, 2009.
- (2) Prescott, C. N. Subsea Separation and Processing of Oil, Gas & Produced Water. Past, Present and Future. Why We Need It Now. In *Rice Global E&C Forum*; Fluor Offshore Solutions, Houston, TX, 2012.
- (3) Wenger, L. M.; Davis, C. L.; Isaksen, G. H. Multiple Controls on Petroleum Biodegradation and Impact on Oil Quality SPE-80168-PA. *SPE Reservoir Eval. Eng.* **2002**, *5* (5), 375.
- (4) Barth, T.; Høiland, S.; Fotland, P.; Askvik, K. M.; Myklebust, R.; Erstad, K. Relationship between the Content of Asphaltenes and Bases in Some Crude Oils. *Energy Fuels* **2005**, *19* (4), 1624–1630.
- (5) Barth, T.; Høiland, S.; Fotland, P.; Askvik, K. M.; Pedersen, B. S.; Borgund, A. E. Acidic compounds in biodegraded petroleum. *Org. Geochem.* **2004**, *35* (11–12), 1513–1525.
- (6) Bernsten, J. S. Qualified technology (TRL 5) to remove produced water, at seafloor or topside, before it becomes difficult to treat. Presented at the *Tekna Produced Water Management Conference*, Stavanger, Norway, 2018.
- (7) Brandal, Ø. Interfacial (o/w) Properties of Naphthenic Acids and Metal Naphthenates, Naphthenic Acid Characterization and Metal Naphthenate Inhibition. Ph.D. Thesis, NTNU, Trondheim, Norway, 2005.
- (8) Shepherd, A. G. A Mechanistic Analysis of Naphthenate and Carboxylate Soap-Forming Systems in Oilfield Exploration and Production. Ph.D. Thesis, Heriot–Watt University, Edinburgh, U.K., 2008.
- (9) Headley, J. V.; McMartin; Dena, W. A Review of the Occurrence and Fate of Naphthenic Acids in Aquatic Environments. *J. Environ. Sci. Health, Part A: Toxic/Hazard. Subst. Environ. Eng.* **2004**, *39* (8), 1989–2010.
- (10) Grewer, D. M.; Young, R. F.; Whittall, R. M.; Fedorak, P. M. Naphthenic acids and other acid-extractables in water samples from Alberta: What is being measured? *Sci. Total Environ.* **2010**, *408* (23), 5997–6010.
- (11) Headley, J. V.; Peru, K. M.; Mohamed, M. H.; Frank, R. A.; Martin, J. W.; Hazewinkel, R. R. O.; Humphries, D.; Gurprasad, N. P.; Hewitt, L. M.; Muir, D. C. G.; Lindeman, D.; Strub, R.; Young, R. F.; Grewer, D. M.; Whittall, R. M.; Fedorak, P. M.; Birkholz, D. A.; Hindle, R.; Reisdorph, R.; Wang, X.; Kasperski, K. L.; Hamilton, C.; Woudneh, M.; Wang, G.; Loescher, B.; Farwell, A.; Dixon, D. G.; Ross, M.; Pereira, A. D. S.; King, E.; Barrow, M. P.; Fahlman, B.; Bailey, J.; McMartin, D. W.; Borchers, C. H.; Ryan, C. H.; Toor, N. S.; Gillis, H. M.; Zuin, L.; Bickerton, G.; McMaster, M.; Sverko, E.; Shang, D.; Wilson, L. D.; Wrona, F. J. Chemical fingerprinting of naphthenic acids and oil sands process waters—A review of analytical methods for environmental samples. *J. Environ. Sci. Health, Part A: Toxic/Hazard. Subst. Environ. Eng.* **2013**, *48*, 1145–1163.
- (12) Qian, K.; Robbins, W. K.; Hughey, C. A.; Cooper, H. J.; Rodgers, R. P.; Marshall, A. G. Resolution and Identification of Elemental Compositions for More than 3000 Crude Acids in Heavy Petroleum by Negative-Ion Microelectrospray High-Field Fourier Transform Ion Cyclotron Resonance Mass Spectrometry. *Energy Fuels* **2001**, *15* (6), 1505–1511.
- (13) Tomczyk, N. A.; Winans, R. E.; Shinn, J. H.; Robinson, R. C. On the Nature and Origin of Acidic Species in Petroleum. 1. Detailed Acid Type Distribution in a California Crude Oil. *Energy Fuels* **2001**, *15* (6), 1498–1504.
- (14) Rudzinski, W. E.; Oehlers, L.; Zhang, Y.; Najera, B. Tandem Mass Spectrometric Characterization of Commercial Naphthenic Acids and a Maya Crude Oil. *Energy Fuels* **2002**, *16* (5), 1178–1185.
- (15) Hemmingsen, P. V.; Kim, S.; Pettersen, H. E.; Rodgers, R. P.; Sjöblom, J.; Marshall, A. G. Structural Characterization and Interfacial Behavior of Acidic Compounds Extracted from a North Sea Oil. *Energy Fuels* **2006**, *20* (5), 1980–1987.
- (16) Barrow, M. P.; McDonnell, L. A.; Feng, X.; Walker, J.; Derrick, P. J. Determination of the Nature of Naphthenic Acids Present in Crude Oils Using Nanospray Fourier Transform Ion Cyclotron Resonance Mass Spectrometry: The Continued Battle Against Corrosion. *Anal. Chem.* **2003**, *75* (4), 860–866.
- (17) Ese, M.-H.; Kilpatrick, P. K. Stabilization of Water-in-Oil Emulsions by Naphthenic Acids and Their Salts: Model Compounds, Role of pH, and Soap: Acid Ratio. *J. Dispersion Sci. Technol.* **2004**, *25* (3), 253–261.
- (18) Häger, M.; Ese, M. H.; Sjöblom, J. Emulsion Inversion in an Oil–Surfactant–Water System Based on Model Naphthenic Acids under Alkaline Conditions. *J. Dispersion Sci. Technol.* **2005**, *26* (6), 673–682.
- (19) Vindstad, J. E.; Bye, A. S.; Grande, K. V.; Hustad, B.; Hustvedt, E.; Nergård, B. Fighting Naphthenate Deposition at the Heidrun Field. In *International Symposium on Oilfield Scale*, Jan. 29 and 30, 2003, Aberdeen, U.K.; Society of Petroleum Engineers: Paper No. SPE 80375, 2003.
- (20) Sarac, S.; Civan, F. Mechanisms, Parameters, and Modeling of Naphthenate-Soap-Induced Formation Damage. *Soc. Pet. Eng. J.* **2009**, *14* (2), 259–266.
- (21) Scarlett, A. G.; West, C. E.; Jones, D.; Galloway, T. S.; Rowland, S. J. Predicted toxicity of naphthenic acids present in oil sands process-affected waters to a range of environmental and human endpoints. *Sci. Total Environ.* **2012**, *425*, 119–127.
- (22) Li, C.; Fu, L.; Stafford, J.; Belosevic, M.; Gamal El-Din, M. The toxicity of oil sands process-affected water (OSPW): A critical review. *Sci. Total Environ.* **2017**, *601*–602, 1785–1802.
- (23) Thomas, K. V.; Langford, K.; Petersen, K.; Smith, A. J.; Tollefsen, K. E. Effect-Directed Identification of Naphthenic Acids as Important in Vitro Xeno-Estrogens and Anti-Androgens in North Sea

- Offshore Produced Water Discharges. *Environ. Sci. Technol.* **2009**, *43* (21), 8066–8071.
- (24) St. John, W. P.; Rughani, J.; Green, S. A.; McGinnis, G. D. Analysis and characterization of naphthenic acids by gas chromatography–electron impact mass spectrometry of *tert*-butyldimethylsilyl derivatives. *J. Chromatogr. A* **1998**, *807* (2), 241–251.
- (25) Scott, A. C.; Young, R. F.; Fedorak, P. M. Comparison of GC–MS and FTIR methods for quantifying naphthenic acids in water samples. *Chemosphere* **2008**, *73* (8), 1258–1264.
- (26) Holowenko, F. M.; MacKinnon, M. D.; Fedorak, P. M. Characterization of naphthenic acids in oil sands wastewaters by gas chromatography–mass spectrometry. *Water Res.* **2002**, *36* (11), 2843–2855.
- (27) Clemente, J. S.; Fedorak, P. M. A review of the occurrence, analyses, toxicity, and biodegradation of naphthenic acids. *Chemosphere* **2005**, *60* (5), 585–600.
- (28) Stanford, L. A.; Kim, S.; Klein, G. C.; Smith, D. F.; Rodgers, R. P.; Marshall, A. G. Identification of Water-Soluble Heavy Crude Oil Organic-Acids, Bases, and Neutrals by Electrospray Ionization and Field Desorption Ionization Fourier Transform Ion Cyclotron Resonance Mass Spectrometry. *Environ. Sci. Technol.* **2007**, *41* (8), 2696–2702.
- (29) Damasceno, F. C.; Gruber, L. D. A.; Geller, A. M.; Vaz de Campos, M. C.; Gomes, A. O.; Guimaraes, R. C. L.; Peres, V. F.; Jacques, R. A.; Caramao, E. B. Characterization of naphthenic acids using mass spectroscopy and chromatographic techniques: Study of technical mixtures. *Anal. Methods* **2014**, *6* (3), 807–816.
- (30) Lewis, A. T.; Tekavec, T. N.; Jarvis, J. M.; Juyal, P.; McKenna, A. M.; Yen, A. T.; Rodgers, R. P. Evaluation of the Extraction Method and Characterization of Water-Soluble Organics from Produced Water by Fourier Transform Ion Cyclotron Resonance Mass Spectrometry. *Energy Fuels* **2013**, *27* (4), 1846–1855.
- (31) Headley, J. V.; Peru, K. M.; McMartin, D. W.; Winkler, M. Determination of dissolved naphthenic acids in natural waters by using negative-ion electrospray mass spectrometry. *J. AOAC Int.* **2002**, *85*, 182–187.
- (32) Anderson, K.; Atkins, M. P.; Goodrich, P.; Hardacre, C.; Hussain, A. S.; Pilus, R.; Rooney, D. W. Naphthenic acid extraction and speciation from Doba crude oil using carbonate-based ionic liquids. *Fuel* **2015**, *146*, 60–68.
- (33) Clingenpeel, A. C.; Rowland, S. M.; Corilo, Y. E.; Zito, P.; Rodgers, R. P. Fractionation of Interfacial Material Reveals a Continuum of Acidic Species That Contribute to Stable Emulsion Formation. *Energy Fuels* **2017**, *31* (6), 5933–5939.
- (34) Stanford, L. A.; Rodgers, R. P.; Marshall, A. G.; Czarniecki, J.; Wu, X. A.; Taylor, S. Detailed Elemental Compositions of Emulsion Interfacial Material versus Parent Oil for Nine Geographically Distinct Light, Medium, and Heavy Crude Oils, Detected by Negative- and Positive-Ion Electrospray Ionization Fourier Transform Ion Cyclotron Resonance Mass Spectrometry. *Energy Fuels* **2007**, *21* (2), 973–981.
- (35) Jones, D. M.; Watson, J. S.; Meredith, W.; Chen, M.; Bennett, B. Determination of Naphthenic Acids in Crude Oils Using Nonaqueous Ion Exchange Solid-Phase Extraction. *Anal. Chem.* **2001**, *73* (3), 703–707.
- (36) Merlin, M.; Guigard, S. E.; Fedorak, P. M. Detecting naphthenic acids in waters by gas chromatography–mass spectrometry. *J. Chromatogr. A* **2007**, *1140* (1–2), 225–229.
- (37) Young, R. F.; Wismer, W. V.; Fedorak, P. M. Estimating naphthenic acids concentrations in laboratory-exposed fish and in fish from the wild. *Chemosphere* **2008**, *73* (4), 498–505.
- (38) Schummer, C.; Delhomme, O.; Appenzeller, B. M. R.; Wennig, R.; Millet, M. Comparison of MTBSTFA and BSTFA in derivatization reactions of polar compounds prior to GC/MS analysis. *Talanta* **2009**, *77* (4), 1473–1482.
- (39) Clemente, J. S.; Fedorak, P. M. Evaluation of the analyses of *tert*-butyldimethylsilyl derivatives of naphthenic acids by gas chromatography–electron impact mass spectrometry. *J. Chromatogr. A* **2004**, *1047* (1), 117–128.
- (40) Shepherd, A. G.; van Mispelaar, V.; Nowlin, J.; Genuit, W.; Grutters, M. Analysis of Naphthenic Acids and Derivatization Agents Using Two-Dimensional Gas Chromatography and Mass Spectrometry: Impact on Flow Assurance Predictions. *Energy Fuels* **2010**, *24* (4), 2300–2311.
- (41) Gutierrez-Villagomez, J. M.; Vázquez-Martínez, J.; Ramírez-Chávez, E.; Molina-Torres, J.; Trudeau, V. L. Analysis of naphthenic acid mixtures as pentafluorobenzyl derivatives by gas chromatography–electron impact mass spectrometry. *Talanta* **2017**, *162*, 440–452.
- (42) Havre, T. E.; Sjöblom, J.; Vindstad, J. E. Oil/Water-Partitioning and Interfacial Behavior of Naphthenic Acids. *J. Dispersion Sci. Technol.* **2003**, *24* (6), 789–801.
- (43) Ahmed, M. M. Characterization, modelling, prediction and inhibition of naphthenate deposits in oilfield production. Ph.D. Thesis, Heriot–Watt University, Edinburgh, U.K., 2010.
- (44) Hsu, C. S.; Dechert, G. J.; Robbins, W. K.; Fukuda, E. K. Naphthenic Acids in Crude Oils Characterized by Mass Spectrometry. *Energy Fuels* **2000**, *14* (1), 217–223.
- (45) West, C. E.; Scarlett, A. G.; Pureveen, J.; Tegelaar, E. W.; Rowland, S. J. Abundant naphthenic acids in oil sands process-affected water: studies by synthesis, derivatisation and two-dimensional gas chromatography/high-resolution mass spectrometry. *Rapid Commun. Mass Spectrom.* **2013**, *27* (2), 357–65.
- (46) Lo, C. C.; Brownlee, B. G.; Bunce, N. J. Mass spectrometric and toxicological assays of Athabasca oil sands naphthenic acids. *Water Res.* **2006**, *40* (4), 655–664.
- (47) Hindle, R.; Noestheden, M.; Peru, K.; Headley, J. Quantitative analysis of naphthenic acids in water by liquid chromatography–accurate mass time-of-flight mass spectrometry. *J. Chromatogr. A* **2013**, *1286*, 166–174.
- (48) Rowland, S. J.; West, C. E.; Scarlett, A. G.; Jones, D. Identification of individual acids in a commercial sample of naphthenic acids from petroleum by two-dimensional comprehensive gas chromatography/mass spectrometry. *Rapid Commun. Mass Spectrom.* **2011**, *25* (12), 1741–1751.
- (49) Saab, J.; Mokbel, I.; Razzouk, A. C.; Ainous, N.; Zydowicz, N.; Jose, J. Quantitative Extraction Procedure of Naphthenic Acids Contained in Crude Oils. Characterization with Different Spectroscopic Methods. *Energy Fuels* **2005**, *19* (2), 525–531.
- (50) West, C. E.; Jones, D.; Scarlett, A. G.; Rowland, S. J. Compositional heterogeneity may limit the usefulness of some commercial naphthenic acids for toxicity assays. *Sci. Total Environ.* **2011**, *409* (19), 4125–31.
- (51) Turner, A. Salting out of chemicals in estuaries: Implications for contaminant partitioning and modelling. *Sci. Total Environ.* **2003**, *314*–316, 599–612.
- (52) Celsie, A.; Parnis, J. M.; Mackay, D. Impact of temperature, pH, and salinity changes on the physico-chemical properties of model naphthenic acids. *Chemosphere* **2016**, *146*, 40–50.
- (53) Kanicky, J. R.; Shah, D. O. Effect of Premicellar Aggregation on the  $pK_a$  of Fatty Acid Soap Solutions. *Langmuir* **2003**, *19* (6), 2034–2038.
- (54) Brient, J. A.; Wessner, P. J.; Doyle, M. N. Naphthenic Acids. In *Kirk-Othmer's Encyclopedia of Chemical Technology*; John Wiley & Sons: New York, 1995; pp 1017–1029.
- (55) Touhami, Y.; Hornof, V.; Neale, G. H. Mechanisms for the Interactions between Acidic Oils and Surfactant-Enhanced Alkaline Solutions. *J. Colloid Interface Sci.* **1996**, *177* (2), 446–455.
- (56) Hurtevent, C.; Bourrel, M.; Rousseau, G.; Brocart, B. Production Issues of Acidic Petroleum Crude Oils. In *Emulsions and Emulsion Stability*; Sjöblom, J., Ed. CRC Press: Boca Raton, FL, 2005; pp 477–516.
- (57) Hutin, A.; Argillier, J.-F.; Langevin, D. Mass Transfer between Crude Oil and Water. Part 1: Effect of Oil Components. *Energy Fuels* **2014**, *28* (12), 7331–7336.
- (58) Nordgård, E. L.; Ahmad, J.; Simon, S.; Sjöblom, J. Oil-Water Partitioning of a Synthetic Tetracarboxylic Acid as a Function of pH. *J. Dispersion Sci. Technol.* **2012**, *33* (6), 871–880.

- (59) Bertheussen, A.; Simon, S.; Sjöblom, J. Equilibrium partitioning of naphthenic acids and bases and their consequences on interfacial properties. *Colloids Surf, A* **2017**, *529*, 45–56.
- (60) Scherrer, R. A.; Howard, S. M. Use of distribution coefficients in quantitative structure-activity relationships. *J. Med. Chem.* **1977**, *20* (1), 53–8.
- (61) Cooke, C. E., Jr.; Williams, R. E.; Kolodzie, P. A. Oil Recovery by Alkaline Waterflooding. *JPT, J. Pet. Technol.* **1974**, *26* (12), 1365–1374.
- (62) Brandal, Ø.; Sjöblom, J. Interfacial Behavior of Naphthenic Acids and Multivalent Cations in Systems with Oil and Water. II: Formation and Stability of Metal Naphthenate Films at Oil–Water Interfaces. *J. Dispersion Sci. Technol.* **2005**, *26* (1), 53–58.
- (63) Havre, T. E. Formation of Calcium Naphthenate in Water/Oil Systems, Naphthenic Acid Chemistry and Emulsion Stability. Ph.D. Thesis, NTNU, Trondheim, Norway, 2002.
- (64) Hanneseth, A. M. D.; Brandal, Ø.; Sjöblom, J. Formation, Growth, and Inhibition of Calcium Naphthenate Particles in Oil/Water Systems as Monitored by Means of Near Infrared Spectroscopy. *J. Dispersion Sci. Technol.* **2006**, *27* (2), 185–192.
- (65) Simon, S.; Reisen, C.; Bersås, A.; Sjöblom, J. Reaction Between Tetrameric Acids and Ca<sup>2+</sup> in Oil/Water System. *Ind. Eng. Chem. Res.* **2012**, *51* (16), 5669–5676.
- (66) Sjöblom, J.; Simon, S.; Xu, Z. The chemistry of tetrameric acids in petroleum. *Adv. Colloid Interface Sci.* **2014**, *205*, 319–338.
- (67) Bertheussen, A.; Simon, S.; Sjöblom, J. Equilibrium Partitioning of Naphthenic Acid Mixture, Part 2: Extracted Naphthenic Acids from a Crude Oil. Submitted.
- (68) Lide, D. R. *CRC Handbook of Chemistry and Physics: A Ready-Reference Book of Chemical and Physical Data*, 77th Edition; CRC Press: Boca Raton, FL, 1997; p 842.
- (69) Lu, Y.; Wang, J.; Deng, Z.; Wu, H.; Deng, Q.; Tan, H.; Cao, L. Isolation and characterization of fatty acid methyl ester (FAME)-producing *Streptomyces* sp. S161 from sheep (*Ovis aries*) faeces. *Lett. Appl. Microbiol.* **2013**, *57* (3), 200–205.
- (70) Barros, E. V.; Dias, H. P.; Pinto, F. E.; Gomes, A. O.; Moura, R. R.; Neto, A. C.; Freitas, J. C. C.; Aquije, G. M. F. V.; Vaz, B. G.; Romão, W. Characterization of Naphthenic Acids in Thermally Degraded Petroleum by ESI(–)-FT-ICR MS and <sup>1</sup>H NMR after Solid-Phase Extraction and Liquid/Liquid Extraction. *Energy Fuels* **2018**, *32*, 2878–2888.
- (71) ThermoScientific. *Reagents, Solvents and Accessories Catalog*, 2012.
- (72) Acevedo, S.; Escobar, G.; Ranaudo, M. A.; Khazen, J.; Borges, B.; Pereira, J. C.; Méndez, B. Isolation and Characterization of Low and High Molecular Weight Acidic Compounds from Cerro Negro Extraheavy Crude Oil. Role of These Acids in the Interfacial Properties of the Crude Oil Emulsions. *Energy Fuels* **1999**, *13* (2), 333–335.
- (73) Mapolelo, M. M.; Rodgers, R. P.; Blakney, G. T.; Yen, A. T.; Asomaning, S.; Marshall, A. G. Characterization of naphthenic acids in crude oils and naphthenates by electrospray ionization FT-ICR mass spectrometry. *Int. J. Mass Spectrom.* **2011**, *300* (2–3), 149–157.
- (74) Wang, Z.; Hollebone, B. P.; Fingas, M.; Fieldhouse, B.; Sigouin, L.; Landriault, M.; Smith, P.; Noonan, J.; Thouin, G. *Characteristics of Spilled Oils, Fuels, and Petroleum Products: 1. Composition and Properties of Selected Oils*; Ecosystems Research Division, United States Environmental Protection Agency, Research Triangle Park, NC, 2003; p 286.
- (75) Jones, D.; West, C. E.; Scarlett, A. G.; Frank, R. A.; Rowland, S. J. Isolation and estimation of the “aromatic” naphthenic acid content of an oil sands process-affected water extract. *J. Chromatogr. A* **2012**, *1247*, 171–175.
- (76) Seifert, W. K.; Teeter, R. M. Identification of polycyclic aromatic and heterocyclic crude oil carboxylic acids. *Anal. Chem.* **1970**, *42* (7), 750–758.
- (77) Bataineh, M.; Scott, A. C.; Fedorak, P. M.; Martin, J. W. Capillary HPLC/QTOF-MS for Characterizing Complex Naphthenic Acid Mixtures and Their Microbial Transformation. *Anal. Chem.* **2006**, *78* (24), 8354–8361.
- (78) Martin, J. W.; Han, X.; Peru, K. M.; Headley, J. V. Comparison of high- and low-resolution electrospray ionization mass spectrometry for the analysis of naphthenic acid mixtures in oil sands process water. *Rapid Commun. Mass Spectrom.* **2008**, *22*, 1919–1924.
- (79) Wei, D.; Orlandi, E.; Barriet, M.; Simon, S.; Sjöblom, J. Aggregation of tetrameric acid in xylene and its interaction with asphaltenes by isothermal titration calorimetry. *J. Therm. Anal. Calorim.* **2015**, *122* (1), 463–471.
- (80) Pradilla, D.; Simon, S.; Sjöblom, J. Mixed interfaces of asphaltenes and model demulsifiers, Part I: Adsorption and desorption of single components. *Colloids Surf, A* **2015**, *466*, 45–56.
- (81) Nenningsland, A. L.; Simon, S.; Sjöblom, J. Influence of Interfacial Rheological Properties on Stability of Asphaltene-Stabilized Emulsions. *J. Dispersion Sci. Technol.* **2014**, *35* (2), 231–243.
- (82) Nenningsland, A. L.; Gao, B.; Simon, S.; Sjöblom, J. Comparative Study of Stabilizing Agents for Water-in-Oil Emulsions. *Energy Fuels* **2011**, *25* (12), 5746–5754.
- (83) Dewick, P. M. Acids and bases. In *Essentials of Organic Chemistry: For Students of Pharmacy, Medicinal Chemistry and Biological Chemistry*; Dewick, P. M., Ed.; Wiley: West Sussex, England, 2006; p 130.
- (84) Passade-Boupat, N.; Rondon Gonzalez, M.; Hurtevent, C.; Brocart, B.; Palermo, T. Risk Assessment of Calcium Naphthenates and Separation Mechanisms of Acidic Crude Oil. In *SPE International Conference and Exhibition on Oilfield Scale*, May 30 and 31, 2012, Aberdeen, U.K.; Society of Petroleum Engineers: Paper No. SPE 155229, 2012.
- (85) Reinsel, M. A.; Borkowski, J. J.; Sears, J. T. Partition Coefficients for Acetic, Propionic, and Butyric Acids in a Crude Oil/Water System. *J. Chem. Eng. Data* **1994**, *39* (3), 513–516.
- (86) Dudek, M.; Kancir, E.; Øye, G. Influence of the Crude Oil and Water Compositions on the Quality of Synthetic Produced Water. *Energy Fuels* **2017**, *31* (4), 3708–3716.
- (87) Christiansen, I. Isolation and Characterization of Oil-Soluble Calcium Naphthenates in North Sea Heavy Crude Oil. M.Sc. Thesis, NTNU, Trondheim, Norway, 2014.

## Supporting Information

Table S1. Mass to charge ratio ( $m/z$ ) for stable ion fragment of naphthenic acid isomer  $C_nH_{2n+Z}O_2$  derivatized with MTBSTFA. The stable ion mass fragment obtained with MTBSTFA has a mass of  $[M+57]$  where  $M$  is the molecular weight of the acid. Some masses are excluded by on the rules set up by <sup>1</sup> except aromatic structures are included here.

Carbon number ( $n$ )	Hydrogen deficiency ( $Z$ )						
	0	-2	-4	-6	-8	-10	-12
5	159						
6	173						
7	187	185			179		
8	201	199			193		
9	215	213			207		
10	229	227	225		221	219	
11	243	241	239		235	233	
12	257	255	253	251	249	247	
13	271	269	267	265	263	261	259
14	285	283	281	279	277	275	273
15	299	297	295	293	291	289	287
16	313	311	309	307	305	303	301
17	327	325	323	321	319	317	315
18	341	339	337	335	333	331	329
19	355	353	351	349	347	345	343
20	369	367	365	363	361	359	357
21	383	381	379	377	375	373	371
22	397	395	393	391	389	387	385
23	411	409	407	405	403	401	399
24	425	423	421	419	417	415	413
25	439	437	435	433	431	429	427
26	453	451	449	447	445	443	441
27	467	465	463	461	459	457	455
28	481	479	477	475	473	471	469
29	495	493	491	489	487	485	483
30	509	507	505	503	501	499	497
31	523	521	519	517	515	513	511
32	538	535	533	531	529	527	525
33	552	550	547	545	543	541	539
34	566	564	562	559	557	555	553
35	580	578	576	574	571	569	567
36	594	592	590	588	586	583	581
37	608	606	604	602	600	598	595

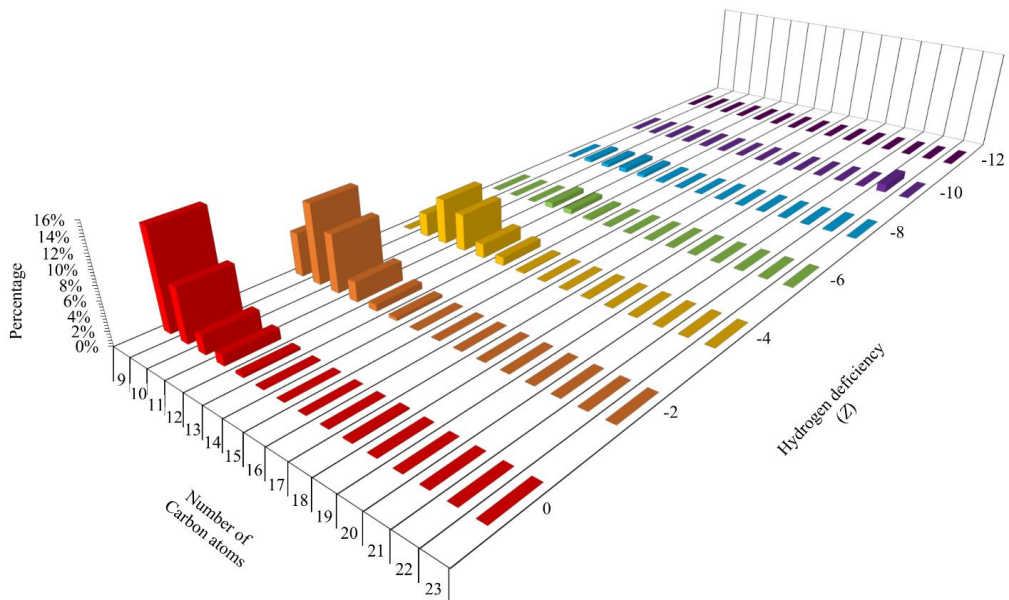
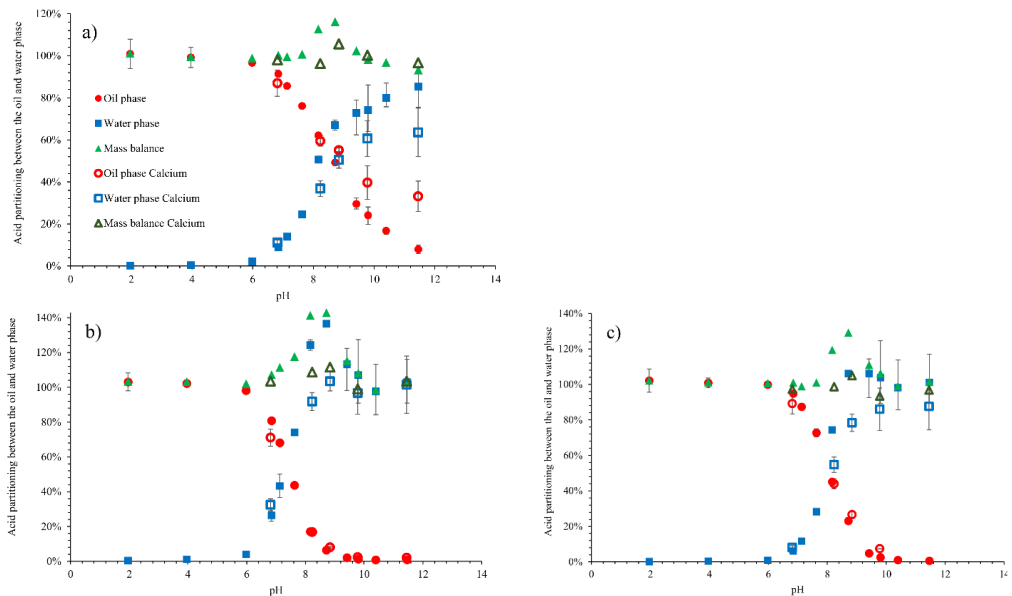


Figure S1 Mass distribution of commercial NA mixture in the water phase after partitioning at pH 8. The mass spectrum was not segmented and recombined to remove fragment contribution due to the limited influence of these fragments had on the distribution as shown in section 4.1.2.2.



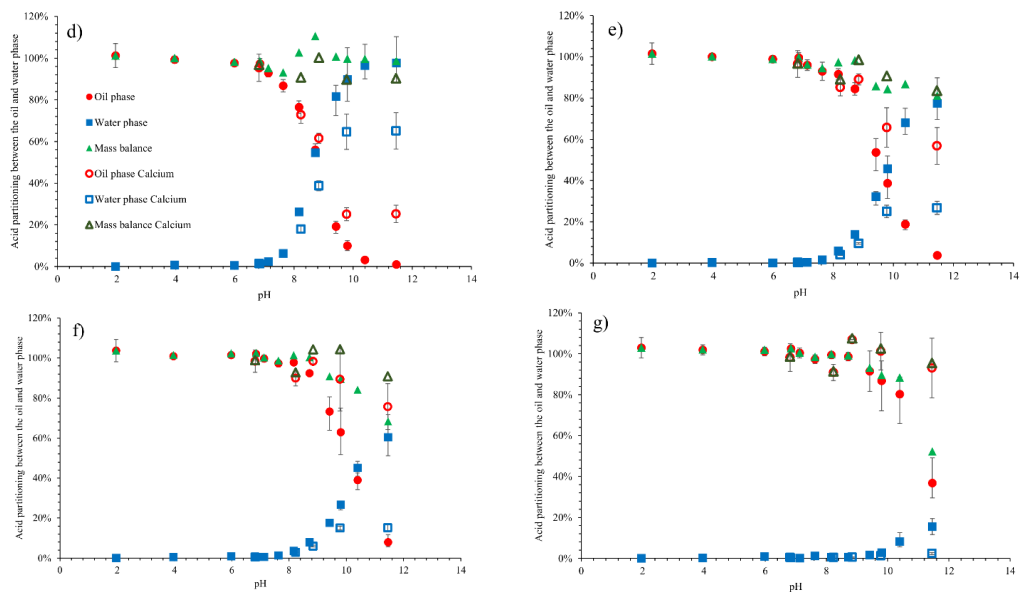


Figure S2 Equilibrium partitioning of the fractions (a) 209 m/z - 600 m/z, (b) 209 m/z - 233 m/z, (c) 234 m/z - 258 m/z (d) 259 m/z - 283 m/z, (e) 284 m/z - 308 m/z, (f) 309 m/z - 333 m/z, (g) 334 m/z - 358 m/z given as a function of equilibrium pH. The total concentration of the commercial NA mixture was 10 mM or 4 mM for pH higher than 9. Aqueous buffers with 3.5wt.% NaCl or 10 mM CaCl<sub>2</sub> and 3.5wt.% NaCl were used as water phase. The values are the average of two or three measurements where the error bars represent the range of obtained values. Some of the error bars are smaller than the symbols. The mass balance error bars are not specified for clarity's sake.

1. Holowenko, F. M.; MacKinnon, M. D.; Fedorak, P. M., Characterization of naphthenic acids in oil sands wastewaters by gas chromatography-mass spectrometry. *Water Research* **2002**, 36, (11), 2843-2855.



## PAPER IV

---

Equilibrium partitioning of naphthenic acid mixture part 2: Crude oil extracted naphthenic acids





# Equilibrium partitioning of naphthenic acid mixture part 2: Crude oil extracted naphthenic acids.

Are Bertheussen\*, Sébastien Simon and Johan Sjöblom

Ugelstad Laboratory, Department of Chemical Engineering, the Norwegian University of Science and Technology (NTNU), N-7491 Trondheim, Norway

## Highlights

- Composition of naphthenic acids by GC/MS
- Partitioning of acids to determine water quality of produced water
- Equilibrium partitioning of crude oil extracted naphthenic acids vs pH

## Abstract:

Crude oil naphthenic acids can partition into the water phase during oil production. Variations in production parameters such as temperature, pressure, pH and water cut affect partitioning. In a previous article, a method has been developed to determine the partition ratio for mixtures of naphthenic acids and tested on a commercial acid mixture. In this study, the method is implemented on a naphthenic acid mixture extracted from an acidic crude oil. Compositional analysis of the extracted acid mixture reveals a broad structural distribution consisting mainly of saturated ring structures with 2 to 3 rings. Examination of the GC/MS method revealed a distribution bias towards low molecular weight compounds and a correction method was explained and applied. The equilibrium partitioning as a function of pH for the acid mixture and molecular mass ranges within the acid mixture was determined by GC/MS. An extracted crude oil acid mixture dissolved in toluene was used as oil phase and 3.5wt.% NaCl aqueous buffers were used as water phase. Dividing the acid mixture into molecular weight ranges, characterized by a single partition ratio  $P_{wo}$  allowed the oil-water partitioning to be successfully modelled. The variation of the cologarithm of the partition ratio  $pP_{wo}$  with naphthenic acid molecular weight was compared with previously published experimental and simulated data. The presence of calcium reduced the partitioning of the acid mixture at high pH for larger acid molecules. Analysis of the resulting oil phase revealed a calcium content consistent with oil-soluble calcium naphthenate, in agreement with results found for a commercial acid mixture.

\*To whom correspondence should be addressed.

Telephone: (+43) 73 55 09 24.

E-mail: [are.bertheussen@ntnu.no](mailto:are.bertheussen@ntnu.no)

---

Keywords

Equilibrium partitioning

GC/MS

Naphthenic acids

Partition ratio

---

## 1. Introduction

Production of acidic crude oil is increasing both worldwide and in the North Sea <sup>1</sup>. With expected growth in deep-sea and arctic production <sup>2</sup>, new subsea separator designs are in development to match the new requirements <sup>3,4</sup>. It is therefore needed to have better tools to model the oil water separation as well as the quality of the separated phases. Variations in pressure and temperature during production can induce the partitioning of crude oil components such as naphthenic acids into the produced water. The presence of these components can alter the stability of water droplets in oil as recently shown <sup>5,6</sup> and oil droplets in water <sup>7</sup>. This paper is the second in a series of two which will discuss and explore the composition and equilibrium partitioning of naphthenic acid mixtures.

## 2. Theory

### 2.1. Definition and prevalence

Naphthenic acids are part of the resin group in crude oils. They are generally described by the raw formula  $C_nH_{2n+Z}O_2$  <sup>8</sup> with a molecular weight of around 200-700 g/mol <sup>9</sup>. As with other crude oil groups, naphthenic acid structures are complex. The analysis of some crude oil acids reveal that more than half of the identified acidic structures contained additional functional groups of oxygen, nitrogen, aromatics or sulphur like alkyl sulphonic acid <sup>10-12</sup>. A new term, naphthenic acid fraction components (NAFC), was defined by Headley, et al. <sup>13</sup>, allows the encompassment of a large

number of structures with functional groups containing hetero elements oxygen, sulphur, nitrogen, aromatic rings and unsaturations in crude oil.

Naphthenic acids have been linked to downstream corrosion<sup>14</sup>, emulsion formation<sup>15, 16</sup>, deposition on processing units<sup>17</sup> and formation pore blockage<sup>18</sup>. Multiple authors have applied mass spectroscopy to characterize naphthenic acids<sup>5, 10-12, 19-27</sup>. Mass spectroscopy have some limitations that need to be accounted for. For instance, Clingenpeel, et al.<sup>28</sup> and Rowland, et al.<sup>29</sup> analyzed surface active compounds including naphthenic acids in bitumen and deasphalted bitumen with FT-ICR MS. They stressed the importance of prior fractionation of the sample by demonstrating that easily ionizable low molecular weight compounds hide the presence of less ionizable and larger compounds. Clingenpeel, et al.<sup>28</sup> also demonstrated that it was these larger and previously hidden surface active compounds which contributed most to the emulsion stability. Ligiero<sup>5</sup> studied the water-soluble compounds in resolved waters from several crude oils with ESI-MS and surprisingly found the crude oil with the lowest TAN value (0.1) to give the broadest naphthenic acid distribution in the resolved water, some of which had asphaltene-like characteristics (double bond equivalent (DBE) > 0.46C<sub>n</sub>). However, the comparison involves only three crude oils, and therefore needs to be extended. When exact molecular structure is not essential, simpler naphthenic acid analysis methods have been developed for standard GC/MS instrumentation. Derivatization with N-methyl-N-(t-butyldimethylsilyl) trifluoroacetamide (MTBSTFA) produces stable ion fragment [M+57] where M is the molecular weight of the naphthenic acid<sup>19</sup>. This method allows for crude classification based on carbon number and hydrogen deficiency Z of naphthenic acids peaks within the unresolved GC/MS elution hump<sup>21</sup>.

The partitioning of naphthenic acids to the water phase have been studied by several authors<sup>23, 30, 31</sup>. Stanford, et al.<sup>23</sup> extracted crude oil acids with pH neutral water and detected water soluble acids up to C<sub>41</sub>(~600 g/mol) with FT-ICR MS. Havre, et al.<sup>30</sup> found that the partition ratio varied depending on the molecular weight of the acids and that naphthenic acids in crude oil water systems had a  $pK_a$  around 4.9. Celsie, et al.<sup>32</sup> simulated the effect of temperature on naphthenic acid partitioning and found that the partition ratio goes towards unity upon increasing temperature. This qualitatively correlates with the finding of Bostick, et al.<sup>33</sup>, studying the concentration of different water soluble organics as a function of pH, salinity, pressure and temperature, who found that increased temperature did not affect the total amount of polar organics in the water phase, but

increased the concentration of C<sub>10</sub>-C<sub>20</sub> components while decreasing the concentration of C<sub>6</sub>-C<sub>10</sub> components. Other factors like the presence of calcium has been shown to affect naphthenic acids behavior in oil water systems<sup>9, 34-38</sup>. In the presence of calcium, oil-soluble calcium naphthenate can form<sup>39</sup> which can cause problems in downstream processing<sup>40</sup>. In order to combat the naphthenate problems<sup>17</sup>, Dyer, et al.<sup>41</sup> made a huge matrix of experimental results on the topic by screening dozens of carboxylic acids in systems with various pH values, concentrations and water phase compositions, before it was discovered that a specific family of naphthenic acids named ARN was the main component behind the calcium naphthenate problems<sup>42</sup>.

This article will study the equilibrium partitioning of an extracted crude oil acid mixture, determine acid partition ratios and present insight into at which pH the phase change occurs.

## 2.2. Modelling of partition ratio with pH

A thermodynamic model for the partitioning of naphthenic acids applied in previous work by Bertheussen, et al.<sup>43 44</sup> is presented. All concentrations are in mol/L, unless otherwise stated.

In an oil-water system, protonated acids would partition themselves between the oil and water phase described by the following partition constant

$$K_{wo,HA} = \frac{[HA]_w}{[HA]_o} \quad (1)$$

where  $[HA]_w$  represents the protonated acid concentration in the water phase,  $[HA]_o$  represents the acid concentration in the oil phase and  $K_{wo,HA}$  represents the partition constant of the acid. As described in previous work<sup>43</sup> it was favored to use the partition ratio,  $P_{wo}$ , instead to avoid considering dimers in the oil phase<sup>45</sup>. Although the partition ratio is not a constant because of its dependence on concentration, it is a practical term with regards to measurements. The partition ratio of 4-heptylbenzoic acid was shown to remain almost constant with concentration<sup>46</sup>. The partition ratio accounts for the non-ionized compounds in each phase as seen in Equation 2.

$$P_{wo} = \frac{[HA]_w}{[HA]_{o,tot}} = \frac{[HA]_w}{[HA]_o + 2[(HA)_2]_o} \quad (2)$$

Water phase dissociation of acids are described by the following dissociation constant

$$K_{a,HA} = \frac{[A^-]_w[H^+]}{[HA]_w} \quad (3)$$

where  $[A^-]_w$  represents the concentration of dissociated acid in the water phase and  $K_{a,HA}$  represents the dissociation constant of the acid.

The following mass balance is valid for a system without precipitation.

$$[HA]_{o,init} V_o = [HA]_{w,tot} V_w + [HA]_{o,tot} V_o \quad (4)$$

where  $[HA]_{o,init}$  represents the initial concentration of acid in the oil phase, and  $[HA]_{w,tot}$  represents the sum of dissociated and undissociated acids in the water phase. The terms  $V_o$  and  $V_w$  denote the volume of the oil and water phase.

Combining equations 2, 3, and 4 gives expressions for the total acid concentration in the oil and water phase.

$$[HA]_{w,tot} = \frac{[HA]_{o,init}}{\frac{[H^+]}{P_{wo,acid}(K_{a,HA}+[H^+])} + \frac{V_w}{V_o}} \quad (5)$$

$$[HA]_{o,tot} = \frac{[HA]_{o,init}}{1 + \frac{V_w P_{wo,acid}(K_{a,HA}+[H^+])}{V_o [H^+]}} \quad (6)$$

It is assumed that the deprotonated acid  $[A^-]$  is completely insoluble in oil phase. The formation of aggregates was not taken into account in the model presented in Equations 5 and 6.

This study is expanding on and comparing with previous work performed on a commercial acid mixture. In this study, two crude oil acid mixtures will be characterized, mainly by GC/MS. Then the equilibrium partitioning of an extracted crude oil acid mixture will be considered over the pH range. The partition ratio  $P_{wo}$  will be obtained through fitting Equations 5 and 6 with a constant  $pK_a$  of 5. The use of this  $pK_a$  value will be justified in section 4.2. The effect of calcium on the partitioning will be also be evaluated. Then the  $P_{wo}$  obtained in this work will be compared with values from the literature, and with measurements using a model naphthenic acid, 4-heptylbenzoic acid.

### 3. Materials and methods

#### 3.1. Chemicals

The chemicals used to perform the partitioning experiments and GC/MS analysis have already been presented in a part I article of this series. Additional chemicals were used in this new study. They were used as received and not further purified. Boron trifluoride-methanol (Sigma Aldrich, 14wt.%), 4-heptyl benzoic acid (VWR, 99%), tridecanoic acid (Fluka, 99.7%), heptane (Sigma Aldrich, >99%) and ultra-pure water (MilliQ resistivity of 18.2 M $\Omega$ -cm millipore). The extracted crude oil acid mixtures, A and B, were provided by Equinor. The acids were obtained through the Acid-IER method<sup>47</sup> performed at Equinor Research Centre Rotvoll and were delivered as amber colored 1.5wt.% solutions in 1:1(wt.) toluene and isopropanol. The crude oils used for extraction come from the same North Sea reservoir, but from different wells. More data are listed in Table 1. The crude oil acid solutions were evaporated to a stable weight at 60°C under nitrogen convection to prepare toluene stock solutions. The color of the dried acids was dark brown.

Table 1 Characteristics of the extracted crude oil acids and their parent crude oil. Data kindly provided by Equinor.

	Extracted crude oil acid mixture A	Extracted crude oil acid mixture B
Average molecular weight**	438 g/mol	454 g/mol
Extraction yield	90%	94%
TAN of the parent crude oil [mg <sub>KOH</sub> /g]	1.7	3.1
Water-cut well at sampling time	58%	19%

\*\*Average values calculated from titration of the isolated acids by assuming monoprotic acids as explained in Mediaas, et al.<sup>47</sup>

#### 3.2. Characterization

A Bruker Avance nuclear magnetic resonance (NMR) spectrometer (400 MHz) was used to obtain hydrogen 1 (<sup>1</sup>H) NMR spectra on a 1% solution in CDCl<sub>3</sub>. The number of scans used was 8. The Laboratory SGS Multilab (Evry, France) determined the elemental composition by thermal conductivity measurements for C, H, and N, by infrared measurements for O and S, by mineralization and ICP/AES for Ca and Na and potentiometric titration for Cl.

### 3.3. Equilibrium partitioning

The partitioning of naphthenic acids were determined according to a procedure developed in Bertheussen, et al. <sup>44</sup>. The procedure is briefly recalled below. At least 2 parallels were performed per condition tested.

#### 3.3.1. In presence of monovalent cations

4 mL of 3.3 mM (1.4 g/L) for pH lower than 10, 1.65 mM (0.7 g/L) for pH higher than 10, extracted crude oil acid mixture A in toluene were mixed with 4 mL of aqueous solution containing 3.5wt.% NaCl and a buffer (Table 2) for 1 day at 250 rpm. Aliquots of oil and aqueous phase were recovered after centrifugation (11000 rpm, 30 minutes). The pH of the aqueous phase was then measured, and 3 mL was adjusted to pH < 2. Then the, now protonated, naphthenic acids were back-extracted in toluene (3 mL, 24 h shaking). Note that, after centrifugation, the centrifugation tube used for the samples prepared at pH 11 and pH 12 had a light brown colored layer along the tube wall in the water phase.

#### 3.3.2. In the presence of divalent cation, Ca<sup>2+</sup>.

The procedure was like the method described in part 3.3.1 with the following modification.

- In addition to NaCl 3.5wt.% and buffers, the aqueous phase also contained 10 mM CaCl<sub>2</sub>.
- pH 11 samples were not buffered owing to the incompatibility between NaHCO<sub>3</sub> and CaCl<sub>2</sub>. This solution did not contain buffer and the initial pH was 11.5 to obtain the correct equilibrium pH.
- Tests were performed by washing the equilibrated oil phase with low pH buffer to determine the influence of calcium naphthenate on the derivatization reaction, but results were similar as without washing.
- Finally, it was not observed any brown layer on the centrifugation tube wall when the water phase contained CaCl<sub>2</sub>.



Elemental analysis of the resulting oil phase after high pH partitioning was performed. High volumes (350 mL of both phases) were required to obtain enough dry sample. Only extracted crude oil acid B was used in this experiment due to the limited amount of extracted crude oil acids available (0.6 g of acid mixture A and 0.5 g of acid mixture B). Due to the similar origin and statistically insignificant mass distribution difference between acid mixtures A and B (see section 4.1.2.2, Figure 6 and Figure 7), elemental analysis results obtained with extracted crude oil acid B were assumed representable to explain partitioning results obtained with extracted crude oil acid A. Likewise, due to the limited amount of sample, only one elemental analysis determination was performed.

### 3.3.3. Model acid 4-heptylbenzoic acid

The equilibrium partitioning for the model acid 4-heptylbenzoic acid was performed similarly as in section 3.3.1, except the concentration of this acid was 1 mM in toluene and 10 mL of each phase were put into contact. Equal volumes of internal standard (tridecanoic acid 0.5 mM in toluene) was added to samples prior to solvent evaporation under nitrogen at 50 degrees. Dry samples were derivatized by addition of 1.5 mL 14wt.% Boron trifluoride-methanol solution before stirring in a 60°C waterbath for 1 h. 2 mL heptane and 1.5 mL MQ water was added to the sample vials before shaking for 30 min at 250 rpm. The final heptane phase was analyzed with GC/FID at Equinor Research Centre Rotvoll and quantitative results obtained by comparison with calibration curves.

*Table 2 List of different aqueous buffers prepared <sup>48</sup>. 3.5wt.% NaCl was also present in these buffers.*

pH	Buffers
4	0.1 M CH <sub>3</sub> COOH adjusted with NaOH
6-7.9	0.1 M KH <sub>2</sub> PO <sub>4</sub> adjusted with NaOH
8.4-9	0.025 M Borax adjusted with HCl
9.5-10	0.025 M Borax adjusted with NaOH
11	0.05 M NaHCO <sub>3</sub> adjusted with NaOH
12	0.01 M NaOH

### 3.4. GC/MS analysis of the extracted naphthenic acids.

The GC/MS analysis was developed in Bertheussen, et al.<sup>44</sup>. The procedure is briefly summarized.

#### 3.4.1. Derivatization and analysis

270 mg of a 0.23 mM capric acid in toluene solution (used as internal standard), was added to 1.6 g of the sample to be analyzed. 0.36 g of this solution was mixed with 0.04 g of N-tert-Butyldimethylsilyl-N-methyltrifluoroacetamide with 1% tert-Butyldimethylchlorosilane (MTBSTFA + 1% TBDMSCl) and heated at 65°C for 30 minutes. Then the derivatized sample was analyzed (injection volume 1.5  $\mu$ L) on an Agilent GC(7890)/MS(5977). The separation was performed on an Agilent J&W DB-1HT Non-polar, 100% Dimethylpolysiloxane, capillary column (30m $\times$ 0.25mm $\times$ 0.10  $\mu$ m film thickness) in splitless mode and at a flow rate of 1 mL helium per minute. The inlet temperature was 360°C and the GC temperature program was the following. The temperature was initially 100°C for 5 minutes, then increased to 350°C at a rate of 5°C/min. This maximum temperature was finally held for 10 minutes.

#### 3.4.2. Identification of naphthenic acid composition by GC/MS

Analysis were performed using the Masshunter Acquisition Data software. First mass spectra were extracted from the chromatogram peak, with a height filter, relative height > 0.1% of largest peak. Spectra from corresponding injection of blank solvents were subtracted from the sample data. The n, Z distribution of naphthenic acids was determined from m/z values using the following procedure: First if m/z is comprised between (x-1).7 (included) and (x).7, then it is rounded to x. For instance:

- m/z values of 237.4 or 237.6 would be rounded to 237.
- m/z values of 237.7 or 238.69 would be rounded to 238.

The integer m/z values then allow for the determination of n and Z using the table presented in the supplementary information (Table S1).

### 3.4.3. Quantification by GC/MS

Different chromatograms could be obtained from raw data:

- Total ion chromatograms (TIC) represent the sum of all intensities for all m/z values included in the mass scan.
- Extracted ion chromatograms (EIC) represent the sum of intensities for a specific mass or mass range.

EIC were obtained from TIC and used, after subtraction of solvent blanks and integration, to obtain naphthenic acid concentration after normalization with the peak of the capric acid (internal standard) and comparison with a calibration curve built beforehand. The calibration curves were performed as advised by the manufacturer. This determination is further explained in section 4.2.

## 4. Results and Discussion

### 4.1. Characterization

#### 4.1.1. Characterization by elemental analysis and NMR

The average molecular weight of NA mixtures A and B was reported by Equinor as 438 g/mol and 454 g/mol respectively (Table 1) by determining the TAN and the mass of the extracted acids. The average molecular weight of the extracted acids can be determined by TAN titration by combining the two equations 7 and 8<sup>47</sup>

$$n_{acid} = \frac{(V_{EP}-V_b) \cdot C_{titrant}}{1000} \quad (7)$$

$$TAN = \frac{(V_{EP}-V_b) \cdot C_{titrant} \cdot M_{KOH}}{m_{sample}} \quad (8)$$

into Equation 9

$$M_{acid} = \frac{m_{sample} \cdot 1000}{(V_{EP}-V_b) \cdot C_{titrant}} = \frac{M_{KOH} \cdot 1000}{TAN} \quad (9)$$

where  $n_{acid}$ ,  $M_{acid}$  and  $m_{sample}$  is the number of mole, average molecular weight and mass of the extracted acid mixture respectively in the units moles, g/mol and g.  $M_{KOH}$  is the molecular mass of potassium hydroxide in g/mol.  $V_{EP}$  and  $V_b$  are the volume of titrant required to the equivalence point for sample and pure solvent (blank) respectively, in mL.  $C_{titrant}$  is the concentration of the titrant used, in mol/L, and  $TAN$  is the total acid number in mg<sub>KOH</sub>/g<sub>sample</sub>.

In house TAN titration was not performed due to the limited amount of sample. The elemental composition of acid mixtures A and B are listed in Table 3. Here it can be seen that the acid mixtures contain almost no nitrogen and a small amount of sulphur. By assuming an overarching raw formula  $C_nH_{2n+Z}O_2$  for all acids in the sample the average molecular weight of the acid mixture can be calculated by finding n and Z values which matches the molar ratio between carbon and hydrogen. The percentages of C, H, O indicate an average molecular weight of 373 g/mol for acid mixture A and 395 g/mol for acid mixture B, assuming only monoacids, both of which are lower than the average molecular weights obtained by titration. As will be discussed in section 4.1.2.2, the difference between the molecular weight from titration and elemental analysis could come from pollution by non-acid compounds in the sample. The difference in average molecular weight between the two acids however, is consistent for both methods, i.e. the average molecular weight for acid mixture A is lower than for acid mixture B in both methods.

Table 3 Elemental composition of the extracted crude oil acid mixtures

Element	Symbol	Composition [wt.%] acid mixture A	Composition [wt.%] acid mixture B
Carbon	C	79.5	80.1
Hydrogen	H	11.0	11.2
Oxygen	O	8.5	8.0
Sulphur	S	0.56	0.60
Nitrogen	N	0.09	0.09

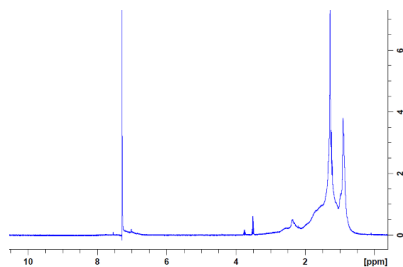


Figure 1  $^1\text{H}$  NMR spectrum for the extracted crude oil acid mixture A in  $\text{CDCl}_3$ .

Figure 1 show the  $^1\text{H}$  NMR spectrum conducted on a 1wt.% solution of acid mixture A. The termination methyl groups give peaks with chemical shifts lower than 1 ppm, while  $\text{CH}_2$  methylene bridges have peaks between 1.15 -2.33 ppm<sup>49, 50</sup>. It appears that there are few aromatic groups in the extracted crude oil acid mixture since aromatic groups would register as peaks in the 7-8 ppm range<sup>51</sup>. The absence of aromatic rings is a typical feature of crude oil naphthenic acids<sup>11, 51, 52</sup>. Saab, et al.<sup>51</sup> reported that based on  $^1\text{H}$  NMR on 1.8% of the analyzed crude oil acids were aromatic. Different theories have been suggested regarding the small amount of aromatic groups found in crude oil acids. Tomczyk, et al.<sup>11</sup> discussed this lack of aromatic acids by suggesting the higher polarity impeded migration from source rock to reservoir. Other authors discuss the role of biodegradation where aromatic hydrocarbons are less susceptible to biodegradation<sup>21, 53</sup>. However, due to their polar nature, aromatic compounds are more prominent in the water phase, Jones, et al.<sup>54</sup> found 30% of oil sands process-affected water (OSPW) acids to have aromatic structures and Stanford, et al.<sup>23</sup>, comparing the water soluble acid fractions to the acid fractions of their parent crude oil, found aromatic groups to be more prominent in the water phase acids. Consequently, it is possible that smaller aromatic acids initially present in crude oil were partitioned into the produced water prior to crude oil sampling.

#### 4.1.2. Characterization by GC/MS

##### 4.1.2.1. Assessment of derivatization efficiency

Through GC/MS analysis more information about the acid mixture compositions can be obtained. Published mass spectra of crude oil and bitumen acids reveal broad distributions with a fraction of large and non-volatile molecules<sup>29, 35, 55</sup>. Even If the GC is not able to analyze non-volatile molecules, the use of GC/MS is deemed valid for this work, due to its focus on compounds with partial water solubility, which mainly encompasses smaller acids. The derivatization agent MTBSTFA converts hydroxyl, carboxyl, thiol groups and primary and secondary amines and creates stable ion fragments [M+57], as shown in a previous publication<sup>44</sup>, where M is the molecular weight of the acid<sup>56</sup>. For clarity real molecular weight of acids will be denoted g/mol while mass fragments of derivatized acids ([M+57]) will be denoted m/z. The category [M+57] is used to denote all types of derivatized acids, even though molecules with various 1+x functional groups technically becomes a [M+57+x·114] mass fragment. Table S1 in the supplementary material lists the masses for the isomer C<sub>n</sub>H<sub>2n+Z</sub>O<sub>2</sub>. As explained in section 3.4.2 this table allows the ascertainment of *n* and *Z* from their molecular weight. The average unsaturation for naphthenic acids structures can be described by the double bond equivalent (DBE) as described in Equation 10<sup>57</sup>. The hydrogen deficiency *Z* is linked to the DBE as described in Equation 11<sup>58</sup>.

$$DBE = \frac{2C+2-H}{2} \quad (10)$$

$$Z = -2DBE + 2 \quad (11)$$

where *C* and *H* are the number of carbon and hydrogen atoms in the formula. Hydrogen deficiency *Z* is used to assign cyclic or aromatic structures due to the absence of alkenes in crude oil<sup>59</sup>.

A hydrogen deficiency of -8 or lower in Table S1 could be attributed to either an aromatic ring or a ring structures with 4 rings or more. Aromatic acids have previously been discounted from mass distribution tables like Table S1<sup>21</sup>. Larger aromatic acids have been reported in both OSPW, crude oil and bitumen<sup>29, 54, 60</sup>. Low molecular weight aromatic acids are however, reportedly not present

in petroleum acid extracts<sup>52</sup>, an absence which might be caused by losses to the produced water during production prior to acids being extracted from the crude oil. To cover as diverse a range of carboxylic acids as possible, this article has included aromatic ring combinations to possible acid structures in Table S1.

A previous article<sup>44</sup> discussed the development of the GC/MS method for analysis of naphthenic acid mixtures. Here it was found that all acid structures produced a dominant [M+57] peak. Fatty acids produced the most dominant ion peaks i.e. the low fragmentation, followed by alicyclic and aromatic structures.

#### 4.1.2.2. GC/MS analysis of the extracted crude oil acid mixture

The extracted crude oil acid mixtures were analyzed by GC/MS to give the chromatogram presented in Figure 2. As usual with complex acid mixtures, the GC cannot separate all the molecules present, and the acids elute as an unresolved hump with one mode and few well-defined peaks. The peak at retention time 15 minutes belongs to the internal standard, capric acid. The most distinct peaks at 313 m/z and 341 m/z corresponds to C<sub>16</sub> and C<sub>18</sub> aliphatic saturated acids, shown to be respectively palmitic and stearic acids by comparison with the retention time of standard samples. The well-defined peak at 647 m/z at retention time 44 min (C<sub>40</sub>, Z=-2) gives credibility to the methods ability to analyze relatively high molecular weight molecules. A response factor of 1 was assumed for all acids.

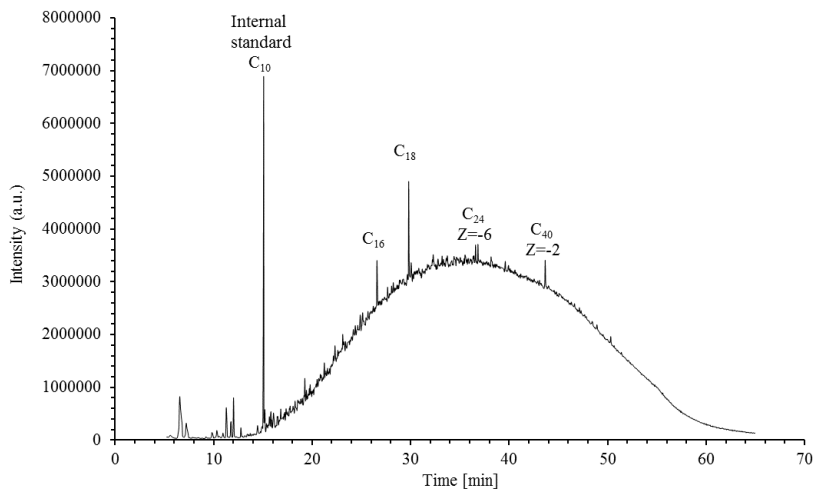


Figure 2 Extracted ion chromatogram of extracted crude oil acid mixture A (159 m/z - 750 m/z). Subtracted by blank solvent chromatogram. The peak at retention time 15 minutes corresponds to the internal standard capric acid C<sub>10</sub>. Some major peaks listed have stable ion fragments consistent with saturated fatty acids. Their carbon number is indicated on the figure. C<sub>16</sub> single peak corresponds to palmitic acids, C<sub>18</sub> single peak correspond to stearic acid, C<sub>24</sub> double peak is presumed to correspond to a 3 ringed acid, C<sub>40</sub> single peak is presumed to correspond to an acid with one ring structure. There is an additional 316 m/z specie at the same retention time as C<sub>40</sub> peak, assumed to be a fragment.

The chromatographic separation in a non-polar column is based on boiling point i.e. the molecular weight. Figure 3 show the elution humps of increasing EIC mass ranges. As the mass of the acids increase they elute successively and with broader peaks due to the increase in possible structural isomer combinations<sup>61</sup>. The EIC mass range 159 m/z - 233 m/z (covering the smallest acids in Table S1) does not have an initial elution hump, but rather present a flat elution from retention time 18 - 60 minutes. These were deemed to be fragments of high molecular weight species and the analysis starts at the next mass range 234-258 m/z or C<sub>11</sub>. The lack of smaller acids apparent absence of small acid molecules have also been noted previously<sup>19</sup> and can be attributed to pre-sampling production conditions like water-cut and pH. There are also fewer possible structures for lower molecular weight acids as seen in Table S1.

The exclusion of masses below 234 m/z is not enough to remove the influence of fragments. Figure 4 show the EIC for two mass ranges, 234 m/z - 258 m/z and 359 m/z - 383 m/z. Here it can be observed that the small acids after an initial elution hump, reemerge with a flat second elution at a retention time were larger acids elute. It is assumed that the initial elution hump for all EIC mass ranges would represent the actual acids in that range whilst the second and flat elution later in the



chromatogram would be interpreted as fragments of higher molecular weight compounds caused by electron impact ionization or non-acid pollutants. For instance, the acids in the mass range 234 m/z – 258 m/z elute from 12 min - 21 min as seen in Figure 4. After 21 minutes signal responses from this EIC mass range in the chromatogram were disregarded.

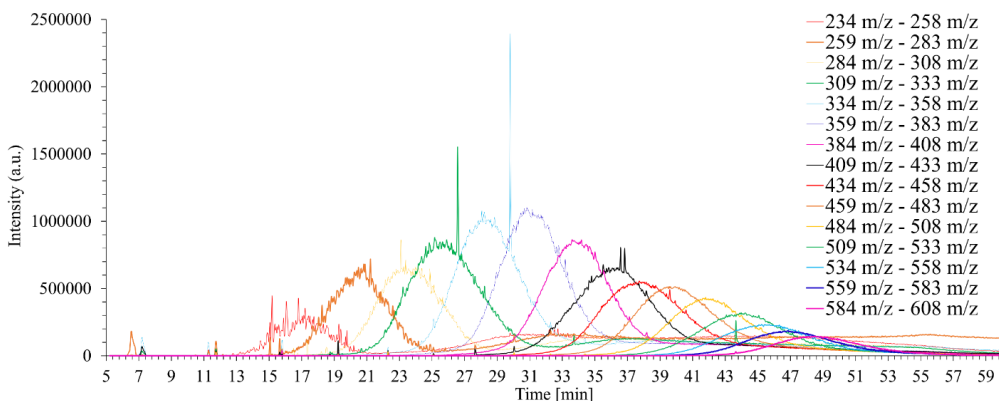


Figure 3 Extracted ion chromatograms (EIC) with increasing mass ranges.

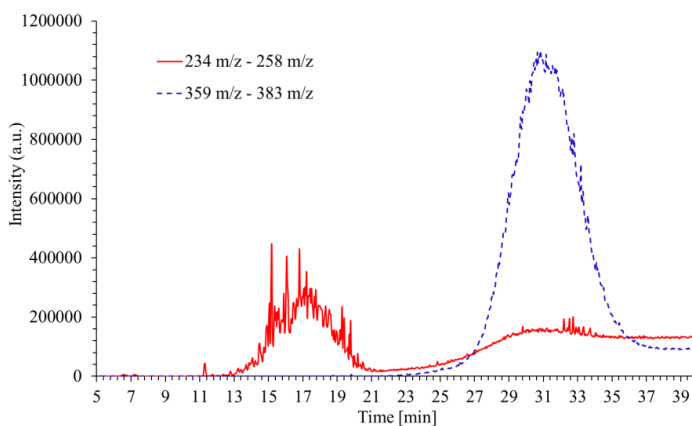


Figure 4 Chromatogram showing response for extracted ion chromatograms (EIC) with mass ranges 234 m/z-258 m/z and 359 m/z-383 m/z. The response of the EIC with mass range 234 m/z-258 m/z from minute 21 is considered as fragments.

Figure 5 displays the mass distribution of the entire elution hump of extracted crude oil acid A. To correct for the bias of fragmentation in the acid distribution the elution humps for different EIC

mass ranges were all given a time segment where the “real” acids elute. Based on these time segments the total chromatogram was split into time segments with increasing minimum  $m/z$  cutoff values as shown in Table 4, before the intensity averages of each time segment were normalized by the elution time range and summed up to reconstruct the mass distribution for the whole chromatogram. Consequently, the unwanted fragments are discarded from the distribution. However, this action would skew the reconstructed distribution to higher molecular weight as the false positives for low molecular weight acids are removed. Figure 6 and Figure 7 show the normalized mass distribution for extracted crude oil acid A and B respectively. Compared to the uncorrected distribution for the extracted crude oil acid mixture A shown in Figure 5, many of the registered naphthenic acids with carbon number  $C_{15}$  and below are absent in the normalized distribution in Figure 6. As shown previously<sup>44</sup>, the higher the molecular weight the more likely it is that a fragment will have high enough mass to register as an acid in Table S1. The extracted crude oil acid mixtures contain many higher molecular weight compounds, which makes them prone to fragmentation bias towards lower molecular weight in this method of low resolution GC/MS and derivatizing with MTBSTFA. Although column bleed should be corrected for through subtracting blank chromatograms and spectra, this method with  $m/z$  cutoff also removes the influence of column bleed (207  $m/z$  and 281  $m/z$  for this column) which gets more prevalent at higher temperatures (later retention times).

By applying the time segment method, it is found that 34% of the extracted chromatogram area between 234  $m/z$  and 750  $m/z$  correspond to fragments. When the same method was applied to a commercial acid mixture<sup>44</sup>, fragments only comprised 10% of the extracted chromatogram area (209  $m/z$  - 600  $m/z$ ). As explained in the same work, fragments with masses high enough to falsely register as  $[M+57]$  naphthenic acid masses are more likely obtained with higher molecular weight and more hydrogen deficient ( $Z$ ) acids. As the commercial acid mixture contains lower molecular weight acids with fewer ring structures the difference in fragment area compared to the fragment area obtained with an extracted acid mixture is consistent. The fragment area obtained on extracted acid mixtures is also consistent with the fragmentation observed in mass spectra obtained with model acids<sup>44</sup>, where for example the  $[M+57]$  peak abundance for: 4-heptylbenzoic acid ( $C_{14}$ ,  $Z=-8$ ) was 76%, behenic acid ( $C_{22}$ ,  $Z=0$ ) was 80%, and 5 $\beta$ -cholanic acid ( $C_{24}$ ,  $Z=-8$ ) was 44%.

*Table 4 Table showing how the chromatogram segments were split to ensure that fragments did not skew the mass distribution in favor of lower molecular weight acids*

Chromatogram segment	Minimum m/z cutoff
12 min - 21 min	233
21 min - 25 min	258
25 min - 29 min	283
29 min – 32 min	308
32 min – 35 min	333
35 min – 38 min	358
38 min – 40 min	383
40 min – 43 min	408
43 min – 45 min	433
45 min – 48 min	458
48 min – 50 min	483
50 min – 52 min	508
52 min – 54 min	533
54 min – 55 min	558
55 min – 60 min	583

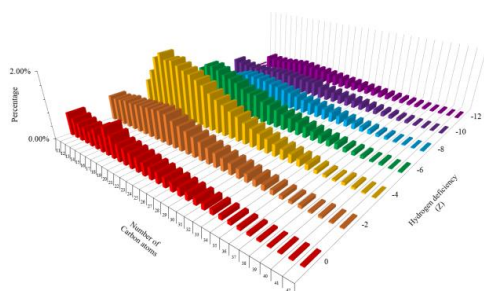


Figure 5 Non normalized mass distribution of extracted crude oil acid mixture A.

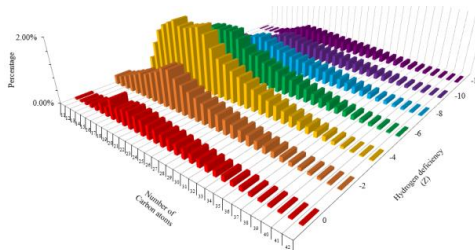


Figure 6 Normalized mass distribution of extracted crude oil acid mixture A. The effect of fragmentation was reduced by splitting up the mass spectrums with different mass range (Table 4) before recombination (see the text for details).

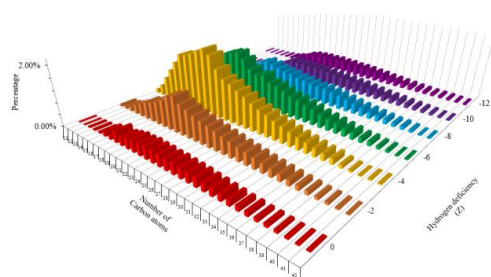


Figure 7 Normalized mass distribution of extracted crude oil acid mixture B. The effect of fragmentation was reduced by splitting up the mass spectrums with different mass range (Table 4) before recombination (see the text for details).

Figure 6 and Figure 7 show that the naphthenic acid mixtures consists of a broad mixture with  $C_{11}$ - $C_{40}$  and  $Z$  varying from 0 to -12.  $Z = 0$  corresponds to aliphatic acids;  $Z$ -values between -2 and -6 corresponds to alicyclic acids. Finally, a  $Z$  lower or equal to -8 would indicate the presence of an aromatic ring or an acid with four or more ring structures. Considering the obtained NRM spectrum ( Figure 1 ) indicating an absence of aromatic structures, these acids are most likely alicyclic ring structures with 4-6 rings. Most peaks appear in the  $C_{13} - C_{27}$  and 1-3 alicyclic ring range. This is similar to the results obtained by Hemmingsen, et al. <sup>55</sup>, who found two ringed acids ( $Z = -4$ ) to be the most abundant in his FT-ICR MS experiments on a North Sea Crude. Qian found three ringed acids ( $Z = -6$ ) to be the most abundant in south American heavy crude. The two mass distributions for the acid mixtures seems to be similar. Clemente, et al. <sup>62</sup> developed

a statistical method to assess the similarities between two naphthenic acid samples by dividing the  $n, Z$  distribution into groups of different carbon number ranges. The groups from each acid mixture distribution are then compared with an independent two-sample  $t$ -test assuming equal variance. The groups are considered different if the  $P$ -value is lower than 0.05. Applying this method to the two distributions indicate there is no significant difference between them (Table S2 in supplementary materials) which is interesting as their parent crude oils come from the same field but from different wells and have different TAN values. This means the two crude oil acids differ by their concentration and not their composition.

From the GC/MS mass distributions the calculated number average molecular weight was 340 g/mol and 360 g/mol for acid mixtures A and B respectively. These numbers are somewhat lower than the numbers obtained through elemental analysis, both of which are much lower than the average molecular weight determined by acid number as seen in Table 5. Some explanations could be proposed to explain this difference. The lower average molecular weight obtained through GC/MS was expected due to the inability of the GC to analyze the heaviest acid fraction and lower response factor of higher molecular weight compounds. None of this holds true for the number derived from the elemental composition however, although the calculations are sensitive to measured oxygen content. The number derived from TAN determination is found from the method and equations in the article by Mediaas, et al.<sup>47</sup> (equations 7, 8 and 9). A pollution by non-acid compounds would give an apparent higher molecular weight and provide a possible explanation. This explanation is strengthened by the data obtained in previous work on a commercial acid mixture from Fluka which show that the average molecular weight obtained from all three methods were similar. This would mean that the methodology is correct and that the discrepancy between the method comes from the composition of the extracted acid sample.

Table 5 Summary of results obtained by characterization of the extracted crude oil acid mixtures.

Method	Average molecular weight	Average molecular weight
	Acid mixture A [g/mol]	Acid mixture B [g/mol]
Elemental analysis	373	395
Titration	438*	454*
GC/MS	340	360

\*TAN determination performed at Equinor facilities

#### 4.2. Determination of the partition ratio in presence of monovalent cation

Extracted crude oil acid mixture A in toluene was shaken to equilibrium with aqueous buffers and the separated phases were derivatized and analyzed with GC/MS. The values reported are measured after one day of shaking and it was assumed that equilibrium was reached, although this was not verified. From the total ion chromatogram of the derivatized naphthenic acids, extracted ion chromatograms (EIC) were created with masses between 233 m/z and 700 m/z (from Table S1 the mass range should have been 159 m/z – 700 m/z, however masses which registered as acids below C<sub>11</sub> were discounted based on their absence in their expected elution time as mentioned in section 4.1.2.2). The area under the chromatogram was used to build calibration curves with the area of the internal standard peak. The calibration curve allows the relationship between the elution area of the internal standard and the elution area of sample to be linked to concentration as shown in Equation 12.

$$\frac{\text{Elution area acid mixture}}{\text{Elution area internal standard}} = a \cdot \frac{\text{Concentration acid mixture}}{\text{Concentration internal standard}} \quad (12)$$

where  $a$  is the slope between the two fractions. Here concentrations refer to the concentrations of the solutions prior to mixing sample and internal standard together and consequently before

derivatization. This relationship allows unknown concentrations in the oil phase to be calculated with Equation 13.

$$\text{Concentration acid mixture} = \frac{\text{Concentration internal standard}}{a} \cdot \frac{\text{Elution area acid mixture}}{\text{Elution area internal standard}} \quad (13)$$

For water the procedure is similar, except the volumes used for acidification and organic solvent extraction are taken into account to calculate the concentration in the water after equilibrium partitioning.

Figure 8 show the equilibrium partitioning for the acid mixture. At low pH values all the acids have a low affinity for the water phase. Partitioning starts at pH 7.2 and at the highest pH value, pH 11.5, around 65% of the acids remain in the oil phase. Only 20 % of the total acids seems to end up in the water phase at the highest studied pH value.

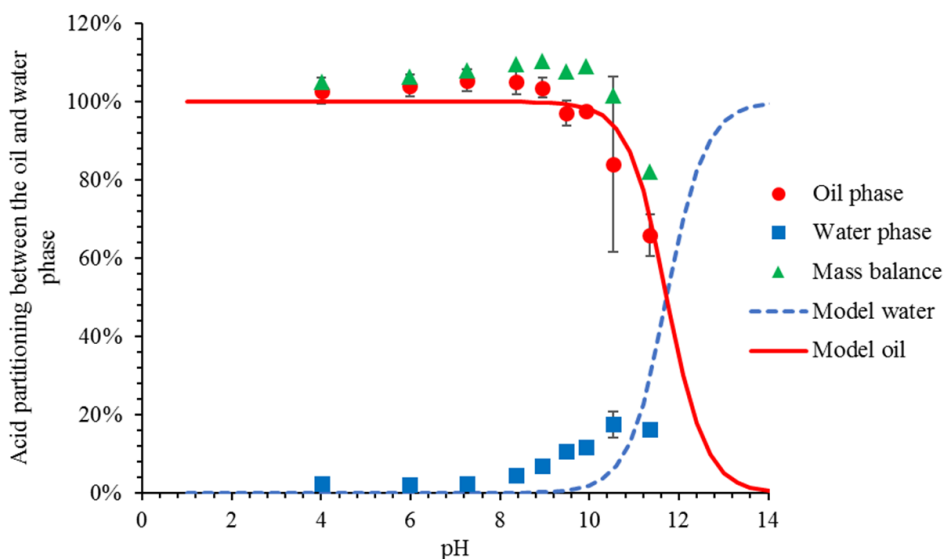


Figure 8 Equilibrium partitioning of the 234 m/z - 700 m/z fraction given as a function of equilibrium pH. Data was fitted with Equations 5 and 6, assuming a single  $pP_{wo}$  ( $pP_{wo}=6.7$ ,  $pK_a=5$ ). The partitioning was calculated by integrating the entire hump from  $RT= 12$  min to  $RT= 60$  min. The values are the average of two or three measurements where the error bars represent the range of obtained values. Some of the error bars are smaller than the symbols. The mass balance error bars are not shown for clarity.

Previous work on carboxylic acids and naphthenic acids indicates  $pK_a$  values between 4 and 6<sup>30, 63, 64</sup>. From more detailed study of previous research<sup>44</sup> it was concluded that it would be a useful assumption to fix the  $pK_a$  in all calculations to a value of 5. The apparent  $pK_a'$ , i.e. the point where the acid(s) is/are equally distributed between the two phases, equal to the sum of  $pP_{wo}$  and  $pK_a$  as shown in Equation 14, is used in the text or equations of several authors<sup>43, 45, 65</sup>

$$pK_a' = pK_a + pP_{wo} \quad (14)$$

From the partitioning of the total acid mixture, a  $pP_{wo}$  of 6.7 is calculated by Equations 5 and 6. An apparent  $pK_a'$  of 11.7 gives an indication of the small fraction of acids that are able to partition into the water phase. The fit is quite good however, a closer look of the MS data reveals that only the naphthenic acids with a molecular weight lower than 327 g/mol (384 m/z) partition into the aqueous phase. Higher molecular weight naphthenic acids do not significantly partition at pH values lower than 12. It was therefore decided to focus on the lower molecular weight naphthenic acids. The equilibrium partitioning of these naphthenic acids is presented in Figure 9. As expected, these naphthenic acids present a more significant partitioning in aqueous phase than the whole crude oil naphthenic acid mixture. Their equilibrium partitioning could not be fitted with a single partitioning ratio  $pP_{wo}$ .



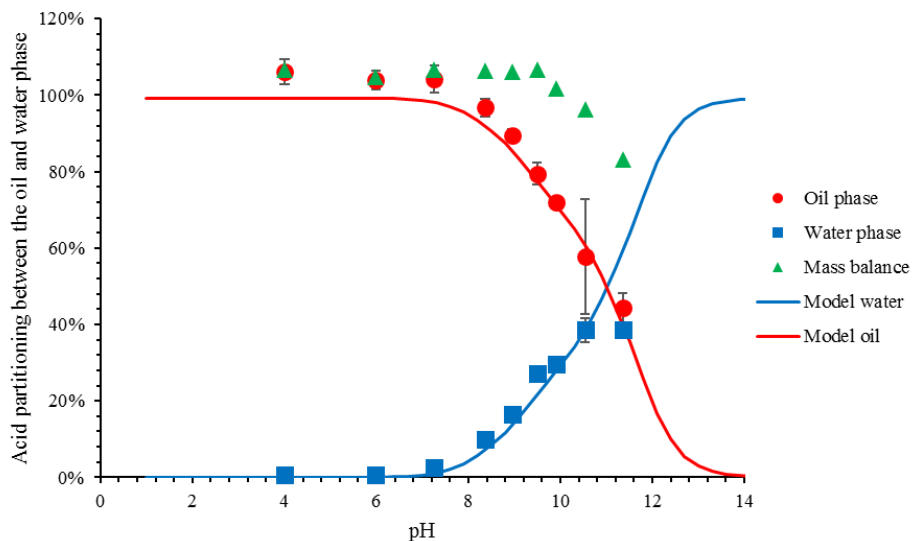


Figure 9 Equilibrium partitioning of the 234 m/z - 383 m/z fraction given as a function of equilibrium pH. Data was fitted with Equations 16 and 17. The values are the average of two or three measurements where the error bars represent the range of obtained values. Some of the error bars are smaller than the symbols. The mass balance error bars are not shown for clarity.

It was decided to divide up the chromatogram into narrower molecular weight ranges using the same method as employed in previous work<sup>44</sup> on a less polydisperse commercial acid mixture. This method will also provide information on the variations of naphthenic acid properties with their molecular weight. Table 6 summarizes the retention times and mass ranges of the different fraction of the chromatogram. This table is consistent with the start of Table 4. The heavier fractions which showed no quantifiable water solubility were disregarded. For every mass range considered in Table 6, a calibration curve was built, normalized by the internal standard. Correlation index  $r^2$  values are also presented in Table 6 (automatically calculated from linear regression fit). In the following sections the partitioning of every mass range is considered and analyzed similarly to the analysis of the commercial acid mixture in Bertheussen, et al.<sup>44</sup>.

Table 6 Mass ranges considered for quantitative partition analysis of extracted ion chromatograms (EIC's) of the extracted crude oil acid mixture A and the elution time segment considered to be whole acids and not fragments.

EIC mass fragment range* [m/z]	Integrated time interval of EIC	r <sup>2</sup>	
		linear range 0.66 mM-6.66 mM 0.28 g/L-2.92g/L	Chromatogram area %
234-700	12 min – 60 min	0.998	100%
234-258	12 min - 21 min	0.997	1%
259-283	16 min - 25 min	0.998	3%
284-308	18 min - 29 min	0.999	3 %
309-333	19 min – 32 min	0.999	5 %
334-358	20 min – 35 min	0.999	6 %
359-383	22 min – 38 min	0.999	6 %

\*Masses included in the mass ranges are based on naphthenic acid masses [M+57] from Table S1 including their isotope [M+57]+1.

The areas used for concentration determination for the different fractions encompassed 24% of the total chromatogram area spanning from 234 m/z to 700 m/z. The remaining 76% correspond to higher masses than 383 m/z (42%) which were not included due to their negligible water partitioning and non-included fragment humps (34%) as described in section 4.1.2.2.

Figure 10a and Figure 10b show the equilibrium partitioning of the mass ranges 234 m/z - 258 m/z and 259 m/z -283 m/z, corresponding to C<sub>11</sub>/C<sub>12</sub> and C<sub>13</sub>/C<sub>14</sub> acids respectively as seen in Table S1. The EIC intensity of this fraction comprises 1% of the total chromatogram area. The acids in the 234 m/z - 258 m/z mass range are completely oil-soluble below pH 6 and has an almost complete transfer to the water phase from pH 6 to 10. Equations 5 and 6 gives an adequate fit with the data when the  $pP_{wo}$  is 3.0, indicating that the molecular weight range is narrow enough to be modeled by a single  $pP_{wo}$ . This is confirmed by the R<sup>2</sup> values calculated from Equation 15<sup>66, 67</sup> and reported in Table 7.

$$R^2 = 1 - \frac{\sum(y - y_{fit})^2}{\sum(y - y_{avg})^2} \quad (15)$$

Here R<sup>2</sup> is the correlation index, y is the data point,  $y_{fit}$  is the calculated value from the fitted curve and  $y_{avg}$  is the arithmetic average of all y data points. The apparent  $pK_a'$  indicates a phase

transfer from pH 8.0. The EIC intensity of the 259 m/z -283 m/z mass range fraction comprises 3% of the total chromatogram area. Equations 5 and 6 give a good fit with the data when the  $pP_{wo}$  is 3.8 (higher than the value found for the mass range 234-258 m/z) which indicates a phase transfer at the apparent  $pK_a'$  of 8.8.

The equilibrium partitioning of the mass ranges 284 m/z -308 m/z and 309 m/z -333 m/z are shown in Figure 10c and Figure 10d. These mass ranges correspond to  $C_{15}/C_{16}$  acids and  $C_{17}$  acids respectively and likewise comprise 3% and 5% of the total chromatogram area. A  $pP_{wo}$  of 4.6 is obtained for the mass range 284 m/z -308 m/z, giving an apparent  $pK_a'$  of 9.6 as seen in Figure 10c. For the mass range 309 m/z -333 m/z, the obtained  $pP_{wo}$  is 5.8 indicating a phase transfer (apparent  $pK_a'$ ) at pH 10.8.

Figure 10e and Figure 10f show the equilibrium partitioning of the mass ranges 334 m/z -358 m/z and 359 m/z -383 m/z. These mass ranges correspond to  $C_{18}/C_{19}$  acids and  $C_{20}/C_{21}$  acids respectively and both comprise 6% of the total chromatogram area. Due to the incomplete partitioning, Equations 5 and 6 do not give a good fit with the data for these two higher mass ranges, consistent with the  $R^2$  values seen in Table 7. The obtained  $pP_{wo}$  values of 6.7 and 6.8 respectively does not accurately predict the system behavior at high pH.

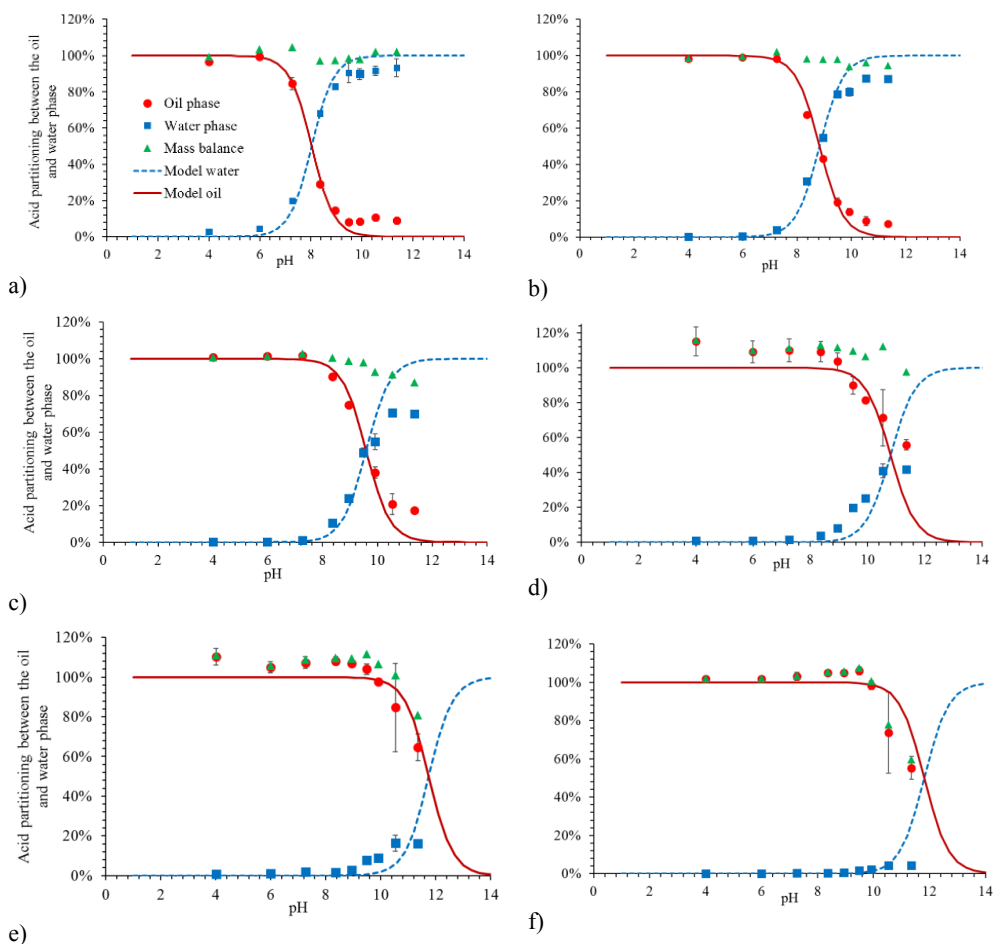


Figure 10 Equilibrium partitioning of the naphthenic acid mass fractions, of the extracted crude oil acid mixture A, given as a function of equilibrium pH. a) 234 m/z - 258 m/z, b) 259 m/z -283 m/z, c) 284 m/z -308 m/z, d) 309 m/z -333 m/z, e) 334 m/z -358 m/z, f) 359 m/z -383 m/z. Data was fitted with Equations 5 and 6, assuming  $pK_a=5$ , and a single  $pP_{wo}$ , a) 3.0, b) 3.8, c) 4.6, d) 5.8, e) 6.7, f) 6.8. The values are the average of two or three measurements where the error bars represent the range of obtained values. Some of the error bars are smaller than the symbols. The mass balance error bars are not shown for clarity.

As can be seen the mass balance determined for all the systems in Figure 8 and Figure 10 are generally close to 100%. One exception comes when higher molecular weight acids partition at high pH (Figure 10e and Figure 10f). Here the mass balance is lower, most likely caused by the light brown colored layer in the water phase at the centrifugation tube wall after centrifugation for experiments with initial pH 11 and 12 ( $pH_i=10.4$  and  $11.4$ ). It was impossible to improve the separation. This trend was also observed for high acid molecular weights at high pH in previous

work<sup>44</sup>. This loss of sample was attributed to the precipitation of sodium salt of naphthenate. The precipitation is only significant for the highest molecular weight acids in their carboxylate form as noticed previously. It can be noticed in Figure 8, 10d and 10e that the mass balances are slightly higher than 100%. This is most likely due to uncertainties in the different steps of the analysis like calibration curve buildup, water phase extraction and mass determination. The error bars presented in the different figures concern the reproducibility of the experiments.

Higher mass ranges (above 383 m/z), which corresponds to 42% of the total chromatogram area, does not have sufficient partitioning to the water phase to be considered with this method. The concentration of the water-soluble fraction of naphthenic acid in oil and water can be determined by the sum of every individual fraction in proportion to their ratios of the total water-soluble fraction chromatogram (24% for masses 234 m/z – 383 m/z) as seen in Equation 16 and 17. Here the  $\omega_i$  and  $P_{wo,acid,i}$  are the chromatogram area fraction and partition ratio for each mass range respectively.

$$[HA]_{w,tot} = \sum_{i=1}^n \omega_i \frac{[HA]_{o,init}}{\frac{[H^+]}{P_{wo,acid,i}(K_{a,HA}+[H^+])} + \frac{V_w}{V_o}} \quad (16)$$

$$[HA]_{o,tot} = \sum_{i=1}^n \omega_i \frac{[HA]_{o,init}}{1 + \frac{V_w P_{wo,acid,i}(K_{a,HA}+[H^+])}{V_o [H^+]}} \quad (17)$$

Figure 9 shows the summation model of the water-soluble fraction of the extracted crude oil acid mixture A. It can be seen that the model gives a good fit to the data.

A summary of the partitioning results for the extracted crude oil acid mixture A, are summarized in Table 7. The  $pP_{wo}$  and consequently the apparent  $pK_a'$  increases with the acid mass.

Table 7 Mass ranges and equivalent molecular weight shown in a summary along with their respective  $pP_{wo}$  calculated by imposing  $pK_a = 5$  in Equations 5 and 6. The area fraction of the elution hump of each mass range is also indicated.  $pK_a = 5$  imposed for naphthenic acids in all mass ranges.

Mass range	Molecular weight	Approximate carbon numbers	$pP_{wo}$	Chromatogram area %	$pK_a$	R <sup>2</sup> Oil phase	R <sup>2</sup> Water phase***
234 – 258 m/z	177 – 201 g/mol	C <sub>11</sub> /C <sub>12</sub>	3.0	1 %	8.0	0.98	0.97
259 – 283 m/z	202 – 226 g/mol	C <sub>13</sub> /C <sub>14</sub>	3.8	3 %	8.8	0.99	0.96
284 – 308 m/z	227 – 251 g/mol	C <sub>15</sub> /C <sub>16</sub>	4.6	3 %	9.6	0.97	0.85
309 – 333 m/z	252 – 276 g/mol	C <sub>17</sub>	5.8	5 %	10.8	0.86	-0.01
334– 358 m/z	277 – 301 g/mol	C <sub>18</sub> /C <sub>19</sub>	6.7*	6 %	11.7	0.92	-0.80
359– 383 m/z	302 – 326 g/mol	C <sub>20</sub> /C <sub>21</sub>	6.8*	6 %	11.8	0.94	-14.76
>384 m/z	>327 g/mol			42 %	-	-	-
234-700 m/z	177-643 g/mol		6.7	100%**	11.7	0.98	-2.30

\* $pP_{wo}$  calculated on incomplete partitioning in water at high pH. \*\* Elution hump area do not add to 100% due to non-included fragment areas as can be seen in Figure 4. \*\*\*low degree of partitioning makes the denominator of the fraction term in Equation 15 small, which gives low or negative R<sup>2</sup> values.

Figure 11 show the linear relationship of the cologarithm of the partition ratio as a function of molecular weight obtained for the extracted crude oil acid mixture A and previously obtained results for a commercial acid mixture from Fluka<sup>44</sup>. In this article we have assumed a  $pK_a$  of 5, based on previous works<sup>30, 63, 64</sup>. Even if this value seems the most likely, we have conducted a small sensitivity analysis on the influence of  $pK_a$  on  $pP_{wo}$  on the data in Figure 10a. When the  $pK_a$  is increased or decreased with 1, the  $pP_{wo}$  decreases or increases with 1 respectively. The shape or location of the predicted oil and water concentration curves in Figure 10a are also unchanged by a change in the assumed  $pK_a$ .

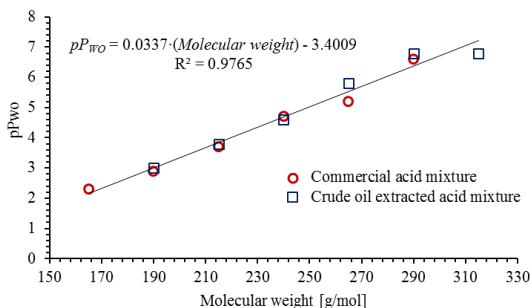


Figure 11 Graph indicating the linearity of the cologarithm of the partition ratio  $pP_{wo}$  of acid mass ranges from the NA mixtures based on molecular weight. Commercial acid mixture data from <sup>44</sup>. The molecular weight indicated corresponds to the middle of the mass ranges.

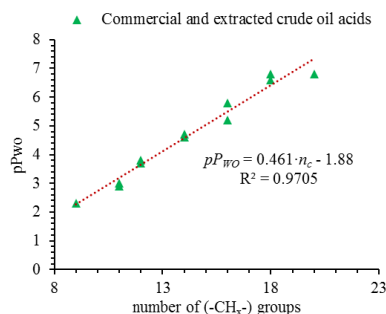


Figure 12 Graph illustrating the link between obtained partition ratio results for a commercial acid mixture <sup>44</sup>, extracted crude oil acids and Equation 18.

### 4.3 Discussion about partition ratio variation with molecular weight

#### 4.3.1 Thermodynamic explanation

Over the years libraries of partition coefficients have been gathered <sup>68</sup> and different models has been used to estimate the partitioning behavior of molecules based on structure <sup>69</sup>. Although the most widely used partition coefficient,  $\log P_{\text{octanol}}$ , refers to an octanol-water system, Leo, et al. <sup>68</sup> also presented solvent correlation to correct for partitioning coefficients between different solvents. Most of these models are dependent on more structural information <sup>70</sup> than what can be obtained through the molecular weight alone due to the impressive number of structural isomers encountered in organic molecules. It should be mentioned that  $\log P_{\text{toluene}}$  is equal to the  $pP_{wo}$  used in this work.

Data from Figure 11 allows the determination of some thermodynamic parameters characterizing the partitioning of naphthenic acids between aqueous solution and toluene.

Cratin <sup>71</sup> demonstrated Equation 18 which presents the variation of the partitioning ratio with the carbon number of homologue series.

$$pP_{wo} = \frac{n\Delta\mu_{L(-CH_2-)}}{2.3RT} + \frac{\Delta\mu_{H(-COOH)}}{2.3RT} + \log \frac{V_w}{V_o} \quad (18)$$

Where  $\Delta\mu_{L(-CH_x-)}$  stands for the free energy change of one lipophilic group of a molecule when the transfer occurs from oil to water.  $\Delta\mu_{H(-COOH)}$  stands for the free energy contribution of the hydrophilic group of the molecule when the transfer occurs from oil to water.  $n$  stands for the number of lipophilic groups.  $\bar{V}_o$  and  $\bar{V}_w$  are the molar volumes of the solvent and water.  $R$  and  $T$  are the ideal gas constant and the temperature. Figure 12 shows how the number of lipophilic groups increase the  $pP_{wo}$  of crude oil acids.

From the slope of 0.461 the free energy change per mole of methylene group  $\Delta\mu_{L(-CH_2-)}$ , when the molecule is transferred from oil to water and the temperature is set to 25 °C, can be calculated to 2.63 kJ/mole. The positive number indicates that this group spontaneously partitions into the oil phase as expected. From the intercept the contribution for the chosen hydrophilic group  $\Delta\mu_{H(-COOH)}$  can be calculated by using molar volumes for toluene and water to be -6.3 kJ/mole.

A value of the free energy change during water to heptane partition for some long chains saturated, linear fatty acids of 3.5 kJ/mole of CH<sub>2</sub> group has been determined by Mukerjee<sup>72</sup>. This value is significantly higher than the one determined in the present study, even if Mukerjee<sup>72</sup> has noticed that the value decreases for the longest tested acids. Two reasons can be pointed out to explain this difference. First, the difference of polarity between the oil phases used in the two study (heptane vs. toluene). Second, the presence of cycloalkyle rings in the commercial and crude oil naphthenic acid mixtures. These differences are consistent with a lower  $\Delta\mu_{L(-CH_x-)}$  compared with the system considered by Mukerjee<sup>72</sup>.

Another interesting comparison to be performed is between oil-water partition coefficient and micellization. The free energy contribution per each CH<sub>2</sub> group is generally considered to be -3.0 kJ/mol<sup>73, 74</sup>. The difference with the CH<sub>2</sub> group contribution for the partition of naphthenic acid found in this article is mostly due to the same factors as previously mentioned i.e. oil phase polarity and presence of cycloalkyle rings in the naphthenic acid structure.

#### 4.3.2 Comparison with model acid 4-heptylbenzoic acid

In previous work<sup>43</sup> the partitioning of the model acids phenyl acetic acid and 4-heptylbenzoic acid between heptane and 3.5% NaCl water was mapped over the pH range. The small acid phenyl



acetic acid was found to be almost completely water soluble even at low pH values and does not lend itself to comparative observations. The larger 4-heptylbenzoic acid had a sharp phase change around pH 8 ( $pK_a'$ ). As discussed in previous work<sup>44</sup>, 4-heptylbenzoic acid would give a stable ion mass fragment covered by the mass range 259 m/z – 283 m/z. This mass range indicated a phase change at the apparent  $pK_a'$  of 8.7 for the commercial acid mixture and 8.8 for the extracted crude oil acids A. However, partitioning in<sup>43</sup> was measured using heptane as the oil phase. To have a meaningful comparison, experiments were repeated in toluene. When 4-heptylbenzoic acid is partitioned in toluene as seen in Figure 13, Equations 5 and 6 gives a  $pP_{wo}$  is 3.8, apparent  $pK_a'$  of 8.8 which overlaps perfectly with the partitioning from the mass range 259 – 283 m/z in the two acid mixtures. The figures also show the influence of the solvent on the  $pK_a'$ : the partition takes place at a lower pH when the polarity of the organic solvent is lower. We can also notice that the partition curve of 4-heptylbenzoic acid in toluene is well-fitted by equations 5 and 6 contrary to heptane. Other equilibria, not taken into account by the model presented in section 2.2, might have an influence in heptane.

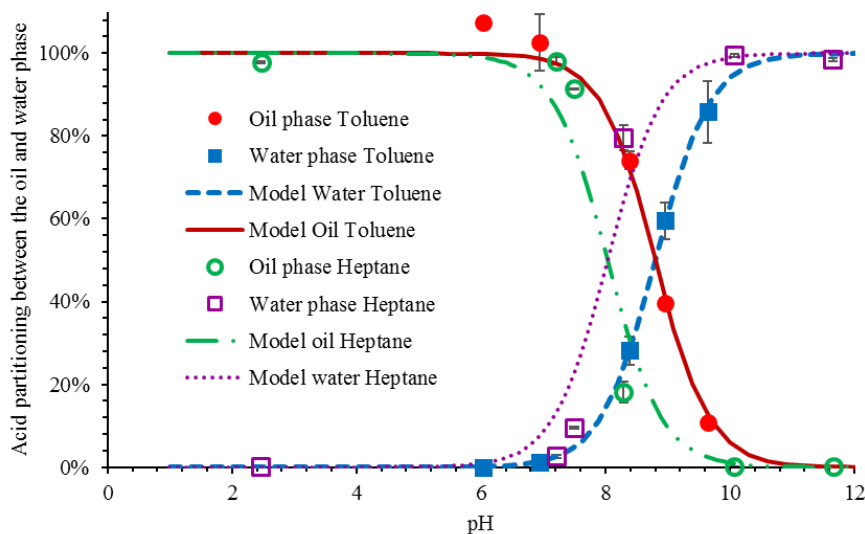


Figure 13 Equilibrium partitioning of 4-heptyl benzoic acid given as a function of equilibrium pH. The system had initial concentration of 1 mM acids in toluene or heptane with aqueous buffer (3.5 wt.% NaCl). Data was fitted with Equations 5 and 6. ( $pP_{wo}$ =3.43,  $pK_a$ =4.6 for heptane,  $pP_{wo}$ =3.8,  $pK_a$ =5 for toluene). Heptane data taken and replotted from Bertheussen, et al.<sup>43</sup>. The values are the average of two measurements where the error bars represent the range of obtained values. Some of the error bars are smaller than the symbols.

### 4.3.3 Comparison of partition ratio with literature

Zhang, et al. <sup>75</sup>, using HPLC ESI/HRMS, reported octanol–water distribution ratios,  $D_{ow}$ , for carboxylic acids from OSPW with increasing carbon number. It is interesting to note a large change in partitioning with structure having increasing DBE number in the work of Zhang, et al. <sup>75</sup>. In order to compare results from different studies, the reported data were converted into  $pP_{wo}$  in toluene and the structure characterized by  $n_c$  and  $Z$  with the following relationships: data reported in octanol were calculated in toluene according to the relationship by Leo, et al. <sup>68</sup>,  $\log P_{\text{toluene}} = 1.135 \log P_{\text{octanol}} - 1.777$ , distribution ratios were converted into partition ratios with equation 9 in Bertheussen, et al. <sup>43</sup> and DBE values are converted to  $Z$  number through Equation 11. As explained in section 4.3.1,  $\log P_{\text{octanol}}$ , commonly refers to an octanol–water system.  $\log P_{\text{toluene}}$  describes the partition coefficient using toluene as the organic solvent instead of octanol.

Experimental data are first compared and can found in Table 8. In general the estimated numbers from Zhang, et al. <sup>75</sup>, differ from the ones obtained for the acid mixtures analyzed in work. Even the most hydrophobic structures reported ( $Z=-4$ ), appears with  $pP_{wo}$  1-2 orders of magnitudes lower, indicating an overestimated water solubility. An argument could be made for the difference in source material. Extracted crude oil acids from a crude oil which has been in contact with water as done in this work, could contain different acid structure isomers compared to oil sands process-affected water (OSPW), as shown by the experiments by Stanford, et al. <sup>23</sup>.

Havre, et al. <sup>30</sup> studied naphthenic acid equilibrium partitioning between a 2wt.% acid content crude oil and aqueous buffers using GC/MS. Reported values for naphthenic acid partitioning is listed in Table 8. As a  $pK_a$  of  $4.9 \pm 0.1$  was given for the acids, this value was used to calculate the  $pK_a'$  values. It should be mentioned that the partition ratio in this instance was between crude oil and water, which is compared to  $pK_a'$  values obtained with partition ratio between toluene and water. Crude oil is a different matrix with thousands of different saturates and aromatics, in addition to the presence of asphaltenes. Despite this limitation, the reported values are very similar to the ones obtained in this work for the acids listed in Table 8. This speaks to the applicability of the obtained results and method to describe crude oil acid mixture behaviors for all crude oils. The data obtained by Havre, et al. <sup>30</sup> show the influence of the number of alicyclic structures ( $Z$ ) at similar carbon number: The higher the carbon number the lower the  $pP_{wo}$ . The values obtained in

the present study are average data for given mass ranges and the influence of  $Z$  on the partitioning is therefore not visible.

Celsie, et al. <sup>32</sup> used COnductor-like Screening MOdel for Realistic Solvents (COSMO-RS) to model how pH would affect naphthenic acid concentrations in water for 55 representative naphthenic acids. Scarlett, et al. <sup>76</sup> reported the partitioning for organic acids based on quantitative structure activity relationship (QSAR) models. A comparison between simulated data and experimental data for some acids is shown in Table 8. All simulated data have been corrected for  $\log P_{\text{octanol}}$  to  $\log P_{\text{toluene}}$ . In general, the data simulated with COSMO-RS predict a more conservative water concentration while the data obtained with QSAR predict higher acid water solubility compared to the experimental data obtained in this work. In addition, COSMO-RS data assumes no salt in the water phase. From the salting out effect <sup>77</sup>, one would assume salinity would decrease the partitioning which was shown by Celsie, et al. <sup>32</sup> who calculated that salinity decreases the partitioning of naphthenic acids slightly. This was also demonstrated on the synthetic and complex tetraacid BP10 <sup>78</sup>, made to mimic the properties of the ARN acid, where the partitioning coefficient  $K_{wo}$  between chloroform and water decreased when salinity increases.

Table 8 Table comparing apparent  $pK_a$  values for carboxylic acids calculated from simulated data, COSMO-RS by Celsie, et al.<sup>32</sup>, QSAR by Scarlett, et al.<sup>76</sup> and experimental values from this work and calculated values from experimental data reported by Havre, et al.<sup>30</sup> and Zhang, et al.<sup>75</sup>.  $\log P$  values have all been converted from octanol to toluene using the correlation by Leo, et al.<sup>68</sup>  $\log P_{\text{toluene}} = 1.135 \log P_{\text{octanol}} - 1.777$ .  $\log P_{\text{toluene}}$  is equal to  $pP_{\text{wo}}$ .

Acids			Apparent $pK_a$ values where phase transfer between oil and water would occur				
Carbon number	Hydrogen deficiency Z-value	Molecular weight [g/mol]	Simulations		Experimental		
			COSMO-RS ** 32	QSAR* 76	Acid mixtures toluene/water partitioning***	Crude oil/water partitioning 30****	OSPW, PDMS partitioning 75*
C <sub>10</sub>	Z=0	172.3	8.5	7.7	7.3	-	-
	Z=-4	168.2	7.1	6.4		7.0	-
C <sub>11</sub>	Z=-2	184.3	11.4	7.6	8.0	7.4	-
	Z=-4	182.3	8.5	6.8		7.3	-
C <sub>12</sub>	Z=-4	196.3	8.8	7.3	8.8	7.9	6.6
C <sub>13</sub>	Z=-4	210.3	12.2	7.9		8.5	6.7
C <sub>14</sub>	Z=-6	222.3	8.8	7.9		8.5	6.7
	Z=-0	228.4	-	10.45	-	-	
C <sub>16</sub>	Z=-6	250	11.6	-	9.7	9.6	7.2
C <sub>18</sub>	Z=0	284.5	-	12.0	11.7	-	-

\*As only  $\log(P)$  was reported the  $pK_a$  was assumed 5 for all acids. \*\*Some reported  $pK_a$  values are much higher than 5, giving high apparent  $pK_a$  values. \*\*\*Average of results for matching naphthenic acid mass range obtained in this work and previously obtained results on a commercial acid mixture<sup>44</sup> as referenced in Figure 11. \*\*\*\*Used reported  $pK_a$  value of 4.9 for all reported partition ratios by Havre; due to the use of crude oil as oil phase solvent, no  $\log P$  solvent correction was attempted.

### 4.3. Influence of divalent cation on partitioning

Adding a divalent cation like calcium to the water phase can affect the partitioning of naphthenic acids as seen in previous work for model acids<sup>43</sup> and a commercial acid mixture<sup>44</sup>. In the case of model acids; calcium only affected the larger of the two acids, 4-heptylbenzoic acid, by forming calcium salt that precipitated at pH values over 7. The smaller of the two acids tested, phenylacetic acid, was not affected. A similar trend was seen for the commercial acid mixture from Fluka for acids with 13 or more carbon atoms, but the mechanism was different: Instead of being due to the formation of insoluble calcium naphthenate, the difference was shown to be caused by the formation of oil-soluble calcium naphthenate. This phenomenon was previously mentioned in the literature<sup>31, 39, 79</sup>. To map how calcium would affect an acid mixture extracted from crude oil, the same experimental setup presented in section 4.2 was repeated with the difference that 10 mM  $\text{CaCl}_2$  was added to the water phase. This concentration is much smaller than the  $\text{NaCl}$

concentration (~600 mM) and therefore the total ionic strength is similar to previous experiments without calcium. Another difference was that the final pH 11 was obtained through pure NaOH addition instead of the bicarbonate buffer due to  $\text{CaCO}_3$  incompatibility. As mentioned the separated water phases from the experiments with the two highest pH values in section 4.2 in absence of  $\text{CaCl}_2$ , had a light brown colored layer along the tube wall in the water phase indicating the presence of particles. No such layer was observed in the partitioning experiments with calcium. The same effect was also observed for the commercial acid mixture<sup>44</sup>. The overall effect of calcium on the whole acid mass range is shown in Figure 14. Here it can be observed that at high pH, calcium has an effect on the partitioning. Due to the low degree of overall partitioning for the crude oil acid mixture, trends are not as well defined. Better mass balances are also obtained when calcium is present, likely due to the clear oil and water phase obtained after centrifugation and no light brown layer.

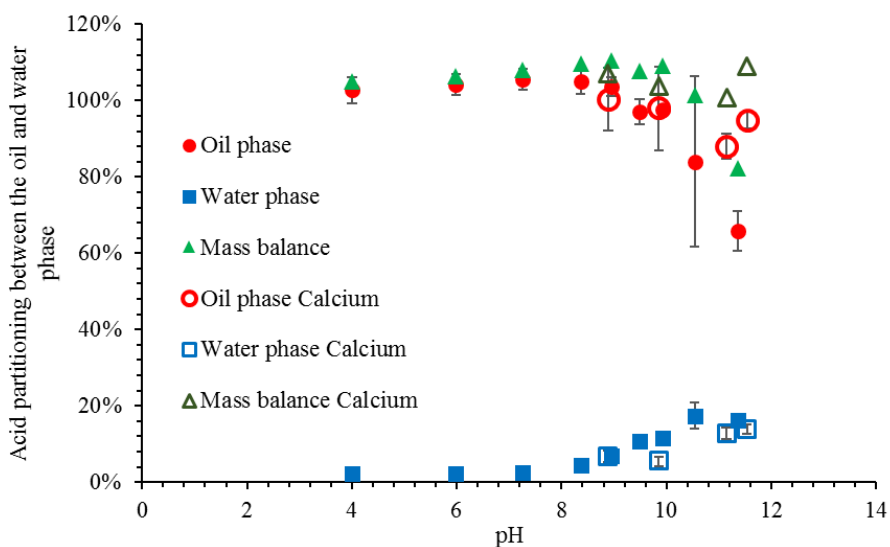


Figure 14. Equilibrium partitioning of the 234 m/z - 700 m/z fraction given as a function of equilibrium pH. The values are the average of two or three measurements where the error bars represent the range of obtained values. Some of the error bars are smaller than the symbols. The mass balance error bars are not shown for clarity.

The mass ranges were evaluated individually as was done previously in section 4.2. Figure 14a show the partitioning of the acids in the mass range 234 m/z - 258 m/z ( $\text{C}_{11}/\text{C}_{12}$ ) in comparison

with the partitioning in the system without calcium. As indicated by the similar partitioning, smaller acids are largely unaffected by the presence of calcium in the water phase, as was the case for the same acid fraction of a commercial acid mixture<sup>44</sup> and the small model acid phenylacetic acid<sup>43</sup>. Figure 14b compares the partitioning of the mass range 259 m/z – 283 m/z (C<sub>13</sub>/C<sub>14</sub>). Here it can be observed that in the system with calcium the partitioning is reduced at pH values higher than pH 9. The large model acid 4-heptylbenzoic acid, falls into this mass range.

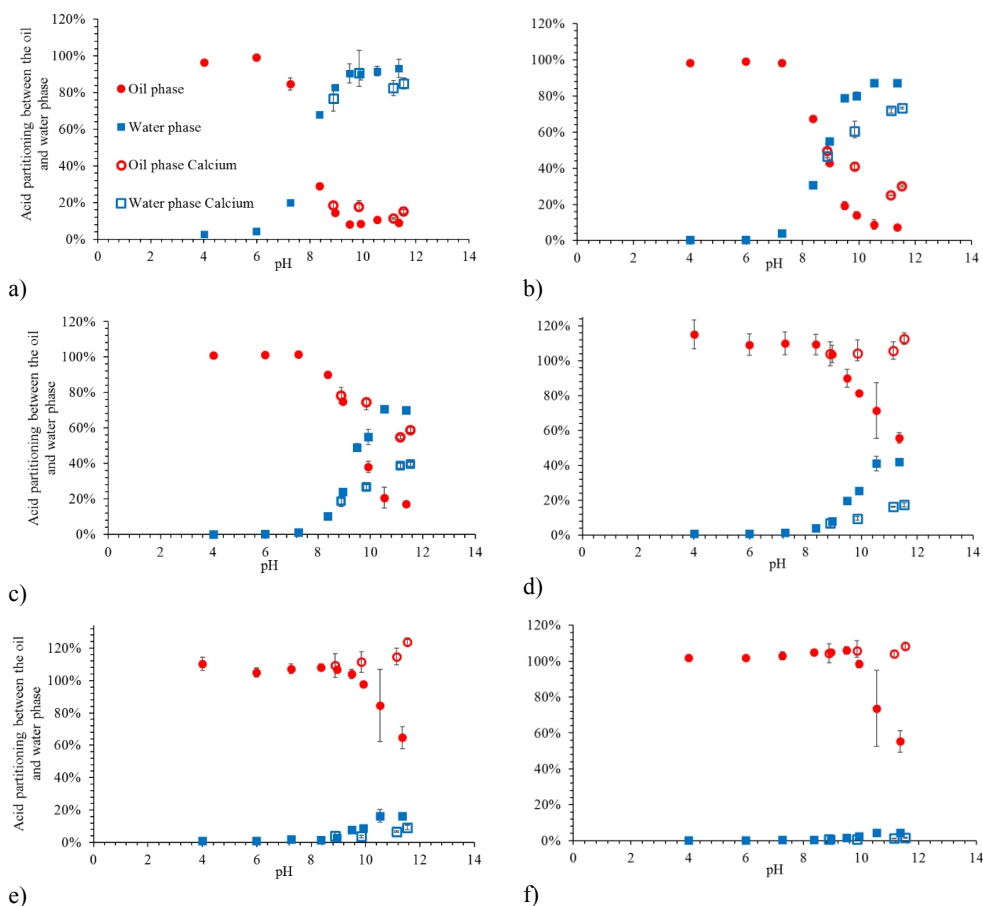


Figure 15 Equilibrium partitioning of the naphthenic acid mass fractions, of the extracted crude oil acid mixture A, given as a function of equilibrium pH. a) 234 m/z - 258 m/z, b) 259 m/z -283 m/z, c) 284 m/z -308 m/z, d) 309 m/z -333 m/z, e) 334 m/z -358 m/z, f) 359 m/z -383 m/z. The values are the average of two or three measurements where the error bars represent the range of obtained values. Some of the error bars are smaller than the symbols. For the sake of clarity, figures without mass balances are presented here, and figures with mass balances are presented in the Supporting Information.

The acid partitioning with and without calcium present for the remaining mass ranges 284 m/z - 308 m/z (C<sub>15</sub>/C<sub>16</sub>), 309 m/z - 333 m/z (C<sub>17</sub>), 334 m/z - 358 m/z (C<sub>18</sub>/C<sub>19</sub>) and 359 m/z - 383 m/z (C<sub>20</sub>/C<sub>21</sub>) is shown in Figure 14 c-f. Here the same trend as shown before prevails. At pH 9, calcium does not affect the partitioning, while at higher pH values the partitioning is reduced as the molecular weight of the acids increases. The mass balances are close to 100%, which indicate little or no loss of sample, such as precipitation of calcium naphthenate particles, as confirmed by visual inspection of the samples after centrifugation. Overall these results are in good agreement with results obtained in previous work on a commercial acid mixture, where it was concluded that at high pH and in the presence of calcium, there is formation of oil-soluble calcium naphthenates. The tendency for calcium to form calcium naphthenate with higher molecular weight acids has been reported previously <sup>79</sup>.

To learn more about the content of the oil phase after partitioning, a high-volume experiment was performed followed by elemental analysis of the oil phase.

Due to the limited amount of sample, only one parallel was performed on the extracted crude oil acid mixture B. The results are considered representative for values obtained with the extracted crude oil acid mixture A, due to the statistically insignificant mass distribution difference between them.

Previous results with a commercial acid mixture <sup>44</sup> showed that after partitioning with calcium present the elemental composition remained unchanged at pH 2, while at pH 10 and 11.5 the amount of oxygen was reduced by a factor of 2, indicating an increase in molecular weight for the acids remaining in the oil phase, in agreement with the relationship between  $pP_{wo}$  and molecular weight seen in Figure 11. Regarding calcium, there was none present in the oil phase at pH 2, while at the higher pH values calcium was present in a calcium to O<sub>2</sub> ratio of 0.25 for pH 10 and 0.5 for pH 11.5. The calcium to O<sub>2</sub> ratio show how many of the carbonyl groups are bound to calcium in the oil (note that 2 RCOO<sup>-</sup> are needed per Ca<sup>2+</sup>).

Comparing the previously obtained results with the commercial acid mixture with the results obtained with the extracted crude oil acids it can be observed in Table 9 that the oxygen content is

half of its original value for the extracted crude oil acids as well. This result was surprising as in contrast to the commercial acid mixture only a small fraction of the total acids of the extracted crude oil acid mixture partition over to the water phase at high pH, as seen in Figure 14. The calcium to O<sub>2</sub> ratio for the extracted crude oil acids at high pH are around 0.5, the same ratio as obtained for the commercial acid mixture, indicating that all the available carboxyl groups in the oil phase are bound to calcium. This result is also surprising, as it seems that even the largest acids have dissociated and formed oil-soluble calcium naphthenates.

Studies by Havre <sup>34</sup> concluded that calcium naphthenate is not formed in the water phase, rather they are formed through interfacial reactions between calcium and dissociated carbonyl groups as discussed by Brandal <sup>35</sup>. At final pH 11.5 the elemental composition indicates an average acid carbon number of C<sub>46</sub> and molecular weight 669 g/mol. This molecular weight is not initially present in the naphthenic acid sample ( Figure 7 ) and indicates that our calculation most likely does not capture some of the reaction happening in the presence of calcium. Consequently, more analyses are required to fully understand the mechanism in presence of calcium.

*Table 9 Elemental composition of evaporated oil phase acids after shaken to equilibrium with pH 12 buffer with 3.5% NaCl and 10 mM CaCl<sub>2</sub>.*

Final pH	Carbon [%]	Hydrogen [%]	Oxygen [%]	Calcium [%]	Sodium [%]	Chlorine [%]	<b>Mol Calcium Mol O<sub>2</sub></b>
pH 11.5	78.4	11.5	4.51	3.0	0.03	<0.4	0.53

In summary it appears that results obtained with an extracted crude oil acid mixture are similar to the ones found with a commercial acid mixture. Calcium reduces the high pH partitioning of C<sub>13</sub>-C<sub>19</sub> acids through the formation of oil-soluble calcium naphthenate, while the smaller acids are seemingly unaffected by calcium.



## 5. Conclusion

This article has continued and expanded previous work, detailing the equilibrium partitioning of a commercial acid mixture, by investigating the equilibrium partitioning of an extracted crude oil acid mixture. Two extracted crude oil acid mixtures from the same field were characterized and found to have statistically insignificant differences in mass distributions, even though their corresponding crude oils presented very different TAN values. A mass distribution bias for the GC/MS analysis method was corrected for and the acid mass distributions obtained reveal broad structural distributions consisting mainly of saturated ring structures with 2 to 3 rings. The partitioning of the extracted crude oil acid mixture A as a function of pH was analyzed with GC/MS. Only the acids with carbon numbers lower than C<sub>22</sub> partitioned to the water phase over the pH range 7-12. To be able to model the partitioning with a single partition ratio,  $P_{wo}$ , the acid mixture analysis was split up into narrower molecular mass ranges with a width of 25 g/mol. Summing up normalized contributions from each mass range, a partitioning curve for the whole water-soluble acid mixture fraction was established. Partition ratios obtained in this work have a complete overlap with previously obtained partition ratios using a commercial acid mixture. The influence of solvents on partitioning was discussed and, through solvent correction factors, previously reported partitioning results, both experimental and simulated, were compared to results obtained in this work. Calcium affected the high pH partitioning of larger acids, while smaller acids were unaffected. Oil phase analysis indicate that all remaining oil phase carboxylic groups are bound to calcium. Results indicate some universal properties for crude oil acids.

## Acknowledgements

This work was carried out as a part of SUBPRO, a Research-based Innovation Centre within Subsea Production and Processing. The authors gratefully acknowledge the financial support from SUBPRO, which is financed by the Research Council of Norway, major industry partners and NTNU. The authors would like to thank Einar Eng Johnsen (Equinor) and Hege Kummernes (Equinor) for providing the North Sea naphthenic acid samples, Gunhild Neverdal (Equinor) for GC/FID analysis and Bicheng Gao (NTNU) for the determination of NMR spectrum. The naphthenic acid extraction was performed at Equinor Research Centre Trondheim.

**Supporting information.** Table S1 displaying the naphthenic acid masses for increasing carbon numbers and hydrogen deficiencies. Table S2 displaying the details in the statistical comparison t-test between the two naphthenic acid mixtures. Figure S1 a-f, graphs showing equilibrium partitioning of naphthenic acids with and without calcium and the mass balances.

## References

1. Warner, R., Western European refineries and acidity in crude oil. In S&P-Global-Platts-Oil, Ed. S&P Global Inc: New York, USA, 2017; pp 1-6.
2. Prescott, C. N., Subsea Separation and Processing of Oil, Gas & Produced Water. Past, Present and Future. Why We Need It Now. In *Rice Global E&C Forum*, Fluor Offshore Solutions: Houston, Texas, 2012.
3. Berntsen, J. S., Qualified technology (TRL 5) to remove produced water, at seafloor or topside, before it becomes difficult to treat. In *Tekna Produced Water Management Conference*, 24th-25th January, Stavanger, Norway, 2018.
4. Shaiek, S.; Laurent, G., SpoolSep for Subsea Produced Water Separation, OTC-25934. In *Offshore Technology Conference*, 4-7 May, Houston, Texas, USA 2015.
5. Ligiero, L. M. Crude oil/water interface characterization and its relation to water-in-oil emulsion stability. University of Pau and Pays de l'Adour (UPPA), Pau, France, 2017.
6. Flesisnki, L. Étude de la stabilité des émulsions et de la rhéologie interfaciale des systèmes pétrole brut/eau: Influence des asphaltènes et des acides naphthéniques. University of Pau and Pays de l'Adour (UPPA), Pau, France, 2011.
7. Dudek, M.; Bertheussen, A.; Dumaire, T.; Øye, G., Microfluidic tools for studying coalescence of crude oil droplets in produced water. *Chemical Engineering Science* **2018**, 191, 448-458.
8. Headley, J. V., McMartin, Dena W., A Review of the Occurrence and Fate of Naphthenic Acids in Aquatic Environments. *Journal of Environmental Science and Health Part A* **2004**, A39, (8), 1989–2010.
9. Shepherd, A. G. A Mechanistic Analysis of Naphthenate and Carboxylate Soap-Forming Systems in Oilfield Exploration and Production. Heriot-Watt University, Edinburg, UK, 2008.
10. Qian, K.; Robbins, W. K.; Hughey, C. A.; Cooper, H. J.; Rodgers, R. P.; Marshall, A. G., Resolution and Identification of Elemental Compositions for More than 3000 Crude Acids in Heavy Petroleum by Negative-Ion Microelectrospray High-Field Fourier Transform Ion Cyclotron Resonance Mass Spectrometry. *Energy & Fuels* **2001**, 15, (6), 1505-1511.
11. Tomczyk, N. A.; Winans, R. E.; Shinn, J. H.; Robinson, R. C., On the Nature and Origin of Acidic Species in Petroleum. 1. Detailed Acid Type Distribution in a California Crude Oil. *Energy & Fuels* **2001**, 15, (6), 1498-1504.
12. Rudzinski, W. E.; Oehlers, L.; Zhang, Y.; Najera, B., Tandem Mass Spectrometric Characterization of Commercial Naphthenic Acids and a Maya Crude Oil. *Energy & Fuels* **2002**, 16, (5), 1178-1185.
13. Headley, J. V.; Peru, K. M.; Mohamed, M. H.; Frank, R. A.; Martin, J. W.; Hazewinkel, R. R. O.; Humphries, D.; Gurprasad, N. P.; Hewitt, L. M.; Muir, D. C. G.; Lindeman, D.; Strub,

- R.; Young, R. F.; Grewer, D. M.; Whittal, R. M.; Fedorak, P. M.; Birkholz, D. A.; Hindle, R.; Reisdorph, R.; Wang, X.; Kasperski, K. L.; Hamilton, C.; Woudneh, M.; Wang, G.; Loescher, B.; Farwell, A.; Dixon, D. G.; Ross, M.; Pereira, A. D. S.; King, E.; Barrow, M. P.; Fahlman, B.; Bailey, J.; McMartin, D. W.; Borchers, C. H.; Ryan, C. H.; Toor, N. S.; Gillis, H. M.; Zuin, L.; Bickerton, G.; McMaster, M.; Sverko, E.; Shang, D.; Wilson, L. D.; Wrona, F. J., Chemical fingerprinting of naphthenic acids and oil sands process waters-A review of analytical methods for environmental samples. *Journal of Environmental Science and Health. Part A, Toxic/hazardous Substances & Environmental Engineering* **2013**, 48, 1145-1163.
14. Barrow, M. P.; McDonnell, L. A.; Feng, X.; Walker, J.; Derrick, P. J., Determination of the Nature of Naphthenic Acids Present in Crude Oils Using Nanospray Fourier Transform Ion Cyclotron Resonance Mass Spectrometry: The Continued Battle Against Corrosion. *Analytical Chemistry* **2003**, 75, (4), 860-866.
15. Ese, M.-H.; Kilpatrick, P. K., Stabilization of Water-in-Oil Emulsions by Naphthenic Acids and Their Salts: Model Compounds, Role of pH, and Soap : Acid Ratio. *Journal Of Dispersion Science And Technology* **2004**, 25, (3), 253-261.
16. Häger, M.; Ese, M. H.; Sjöblom, J., Emulsion Inversion in an Oil-Surfactant-Water System Based on Model Naphthenic Acids under Alkaline Conditions. *Journal of Dispersion Science and Technology* **2005**, 26, (6), 673-682.
17. Vindstad, J. E.; Bye, A. S.; Grande, K. V.; Hustad, B.; Hustvedt, E.; Nergård, B., Fighting Naphthenate Deposition at the Heidrun Field. In *International Symposium on Oilfield Scale*, Society of Petroleum Engineers: January 29-30th, Aberdeen, UK, SPE 80375, 2003.
18. Sarac, S.; Civan, F., Mechanisms, Parameters, and Modeling of Naphthenate-Soap-Induced Formation Damage. *Society of Petroleum Engineers Journal* **2009**, 14, (2), 259-266.
19. St. John, W. P.; Rughani, J.; Green, S. A.; McGinnis, G. D., Analysis and characterization of naphthenic acids by gas chromatography–electron impact mass spectrometry of tert.-butyldimethylsilyl derivatives. *Journal of Chromatography A* **1998**, 807, (2), 241-251.
20. Scott, A. C.; Young, R. F.; Fedorak, P. M., Comparison of GC–MS and FTIR methods for quantifying naphthenic acids in water samples. *Chemosphere* **2008**, 73, (8), 1258-1264.
21. Holowenko, F. M.; MacKinnon, M. D.; Fedorak, P. M., Characterization of naphthenic acids in oil sands wastewaters by gas chromatography-mass spectrometry. *Water Research* **2002**, 36, (11), 2843-2855.
22. Clemente, J. S.; Fedorak, P. M., A review of the occurrence, analyses, toxicity, and biodegradation of naphthenic acids. *Chemosphere* **2005**, 60, (5), 585-600.
23. Stanford, L. A.; Kim, S.; Klein, G. C.; Smith, D. F.; Rodgers, R. P.; Marshall, A. G., Identification of Water-Soluble Heavy Crude Oil Organic-Acids, Bases, and Neutrals by Electrospray Ionization and Field Desorption Ionization Fourier Transform Ion Cyclotron Resonance Mass Spectrometry. *Environmental Science & Technology* **2007**, 41, (8), 2696-2702.
24. Damasceno, F. C.; Gruber, L. D. A.; Geller, A. M.; Vaz de Campos, M. C.; Gomes, A. O.; Guimaraes, R. C. L.; Peres, V. F.; Jacques, R. A.; Caramao, E. B., Characterization of naphthenic acids using mass spectroscopy and chromatographic techniques: study of technical mixtures. *Analytical Methods* **2014**, 6, (3), 807-816.
25. Lewis, A. T.; Tekavec, T. N.; Jarvis, J. M.; Juyal, P.; McKenna, A. M.; Yen, A. T.; Rodgers, R. P., Evaluation of the Extraction Method and Characterization of Water-Soluble Organics from Produced Water by Fourier Transform Ion Cyclotron Resonance Mass Spectrometry. *Energy & Fuels* **2013**, 27, (4), 1846-1855.

26. Grewer, D. M.; Young, R. F.; Whittal, R. M.; Fedorak, P. M., Naphthenic acids and other acid-extractables in water samples from Alberta: what is being measured? *Science of the Total Environment* **2010**, 408, (23), 5997–6010.
27. Headley, J. V.; Peru, K. M.; McMartin, D. W.; Winkler, M., Determination of dissolved naphthenic acids in natural waters by using negative-ion electrospray mass spectrometry. *Journal of AOAC International* **2002**, 85, 182-187.
28. Clingenpeel, A. C.; Rowland, S. M.; Corilo, Y. E.; Zito, P.; Rodgers, R. P., Fractionation of Interfacial Material Reveals a Continuum of Acidic Species That Contribute to Stable Emulsion Formation. *Energy & Fuels* **2017**, 31, (6), 5933-5939.
29. Rowland, S. M.; Robbins, W. K.; Corilo, Y. E.; Marshall, A. G.; Rodgers, R. P., Solid-Phase Extraction Fractionation To Extend the Characterization of Naphthenic Acids in Crude Oil by Electrospray Ionization Fourier Transform Ion Cyclotron Resonance Mass Spectrometry. *Energy & Fuels* **2014**, 28, (8), 5043-5048.
30. Havre, T. E.; Sjöblom, J.; Vindstad, J. E., Oil/Water-Partitioning and Interfacial Behavior of Naphthenic Acids. *Journal of Dispersion Science and Technology* **2003**, 24, (6), 789-801.
31. Hurtevent, C.; Bourrel, M.; Rousseau, G.; Brocart, B., Production Issues of Acidic Petroleum Crude Oils. In *Emulsions and Emulsion Stability*, Sjöblom, J., Ed. CRC Press: Boca Raton, FL, USA, 2005; pp 477-516.
32. Celsie, A.; Parnis, J. M.; Mackay, D., Impact of temperature, pH, and salinity changes on the physico-chemical properties of model naphthenic acids. *Chemosphere* **2016**, 146, 40-50.
33. Bostick, D. T.; Luo, H.; Hindmarsh, B. *Characterization of soluble organics in produced water*; Oak Ridge, Tennessee, US, 2002; pp 25-26.
34. Havre, T. E. Formation of Calcium Naphthenate in Water/Oil Systems, Naphthenic Acid Chemistry and Emulsion Stability. PhD thesis, NTNU, Trondheim, Norway, Trondheim, 2002.
35. Brandal, Ø. Interfacial (o/w) Properties of Naphthenic Acids and Metal Naphthenates, Naphthenic Acid Characterization and Metal Naphthenate Inhibition. PhD thesis, NTNU, Trondheim, Norway, 2005.
36. Haneseth, A. M. D.; Brandal, Ø.; Sjöblom, J., Formation, Growth, and Inhibition of Calcium Naphthenate Particles in Oil/Water Systems as Monitored by Means of Near Infrared Spectroscopy. *Journal of Dispersion Science and Technology* **2006**, 27, (2), 185-192.
37. Simon, S.; Reisen, C.; Bersås, A.; Sjöblom, J., Reaction Between Tetrameric Acids and Ca<sup>2+</sup> in Oil/Water System. *Industrial & Engineering Chemistry Research* **2012**, 51, (16), 5669-5676.
38. Sjöblom, J.; Simon, S.; Xu, Z., The chemistry of tetrameric acids in petroleum. *Advances in Colloid and Interface Science* **2014**, 205, (0), 319-338.
39. Cooke, C. E., Jr.; Williams, R. E.; Kolodzie, P. A., Oil Recovery by Alkaline Waterflooding. *Journal of Petroleum Technology* **1974**, 26, (12), 1365-1374.
40. Speight, J. G., Chapter 4 - Effects in Refining. In *High Acid Crudes*, Speight, J. G., Ed. Gulf Professional Publishing: Boston, US, 2014; pp 77-109.
41. Dyer, S. J.; Graham, G. M.; Arnott, C., Naphthenate Scale Formation - Examination of Molecular Controls in Idealised Systems. In *International Symposium on Oilfield Scale, 29-30 January*, Society of Petroleum Engineers: Aberdeen, United Kingdom, 2003.
42. Mediaas, H.; Wolf, N. O.; Baugh, T. D.; Grande, K. V.; Vinstad, J. E., The Discovery of High Molecular Weight Naphthenic Acids (ARN Acid) Responsible for Calcium Naphthenate

Deposits. In *SPE International Symposium on Oilfield Scale, 11-12 May*, SPE 93011: Society of Petroleum Engineers: Aberdeen, United Kingdom, 2005.

43. Bertheussen, A.; Simon, S.; Sjöblom, J., Equilibrium partitioning of naphthenic acids and bases and their consequences on interfacial properties. *Colloids and Surfaces A: Physicochemical and Engineering Aspects* **2017**, 529, (Supplement C), 45-56.

44. Bertheussen, A.; Simon, S. C.; Sjöblom, J., Equilibrium partitioning of naphthenic acid mixture part 1: Commercial naphthenic acid mixture. *Energy & Fuels* **2018**.

45. Scherrer, R. A.; Howard, S. M., Use of distribution coefficients in quantitative structure-activity relationships. *J Med Chem* **1977**, 20, (1), 53-8.

46. Spildo, K.; Hoiland, H., Interfacial Properties and Partitioning of 4-Heptylbenzoic Acid between Decane and Water. *Journal of Colloid and Interface Science* **1999**, 209, (1), 99-108.

47. Mediaas, H.; Grande, K. V.; Hustad, B. M.; Rasch, A.; Rueslåtten, H. G.; Vindstad, J. E., The Acid-IER Method - a Method for Selective Isolation of Carboxylic Acids from Crude Oils and Other Organic Solvents. In *International Symposium on Oilfield Scale, 29-30 January*, SPE 80404: Society of Petroleum Engineers: Aberdeen, United Kingdom, 2003.

48. Lide, D. R., CRC handbook of chemistry and physics: A ready-reference book of chemical and physical data. In 77 ed.; CRC Press Inc.: Boca Raton, Florida, US, 1997; p 842.

49. Lu, Y.; Wang, J.; Deng, Z.; Wu, H.; Deng, Q.; Tan, H.; Cao, L., Isolation and characterization of fatty acid methyl ester (FAME)-producing *Streptomyces* sp. S161 from sheep (*Ovis aries*) faeces. *Lett Appl Microbiol* **2013**, 57, (3), 200-5.

50. Barros, E. V.; Dias, H. P.; Pinto, F. E.; Gomes, A. O.; Moura, R. R.; Neto, A. C.; Freitas, J. C. C.; Aquije, G. M. F. V.; Vaz, B. G.; Romão, W., Characterization of Naphthenic Acids in Thermally Degraded Petroleum by ESI(-)-FT-ICR MS and 1H NMR after Solid-Phase Extraction and Liquid/Liquid Extraction. *Energy & Fuels* **2018**, 32, (3), 2878-2888.

51. Saab, J.; Mokbel, I.; Razzouk, A. C.; Ainous, N.; Zydowicz, N.; Jose, J., Quantitative Extraction Procedure of Naphthenic Acids Contained in Crude Oils. Characterization with Different Spectroscopic Methods. *Energy & Fuels* **2005**, 19, (2), 525-531.

52. Jones, D. M.; Watson, J. S.; Meredith, W.; Chen, M.; Bennett, B., Determination of Naphthenic Acids in Crude Oils Using Nonaqueous Ion Exchange Solid-Phase Extraction. *Analytical Chemistry* **2001**, 73, (3), 703-707.

53. Cassani, F.; Eglinton, G., Organic geochemistry of Venezuelan extra-heavy crude oils 2. Molecular assessment of biodegradation. *Chemical Geology* **1991**, 91, (4), 315-333.

54. Jones, D.; West, C. E.; Scarlett, A. G.; Frank, R. A.; Rowland, S. J., Isolation and estimation of the 'aromatic' naphthenic acid content of an oil sands process-affected water extract. *Journal of Chromatography A* **2012**, 1247, (1873-3778 (Electronic)), 171- 175.

55. Hemmingsen, P. V.; Kim, S.; Pettersen, H. E.; Rodgers, R. P.; Sjöblom, J.; Marshall, A. G., Structural Characterization and Interfacial Behavior of Acidic Compounds Extracted from a North Sea Oil. *Energy & Fuels* **2006**, 20, (5), 1980-1987.

56. ThermoScientific, Reagents, Solvents and Accessories catalogue. In 2012.

57. Acevedo, S.; Escobar, G.; Ranaudo, M. A.; Khazen, J.; Borges, B.; Pereira, J. C.; Méndez, B., Isolation and Characterization of Low and High Molecular Weight Acidic Compounds from Cerro Negro Extraheavy Crude Oil. Role of These Acids in the Interfacial Properties of the Crude Oil Emulsions. *Energy & Fuels* **1999**, 13, (2), 333-335.

58. Mapolelo, M. M.; Rodgers, R. P.; Blakney, G. T.; Yen, A. T.; Asomaning, S.; Marshall, A. G., Characterization of naphthenic acids in crude oils and naphthenates by electrospray

- ionization FT-ICR mass spectrometry. *International Journal of Mass Spectrometry* **2011**, 300, (2–3), 149-157.
59. Wang, Z.; Hollebone, B. P.; Fingas, M.; Fieldhouse, B.; Sigouin, L.; Landriault, M.; Smith, P.; Noonan, J.; Thouin, G., Characteristics of Spilled Oils, Fuels, and Petroleum Products: 1. Composition and Properties of Selected Oils. In Research Triangle Park, North Carolina 27711, USA: Ecosystems Research Division, United States Environmental Protection Agency, 2003; p 286.
60. Seifert, W. K.; Teeter, R. M., Identification of polycyclic aromatic and heterocyclic crude oil carboxylic acids. *Analytical Chemistry* **1970**, 42, (7), 750-758.
61. Hindle, R.; Noestheden, M.; Peru, K.; Headley, J., Quantitative analysis of naphthenic acids in water by liquid chromatography–accurate mass time-of-flight mass spectrometry. *Journal of Chromatography A* **2013**, 1286, (Supplement C), 166-174.
62. Clemente, J. S.; Prasad, N. G. N.; MacKinnon, M. D.; Fedorak, P. M., A statistical comparison of naphthenic acids characterized by gas chromatography–mass spectrometry. *Chemosphere* **2003**, 50, (10), 1265-1274.
63. Brient, J. A.; Wessner, P. J.; Doyle, M. N., Naphthenic Acids. In *Encyclopedia of Chemical Technology*, Kirk-Othmer, Ed. John Wiley & Sons, Inc.: New York, 1995; pp 1017-1029.
64. Dewick, P. M., Acids and bases. In *Essentials of Organic Chemistry: For Students of Pharmacy, Medicinal Chemistry and Biological Chemistry*, Dewick, P. M., Ed. WILEY: West Sussex, England, 2006; p 130.
65. Passade-Boupat, N.; Rondon Gonzalez, M.; Hurtevent, C.; Brocart, B.; Palermo, T., Risk Assessment of Calcium Naphtenates and Separation Mechanisms of Acidic Crude Oil. In *SPE International Conference and Exhibition on Oilfield Scale*, Society of Petroleum Engineers: Aberdeen, UK, 30-31 May, SPE 155229, 2012.
66. Brown, A. M., A step-by-step guide to non-linear regression analysis of experimental data using a Microsoft Excel spreadsheet. *Comput Methods Programs Biomed* **2001**, 65, (3), 191-200.
67. Colin Cameron, A.; Windmeijer, F. A. G., An R-squared measure of goodness of fit for some common nonlinear regression models. *Journal of Econometrics* **1997**, 77, (2), 329-342.
68. Leo, A.; Hansch, C.; Elkins, D., Partition coefficients and their uses. *Chemical Reviews* **1971**, 71, (6), 525-616.
69. Leo, A. J., Calculating log P<sub>oct</sub> from structures. *Chemical Reviews* **1993**, 93, (4), 1281-1306.
70. Wang, R.; Fu, Y.; Lai, L., A New Atom-Additive Method for Calculating Partition Coefficients. *Journal of Chemical Information and Computer Sciences* **1997**, 37, (3), 615-621.
71. Cratin, P. D., Partitioning at the liquid-liquid interface. *Industrial & Engineering Chemistry* **1968**, 60, (9), 14-19.
72. Mukerjee, P., Dimerization of Anions of Long-Chain Fatty Acids in Aqueous Solutions and the Hydrophobic Properties of the Acids. *The Journal of Physical Chemistry* **1965**, 69, (9), 2821-2827.
73. Pestman, J. M.; Kevelam, J.; Blandamer, M. J.; van Doren, H. A.; Kellogg, R. M.; Engberts, J. B. F. N., Thermodynamics of Micellization of Nonionic Saccharide-Based N-Acyl-N-alkylaldosylamine and N-Acyl-N-alkylamino-1-deoxyalditol Surfactants. *Langmuir* **1999**, 15, (6), 2009-2014.

74. Heerklotz, H.; Eppard, R. M., The Enthalpy of Acyl Chain Packing and the Apparent Water-Accessible Apolar Surface Area of Phospholipids. *Biophysical Journal* **2001**, 80, (1), 271-279.
75. Zhang, K.; Pereira, A. S.; Martin, J. W., Estimates of Octanol–Water Partitioning for Thousands of Dissolved Organic Species in Oil Sands Process-Affected Water. *Environmental Science & Technology* **2015**, 49, (14), 8907-8913.
76. Scarlett, A. G.; West, C. E.; Jones, D.; Galloway, T. S.; Rowland, S. J., Predicted toxicity of naphthenic acids present in oil sands process-affected waters to a range of environmental and human endpoints. *Sci Total Environ* **2012**, 425, 119-27.
77. Turner, A., Salting out of chemicals in estuaries: implications for contaminant partitioning and modelling. *Science of The Total Environment* **2003**, 314–316, 599-612.
78. Nordgård, E. L.; Ahmad, J.; Simon, S.; Sjöblom, J., Oil-Water Partitioning of a Synthetic Tetracarboxylic Acid as a Function of pH. *Journal of Dispersion Science and Technology* **2012**, 33, (6), 871-880.
79. Christiansen, I. Isolation and Characterization of Oil-Soluble Calcium Naphthenates in North Sea Heavy Crude Oil. M.Sc. Thesis, NTNU, Trondheim, Norway, 2014.





## Supplementary information

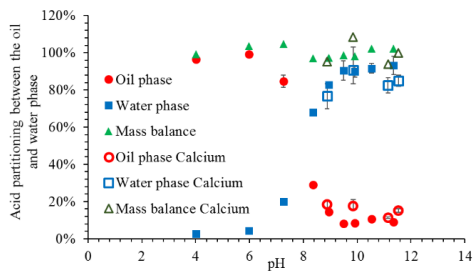
Table S1. Mass to charge ratio ( $m/z$ ) for stable ion fragment of naphthenic acid isomer  $C_nH_{2n+2}O_2$  derivatized with MTBSTFA. The stable ion mass fragment obtained with MTBSTFA has a mass of  $[M+57]$  where  $M$  is the molecular weight of the acid. Some masses are excluded by on the rules set up by Holowenko, et al. <sup>1</sup> except aromatic structures are included here as was done in Bertheussen, et al. <sup>2</sup>

Carbon number ( $n$ )	Hydrogen deficiency ( $Z$ )						
	0	-2	-4	-6	-8	-10	-12
5	159						
6	173						
7	187	185			179		
8	201	199			193		
9	215	213			207		
10	229	227	225		221	219	
11	243	241	239		235	233	
12	257	255	253	251	249	247	
13	271	269	267	265	263	261	259
14	285	283	281	279	277	275	273
15	299	297	295	293	291	289	287
16	313	311	309	307	305	303	301
17	327	325	323	321	319	317	315
18	341	339	337	335	333	331	329
19	355	353	351	349	347	345	343
20	369	367	365	363	361	359	357
21	383	381	379	377	375	373	371
22	397	395	393	391	389	387	385
23	411	409	407	405	403	401	399
24	425	423	421	419	417	415	413
25	439	437	435	433	431	429	427
26	453	451	449	447	445	443	441
27	467	465	463	461	459	457	455
28	481	479	477	475	473	471	469
29	495	493	491	489	487	485	483
30	509	507	505	503	501	499	497
31	523	521	519	517	515	513	511
32	538	535	533	531	529	527	525
33	552	550	547	545	543	541	539
34	566	564	562	559	557	555	553
35	580	578	576	574	571	569	567
36	594	592	590	588	586	583	581
37	608	606	604	602	600	598	595
38	622	620	618	616	614	612	610
39	636	634	632	630	628	626	624
40	650	648	646	644	642	640	638

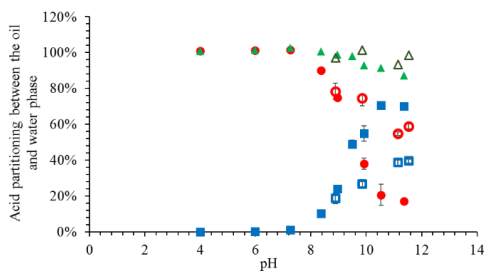
41	664	662	660	658	656	654	652
42	678	676	674	672	670	668	666
43	692	690	688	686	684	682	680
44	706	704	702	700	698	696	694
45	720	718	716	714	712	710	708
46	734	732	730	728	726	724	722
47	748	746	744	742	740	738	736

Table S2. A statistical comparison between naphthenic acid mass distributions through the method developed by Clemente, et al.<sup>3</sup>. The intensity of each n, Z specie is transformed to their arcsine value before statistical comparison with the "data analysis" tool of Excel.

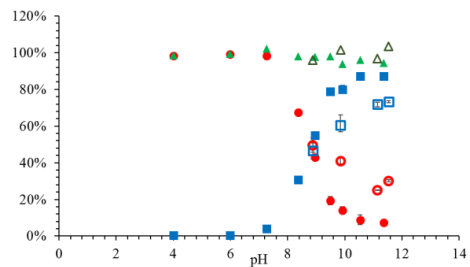
		Acid mixture A	Acid mixture B	P-value	Degrees of freedom	Variance mixture A	Variance mixture B
C <sub>11</sub> -C <sub>14</sub>	Group 1	8 %	4 %	0.091	48	2 · 10 <sup>-5</sup>	6 · 10 <sup>-6</sup>
C <sub>15</sub> -C <sub>21</sub>	Group 2	42 %	38 %	0.493	96	3 · 10 <sup>-5</sup>	4 · 10 <sup>-5</sup>
C <sub>22</sub> -C <sub>33</sub>	Group 3	42 %	49 %	0.065	166	7 · 10 <sup>-6</sup>	9 · 10 <sup>-6</sup>
C <sub>34</sub> -C <sub>45</sub>	Group 4	7 %	9 %	0.057	166	5 · 10 <sup>-7</sup>	8 · 10 <sup>-7</sup>



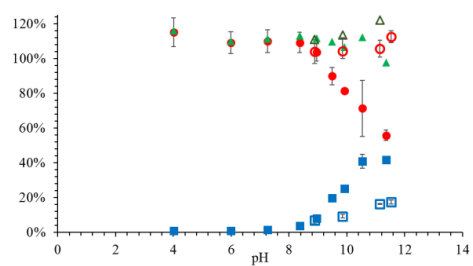
a)



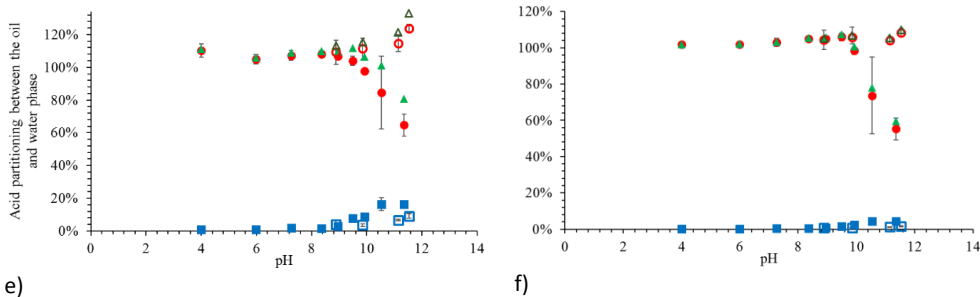
c)



b)



d)



e) f)  
 Figure S1 Equilibrium partitioning of the naphthenic acid mass fractions, of the extracted crude oil acid mixture A, given as a function of equilibrium pH. a) 234 m/z - 258 m/z, b) 259 m/z - 283 m/z, c) 284 m/z - 308 m/z, d) 309 m/z - 333 m/z, e) 334 m/z - 358 m/z, f) 359 m/z - 383 m/z. The total concentration of the extracted crude oil acid mixture A was 3.3 mM or 1.65 mM for pH higher than 10. Aqueous buffers with 3.5wt.% NaCl or 10 mM CaCl<sub>2</sub> and 3.5wt.% NaCl were used as water phase. The values are the average of two or three measurements where the error bars represent the range of obtained values. Some of the error bars are smaller than the symbols

1. Holowenko, F. M.; MacKinnon, M. D.; Fedorak, P. M., Characterization of naphthenic acids in oil sands wastewaters by gas chromatography-mass spectrometry. *Water Research* **2002**, 36, (11), 2843-2855.
2. Bertheussen, A.; Simon, S. C.; Sjoblom, J., Equilibrium partitioning of naphthenic acid mixture part 1: Commercial naphthenic acid mixture. *Energy & Fuels* **2018**.
3. Clemente, J. S.; Prasad, N. G. N.; MacKinnon, M. D.; Fedorak, P. M., A statistical comparison of naphthenic acids characterized by gas chromatography-mass spectrometry. *Chemosphere* **2003**, 50, (10), 1265-1274.

PAPER V

---

Microfluidic tools for studying coalescence of crude oil droplets in produced water





ELSEVIER

Contents lists available at ScienceDirect

## Chemical Engineering Science

journal homepage: [www.elsevier.com/locate/ces](http://www.elsevier.com/locate/ces)

# Microfluidic tools for studying coalescence of crude oil droplets in produced water

Marcin Dudek<sup>a</sup>, Are Bertheussen<sup>a</sup>, Thomas Dumaire<sup>b</sup>, Gisle Øye<sup>a,\*</sup>

<sup>a</sup>Ugelstad Laboratory, Department of Chemical Engineering, Norwegian University of Science and Technology (NTNU), Trondheim, Norway

<sup>b</sup>Sorbonne Universités, UPMC University of Paris 6, Paris, France

## HIGHLIGHTS

- Microfluidic technique is developed for probing coalescence of crude oil droplets.
- Diluted and non-diluted crude oils are used as the dispersed phase.
- Composition of the water phase is systematically varied.
- The effect of pressure on the coalescence is reported.

## ARTICLE INFO

### Article history:

Received 11 April 2018

Received in revised form 24 June 2018

Accepted 3 July 2018

Available online 4 July 2018

### Keywords:

Coalescence

Drop

Emulsion

Microfluidics

Produced water

## ABSTRACT

The major contaminant targeted during the treatment of the oilfield produced water is dispersed oil. The efficiency of most separation processes highly relies on the size of the droplets, which can be increased through coalescence. Crude oil has a complex and field-dependent composition, which can affect the interfacial properties of the drops, and consequently the merging process in different ways. This study focused on the development of microfluidic techniques for investigating coalescence between crude oil drops. The experiments were performed with six diluted crude oils and three neat oils, the latter in the presence of an oil-soluble surfactant. The composition of the water phase was systematically varied (pH, ionic composition, presence of dissolved components). In general, crude oil droplets coalesced more readily in lower or neutral pH. The addition of dissolved Fluka acids to the water phase had a unique effect on each crude oil, reflecting their composition. What is more, this effect was similar to the presence of water-soluble crude oil components in the aqueous phase. The pressure did not have a significant effect on the coalescence, which was explained by the lack of the lightest components (C1–C4) in the system. In summary, the results revealed several trends, however it was clear that the coalescence highly depended on the oil composition. This underlined the necessity for experimental methods, such as microfluidics, which allow for quick assessment of the stability of crude oil droplets.

© 2018 Published by Elsevier Ltd.

## 1. Introduction

During petroleum production, large volumes of water are co-produced with crude oil and natural gas. This produced water (PW) can be composed of formation water, injected fluids (e.g. seawater or production chemicals), dispersed crude oil, solid particles, and dissolved inorganic and organic components. Globally, it is estimated that the produced water to oil ratio is approximately 3:1 (Fakhru'l-Razi et al., 2009).

Before the produced water is disposed of (e.g. by re-injection to the reservoir or discharge), it has to undergo quality improving

\* Corresponding author at: Sem Sælandsvei 4, 7491 Trondheim, Norway.  
E-mail address: [gisle.oye@chemeng.ntnu.no](mailto:gisle.oye@chemeng.ntnu.no) (G. Øye).

treatment. The main contaminant targeted during the produced water treatment (PWT) processes is the dispersed crude oil. The limit for the discharge of the PW to the sea is between 30 and 40 ppm of oil in water (OiW), depending on the local regulation. However, due to increasing environmental concerns, many countries push for even stricter regulations (Igunnu and Chen, 2014). The 'Zero Harmful Discharge' policy, initiated at the Norwegian Continental Shelf, not only decreases the limit of the dispersed OiW concentration, but also underlines the necessity for targeting dissolved components during water treatment. Re-injection of the produced water can waive the problem of aquatic pollution, as the oily water is pumped back to an underground formation. Moreover, it can also be used as an increased oil recovery technique that sustains the pressure in the production reservoir. Nevertheless, to

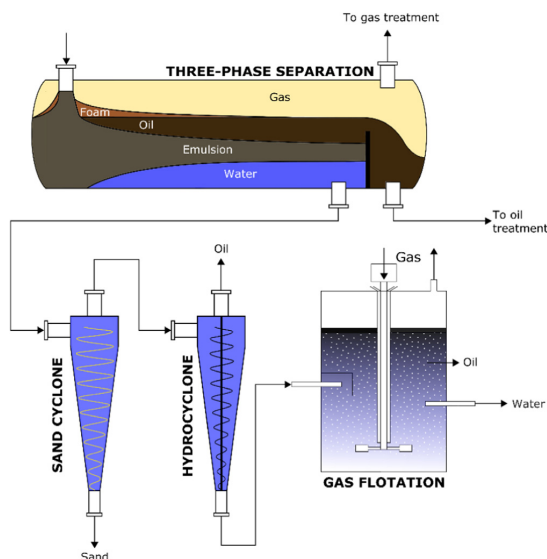


Fig. 1. Typical produced water treatment process.

avoid formation damage, the requirements for the quality of the produced water must be tailored to the reservoir characteristics and can be similar to those for the discharge (Bader, 2007).

A typical offshore produced water system is composed of a bulk gravity separator, a sand handling system, a hydrocyclone and a gas flotation unit (Fig. 1).

The water leaving the gravity separator typically contains 1000 ppm or less of crude oil. The hydrocyclone treatment reduces it further down to 100–300 ppm of OiW, while the gas flotation unit can decrease the oil concentration below the discharge limit. As the oil fields mature, the water cut increases and can reach as high as 95%. Therefore, at some point of the production, the handling of the produced water can bottleneck the entire process. For this reason, subsea treatment of the produced water is considered as a viable alternative to the topside PWT.

Subsea production and processing of crude oil and gas is one of the few options when moving into deeper and more remote waters. In the past two decades, the underwater installations around the world evolved from single satellite wells to complex systems that can perform boosting, compression and separation operations (Lim and Gruehagen, 2009). The subsea treatment of the produced water not only carries the advantage of the reduced volumes of pumped fluids and decreased pressure drop, but can also be beneficial to the separation process. Higher pressure and temperature, maintained in the subsea separation system, can enhance the density difference between the separated phases and reduce the viscosity of the fluids. As a result, the separation efficiency should be higher subsea, compared to the topside conditions (Bringedal et al., 1999).

Most of the produced water treatment processes, such as gravity separation, hydrocyclone or gas flotation, highly rely on the droplet size. As described by Stokes law, the creaming velocity in the gravity separators is directly proportional to the square of the drop diameter. In addition, larger drops are easier to encounter by gas bubbles during gas flotation. With the increase of the drop size, the PWT processes are quicker and more effective, resulting in less dispersed OiW in the discharged or reinjected water.

Coalescence is the main process controlling the droplet growth. It can be split into three steps (Chesters, 1991): (1) droplet

approach (and collision), (2) thin film drainage and (3) film rupture and fusion of two drops into one. Since the stability of emulsions is an important aspect of many industrial processes, either as a goal to reach or a problem to overcome, it has been extensively studied for many years. Several studies of the coalescence of model oil-in-water drops had been conducted (Kourio et al., 1994; Podgórska, 2007; Kamp and Kraume, 2014). Regarding the crude oil systems, the researchers have paid more attention to the coalescence of water drops in the continuous oil phase (Bhardwaj and Hartland, 1994; Frising et al., 2006; Bresciani et al., 2010; Opedal et al., 2011), leaving the crude oil-in-water systems a relatively unexplored topic (Sterling et al., 2002; Gawel et al., 2015). In addition, there are hardly any research tools that allow systematically investigating the coalescence of crude oil drops in water.

Crude oil has a very complex composition and can contain a variety of species that influence their interfacial properties, such as resins, asphaltenes (Poteau et al., 2005; Sjöblom et al., 2001), and acidic species (Havre et al., 2003). The dissolved components in the water, partitioned from the oil phase (Bertheussen et al., 2017), can also adsorb at interfaces (Eftekhardkhan et al., 2016) and affect the coalescence process. Moreover, crude oil drops may behave differently, when subjected to subsea conditions (i.e. high pressure or temperature). To the best of our knowledge, the effect of pressure on the merging of crude oil drops has not been reported in the literature.

Microfluidics proved to be a very useful tool for studying emulsion stability. Both model oil-in-water (Krebs et al., 2012; Krebs et al., 2013; Mazutis and Griffiths, 2012) and water-in-oil systems (Tan et al., 2007; Baret et al., 2009; Zagnoni and Cooper, 2009) were previously reported in the literature. In the petroleum science, however, the focus of microfluidic applications is rather shifted towards fluid analysis (Fisher et al., 2013; Alabi et al., 2014; Floquet et al., 2016) and very few papers concerning separation can be found (Nowbahar et al., 2017). While in microfluidics the effect of gravity is negligible, it still allows to systematically study the merging of drops during flow, in contrast to other techniques that study coalescence in more static conditions (Won et al., 2014).

Previously we have presented a microfluidic approach to study the coalescence of model oil-in-water systems at increased pressure (Dudek et al., 2018). The objective of the current work was to develop methodology for studying coalescence of crude oil drops under different conditions using microfluidics. The investigated parameters included the composition of the oil phase (different crude oils, diluted and neat), water phase (salinity, pH, dissolved components) and pressure.

## 2. Experimentals

### 2.1. Chemicals

The physical and chemical properties of six crude oils, produced at the Norwegian Continental Shelf, are summarized in Table 1. Additional characterization (except of crude oil F) and description of methods were reported elsewhere (Dudek et al., 2017).

The crude oils were initially diluted to 25% wt. with xylene (Mix of isomers, AnalaR, VWR, USA) to be used as the dispersed phase in the microfluidic investigations. During further tests, three crude oils (B, E, F) were used without dilution and upon addition of 200 ppm of a de-emulsifier. Unless stated otherwise, the measurements were performed with one de-emulsifier (A few experiments in the Section 3.2.1. were also conducted with another de-emulsifier). These additives will later be referred to as oil-soluble surfactants.

**Table 1**  
Physicochemical properties of crude oils.

Crude oil	API [°]	Viscosity [mPa s] @20 °C	TAN [mg KOH/g oil]	TBN [mg KOH/g oil]	SARA [% wt.]			
					Saturates	Aromatics	Resins	Asphaltenes
A	19.2	354.4	2.2	2.8	50.6	31.2	15.7	2.5
B	35.8	14.2	ND	1.0	84.0	13.4	2.3	0.3
C	23.0	74.4	2.7	1.1	64.9	26.3	8.4	0.4
D	36.3	10.2	0.2	1.1	71.5	23.1	5.1	0.3
E	37.9	8.3	0.5	0.4	74.8	23.2	1.9	0.1
F	39.7	7.5	0.1	0.6	78.5	18.9	2.5	0.1

Two types of brine were used to simulate produced water salinities at the Norwegian Continental Shelf (Water, 1992) and to investigate the effect of the divalent ions on the coalescence of the crude oil droplets. Both brines had equal ionic strength ( $I = 0.59 \text{ M}$ ). The first brine, referred to as Na-Brine, contained only sodium chloride (p.a., Merck Millipore, USA). The other, NaCa-Brine, was a mixture of NaCl and  $\text{CaCl}_2$  (p.a., Sigma-Aldrich, USA) with Ca/Na molar ratio of 1:35. The brines were adjusted to pH 4 and 10 by using solutions of diluted HCl (AnalaR, VWR, USA) and dissolved NaOH (AnalaR, VWR, USA). The natural pH of the brines, later referred to as pH 6, ranged between 5.8 and 6.6. All aqueous solutions were prepared with deionized water (Millipore Simplicity Systems, Darmstadt, Germany).

## 2.2. Dissolved components

Three kinds of components were dissolved in water and used as the continuous phase in different microfluidic experiments.

**4-Heptyl benzoic acid (4-HBA).** 100 ppm of the 4-HBA (99%, Alfa Aesar, USA) was dissolved in Na-Brine at high pH. Subsequently, the solution was adjusted to pH 10.

**Fluka acids.** The water phase with a commercial naphthenic acid mixture (Fluka, Sigma Aldrich, USA; later denoted as Fluka acids) was obtained through partitioning. Heptane (HPLC  $\geq 99\%$ , Sigma-Aldrich, USA) containing Fluka acids was poured into Schott bottles with buffered Na-Brine at pH 6 and 9, respectively. After 12 h of horizontal shaking, the phases were separated by centrifugation (30 min at 11,000 rpm). Part of the water was acidified to pH  $< 2$  with hydrochloric acid and shaken with pure

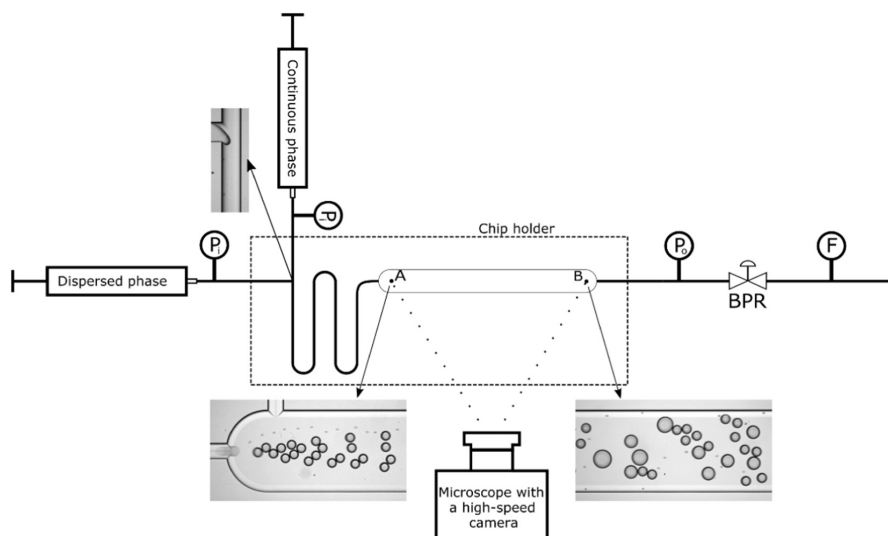
heptane to back-extract the organic content for concentration measurement. Samples were silylated with *N-tert*-Butyldimethylsilyl-*N*-methyltrifluoroacetamide (MTBSTFA) with 1% *tert*-Butyldimethylchlorosilane (Sigma-Aldrich, USA) and then analysed with GC/MS for quantification. Finally, the samples were diluted with Na-Brine to contain 100 ppm of acids and adjusted to pH 6 and 10, respectively.

**Dissolved components from crude oils.** Each of the crude oils were mixed with Na-Brine at pH 4, 6 and 10 in order to saturate the water phase with water-soluble oil components. Approximately 100 ml of brine and crude oil were poured into Schott bottles and put on a vertical shaker (200 rpm) for 48 h. Subsequently, the water phase was extracted and centrifuged to remove any dispersed oil. The pH was measured and afterwards readjusted to the original level. Some water phase was collected, acidified to pH  $< 2$  with sulphuric acid, and analysed for the total organic carbon content (TOC-L<sub>CPH</sub> Analyser, Shimadzu, Japan). The measurements were performed at GIG Research Institute in Katowice, Poland.

## 2.3. Microfluidic chips and setup

The design of the chips and the microfluidic setup is illustrated in Fig. 2.

Custom-designed glass microfluidic chips were delivered by Micronit Microtechnologies B.V. (The Netherlands). The inlet channels had a width of  $100 \mu\text{m}$  and led to a T-junction, where the droplets were generated. The drops then passed a meandering channel and entered a coalescence chamber with the width of  $500 \mu\text{m}$  and length of ca. 33 mm, where they could get in contact



**Fig. 2.** Illustration of the microfluidic setup and chips.



and possibly undergo coalescence. The wider channel led to the outlet of the chip. All channels had a uniform depth of 45  $\mu\text{m}$ . During the experiments, the chip was placed in a chip holder (Fluidic Connect PRO, Micronit Microtechnologies B.V., The Netherlands) and connected to the rest of the flow setup with FFKM ferrules and PEEK tubing (inner diameter 250  $\mu\text{m}$ , Sigma-Aldrich, USA). The high-pressure measurements were performed with another chip holder (Fluidic Connect 4515, Micronit Microtechnologies B.V., The Netherlands). After the experiment, the chips were cleaned through sonication in three different solvents: toluene/acetone mixture (3:1 v/v), isopropanol and deionized water. Each cleaning step lasted 15 min. Finally, the chips were dried with compressed air and baked in an ashing furnace for six hours at 475  $^{\circ}\text{C}$ . Shortly before the experiments, the chips were treated in low-pressure oxygen plasma chamber (Zepto, Diener electronic GmbH, Germany) for 10 min.

The liquids were pumped with syringe pumps (neMESYS mid-pressure module V3, Cetoni GmbH, Germany). The pressure level in the system was controlled by a backpressure regulator (BPR in Fig. 2, JR-BPR2, VICI AG International, Switzerland) and monitored with pressure sensor modules (Qmix P, Cetoni GmbH, Germany) at the inlet and outlet of the chip ( $P_i$  and  $P_o$  in Fig. 2, respectively). The flow was measured with a flowmeter (F in Fig. 2, mini CORI-FLOW, Elveflow, France). The droplets were observed with a high-speed camera (AX100, Photron, Japan), connected to an inverted microscope (Ti-U Eclipse, Nikon, Japan) with an external LED light source (HDF7010, Hayashi, Japan) at a constant framerate of 8500 frames per second.

#### 2.4. Microfluidic experiment, data acquisition and image analysis

The experiments were conducted similar to a previous report (Dudek et al., 2018). In short, the oil and water flow rates were set to 10 and 160  $\mu\text{l}/\text{min}$ , respectively. In these conditions the droplets had a diameter of approx. 50  $\mu\text{m}$ . Due to the smaller channels at the inlet of the chip, the readings from the pressure sensor located there indicated approx. 2 bar higher pressure, compared to the outlet of the chip. This pressure drop was present in all tested pressure levels. The Reynolds number inside the coalescence channel ( $Re = \frac{\rho v l}{\eta}$ , where  $\rho$  and  $\eta$  are the density and viscosity of the continuous phase,  $v$  is the velocity and  $l$  is the width of the channel) was equal to 50. The Weber number ( $We = \frac{\rho v^2 l}{\gamma}$ , where  $\gamma$  is the interfacial tension between oil and water), which compares the inertial forces to interfacial tension, in our case was typically below 1. Both Reynolds and Weber numbers are typically low for microfluidic applications (Anna, 2016). The Capillary number ( $Ca = \frac{\rho v l}{\gamma}$ ), describing the ratio of viscous stresses to stresses due to interfacial tension, was in the range of  $10^{-2}$ . Even though both the Reynolds and Weber number were much lower than in a process taking place in a gravity separator, the velocity of the droplets in our system (ca. 0.1 m/s) was comparable to the water flow during the separation process (Hansen and Rørtveit, 2006).

Two sets of images were taken for each experiment – at the inlet and the outlet of the microfluidic chip (points A and B in Fig. 2, respectively). The series from the inlet was used to retrieve the initial size and number of the droplets, and additionally used to verify the accuracy of the recordings from the outlet of the chip. Next, a series of 7000 frames was recorded at the end of the coalescence chamber to assess the extent of coalescence. Both image sequences were processed with the ImageJ software. The frames were first converted into a binary mask and then the areas and the centre of mass coordinates of droplets were retrieved with the Analyse Particle feature. The data was then copied to a Microsoft Excel spreadsheet. It was found that the droplet area increased

proportionally with the number of coalescence events. For this reason, the droplets could be sorted into several size classes. It is worth pointing out that the same droplets were detected several times in the consecutive frames. Therefore, the actual number of droplets in each size class ( $N_i$ ), used for further analysis, was calculated with the average droplet velocity, the width of the detection box and the mean droplet diameter in each size class. The number of initially created droplets ( $N_{in}$ ) was given by  $N_{in} = \sum_{i=1}^n n_i * \frac{A_i}{A_{in}}$ , where  $n_i$  was the number of class  $i$  drops,  $A_i$  the area of class  $i$  droplets at the outlet of the channel and  $A_{in}$  the area of the initially formed droplets. On average, each dataset consisted of 1500 droplets of the original size. The coalescence frequency was the main parameter for the comparison between different conditions. It was calculated by  $f = \frac{(N_{in} - 1)}{t_{res}}$ , where  $t_{res}$  is the residence time of droplets in the channel (channel length divided by the average drop velocity). All reported values are an average of three parallels with standard deviation.

#### 2.5. Interfacial tension measurements

The interfacial tension (IFT) measurements were conducted using a pendant drop tensiometer (PAT-1M, Sinterface Technologies, Germany). Images of a crude oil drop, immersed in a brine solution were recorded over time. The measurements lasted 100 s. The interfacial tensions were calculated by fitting the drop profiles to the Young-Laplace equation. All measurements were performed at room temperature (22  $^{\circ}\text{C}$ ).

### 3. Results and discussion

#### 3.1. Diluted crude oils

Initially, we tried to use crude oils as is, however they partially wetted and adsorbed to the glass surface, which prevented droplet generation. Diluting crude oils with an aromatic solvent (xylene) mitigated that issue, allowing us to study the effect of the crude oil chemistry and water composition. The coalescence frequencies of the diluted crude oils are illustrated in Fig. 3.

In general, the coalescence between the light crude oil drops (B, D, E, F) was more extensive, compared to the heavier ones (A and C). Notably, the viscosity of the oil phases after dilution did not vary much. The final droplet size also depended on the water phase. The highest coalescence frequency was usually observed at the lowest pH and it declined with increasing pH of the water. At low pH, the coalescence between heavier crude oils was difficult to measure, most likely due to the higher TBN values and the fact that in lower pH the glass surfaces often become wetted by crude oils (Brown and Neustadter, 1980) (Fig. S1 in SI). In addition, it was impossible to measure the coalescence frequency of crude oil C at pH 10 (Na-Brine) due to the formation very small droplets (Fig. S2 in SI), most likely because of high TAN. When calcium was added to the system, the most systematic trend was noticed at pH 10, where its presence boosted the coalescence in almost all cases, compared to the brine without divalent ions. At the other pHs, we did not see any systematic changes in the coalescence frequencies.

Crude oils contain many surface-active components that can be more or less interfacially active in specific conditions. Their interfacial tension (IFT) varies with the pH of the water phase (Arla et al., 2007). This is attributed to the presence of protonated basic species at low pH or dissociated acidic components at higher pH. In general, basic components do not lower the IFT as much as the acids, which has been confirmed both for model (Bertheussen et al., 2017) and crude oil (Nenningsland et al., 2010) systems. This effect was reflected in the present coalescence studies, where the droplets coalesced more readily in pH 4 or 6. When the pH was increased to 10,

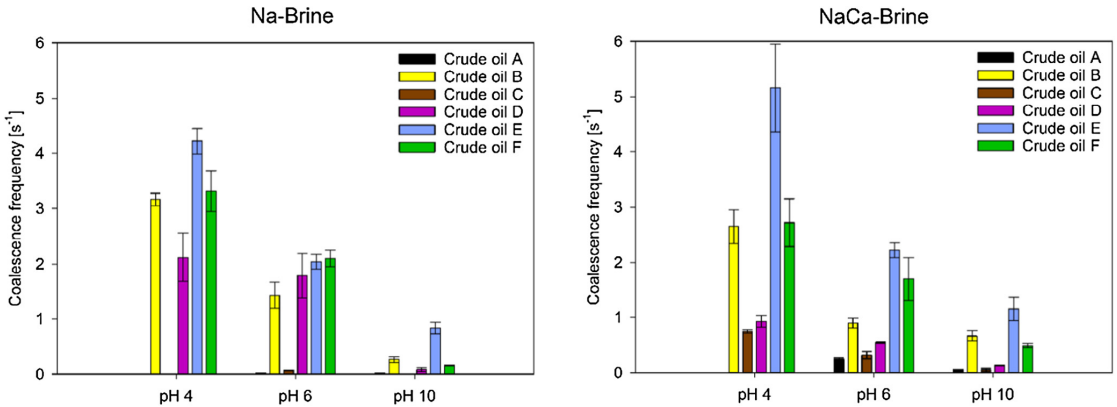


Fig. 3. Coalescence frequencies of diluted crude oils in Na- and NaCa-Brine at three pH levels.

the oil-water interface was controlled by the acids and prevented the droplets from merging with each other through increased interfacial concentration of surface-active components. The acidic species in crude oils are often called naphthenic acids. This group includes a wide range of short- and long-chained carboxylic acids, often with aromatic moieties. They can contribute to a variety of undesirable phenomena during the crude oil production, such as emulsion formation, precipitation or corrosion of the pipelines and process units (Havre et al., 2003). Due to their amphiphilic nature, they can adsorb at the oil-water interface (Arla et al., 2007) or even, in the case of low molecular weight compounds, partition to the water phase (Hutin et al., 2014). Their interfacial activity in neutral or higher pH is probably the main reason behind the increased stability of droplets. The increase of pH deprotonates more acidic species, which leads to increased interfacial concentration and provides additional stability against coalescence. Moreover, this mechanism is further supported by the results obtained with NaCa-Brine at pH 10. Depending on the molecular structure, naphthenic acids in the presence of an electrolyte in water can form soaps or deposits (Hurtevent et al., 2006). These complexes are generally more stable with multivalent ions. High-molecular tetraprotic acids, so called ARN acids, are more likely to form scale (Sjöblom et al., 2014), whereas low molecular monoacids contribute to forming stable emulsions (Mapolelo et al., 2011). In the case of water-in-crude oil emulsions, the latter naph-

thenates can agglomerate at the interface and lead to problems in flow assurance or separation process (Havre, 2004). In the case of oil-in-water emulsions, however, it is likely that the addition of calcium removed acids from the interface. These acid-calcium complexes are less interfacially active and more lipophilic in character, which facilitates their diffusion from the interface to the oil phase (Tichelkamp et al., 2015), reducing their interfacial concentration and most likely leading to the increased coalescence.

Fig. 4 depicts the coalescence frequencies plotted against TAN and TBN values.

The crude oils used in this study had the total base numbers ranging from 0.4 to 2.8. At pH 4, the coalescence frequency was found to be inversely proportional to the TBN of the crude oils. This effect was similar for both brines. The total base number is traditionally considered as an indicator for the basic species in crude oils. At lower pH, these components become protonated and affect the interfacial properties of the crude oil drops (Nenningsland et al., 2010). This effect can depend both on the type of the basic components and their concentration, as observed in our case.

The coalescence behaviour at higher pH was better explained with the total acid number values, as the interfacial properties of crude oil drops are governed by the acidic species. At pH 6 and 10 in Na-Brine, the crude oils could be divided into two groups (plot for pH 10 in Fig. S3 in SI). Crude oils with lower TAN value (<0.5)

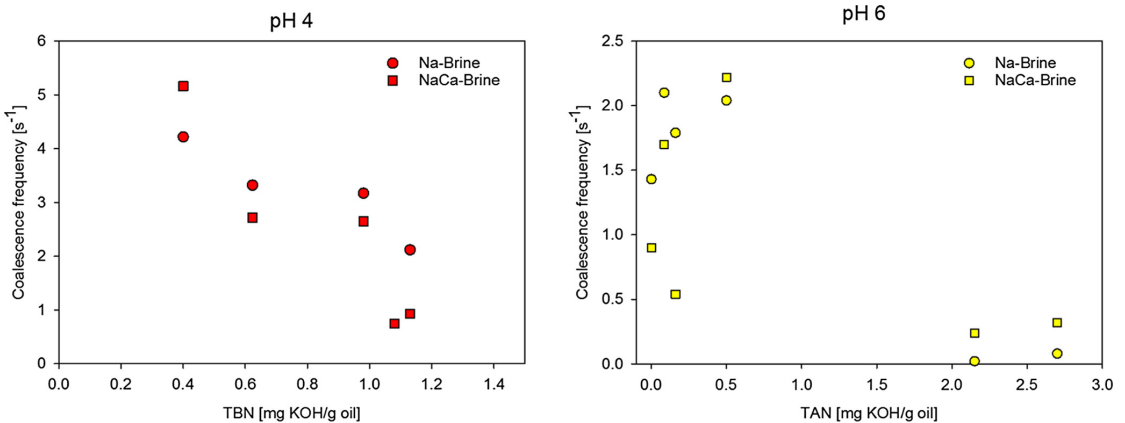


Fig. 4. Coalescence frequencies of diluted crude oil plotted against TBN (left) and TAN (right) values of crude oils. The order of crude oils from left to right: E, F, B, C, D (TBN) and B, F, D, E, A, C (TAN).

coalesced quite extensively, while hardly any coalescence was observed for the crude oils with high TAN values (>2). This effect can be probably related to the concentration of the acidic species in the crude oils. At pH 6 only the crude oils with TAN value equal to or higher than 0.5 (A, C, E) experienced an increase of coalescence when calcium was present in the water phase. Firstly, it was entirely possible that the interfacial concentration of the naphthenic acids in the less acidic oils might have been too low to observe the effect of calcium. Secondly, the type of acidic components and the extent of dissociation at the oil-water interface could have also played a role (Dyer et al., 2003; Brandal and Sjöblom, 2005). At pH 10, significantly more acids were dissociated, which lead to an increase of coalescence upon addition of calcium, based on the mechanism outlined above. At low pH, the surface charge of oil drops was probably close to neutral or even slightly positive (Brown and Neustadter, 1980; Parra-Barraza et al., 2003). The addition of calcium ions might have increased the positive charge at the surface through induced dipole-ion interactions between the non-dissociated acidic chain and the cation (Wolstenholme and Schulman, 1950), resulting in increased repulsive forces and lower coalescence in most cases. However, it should be stated that each crude oil has a unique composition that will affect the charge of droplets at given pH. If the acids in the oil have a low  $pK_a$ , then even at low pH the coalescence might increase, as was the case for crude oil E.

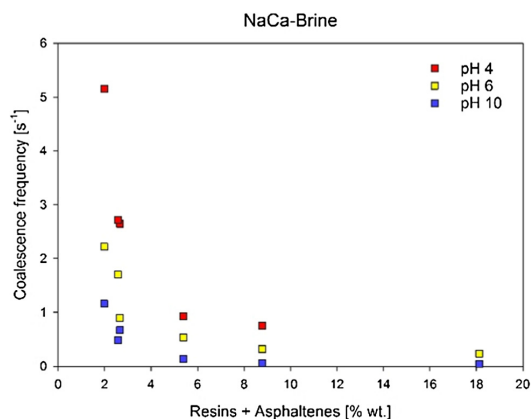


Fig. 5. Coalescence frequencies of diluted crude oils plotted against the sum of resins and asphaltenes of respective crude oils.

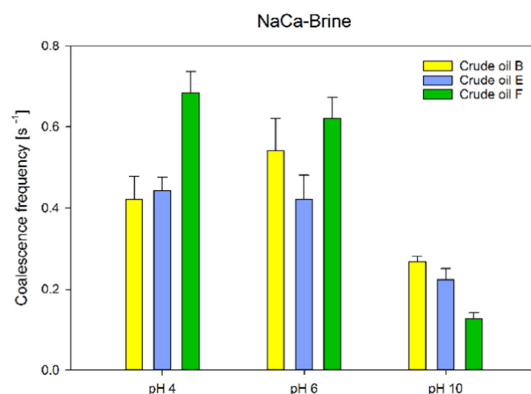
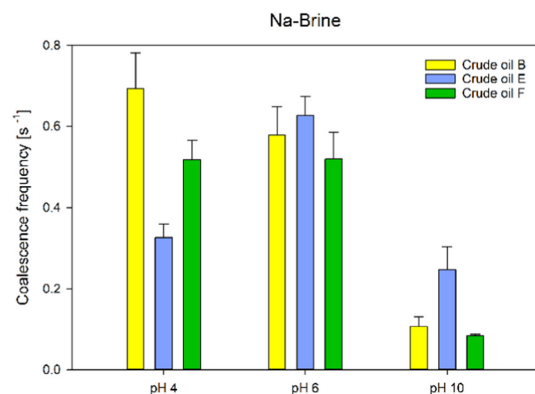


Fig. 6. Coalescence frequencies for three crude oils in Na- and NaCa-Brines at different pH levels.

A trend was also observed when the coalescence frequencies were plotted against the sum of resin and asphaltene weight fractions of the crude oils (Fig. 5).

The coalescence frequencies decayed exponentially with the increasing total resin and asphaltene weight fractions of the crude oils. The coalescence of crude oils with the lowest concentration of these fractions was quite extensive, whereas very little merging occurred at the highest amounts. These trends were similar regardless of the pH or ionic composition (Fig. S4 in SI).

The majority of the interfacially active molecules can be found in the resin and asphaltene fractions, which explains their significance for the coalescence frequency. The presence of these species can affect the coalescence between oil drops in several ways. First, the dissociated, charged groups can create electrostatic repulsion, analogous to the effect of ionic surfactants. However, in our system this type of repulsion was significantly decreased due to high electrolyte concentrations. Secondly, the approach and collision between drops may cause gradients in the interfacial concentrations. This will cause a flux of surface-active molecules in the opposite direction of the film drainage process (Marangoni effect), which will impede drainage. Notably, the crude oils were diluted with an aromatic solvent, which effectively eliminated any asphaltene solubility issues. Nevertheless, asphaltenes in a good solvent could still be present as nanoaggregates (Mullins, 2010) and impact the formation of viscoelastic films, and subsequently influence the coalescence between oil drops. In general, the emulsion stability is enhanced with the increase of the elastic properties of the interface (Georgieva et al., 2009). Solutions of asphaltenes in aromatic solvents typically exhibit a maximum of elasticity at a certain concentration (Angle and Hua, 2012; Nenningsland et al., 2014). In our case, the decreasing coalescence frequency with increasing weight fraction of resins and asphaltenes could also be seen for the increasing percentage of asphaltenes alone (Table 1).

### 3.2. Crude oils

Method development revealed that the addition of an oil-soluble surfactant facilitated the droplet generation process for some of the crude oils without the need of dilution. Therefore, three light crude oils (B, E, F) were used to investigate the effect of the water composition on the coalescence of *non-diluted* crude oil drops.

#### 3.2.1. Water phase effect

Fig. 6 depicts the coalescence frequencies for the non-diluted crude oils in different brines.

Notably, all coalescence frequencies were significantly lower than for the diluted crude oils. In both brines, the highest coalescence frequencies were observed at pH 4 or 6, and the lower values at pH 10. When considering the effect of divalent ions at pH 10, the coalescence was either higher (B, F) or did not change (E) upon the addition of calcium. The effect of calcium at other pH varied with the crude oil type.

The complex composition of crude oils will definitely have an impact on the coalescence process during the produced water treatment. Like in the Section 3.1, we attempted to connect the crude oil physical and chemical properties to the observed coalescence behaviour. In this case, however, the addition of the oil-soluble surfactant affected the interfacial behaviour of the crude oil droplets, rendering any analysis based on composition unclear. In general, crude oils react differently to various types and concentrations of oil-soluble surfactants. This was confirmed by the experiments performed with another oil-soluble surfactant (Fig. S5 in SI). Nevertheless, the trends observed upon changing the water composition remained quite similar to the results obtained with the diluted crude oils.

### 3.2.2. Dissolved components – model systems

Certain components of crude oils are water-soluble. Their partitioning to the water phase can occur in the geological formation, where the two phases spend millions of years in contact, and additionally during the production process, where pressure drops and turbulent flow create further opportunities for mixing and mass transfer. Especially the water pH will affect the partitioning in crude oil systems (Bertheussen et al., 2018). The concentration of the dissolved components is highly field-dependent, but it can reach several hundreds of ppm in the discharged PW (Hansen and Davies, 1994). These components can be toxic and pollute the marine environment (Rogers et al., 2002). Furthermore, they can affect the oil-water separation process. Our group has previously demonstrated the effect of the dissolved components on the air-water interface (Eftekhardakhah et al., 2016; Eftekhardakhah et al., 2013; Eftekhardakhah and Øye, 2013) and the flotation performance (Eftekhardakhah et al., 2015). In this section we discuss their influence on the coalescence between crude oil droplets.

The results of the coalescence frequency in Na-Brine with and without the partitioned naphthenic acids at pH 6 is shown in Fig. 7.

Each of the crude oils reacted uniquely to the presence of the dissolved components in the water phase. An increase of coalescence was observed for crude oil B, while the opposite effect was noticed for crude oil E. The dissolved components had little effect on the coalescence with crude oil F. Similar results were obtained

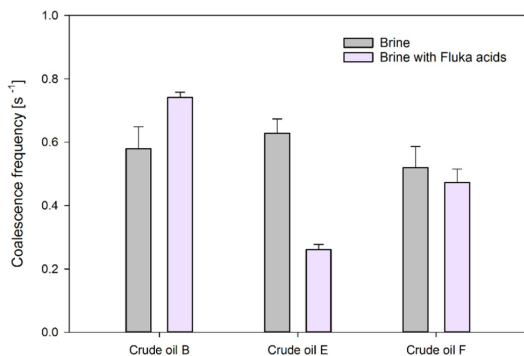


Fig. 7. Coalescence frequency of Na-Brine at pH 6 with and without partitioned Fluka naphthenic acids.

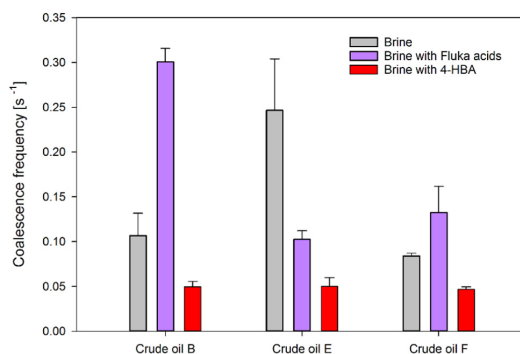


Fig. 8. Coalescence frequency of Na-Brine at pH 10 with Fluka partitioned acids, dissolved 4-HBA and without any dissolved components.

for the Fluka acids partitioned at higher pH, presented in Fig. 8, together with the results for the 4-heptylbenzoic acid. Also in this case the effect of the dissolved Fluka acids was crude oil-dependent. The acids either promoted coalescence (B, slight increase in F) or reduced it (E).

Noteworthy, all the oils reacted in a very similar way to the presence of 4-HBA in the continuous phase. The coalescence frequency was reduced to almost identical values of  $0.05 \text{ s}^{-1}$ , meaning approximately 20 coalescence events for more than 1500 droplets during the recording time.

One possible explanation for the oil-specific response to the presence of the dissolved components is the oil composition, or more precisely the nature of the surface-active components in the crude oils. In the diluted system, crude oil B had lower coalescence frequencies than the other oils. It also had lower resin to asphaltene ratio (R/A) and less aromatic components. Resins are the most polar fraction that is soluble in aliphatic solvents. Although surface-active, they cannot stabilize emulsions by themselves (Spiecker et al., 2003). They are, however, crucial in the emulsion stabilization mechanisms provided by the asphaltenes. Resins were found to increase the stability of asphaltenes in crude oils through solvation (Murgich and Strausz, 2001), and their weight ratio to asphaltene in crude oils correlates inversely with the water-in-oil emulsion stability (Spiecker et al., 2003; Schorling et al., 1999). Additionally, the R/A ratio has an effect on the film rigidity, which also corresponds to the stability of emulsions (Strassner, 1968). Furthermore, the low fraction of aromatics can contribute to destabilization of asphaltenes. Crude oil B has the lowest R/A ratio (ca. 8) and lowest aromatic weight fraction. This might have affected the stability of asphaltenes and increased the film rigidity in the system with standard brine. Upon the addition of dissolved acids, the less stable asphaltenes might have been replaced by the smaller acidic species, diffusing from the water phase, at the interface. Short-chained acids that partitioned at pH 6 might not retard the coalescence between drops to the same extent as the polar, high-molecular weight components from crude oil B. In addition, crude oil B has also slightly higher viscosity, which reduced the diffusion rate from the oil phase to the interface. In the case of crude oil E and F, the smaller amount of more stable asphaltenes (R/A values of 19 and 25, respectively) should have less effect on the coalescence process. While there was hardly any difference in the coalescence behaviour for crude oil F, the crude oil E experienced a significant decrease of coalescence in the presence of the dissolved acids. Taking the TOC values from Table 2 into consideration, it could be noticed that crude oil F had almost twice as much components that partitioned to the water phase as crude oil E. Moreover, these were predominantly

**Table 2**

Interfacial tensions of crude oils against different water phases. <sup>†</sup>value reported after 50 s; <sup>‡</sup>value reported after 10 s. The shorter measurements were due to instability of the generated drop.

Brine type Oil phase ↓      pH →		Interfacial tension [mN/m]								
		Na-Brine			NaCa-Brine			Dissolved components		
		4	6	10	4	6	10	6 (Fluka)	10 (Fluka)	10 (4-HBA)
Crude oil B		14.9	14.1	6.2 <sup>‡</sup>	14.6	13.8	8.7	13.5	4.9	3.8 <sup>†</sup>
Crude oil E		14.9	12.9	9.1	12.8	13.1	10.9	13.5	7.9	4.58 <sup>†</sup>
Crude oil F		6.02 <sup>†</sup>	5.62 <sup>†</sup>	5.88 <sup>†</sup>	5.72 <sup>†</sup>	5.82 <sup>†</sup>	5.62 <sup>†</sup>	5.62 <sup>†</sup>	4.78 <sup>†</sup>	–

short-chained acids, as the decrease of pH from the initial pH 6 value was much more substantial for that crude oil. Therefore, a competitive mass transfer probably took place between the short-chained acids coming from bulk oil and the acidic species diffusing from the water phase. Even though crude oil E has the highest TAN, it probably contains larger acidic molecules that will diffuse more slowly and will be replaced at the interface by the more mobile short-chained Fluka acids. In addition, it could be possible that some of the acidic species in the water phase partitioned into the oil droplet. Groothuis and Zuiderweg (Groothuis and Zuiderweg, 1960) stated that the decreased coalescence rate was expected in systems where mass transfer occurred from the continuous to the dispersed phase. These observations were later confirmed by other groups, who reported that the direction of mass transfer affected the film drainage time (Chevaillier et al., 2006). This phenomenon is often explained with the Marangoni effect. If the mass transfer occurs from the dispersed to the continuous phase, the concentration of the transferred solute in the thin film region is increased, which will often decrease the local interfacial tension. The interfacial tension gradient will facilitate movement of the fluid outside of the film region, thus promoting film drainage (Kopriwa et al., 2012). Conversely, mass transfer from the continuous to the dispersed phase will retard the drainage process by pushing the liquid into the thin film region. In our case, the mass transfer from the water phase to the crude oil E droplet might have inhibited coalescence, compared to the standard brine. Crude oil F contained more water-soluble acidic components, which possibly limited the mass transfer to the oil phase at pH 6, and did not affect the coalescence in the same way.

Interestingly, the dissolved Fluka acids at pH 6 did not influence the interfacial tension of crude oils Table 2.

The oil-soluble surfactant significantly changed the interfacial properties of the oils. The values without the surfactant ranged from 12 to 22 mN/m (for precise values, please refer to our previous report (Dudek et al., 2017)). In some cases, the drop could not be held for longer than 50 or even 10 s. Nevertheless, some trends can be observed. At low and neutral pH, the interfacial tension was almost identical, even when using the brine with Fluka acids. Crude oil F had similar values, regardless of the composition of the water phase. For the two other oils, the IFT at pH 10 was lower. However, it increased upon the addition of calcium, which agrees with the previously proposed mechanisms for the calcium – naphthenic acids interactions. The values of the interfacial tension at pH 10 were somewhat lower when Fluka acids were present, whereas the detection limit (ca. 5 mN/m) of the instrument was reached

within 10 s after generating the droplet for the brine with 4-HBA. The distributions of Fluka acids are depicted in Figs. S6 and S7 in SI.

In all cases, Fluka acids at pH 6 had no effect on the interfacial tension and in the same time affected the coalescence frequency in different ways. This might indicate that their limited surface-activity could have played a role in either increasing the coalescence frequency by replacing some of the high-molecular weight molecules in the case of crude oil B or decreasing it through diffusion from the continuous phase to the oil phase in the case of crude oil E. Finally, all the crude oils experienced a universal drop of coalescence frequency when 4-HBA was in the water phase. At this high pH, 4-heptylbenzoic acid has very high affinity to the oil-water interface (Spildo and Høiland, 1999), significantly reduces the IFT and stabilizes the droplets against coalescence. The 4-HBA completely filled the oil-water interface and ‘neutralized’ the indigenous surfactants. In contrast to the polydisperse species in the Fluka acids solutions, the 4-heptylbenzoic acid is a single molecule, that packed more efficiently at the interface.

### 3.2.3. Dissolved components – water-soluble crude oil species

Table 3 shows the total organic carbon and pH (before readjustment) after 48 h of contact between the crude oil and water.

The amount of the organic content that partitioned from the oil to the water phase depended on the oil, but also differed slightly with the pH. In some cases, the change of pH after mixing was quite significant, which indicated the nature of the partitioned components. In all cases, the lowest amount of TOC was obtained for the neutral pH, while the most marked pH changes were observed at the highest pH. The water phase from crude oil B contained the smallest amount of dissolved organics and experienced relatively small changes of pH, indicating high molecular weights of both acidic and basic species. Similar observations can be made for crude oil E, with a small exception at pH 4, suggesting the presence of smaller basic molecules, which is supported by the significant decrease of coalescence at that pH for that oil. Brines after mixing with crude oil F contained twice the amount of the detected organic carbon compared to other oils, and experienced significant decreases of pH at pH 6 and 10. This implied significant amount of short-chained acids.

The coalescence frequencies in the water phase containing dissolved crude oil components are illustrated in Fig. 9.

Also here, the values were oil-specific. The presence of any dissolved components generally resulted in increased coalescence for crude oil B. The opposite effect was observed for crude oil E, while crude oil F experienced only minor changes in coalescence

**Table 3**

TOC and pH values of water after contact with crude oils.

Initial pH	Crude oil B		Crude oil E		Crude oil F	
	TOC [ppm]	pH	TOC [ppm]	pH	TOC [ppm]	pH
pH 4	21	4.33	31	4.93	52	4.07
pH 6	17	5.90	30	6.03	49	4.61
pH 10	21	8.91	33	8.67	52	7.21

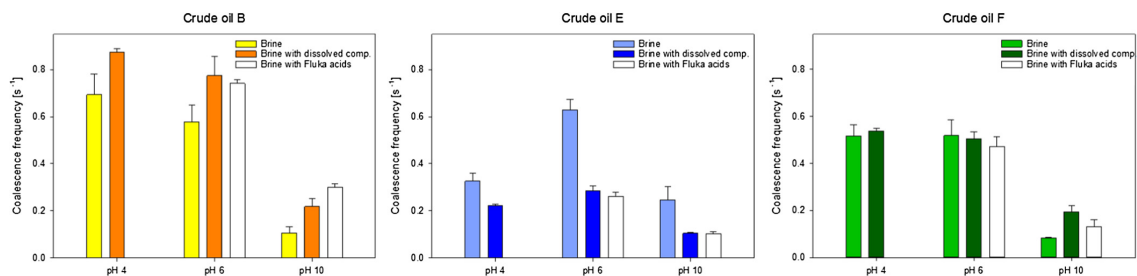


Fig. 9. Coalescence frequency of different crude oils in Na-Brines with dissolved crude oil components and Fluka acids.

behaviour, limited to the highest pH. Remarkably, the results for the brines with dissolved crude oil components resembled the values acquired with the water phase containing Fluka acids (white bars in Fig. 9).

Water-soluble crude oil species are not only of growing environmental concern, but can also affect some aspects of the PW treatment processes. There was no correlation between the crude oil properties and the amount of dissolved organics in the water phase. Moreover, the concentration of the dissolved components did not affect the coalescence frequency in any systematic way. The biggest effects were observed for crude oils B and E, which water phases contained significantly less TOC compared to crude oil F. The results were very similar to the ones presented in the Section 3.2.2., so the previously discussed effect of the dissolved components on the coalescence process also applies here. Since our study was performed with only three crude oils, it is difficult to unambiguously state the impact of the dissolved components on the coalescence process. However, the results demonstrate that their presence in the produced water cannot be neglected. It should also be noted that the striking similarity of coalescence between the water-soluble crude oil components and Fluka acids suggests that the majority of surface-active components affecting coalescence has acidic nature.

### 3.2.4. Pressure

Two oils and brines were chosen for experiments at elevated pressure conditions. The results are depicted in Fig. 10.

The results show that in the tested pressure range, the extent of coalescence between oil droplets was relatively similar, independent of the pH of the brine and the crude oil (data for crude oil F shown in Fig. S8 in SI). The data analysis proved that the

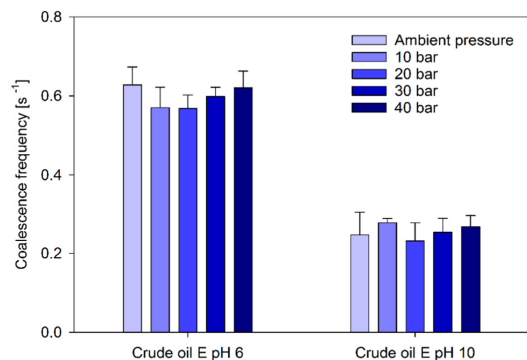


Fig. 10. Coalescence frequencies for crude oil E in Na-Brines pH 6 and pH 10 at elevated pressures.

differences between the values were statistically insignificant ( $t$ -Student,  $\alpha = 0.05$ ).

During the course of experiments, we used 'dead' crude oils, meaning that the samples were depressurized and stored at ambient conditions. As a result, the samples were missing the lightest components ( $C_1$ – $C_4$ ) that usually flash off during depressurization. This means that, in this range, pressure had minor effect on the physical properties of the crude oils (Al-Besharah et al., 1989; Karnanda et al., 2013). Increased system pressure would lead to increased solubility of the shortest hydrocarbons in the crude oil. This would have several effects on the sample, such as decrease of density or viscosity, and change in the interfacial tension. Higher pressure and change in the crude oil composition can also affect other phenomena associated with crude oil, for instance wax crystallization (Vieira et al., 2010) and asphaltene behaviour (Golkari and Riazzi, 2016), which can cause further variations in the oil-water interface and alter the coalescence between drops. Nevertheless, our results showed that the drop fusion remained unaffected by the increased system pressure, showing that the pressure factor will only contribute to the changes in the chemistry of crude oil drops and not influence the mechanisms of the coalescence process.

## 4. Conclusions

We have presented microfluidic methods for investigating coalescence between crude oil drops in water phase. The experiments were first performed with diluted crude oils, followed by a study conducted on crude oil drops with the addition of an oil-soluble surfactant. It was demonstrated that both the composition of the oil and water phases influenced the extent of coalescence in our systems. We have also shown that the dissolved components in the water phase can play a crucial role in the merging process and that this effect is likely to be oil-specific. Furthermore, amongst the various water-soluble components from crude oils, the effect of the acids is dominant in the interfacial behaviour of crude oil drops in water. The pressure did not affect coalescence in any way, which was attributed to the lack of light components ( $C_1$ – $C_4$ ) in the crude oils.

We believe that the microfluidic coalescence tool in the present paper will help understand the role of crude oil chemistry in the produced water treatment, and become a useful method for probing the stability of crude oil drops in water. With this paper we aimed to present the applicability of microfluidics to the produced water field and its certain advantages over the other available methodologies. With the knowledge on how different parameters affect coalescence of oil drops, the treatment process can be adjusted to promote droplet growth, leading to more efficient separation. Other aspects, for example the presence and concentration of the production chemicals, will be the scope of our future work.



## Acknowledgments

This work was carried out as a part of SUBPRO, a Research-based Innovation Centre within Subsea Production and Processing. The authors gratefully acknowledge the financial support from SUBPRO, which is financed by the Research Council of Norway, major industry partners and NTNU. We additionally thank Kelly Muijlwijk, Karin Schroën and Maurice Strubel for their assistance and advice during the method development process.

## Appendix A. Supplementary material

Supplementary data associated with this article can be found, in the online version, at <https://doi.org/10.1016/j.ces.2018.07.006>.

## References

- Alabi, O.O., Bowden, S.A., Parnell, J., 2014. Simultaneous and rapid asphaltene and TAN determination for heavy petroleum using an H-cell. *Anal. Methods* 6 (11), 3651–3660.
- Al-Besharah, J.M., Akashah, S.A., Mumford, C.J., 1989. The effect of temperature and pressure on the viscosities of crude oils and their mixtures. *Ind. Eng. Chem. Res.* 28 (2), 213–221.
- Angle, C.W., Hua, Y., 2012. Dilational interfacial rheology for increasingly deasphalted bitumens and  $\eta$ -C5 asphaltenes in toluene/NaHCO<sub>3</sub> solution. *Energy Fuels* 26 (10), 6228–6239.
- Anna, S.L., 2016. Droplets and bubbles in microfluidic devices. *Annu. Rev. Fluid Mech.* 48 (1), 285–309.
- Arla, D., Sinquin, A., Palermo, T., Hurtevent, C., Graciaa, A., Dicharry, C., 2007. Influence of pH and water content on the type and stability of acidic crude oil emulsions. *Energy Fuels* 21 (3), 1337–1342.
- Bader, M.S.H., 2007. Seawater versus produced water in oil-fields water injection operations. *Desalination* 208 (1), 159–168.
- Baret, J.-C., Kleinschmidt, F., El Harrak, A., Griffiths, A.D., 2009. Kinetic aspects of emulsion stabilization by surfactants: a microfluidic analysis. *Langmuir* 25 (11), 6088–6093.
- Bertheussen, A., Simon, S., Sjöblom, J., 2017. Equilibrium partitioning of naphthenic acids and bases and their consequences on interfacial properties. *Colloids Surf. Physicochem. Eng. Aspects* 529 (Suppl. C), 45–56.
- Bertheussen, A., Simon, S.C., Sjöblom, J., 2018. Equilibrium partitioning of naphthenic acid mixture part 1: commercial naphthenic acid mixture. *Energy Fuels*.
- Bhardwaj, A., Hartland, S., 1994. Kinetics of coalescence of water droplets in water-in-crude oil emulsions. *J. Dispersion Sci. Technol.* 15 (2), 133–146.
- Brandal, Ø., Sjöblom, J., 2005. Interfacial behavior of naphthenic acids and multivalent cations in systems with oil and water. II: formation and stability of metal naphthenate films at oil-water interfaces. *J. Dispersion Sci. Technol.* 26 (1), 53–58.
- Bresciani, A.E., Alves, R.M.B., Nascimento, C.A.O., 2010. Coalescence of water droplets in crude oil emulsions: analytical solution. *Chem. Eng. Technol.* 33 (2), 237–243.
- Bringedal, B., Ingebretsen, T., Haugen, K., 1999. Subsea separation and reinjection of produced water. In *Offshore Technology Conference, Offshore Technology Conference: Houston, Texas*.
- Brown, C.E., Neustadter, E.L., 1980. The wettability of oil/water/silica systems with reference to oil recovery.
- Chesters, A.K., 1991. The modelling of coalescence processes in fluid-liquid dispersions: a review of current understanding. *Chem. Eng. Res. Des.* 69 (A4), 259–270.
- Chevallier, J.P., Klaseboer, E., Masbernat, O., Gourdon, C., 2006. Effect of mass transfer on the film drainage between colliding drops. *J. Colloid Interface Sci.* 299 (1), 472–485.
- Dudek, M., Kancir, E., Øye, G., 2017. Influence of the crude oil and water compositions on the quality of synthetic produced water. *Energy Fuels* 31 (4), 3708–3716.
- Dudek, M., Muijlwijk, K., Schroën, C.G.P.H., Øye, G., 2018. The effect of dissolved gas on coalescence of oil drops studied with microfluidics. *J. Colloid Interface Sci.* 528, 166–173.
- Dyer, S.J., Graham, G.M., Arnott, C., 2003. Naphthenate scale formation - examination of molecular controls in idealised systems. In *International Symposium on Oilfield Scale*, Society of Petroleum Engineers, Aberdeen, United Kingdom.
- Eftekhardakhah, M., Øye, G., 2013. Dynamic adsorption of organic compounds dissolved in synthetic produced water at air bubbles: the influence of the ionic composition of aqueous solutions. *Energy Fuels* 27 (9), 5128–5134.
- Eftekhardakhah, M., Reynders, P., Øye, G., 2013. Dynamic adsorption of water soluble crude oil components at air bubbles. *Chem. Eng. Sci.* 101, 359–365.
- Eftekhardakhah, M., Aanesen, S.V., Rabe, K., Øye, G., 2015. Oil removal from produced water during laboratory- and pilot-scale gas flotation: the influence of interfacial adsorption and induction times. *Energy Fuels* 29 (11), 7734–7740.
- Eftekhardakhah, M., Klöcker, K.N., Trapnes, H.H., Gaweł, B., Øye, G., 2016. Composition and dynamic adsorption of crude oil components dissolved in synthetic produced water at different pH values. *Ind. Eng. Chem. Res.* 55 (11), 3084–3090.
- Fakhrul-Razi, A., Pendashteh, A., Abdullah, L.C., Biak, D.R., Madaeni, S.S., Abidin, Z.Z., 2009. Review of technologies for oil and gas produced water treatment. *J. Hazard. Mater.* 170 (2–3), 530–551.
- Fisher, R., Shah, M.K., Eskin, D., Schmidt, K., Singh, A., Molla, S., Mostowfi, F., 2013. Equilibrium gas-oil ratio measurements using a microfluidic technique. *Lab Chip* 13 (13), 2623–2633.
- Floquet, C.F.A., Sieben, V.J., MacKay, B.A., Mostowfi, F., 2016. Determination of boron concentration in oilfield water with a microfluidic ion exchange resin instrument. *Talanta* 154, 304–311.
- Frising, T., Noik, C., Dalmazzone, C., 2006. The liquid/liquid sedimentation process: from droplet coalescence to technologically enhanced water/oil emulsion separation: a review. *J. Dispersion Sci. Technol.* 27 (7), 1035–1057.
- Gaweł, B., Lesaint, C., Bandyopadhyay, S., Øye, G., 2015. Role of physicochemical and interfacial properties on the binary coalescence of crude oil drops in synthetic produced water. *Energy Fuels* 29 (2), 512–519.
- Georgieva, D., Schmitt, V., Leal-Calderon, F., Langevin, D., 2009. On the possible role of surface elasticity in emulsion stability. *Langmuir* 25 (10), 5565–5573.
- Golkari, A., Razi, M., 2016. Experimental Investigation of Miscibility Conditions of Dead and Live Asphaltic Crude Oil-CO<sub>2</sub> Systems. vol. 7.
- Groothuis, H., Zuiderweg, F.J., 1960. Influence of mass transfer on coalescence of drops. *Chem. Eng. Sci.* 12 (4), 288–289.
- Hansen, E.W.M., Rørtveit, G.J., 2006. Numerical simulation of fluid mechanisms and separation behavior in offshore gravity separators. In: Sjöblom, J. (Ed.), *Emulsions and Emulsion Stability*, Taylor & Francis, Boca Raton, FL, vol. 132.
- Hansen, B.R., Davies, S.H., 1994. Review of potential technologies for the removal of dissolved components from produced water. *Chem. Eng. Res. Des.* 72 (A2), 176–188.
- Havre, T.E., 2004. Near-IR spectroscopy as a method for studying the formation of calcium naphthenate. *Colloid. Polym. Sci.* 282 (3), 270–279.
- Havre, T.E., Sjöblom, J., Vindstad, J.E., 2003. Oil/water-partitioning and interfacial behavior of naphthenic acids. *J. Dispersion Sci. Technol.* 24 (6), 789–801.
- Hurtevent, C., Rousseau, G., Bourrel, M., Brocart, B., 2006. Production issues of acidic petroleum crude oils. In: Sjöblom, J. (Ed.), *Emulsions and Emulsion Stability*, Taylor & Francis Group LLC, Boca Raton, FL, pp. 477–516.
- Hutin, A., Argillier, J.-F., Langevin, D., 2014. Mass transfer between crude oil and water. Part 1: effect of oil components. *Energy Fuels* 28 (12), 7331–7336.
- Igunnu, E.T., Chen, G.Z., 2014. Produced water treatment technologies. *Int. J. Low-Carbon Technol.* 9 (3), 157–177.
- Kamp, J., Kraume, M., 2014. Influence of drop size and superimposed mass transfer on coalescence in liquid/liquid dispersions – test cell design for single drop investigations. *Chem. Eng. Res. Des.* 92 (4), 635–643.
- Karnanda, W., Benzagouta, M.S., AlQuraishi, A., Amro, M.M., 2013. Effect of temperature, pressure, salinity, and surfactant concentration on IFT for surfactant flooding optimization. *Arabian J. Geosci.* 6 (9), 3535–3544.
- Kopriwa, N., Buchbender, F., Ayesterán, J., Kalem, M., Pfennig, A., 2012. A critical review of the application of drop-population balances for the design of solvent extraction columns: I. Concept of solving drop-population balances and modelling breakage and coalescence. *Solvent Extr. Ion Exch.* 30 (7), 683–723.
- Kourio, M.J., Gourdon, C., Casamatta, G., 1994. Study of drop-interface coalescence: drainage time measurement. *Chem. Eng. Technol.* 17 (4), 249–254.
- Krebs, T., Schroën, K., Boom, R., 2012. Coalescence dynamics of surfactant-stabilized emulsions studied with microfluidics. *Soft Matter* 8 (41), 10650–10657.
- Krebs, T., Schroën, C.G.P.H., Boom, R.M., 2013. Coalescence kinetics of oil-in-water emulsions studied with microfluidics. *Fuel* 106, 327–334.
- Lim, D., Gruenhagen, H., 2009. Subsea separation and boosting—an overview of ongoing projects. In *Asia Pacific Oil and Gas Conference & Exhibition, Society of Petroleum Engineers: Jakarta, Indonesia*.
- Mapolelo, M.M., Rodgers, R.P., Blakney, G.T., Yen, A.T., Asomaning, S., Marshall, A.G., 2011. Characterization of naphthenic acids in crude oils and naphthenates by electrospray ionization FT-ICR mass spectrometry. *Int. J. Mass Spectrom.* 300 (2), 149–157.
- Mazutis, L., Griffiths, A.D., 2012. Selective droplet coalescence using microfluidic systems. *Lab Chip* 12 (10), 1800–1806.
- Mullins, O.C., 2010. The modified yen model. *Energy Fuels* 24 (4), 2179–2207.
- Murgich, J., Strausz, O.P., 2001. Molecular mechanics of aggregates of asphaltenes and resins of the athabasca oil. *Pet. Sci. Technol.* 19 (1–2), 231–243.
- Nenningsland, A.L., Simon, S., Sjöblom, J., 2010. Surface properties of basic components extracted from petroleum crude oil. *Energy Fuels* 24 (12), 6501–6505.
- Nenningsland, A.L., Simon, S., Sjöblom, J., 2014. Influence of interfacial rheological properties on stability of asphaltene-stabilized emulsions. *J. Dispersion Sci. Technol.* 35 (2), 231–243.
- Nowbahar, A., Whitaker, K.A., Schmitt, A.K., Kuo, T.-C., 2017. Mechanistic study of water droplet coalescence and flocculation in diluted bitumen emulsions with additives using microfluidics. *Energy Fuels*.
- Opedal, N.v.d.T., Kralova, I., Lesaint, C., Sjöblom, J., 2011. Enhanced sedimentation and coalescence by chemicals on real crude oil systems. *Energy Fuels* 25 (12), 5718–5728.
- Parra-Barraza, H., Hernández-Montiel, D., Lizardi, J., Hernández, J., Herrera Urbina, R., Valdez, M.A., 2003. The zeta potential and surface properties of asphaltenes obtained with different crude oil/n-heptane proportions. *Fuel* 82 (8), 869–874.

- Podgórska, W., 2007. Influence of dispersed phase viscosity on drop coalescence in turbulent flow. *Chem. Eng. Res. Des.* 85 (5), 721–729.
- Poteau, S., Argillier, J.-F., Langevin, D., Pincet, F., Perez, E., 2005. Influence of pH on stability and dynamic properties of asphaltenes and other amphiphilic molecules at the oil–water interface. *Energy Fuels* 19 (4), 1337–1341.
- Rogers, V.V., Wickstrom, M., Liber, K., MacKinnon, M.D., 2002. Acute and subchronic mammalian toxicity of naphthenic acids from oil sands tailings. *Toxicol. Sci.* 66 (2), 347–355.
- Schorling, P.C., Kessel, D.G., Rahimian, I., 1999. Influence of the crude oil resin/asphaltene ratio on the stability of oil/water emulsions. *Colloids Surf. Physicochem. Eng. Aspects* 152 (1), 95–102.
- Sjöblom, J., Marit-Helen, E., Wanzhen, L., Xiaoli, Y., 2001. Film properties of asphaltenes and resins. In: *Encyclopedic Handbook of Emulsion Technology*. CRC Press, pp. 525–540.
- Sjöblom, J., Simon, S., Xu, Z., 2014. The chemistry of tetrameric acids in petroleum. *Adv. Colloid Interface Sci.* 205, 319–338.
- Spiecker, P.M., Gawrys, K.L., Trail, C.B., Kilpatrick, P.K., 2003. Effects of petroleum resins on asphaltene aggregation and water-in-oil emulsion formation. *Colloids Surf. Physicochem. Eng. Aspects* 220 (1), 9–27.
- Spildo, K., Høiland, H., 1999. Interfacial properties and partitioning of 4-heptylbenzoic acid between decane and water. *J. Colloid Interface Sci.* 209 (1), 99–108.
- Sterling Jr., M.C., Ojo, T., Autenrieth, R.L., Bonner, J.S., Page, C.A., Ernest, A.N.S., 2002. Coalescence kinetics of dispersed crude oil in a laboratory reactor. In: *Environment Canada Arctic and Marine Oil Spill Program Technical Seminar (AMOP) Proceedings*, pp. 741–753.
- Strassner, J.E., 1968. Effect of pH on interfacial films and stability of crude oil-water emulsions.
- Tan, Y.-C., Ho, Y.L., Lee, A.P., 2007. Droplet coalescence by geometrically mediated flow in microfluidic channels. *Microfluid. Nanofluid.* 3 (4), 495–499.
- Tichelkamp, T., Teigen, E., Nourani, M., Øye, G., 2015. Systematic study of the effect of electrolyte composition on interfacial tensions between surfactant solutions and crude oils. *Chem. Eng. Sci.* 132, 244–249.
- Vieira, L.C., Buchuid, M.B., Lucas, E.F., 2010. Effect of pressure on the crystallization of crude oil waxes. I. Selection of test conditions by microcalorimetry. *Energy Fuels* 24 (4), 2208–2212.
- Produced Water: Technological/Environmental Issues and Solutions*, 2002. Springer, US, vol. 46, p. 632.
- Wolstenholme, G.A., Schulman, J.H., 1950. Metal-monolayer interactions in aqueous systems. Part I. -The interaction of monolayers of long-chain polar compounds with metal ions in the underlying solution. *Trans. Faraday Soc.* 46, 475–487.
- Won, J.Y., Krägel, J., Makievski, A.V., Javadi, A., Gochev, G., Loglio, G., Pandolfini, P., Leser, M.E., Gehin-Delval, C., Miller, R., 2014. Drop and bubble micro manipulator (DBMM)—A unique tool for mimicking processes in foams and emulsions. *Colloids Surf. Physicochem. Eng. Aspects* 441, 807–814.
- Zagnoni, M., Cooper, J.M., 2009. On-chip electrocoalescence of microdroplets as a function of voltage, frequency and droplet size. *Lab Chip* 9 (18), 2652–2658.



# Microfluidic tools for studying coalescence of crude oil droplets in produced water

*Marcin Dudek<sup>1</sup>, Are Bertheussen<sup>1</sup>, Thomas Dumaire<sup>2</sup> and Gisle Øye<sup>1,†</sup>*

<sup>1</sup> Ugelstad Laboratory, Department of Chemical Engineering, Norwegian University of Science and Technology (NTNU), Trondheim, Norway

<sup>2</sup> Université Pierre-et-Marie-Curie (UPMC), Paris, France

† Corresponding author: [gisle.oye@chemeng.ntnu.no](mailto:gisle.oye@chemeng.ntnu.no); Sem Sælandsvei 4, 7491 Trondheim, Norway

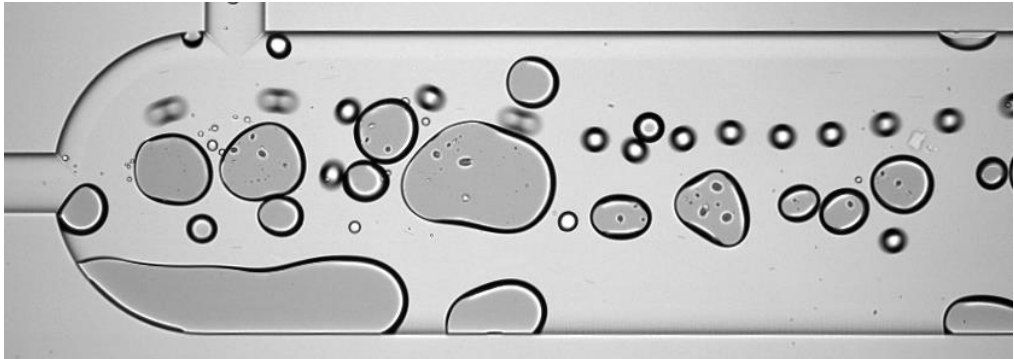


Figure S1 Snapshot of crude oil C droplets in Na-Brine at pH 4.

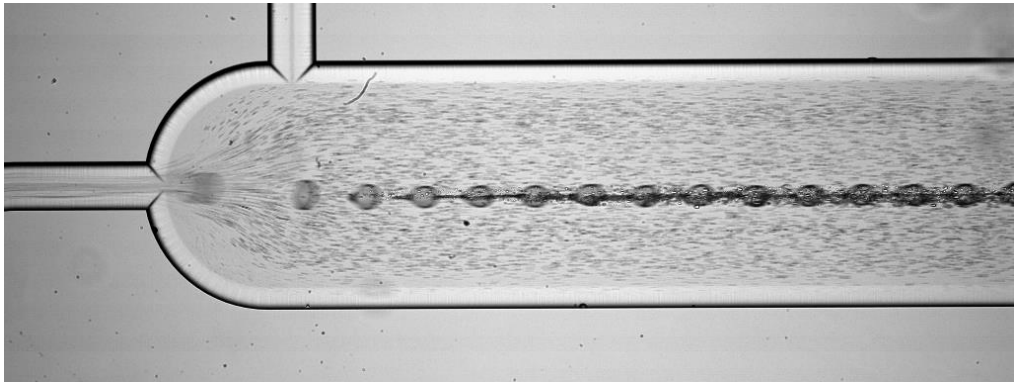


Figure S2 Snapshot of crude oil C droplets in Na-Brine at pH 10. Small dots in the picture are 1-2  $\mu\text{m}$  droplets that split from the generated droplet.

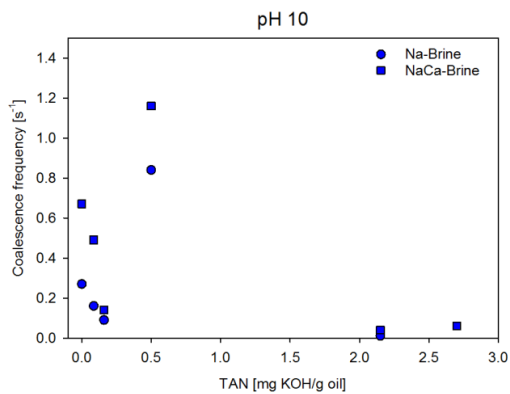


Figure S3 Coalescence frequencies of diluted crude oils at pH 10 plotted against their TAN values. The order of crude oils from left to right: B, F, D, E, A, C.

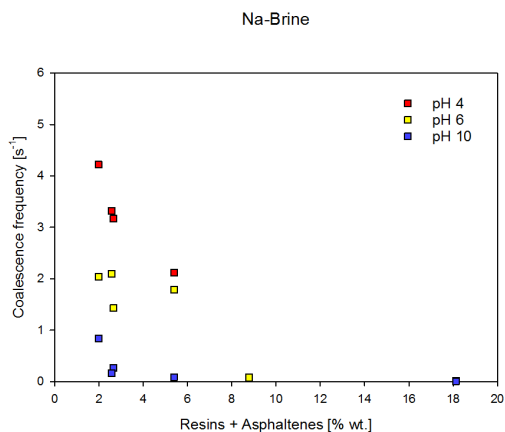


Figure S4 Coalescence frequencies of diluted crude oils in Na-Brine plotted against the sum of resin and asphaltene weight fractions of respective crude oils.

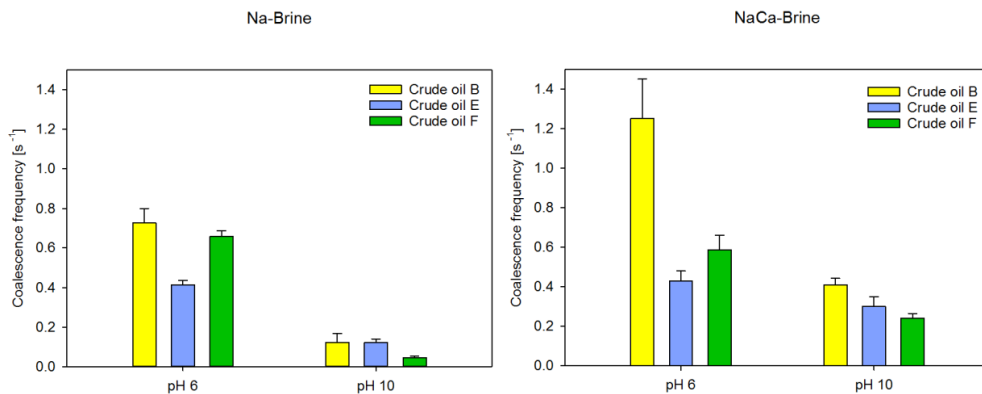


Figure S5 Coalescence frequencies of three crude oils with the second type of an oil-soluble surfactant.

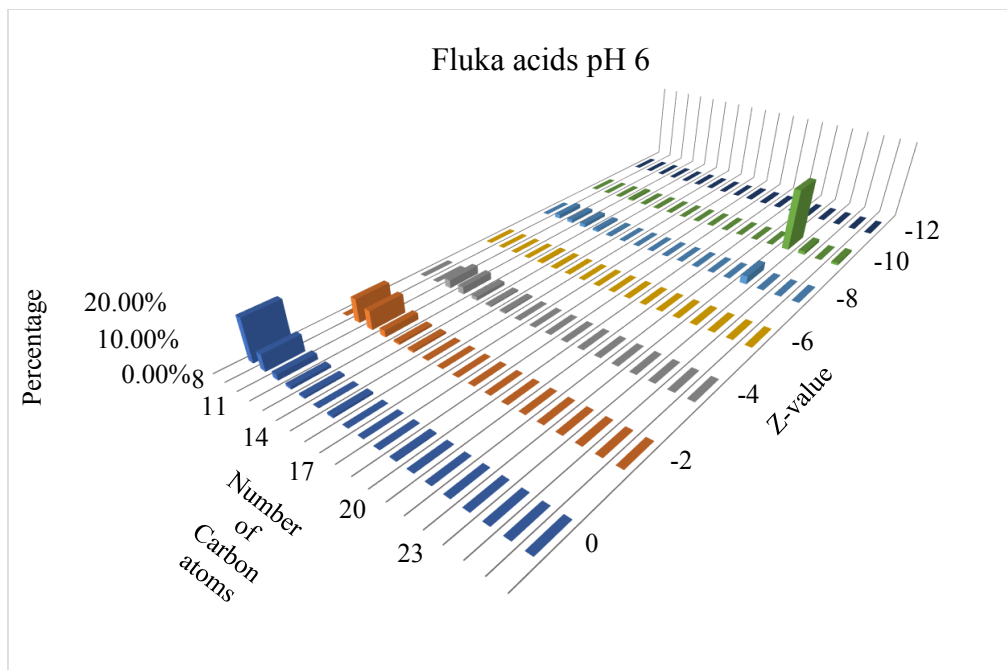


Figure S6 Distribution of dissolved Fluka acids at pH 6.

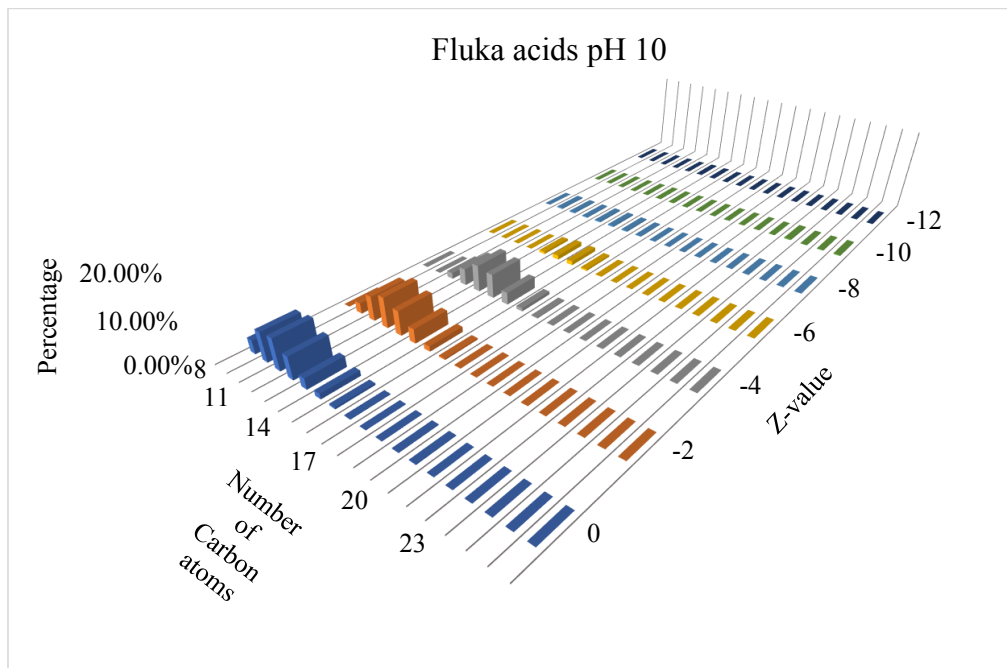


Figure S7 Distribution of dissolved Fluka acids at pH 10.

Figures S6 and S7 represent the distribution of the acids in the water phase after equilibrium partitioning, back-extraction at low pH to oil phase, derivatization with MTBSTFA + 1% TBDMSCI (Sigma Aldrich), analysed with low resolution GC EI MS, extracted spectra are rounded to nominal masses and classified by n/Z distribution table as described in Holowenko et al. *Water Research* **36**(11), 2002.

At pH 6, only 2% of the Fluka naphthenic acids have partitioned into the water phase. As seen on the n/Z distribution at pH 6, most of the species correspond to naphthenic acids with low carbon numbers and hydrogen deficiencies, n from 8 to 10 and Z from 0 to -2. The only exception is the peak at is n=22 Z=-10. This peak corresponds to 24% of the intensities. However, it seems that this peak doesn't correspond to a regular naphthenic acid i.e. hydrocarbons with single COOH function, since it partitions into water at any pH as explained by Bertheussen et al. *Energy Fuels* (DOI: 10.1021/acs.energyfuels.8b01494). This peak is also present at pH 9, but does not represent a significant amount of naphthenic acids present in the water phase. Interfacial tension measurement of 10 mM Fluka acids in toluene with pH 6 buffer in sinterface show negligible IFT reduction.

At pH 9 more of the Fluka naphthenic acids (70%) have partitioned into the water phase which is evident by a broader n/Z distribution with n from 8 to 14 and Z from 0 to -6.

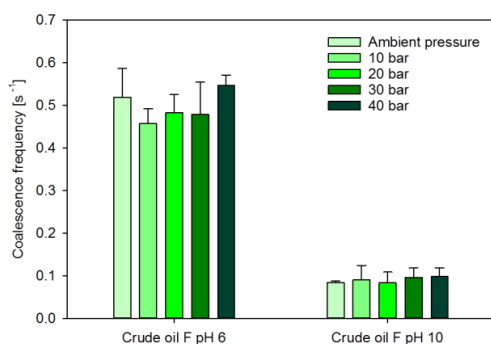


Figure S8 The effect of pressure on the coalescence of crude oil F in Na-Brine.